HUMAN MICROGLIA IMPACT NEURONAL DEVELOPMENT IN RETINAL ORGANOIDS

by

Verena Schmied

June, 2025

A thesis submitted to the
Graduate School
of the
Institute of Science and Technology Austria
in partial fulfillment of the requirements
for the degree of
Doctor of Philosophy

Committee in charge:
Caroline Jane Muller, PhD, Chair
Dr. Sandra Siegert
Dr. Mario de Bono
J. Gray Camp, PhD

The thesis of Verena Schmied, titled *HUMAN MICROGLIA IMPACT NEURONAL DEVELOPMENT IN RETINAL ORGANOIDS*, is approved by:

Supervisor: Sandra Siegert, ISTA, Klosterneuburg, Austria

Signature: _____

Committee Member: Mario de Bono, ISTA, Klosterneuburg, Austria

Signature: _____

Committee Member: J. Gray Camp, IHB, Basel, Switzerland

Signature: _____

Defense Chair: Caroline Jane Muller, PhD, ISTA, Klosterneuburg, Austria

Signature: _____

Signed page is on file

ISTA Thesis, ISSN: 2663-337X

ISBN: 978-3-99078-060-2

I hereby declare that this thesis is my own work and that it does not contain other people's work without this being so stated; this thesis does not contain my previous work without this being stated, and the bibliography contains all the literature that I used in writing the dissertation.

I accept full responsibility for the content and factual accuracy of this work, including the data and their analysis and presentation, and the text and citation of other work.

I declare that this is a true copy of my thesis, including any final revisions, as approved by my thesis committee, and that this thesis has not been submitted for a higher degree to any other university or institution.

I certify that any republication of materials presented in this thesis has been approved by the relevant publishers and co-authors.

Signature: _____
Verena Schmied

Signed page is on file

Abstract

Prenatal immune challenges pose significant risks to human embryonic brain and eye development. However, we still lack knowledge about the safe usage of anti-inflammatory drugs during pregnancy. Human induced pluripotent stem cell (hIPSC)-derived brain organoid models provide a unique opportunity to investigate neuronal development and have started to explore functional consequences upon viral infection. However, brain organoids usually lack microglia, the brain-resident immune cells. They are present in the early human embryonic brain and actively participate in neuronal circuit development. At the same time, microglia are known for their immune-sensing properties and will influence viral-mediated effects. In my thesis, I was interested to study the multifunctional role of human microglia during retinal development.

In chapter 1, I characterize the innate occurrence of IBA1^{+}-microglia-like cells within the retinal organoid differentiation (Bartalska et al., 2022). Therefore, we differentiate hIPSC using an unguided retinal organoid differentiation protocol and observe the presence of IBA1^{+}-microglia-like cells alongside retinal cups between week 3 and 4 in 2.5D culture. However, instead of infiltrating the neuroectodermal sides, they enrich within non-pigmented, 3D-cystic compartments that develop in low numbers parallel to 3D-retinal organoids. To enrich for IBA1^{+}-microglia precursors (preMG), we guided the differentiation with a low-dosed BMP4 application, which prevents retinal cup development and enhances microglia and 3D-cysts formation. We characterize the differentiated preMG for their microglia-like identity and validated their functionality. In parallel, mass spectrometry identifies the 3D-cysts to express mesenchymal and epithelial markers. We confirm that comparable 3D-cysts are also the preferential environment for IBA1^{+}-microglia-like cells within the unguided retinal organoid differentiation.

In chapter 2, I investigate how microglia influence retinal development and whether they contribute to viral-mediated consequences (Schmied et al., 2025). Here, we assemble preMG, which we have characterized in chapter 1, into 3D-retinal organoids. Once the outer plexiform layer forms, microglia-like cells (iMG) populate them and interact with retinal cell types. However, at this developmental stage, the ganglion cell number decreases in 3D-retinal organoids. Thus, we adapted the model into 2D which promotes their survival. Integrated iMG engulf ganglion cells and control their cell number. In parallel, we apply the immunostimulant POLY(I:C) to mimic a fetal viral infection. Although POLY(I:C) stimulation affects iMG phenotype, it does not influence their interaction with ganglion cells. Furthermore, iMG presence significantly contributes to the supernatant's inflammatory secretome and increases retinal cell proliferation. Simultaneous exposure to the non-steroidal anti-inflammatory drug (NSAID) ibuprofen dampens POLY(I:C)-mediated consequences of the iMG phenotype and ameliorates cell proliferation. Remarkably, while POLY(I:C) disrupts neuronal calcium dynamics independent of iMG presence, ibuprofen rescues this effect only in the presence of iMG. Mechanistically, ibuprofen blocks the enzymes cyclooxygenase 1 and 2 (COX1/ PTGS1 and COX2/ PTGS2) simultaneously, from which iMG predominantly express COX1. Selective inhibition of COX1 does not restore the calcium peak amplitude upon POLY(I:C) stimulation, indicating ibuprofen's effect depends on the presence and interplay of both, COX1 and COX2.

In summary, we characterized the 3D-retinal organoid model for the occurrence of IBA1^{+}-microglia like cells. As the innately developing IBA1^{+}-cells enrich in mesenchymal over retinal

structures, we optimized a protocol to differentiate IBA1^{+}-microglia precursors. By combining these two models we generate microglia-assembled retinal organoids. Our results underscore the importance of microglia during neurodevelopment, in the context of prenatal immune challenges and provide insight into the mechanisms by which ibuprofen exerts its protective effects during embryonic development.

Acknowledgments

I would like to express my sincere gratitude to my supervisor **Dr. Sandra Siegert** for all her support and navigation through scientific and personal challenges. Thank you for the opportunity to follow this project from creating the idea and establishing the methodology to publishing the results.

Thank you to the members of the committee of my thesis **Dr Mario de Bono and J. Gray Camp, PhD** for assessing and approving my thesis.

My PhD was special because of special people in our group. Thank you to **Alessandro, Amin, Arsalan, Balint, Fleur, Filo, Gabi, Gloria, Iris, Juan Pablo, Katharina, Maggie, Medina, Nathalie, Negar, Rouven and Yari** for scientific and non-scientific discussions, lunches and coffee breaks. Thank you for sharing demanding times and celebrating successful moments. In particular, I want to thank Alessandro, my favorite office neighbor for evolving and discussing projects ideas and analysis as well as your mental support. Special thanks to Medina and Fleur for sharing weekend duties, jumping in during holidays and sickness. Iris without you I would not have started this journey, thank you for being there for me in such a special and demanding time.

Thank you to the scientific service units at ISTA including the life science facility, specifically Margarita Eustacchio; the imaging and optics facility for their support; Nicolas Armel for performing the mass spectrometry and the virus services team, specifically Flavia Gama Gomes Leite and Mark Andrew Smyth for the virus production. Thanks to Alexandra Lang and Tanja Peilnsteiner for their help in human brain tissue collection. Thanks to Ana Freeman for your support in the cell culture and our chats.

Thank you to the Gesellschaft für Forschungsförderung Niederösterreich m.b.H. for financially supporting my research with the grant Science Call 2019 (grant No. Sc19-017).

Thanks to my cohort, especially Lena and Nathalie, Andrea and Elizabeth for sharing challenging and successful moments and understanding each other's situations. I will miss our lunches and coffee breaks.

Finally, I would like to thank my family and friends for supporting my weekend and your mental support. Thanks to Michi for our discussions about statistical analysis and planning our vacations around my cell culture schedules. Dad, without you I would have stopped this journey at a very early stage.

About the Author

Verena Schmied completed her BSc in Food Science and Biotechnology and an MSc in Biotechnology at the University of Natural Resources and Life Science Vienna, Austria. In February 2017, she joined the group of Dr. Sandra Siegert at the Institute of Science and Technology Austria (ISTA) to conduct her master thesis, during which she focused on generating and characterizing microglia-like cells differentiated from human induced pluripotent stem cells. In September 2018, she joined the ISTA graduate school program and affiliated with Dr. Sandra Siegert in May 2019. For her PhD project, Verena developed a human model system to investigate microglia-neuron interaction during embryonic development. She used microglia-assembled retinal organoids to understand developmental consequences upon viral infection and their treatment using the anti-inflammatory drug *Ibuprofen*. Her results highlight, that microglia contribute to viral-mediated as well as drug-mediated effects.

Verena's Ph.D. was supported with a fellowship from the Gesellschaft für Forschungsförderung Niederösterreich m.b.H. In 2023, she received travel support from Erasmus+ to attend the Neuroscience School of Advanced Studies in Venice, where she attended the course 'Organoid modeling and Neural Reprogramming'.

The results of her research led to a first-author publication in the *Journal of Neuroinflammation* (2025) and two co-first-author publications in *IScience* (2022) and a Cell *STAR protocol* (2022). She presented her work at several national and international conferences and was invited to give an oral presentation at the *ProRetina* meeting 2024 in Potsdam, Germany. Her publication was mentioned in several national newspapers and she was invited for an interview for the radio station OE1. She also shared her research with the general public during events such as the Open Campus or the Pint of Science and fostered children's interest who joined the Wifzac Academy.

List of Collaborators and Publications

Chapter 1 is based on the following publication:

Bartalska, K.*, **Hübschmann, V.*, #**, Korkut-Demirbaş, M.*, Cubero, R.J.A., Venturino, A., Rössler, K., Czech, T., and Siegert, S. (2022). A systematic characterization of microglia-like cell occurrence during retinal organoid differentiation. iScience *25*, 104580. https://doi.org/10.1016/j.isci.2022.104580.

***** shared authorship: We used two human induced pluripotent stem cell (hIPSC) lines for this study. **Verena Schmied** focused on the hIPSC line SC 102A-1 and Medina Korkut-Demirbaş focused on the hIPSC line CR0000005. Katharina Bartalska initiated this project.

[#] Verena Hübschmann changed to Verena Schmied

List of Contributions:
Conceptualization – Sandra Siegert, PhD
Methodology – **Verena Schmied**; Katharina Bartalska; Medina Korkut-Demirbaş; Ryan John A. Cubero, PhD, Sandra Siegert, PhD
Validation – **Verena Schmied**; Katharina Bartalska; Medina Korkut-Demirbaş
Formal analysis – **Verena Schmied**; Ryan John A. Cubero, PhD
Investigation – **Verena Schmied**; Katharina Bartalska; Medina Korkut-Demirbaş
Resources – Alessandro Venturino, PhD; Karl Rössler, Prof.; Thomas Czech, Prof.
Data Curation – **Verena Schmied**; Ryan John A. Cubero, PhD
Writing original draft and visualization – **Verena Schmied**; Sandra Siegert, PhD, with input from Katharina Bartalska and Medina Korkut-Demirbaş
Supervision, project administration, funding acquisition – Sandra Siegert, PhD

Chapter 2 is based on the following publication:

Schmied, V., Korkut-Demirbaş, M., Venturino, A., Maya-Arteaga, J.P., and Siegert, S. (2025). Microglia determine an immune-challenged environment and facilitate ibuprofen action in human retinal organoids. J Neuroinflammation *22*, 98. https://doi.org/10.1186/s12974-025-03366-x.

List of Contributions:
Conceptualization – **Verena Schmied**; Sandra Siegert, PhD
Methodology – **Verena Schmied**; Medina Korkut-Demirbaş; Alessandro Venturino, PhD; Sandra Siegert, PhD
Validation – **Verena Schmied;** Sandra Siegert, PhD
Formal analysis – **Verena Schmied**; Juan Pablo Maya Arteaga
Investigation –**Verena Schmied**; Medina Korkut-Demirbaş; Alessandro Venturino, PhD; Sandra Siegert, PhD
Writing original draft and visualization – **Verena Schmied**; Sandra Siegert, PhD
Reviewing & editing – **Verena Schmied**; Medina Korkut-Demirbaş; Alessandro Venturino, PhD; Sandra Siegert, PhD
Supervision, project administration, funding acquisition – Sandra Siegert, PhD

Publication not included in the thesis:

Hübschmann, V.*, #, Korkut-Demirbaş, M.*, and Siegert, S. (2022). Assessing human iPSC-derived microglia identity and function by immunostaining, phagocytosis, calcium activity, and inflammation assay. STAR Protocol *3*, 101866. https://doi.org/10.1016/j.xpro.2022.101866.

* shared authorship

Verena Hübschmann changed to Verena Schmied

Table of Contents

List of Figures

List of Tables

List of Abbreviations

$_{3D}$RO	3D-retinal organoid
Aβ	Beta-amyloid.
AAV	Adeno-associated virus
AAVS1	Adeno-associated virus integration site 1 locus
APB	2-aminoethoxydiphenyl borate
AC	Amacrine cells
ATP	Adenosintriphosphat
BAM	Brain-border associated macrophages
BBB	Blood brain barrier
BC	Bipolar cells
BDNF	Brain derived neurotrophic factor
BMP4	Bone morphogenetic protein 4
BRN3/ POU4F2	Brain-specific homeobox/POU domain protein 3B
C1QA	Complement component C1q
Ca^{2+}	Calcium
CAG	CMV immediate enhancer/β-actin promoter
CALB1	Calbindin
CALB2	Calretinin
CCAS3	Cleaved caspase-3
CCL2	C-C motif chemokine ligand 2
CD11c	Integrin Subunit Alpha X
CD14	Cluster of differentiation 14/ monocyte differentiation antigen CD14
CD31	Platelet endothelial cell adhesion molecule
CD36	CD36 antigen/ Thrombospondin receptor
CD38	CD38 antigen/ ADP-ribosyl cyclase 1
CD45	Cluster of differentiation 45/ protein tyrosine phosphatase receptor
CD163	Cluster of differentiation 163/ scavenger receptor cysteine-rich type 1 protein M130
CD169	Sialic acid-binding Ig-like lectin 1
CD206	Mannose receptor C-type 1
CDH1	E-cadherin
CHAT	Choline acetyltransferase
CNS	Central nervous system
COX-1/ PTGS1	Cyclooxygenase-1/ Prostaglandin-endoperoxide synthase 1
COX-2/ PTGS2	Cyclooxygenase-2/ Prostaglandin-endoperoxide synthase 2
CPP	4-(3-phosphonopropyl)piperazine-2-carboxylic acid
CRALBP	Cellular retinaldehyde-binding protein
CSF1R	Colony stimulating factor 1 receptor
CTBP2	C-terminal-binding protein 2
CTIP2/BCL11b	BAF chromatin remodeling complex subunit
CTRL	Untreated control
CX3CR1	C-X3-C motif chemokine receptor 1
D	Days of differentiation
DAMPs	Damage associated molecular pattern
DCX	Doublecortin

$_{diss}$RO	Dissociated retinal organoid (without iMG)
DSN	Double-strand break
E	Embryonic day
EB	Embryoid bodies
EGTA	Ethylene glycol tetraacetic acid
EMP	Erythro-myeloid progenitors
FN1	Fibronectin
GAPDH	Glyceraldehyde 3-phosphate dehydrogenase
GC	Ganglion cells
GCL	Ganglion cell layer
GFAP	Glial fibrillary acidic protein
CHAT	Choline acetyltransferase
GMCSF/ CSF2	Granulocyte-macrophage colony stimulating factor
GW	Gestational week
H	Hour
HA-L/ HA-R	Homologous arm left/ right
HC	Horizontal cells
HR	Homologous recombination
hESC	Human embryonic stem cells
hIPSC	Human induced pluripotent stem cells
HMC3	human microglial clone 3
hPSC	Human pluripotent stem cells
HSV1	Herpes simplex virus type 1
Hz	Hertz
IBA1/AIF1	Ionized Calcium-Binding Adapter Molecule 1/ Allograft Inflammatory Factor 1
IBU	S(+)-ibuprofen
IFNA1	Interferon alpha 1
IFNB1	Interferon beta 1
IGF-1	Insulin-like growth factor 1
IL1B/ IL1β	Interleukin 1 beta
IL6	Interleukin 6
IL34	Interleukin 34
iMG	hIPSC derived microglia-like cells
iMG-$_{3D}$RO	Microglia assembled 3D-retinal organoid
iMG-$_{diss}$RO	Microglia assembled dissociated retinal organoid
IFNα	Interferon alpha
IFNγ	Interferon gamma
INL	Inner nuclear layer
IPL	Inner plexiform layer
IRF8	Interferon regulatory factor 8
ITGAM/CD11b	Integrin subunit alpha M
Kbp	Kilobase pair
KI67	Proliferation marker protein Ki-67
KLF4	Kruppel like factor 4
LAMB1	Laminin β1
LIF	Leukemia inhibitory factor

LIN28	Zinc finger CCHC domain-containing protein
LPS	Lipopolysaccharide
LYVE1	Lymphatic vessel endothelial hyaluronan receptor 1
MAP2	Microtubule-associated protein 2
MC	Müller glia cell
MCSF/CSF1	Macrophage colony stimulating factor/ Colony stimulation factor 1
MIA	Maternal immune activation
mRNA	Messenger ribonucleic acid
MYB	MYB proto-oncogene
MYC	MYC proto-oncogene
n.d.	Not detectable
NANOG	Nanog homeobox
Nbl	Neuroblastic layer
NBQX	2,3-dioxo-6-nitro-7-sulfamoyl-benzo[f]quinoxaline
NPC	Neuronal progenitor cell
NTC	Non-template control
OCT3/4	Octamer-binding protein 3/4
ONL	Outer nuclear layer
OPL	Outer plexiform layer
OTX2	Orthodenticle homolog 2/ orthodenticle homeobox 2
P2RY12/P2Y12	Purinergic receptor P2Y, G-protein coupled, 12
PAMP	Pathogen associated molecular pattern
PAX6	Paired box 6
PCNA	Proliferating cell nuclear antigen
PCR	Polymerase chain reaction.
PHH3	Phosphohistone H3
POU5F1	POU Domain, class 5, transcription factor 1
PR	Photoreceptor cells
PGE2	Prostaglandin E2
POLY(I:C)	Polyinosinic:polycytidylic acid
POLY(I:C) +IBU	POLY(I:C) and S(+)-ibuprofen in combination
preMG	Microglia precursors
PRKCA	Protein kinase C alpha
PSD95	Postsynaptic density protein 95
PU.1/ SPI1	Hematopoietic transcription factor PU.1/ Spi-1 proto-oncogene
PURO	Puromycin selection side
RCVRN	Recoverin
RLBP1	Cellular retinaldehyde-binding protein
Rod	Rod photoreceptor cell
ROI	Region of interest
RPE	Retinal pigment epithelium
RT-qPCR	Real-time quantitative polymerase chain reaction
RUNX1	Runt-related transcription factor 1
SC-560	PTGS1/COX-1 selective inhibitor
SCF	Stem cell factor
Sec	Seconds
SEM	Standard error of the mean

SOX2	Sex determining region Y-Box 2
SSEA-4	Stage-specific embryonic antigen 4
SV40	SV40 transcriptional enhancer factor
TBR2	T-box brain protein 2
TGFB	Transforming growth factor beta
TLR	Toll-like receptor
TMEM119	Transmembrane protein 119
TNF	Tumor necrosis factor alpha
TORCH	Toxoplasmosis, others, rubella, cytomegalovirus, herpes simplex
TREM2	Triggering receptor expressed on myeloid cells 2
TTX	Tetrodotoxin
RUNX1	Runt-related transcription factor 1
UMAP	Uniform manifold approximation and projection
VEGF	Vascular endothelial growth factor
VIM	Vimentin
VGLUT1	Vesicular glutamate transporter 1
WK	Week after the start of the differentiation
ZIKV	Zika virus

1. General introduction

The central nervous system (CNS) summarizes the dense neuronal networks of the brain and the spinal cord (Thau et al. 2022). The neurons are surrounded by non-neuronal cells known as '*neuroglia*', which support neuronal development, maintenance and function. (Allen and Barres 2009; Kettenmann et al. 1996) The term 'glia' derives from the Greek word for 'glue' reflecting the historical concept that these cells hold neurons together (Somjen 1988).

Microglia are the primary resident macrophage population located in the CNS parenchyma (Colonna and Butovsky 2017), and depending on the brain region, represent up to 10% of all cells in the adult mouse (Lawson et al. 1990) and human brain (Mittelbronn et al. 2001). Microglia were first described by Pio del Rio-Hortega in 1919 as cells with small cell bodies and long, thin processes (Sierra et al. 2016). Beyond their role as immune cells to defend against invading pathogens, microglia play a multifunctional role during neuronal development, tissue homeostasis, and degeneration (Colonna & Butovsky, 2017; Hanisch & Kettenmann, 2007; Kettenmann et al., 2011). *In vivo* imaging of adult microglia has shown that they are highly dynamic cells, continuously extending and retracting their processes (Davalos et al. 2005; Nimmerjahn et al. 2005). Through this activity, microglia constantly monitor their local environment and can sense a wide range of stimuli, including molecular patterns or neuronal signals (Hickman et al. 2013; Pocock and Kettenmann 2007).

1.1. Ontogeny of CNS macrophages

1.1.1. Microglia origin

Fate mapping studies have identified that microglia derive from erythro-myeloid progenitors (EMPs), which are generated during the primitive (first) wave of hematopoiesis starting at embryonic day (E) 7.0 in the blood islands of the yolk sac in mice (Ginhoux et al., 2010; Schulz et al., 2012). Thus, microglia derive from the mesoderm while neurons and astrocytes differentiate from the ectoderm (Ginhoux and Prinz 2015). EMPs give rise to primitive macrophages that colonize the developing embryo, including the brain rudiment, between E8.5 and E9.5 (Alliot et al. 1999; Hoeffel et al. 2015; Kierdorf et al. 2013). In humans, microglia precursor cells also originate in the yolk sac (Bian et al. 2020) and populate the fetal brain as early as gestational week (GW) 4.5 (Monier et al. 2006, 2007). They enter from the ventricular lumen, leptomeninges, and choroid plexus (Hattori et al. 2020; Monier et al. 2006, 2007; Rezaie and Male 2003).

In mice, the blood-brain barrier is established around E13.5, separating the CNS from the body periphery (Daneman et al. 2010). Influenced by local environmental cues, primitive macrophages mature to parenchymal and retinal microglia (Ginhoux et al. 2010; O'Koren et al. 2019). This maturation is associated with the gradual decrease in c-kit and an increase in CD45 and CX3CR1 expression (Kierdorf et al. 2013). Throughout life, microglia maintain by local self-renewal and exhibit slow turnover rates: in humans, 28% of the microglia population are replaced every year resulting in an average microglia age of 4.2 years (Lawson et al. 1990; Réu et al. 2017).

Microglia are distinct from monocytes and peripheral tissue macrophages, which originate from hematopoietic stem cells generated during the definitive (second) wave of hematopoiesis, starting at E8.5 in the yolk sac (Lux et al. 2008). These progenitors replace primitive macrophages in the periphery and not the CNS (Ginhoux et al. 2010; Hoeffel and

Ginhoux 2015). The two hematopoietic waves differ in their dependency on transcription factors: the runt-related transcription factor 1 (RUNX1) is highly expressed by EMPs, while microglia precursor cells rely on Spi1 proto-oncogene (SPI1, also known as PU.1) and interferon regulatory factor 8 (IRF8) (Ginhoux et al. 2010; Hagemeyer et al. 2016). Progenitors generated during the second wave of hematopoiesis depend on c-myb expression, which is lacking in microglia precursor cells (Schulz et al. 2012).

1.1.2. Origin of brain-border associated macrophages

In addition to microglia, the CNS also contains brain-border associated macrophages (BAMs) which are located in the meninges (meningeal macrophages), the perivascular space (perivascular macrophages), and the choroid plexus (choroid plexus macrophages) (Goldmann et al. 2016; Prinz et al. 2017). Unlike microglia, BAMs have a heterogeneous ontogeny. They partially derive from EMPs produced during the first hematopoietic wave, similar to microglia. In addition, BAMs in the choroid plexus and meninges are supplemented by precursors from the second hematopoietic wave (Goldmann et al. 2016; Van Hove et al. 2019; Utz et al. 2020). Although, microglia and BAMs partially share their origin, their common precursors differentiate into distinct cell types with unique transcriptional profiles which allows to distinguish $CD206^{+}$ (Mannose Receptor C-Type 1)/ $CD163^{+}$ (cluster of differentiation 163/ scavenger receptor cysteine-rich type 1 protein M130) BAMs and $CD206^{-}$ / $CD163^{-}$ microglia already early during fetal development (Utz et al. 2020).

In adulthood, microglia express markers like TMEM119 and P2RY12 while BAMs are positive for CD206, CD163, CD169, LYVE1, CD38 and CD11c (Mrdjen et al. 2018). Due to their specific locations between the parenchyma and peripheral tissues, BAMs acquire specialized roles (Dermitzakis et al. 2023; Mrdjen et al. 2018). They are crucial for immune surveillance by monitoring for pathogens and foreign molecules, antigen representation and BBB integrity (Fabriek et al. 2005; Goddery et al. 2021; Rustenhoven et al. 2021).

1.2. Retinal development and microglia colonization

The retina develops from the posterior part of the forebrain, the diencephalon (Jacobson and Hirose 1978). Two eye fields split form the neural tube and give rise to the optic vesicles, which invaginate to form the optic cup (Adler and Canto-Soler 2007; Pei and Rhodin 1970). The retinal progenitors undergo symmetric proliferation and differentiate to generate the five major neuronal cell classes: photoreceptors, horizontal-, bipolar-, amacrine-, and ganglion cells. By mid-gestation, the neuronal cell bodies are organized within the three nuclear layers with their processes localized in two synaptic layers, the outer- and the inner plexiform layers (OPL and IPL, respectively) (**Figure 1**) (Gupta et al. 2016; Kolb et al. 1995). The outer nuclear layer (ONL), adjacent to the choroid, consists of photoreceptor cells, while the inner nuclear layer (INL) contains bipolar-, amacrine- and horizontal cells. The ganglion cell layer (GCL), located close to the vitreous, consists of ganglion cells and displaced amacrine cells (Hendrickson 2016; Hoshino et al. 2017). In humans, the IPL forms first by GW11-12, followed by the OPL, which becomes visible by GW16-17 (Hendrickson 2016; Hoshino et al. 2017; Nag and Wadhwa 2001). In addition to the six major neuronal cell types, retinal progenitors also give rise to Müller glia cells, whose cell bodies are located in the INL with processes spanning the entire retina (Hendrickson et al. 2012).

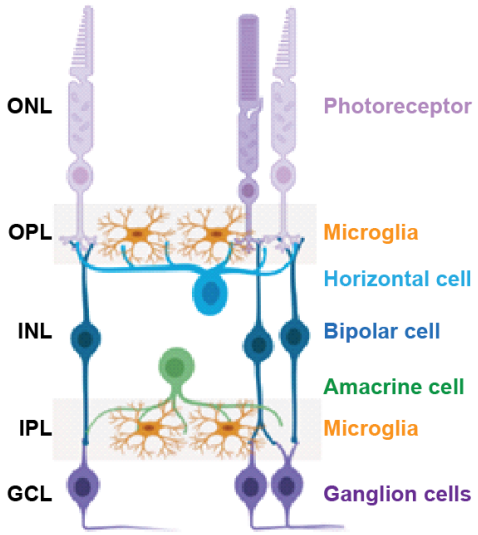

Figure 1 – Schematic side view of the adult retina.
ONL: outer nuclear layer, OPL: outer plexiform layer, INL: inner nuclear layer, IPL: inner plexiform layer, GCL: ganglion cell layer. Figure designed with Biorender.

In the retina, microglia are present by E11.5 in mice (Anderson et al. 2019; Santos et al. 2008) and by GW5 in humans (Hu et al. 2019; Mellough et al. 2019). Microglia precursors have been suggested to enter the retina via two routes: Before vascularization is established, they migrate from the ciliary margin zone and cross the vitreous-retina surface (Diaz-Araya et al. 1995; Santos et al. 2008).

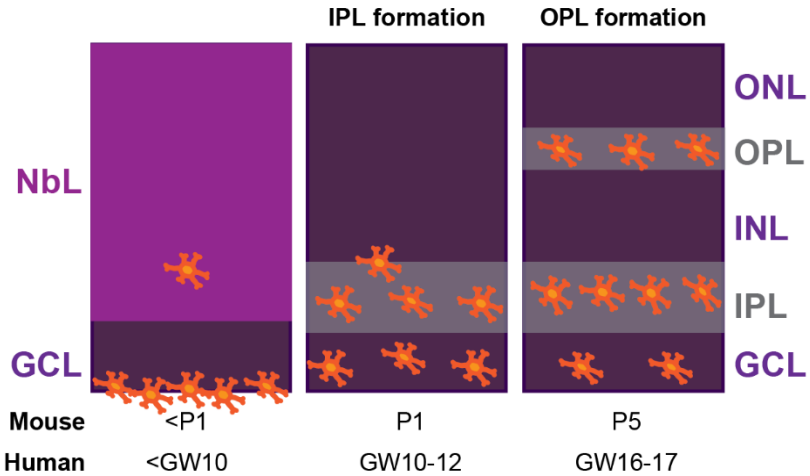

Figure 2 – Timepoint of retinal lamination in mouse and human.
GCL: ganglion cell layer. GW: gestational week. INL: inner nuclear layer. IPL: inner plexiform layer. NbL: neuroblastic layer. ONL: outer nuclear layer. OPL: outer plexiform layer. P: postnatal day. Orange cells: microglia.

After vascularization, they enter from the optic nerve or via blood vessels (Diaz-Araya et al. 1995; Li, Jiang, and Samuel 2019). During development, the distribution of microglia correlates with the retinal cell layer formation (**Figure 2**): Before retinal lamination, most microglia localize close to or within the developing GCL. Only few colonize the neuroblastic layer (NbL), which consists of

neuronal progenitor cells (Anderson et al. 2019; Santos et al. 2008). Once the IPL forms between the NbL and the GCL, approximately 80% of microglia populate the newly formed synaptic layer (Nag and Wadhwa 2001; Santos et al. 2008). Following OPL formation, microglia colonization occurs, while they avoid the ONL (Diaz-Araya et al. 1995; Santos et al. 2008; Li et al. 2019). In the adult healthy retina, 47% of the retinal microglia reside in the OPL and 53% populate the IPL/GCL (Li et al. 2019; O'Koren et al. 2019).

1.3. The multifunctional role of microglia

1.3.1. Microglia function during embryonic development

During brain development, neurons are generated, organized and connected to each other (Barresi 2020; Kelley and Pașca 2022). Microglia have been identified to play a multifunctional role during various steps of development, from neurogenesis to neuronal organization and connectivity (**Figure 3**).

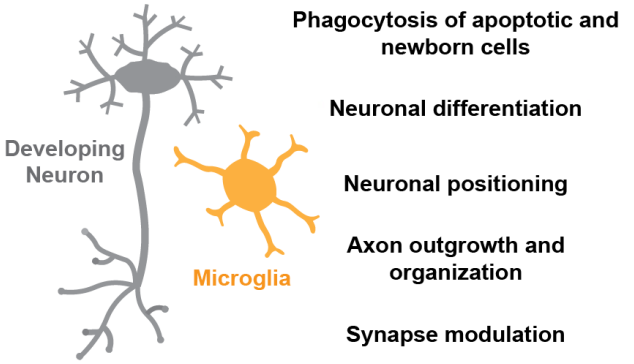

Figure 3 – The multifunctional role of microglia during neuronal development.

Microglia influence neurogenesis and neuronal survival

During embryonic development, multiple studies suggest that microglia promote the differentiation of neural stem cells into intermediate progenitors. In zebrafish, the absence of microglia prolongs retinal progenitor cell proliferation, thereby inhibiting neuronal differentiation resulting in microphthalmia (Huang et al. 2012). Microglia repopulation partially recovered this phenotype. Also in mice, microglia elimination results in a decreased number of $TBR2^+$ (t-box brain protein 2) intermediate progenitors, concurrently an increase of $PAX6^+$ (paired box 6) neural stem cells in the developing forebrain (Arnò et al. 2014; Hattori and Miyata 2018).

Moreover, microglia regulate neuronal cell population size. They phagocytose cleaved-$caspase3^+$ apoptotic cells as well as viable neurons including $TBR2^+$-$PAX6^+$ neuronal progenitors and $PCNA^+$ (proliferating cell nuclear antigen) postmitotic neurons (Cunningham et al. 2013). Also in the prenatal retina, microglia have been shown to control RGC number (Anderson et al. 2019). Beside their phagocytic activity they are also involved in programmed cell death. By releasing superoxide ions, microglia actively induce apoptosis of developing Purkinje cells in the mouse cerebellum (Marín-Teva et al. 2004).

Moreover, microglial processes control neuronal proliferation by interacting with somas of DCX^+-(doublecortin) immature postmitotic neurons via purinergic signaling (P2RY12) (Cserép et al. 2022). Deletion of microglial P2RY12 results in the decrease of proliferating DCX^+-neuron. Postnatally, this interaction assists cortical layer formation and controls neuronal density in cortical layer 1 and 6.

In addition, microglia influence neuronal survival. They secrete multiple neurotrophins in a brain region dependent manner (Elkabes et al. 1996) exemplified in the white matter where a subset of microglia release insulin-like growth factor 1 (IGF-1), which promotes survival of layer V pyramidal neurons (Ueno et al. 2013).

Microglia assist neuronal circuit formation

Beside their role during neurogenesis, microglia fine-tune neuronal positioning as shown for Lhx6^{+}-interneurons, progenitors of somatostatin-positive interneurons and fast-spiking interneurons, in a CX3CR1-dependent manner (Squarzoni et al. 2014). In the retina, microglia influence horizontal cell positioning as well as their shape (Burger et al. 2020). Moreover, embryonic microglia impact neuronal wiring by restricting dopaminergic axonal outgrowth (Squarzoni et al. 2014) and influencing the organization and bundling of axonal fibers within the corpus callosum (Pont-Lezica et al. 2014).

On a synaptic level, microglia promote the formation (Miyamoto et al. 2016; Paolicelli et al. 2011; Parkhurst et al. 2013), and selective elimination known as *'sy*naptic pruning' of immature synapses via the fractalkine receptor CX3CR1 (Paolicelli et al. 2011) or in a complement-dependent manner (Schafer et al. 2012; Stevens et al. 2007) to refine neuronal connections during postnatal development.

Microglia impact gliogenesis and vascularization

Besides regulating neuronal development, microglia-derived factors such interleukin 6 (IL6) and leukemia inhibitory factor (LIF) impact astrocyte- and oligodendrocyte differentiation and survival (Marsters et al. 2020; Nakanishi et al. 2007). Similar as shown for neuronal progenitors, microglia phagocytose oligodendrocyte progenitors, thus influencing their maturation into oligodendrocytes which in turn affects neuronal myelination (Nemes-Baran et al. 2020).

In addition, microglia have proangiogenic properties, thereby promoting vascularization. By migrating towards endothelial tip-cells, they stimulate their sprouting via the release of soluble mediators (Rymo et al. 2011). Moreover, their presence affects the branching complexity of the developing vasculature in a region-specific and age-dependent manner (Chen et al. 2024).

1.3.2. Microglia phenotype during development

Transcriptional profiling has identified that microglia are highly heterogenous during development and that this diversity decreases with age, resulting in limited heterogeneity in the healthy adult CNS in mice (Hammond et al., 2019; Li et al., 2019; Masuda et al., 2019; Matcovitch-Natan et al., 2016) and human (Kracht et al. 2020; Yaqubi et al. 2023). Human prenatal microglia show a gene signature associated to a high phagocytic capacity and a high activity of transcription factors that control cell proliferation compared to postnatal microglia, which acquire an immune-responsive profile (Han et al. 2023; Kracht et al. 2020; Yaqubi et al. 2023).

Microglia maturation is further indicated by their morphology. During development, they commonly represent an amoeboid or bipolar-like shape, with large and rounded cell bodies and short, thick branches (Diaz-Araya et al. 1995; Monier et al. 2007; Santos et al. 2008). In contrast, in adulthood, microglia exhibit a ramified shape under homeostatic condition (Sierra et al. 2016). Although less ramified, also embryonic microglia monitor their environment by constantly extending and retracting their processes (Hattori and Miyata 2018; Rosin et al. 2021).

1.3.3. Microglia function as immune cells

As the main resident immune cells of the CNS, microglia play a key role in neuroinflammation (Hanisch and Kettenmann 2007; Kreutzberg 1996). They express a set of pattern recognition receptors, such as toll-like receptors (TLRs), to detect damage-associated molecular patterns (DAMPs) and pathogen-associated molecular patterns (PAMPs) to recognize injuries and diseases or potential infections respectively (Bsibsi et al. 2002; Davalos et al. 2005; Hickman et al. 2013; Venegas and Heneka 2017).

In the CNS, microglia express various TLRs (Bsibsi et al. 2002) to either sense viral components such as double-stranded RNA via TLR3 (Alexopoulou et al. 2001; Town et al. 2006) or single-stranded RNA via TLR7 and TLR8 (Seitz et al. 2018; Wheeler et al. 2018). Upon receptor stimulation, a signaling cascade involving the NFkB- and the interferon pathway is triggered, resulting in the release of inflammatory mediators including cytokines and chemokines (Alexopoulou et al. 2001; Kawai and Akira 2010; Matsumoto and Seya 2008; Town et al. 2006). These signaling molecules are important to recruit peripheral immune cell populations including monocytes, neutrophils, dendritic cells and T-cells into the CNS to resolve the infection (Chen et al. 2003; Fife et al. 2001; Johnson et al. 2011; Romagnani and Crescioli 2012; Ubogu et al. 2006).

Beside secreting inflammatory mediator, microglia response to viral infections is associated to morphological changes (Quick et al. 2014), and that they phagocytose infected, damaged or dead cells (Chhor et al. 2013; Colonna and Butovsky 2017; Quick et al. 2014). Upon viral infection, microglia exhibit a dual role: On one hand, they are protective as microglia restrict viral growth and reduce mortality (Seitz et al., 2018; Wheeler et al., 2018). On the other hand, they have destructive effects by removing synapses (Garber et al. 2019).

1.4. Establishing a human model system

Although rodent models have provided important insights into the multifunctional role of microglia, there is still limited knowledge about their role in humans. Beside their brain size, human and rodents differ in their developmental timeline, neuronal composition and diversification as well as brain complexity and organization (Agoston, 2017; Boldog et al., 2018; Vanderhaeghen & Polleux, 2023; Zeiss, 2021). Their difference is also reflected by microglial transcriptional signature and metabolic reprogramming associated with immune response and neurodegenerative diseases (Geirsdottir et al. 2019; Sabogal-Guáqueta et al. 2023) emphasizing the necessity to establish and investigate human models.

Primary human microglia cultures

One possible strategy to study human microglia is to generate primary microglia cultures by isolating them acutely from human fetal and post-mortem tissue, or disease surgical explants (Mizee et al. 2017; Rustenhoven et al. 2016). Besides ethical concerns and accessibility, several biological concerns exist such as tissue origin and age of the donor or cell manipulation due to the isolation procedure which affects microglia survival rates (Pesti et al. 2024). Moreover, it has been shown that isolated microglia quickly adapt to their local microenvironment upon removal from their native tissue context (Bohlen et al. 2017; Butovsky et al. 2014; Gosselin et al. 2017). *In vitro*, microglia adapt their morphology from a ramified homeostatic to a more ameboid shape (Bohlen et al. 2017) and alter their transcriptional profile by downregulating microglia specific genes like P2RY12 and TMEM119 (Gosselin et al. 2017).

Microglia cell lines

Human microglia cell lines such as the human microglial clone 3 cell line (HMC3) provide an alternative to primary cultures. HMC3 cells originate from primary human embryonic microglia cultures immortalized through transduction of the oncogene SV40 (SV40 Transcriptional Enhancer Factor) (Janabi et al. 1995; Timmermanet al. 2018). The immortalization induces an unrestricted proliferative capacity, which might interfere with the microglia phenotype (Dello Russo et al. 2018). In parallel, it allows to overcome limitations in availability and variability in donor origin compared to primary cultures. Since these cell lines are derived from primary microglia similar disadvantages apply as described for primary microglia cultures.

1.4.1. Human pluripotent stem cells (hPSC)

Human embryonic stem cells (hESC)

Human pluripotent stem cells (hPSC) provide the unique possibility to establish human-related models. In 1998, Thompson *et al.* generated the first human embryonic stem cell (hESC) line, derived from an embryo's inner cell mass at the blastocyst stage. These cells express pluripotency markers like SSEA-4 (stage-specific embryonic antigen 4), or the podocalyxin (TRA-1-60 and TRA-1-81), and have the potential to differentiate into cells from all three germ layers endoderm, mesoderm and ectoderm *in vitro* (Thomson et al. 1998). Since hESCs are obtained from *in vitro* fertilized human embryos, which raises strong ethical concerns, researchers have investigated alternative methods to generate pluripotent stem cells from somatic tissue.

Human induced pluripotent stem cells (hIPSC)

In 2007, human induced pluripotent stem cells (hIPSC) were reprogrammed from human dermal fibroblasts via the expression of a cocktail of four transcriptions factors (pluripotency factors): octamer-binding transcription factors 4 (OCT4), sex determining region Y-box 2 (SOX2), kruppel-like factor 4 (KLF4), and bHLH transcription factor MYC proto-oncogene c-Myc (Takahashi et al. 2007); or OCT4, SOX2, nanog homeobox (NANOG) and zinc finger CCHC domain-containing protein (LIN28) (Yu et al. 2007). hIPSC can be derived from various somatic cell types using different approaches to deliver the reprogramming factors (Malik and Rao 2013). hIPSCs show similar characteristics as hESCs because they self-renew and can differentiate into any somatic adult cell type from all three germ layers endo-, meso-, and ectoderm **Figure 4** (Takahashi et al. 2007; Yu et al. 2007).

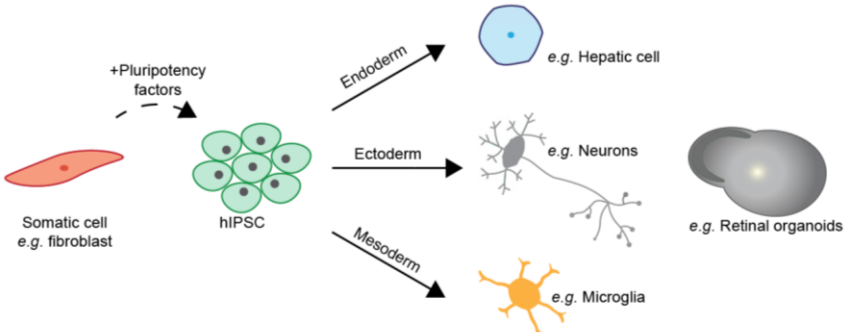

Figure 4 – Schematic overview of hIPSCs. HIPSC: human in human induced pluripotent stem cells.

1.4.2. Differentiation of hPSC-derived microglia precursors

hESCs and hIPSCs can be differentiated into diverse cell types, from neurons to astrocytes (Emdad et al. 2012; Qi et al. 2017; TCW et al. 2017). In 2012, the first study described the differentiation of microglia-like precursors (Roy 2012). Several groups have guided iPSC-differentiation to specifically obtain EMPs or microglia precursors (Abud et al. 2017; Douvaras et al. 2017; Guttikonda et al. 2021; Haenseler et al. 2017; Konttinen et al. 2019; McQuade et al. 2018; Muffat et al. 2016; Pandya et al. 2017; Takata et al. 2017). These protocols aim to mirror the main characteristics of microglia development, inspired by ontogeny studies (Ginhoux et al. 2010; Kierdorf et al. 2013). The steps include mesoderm induction, followed by hematopoietic lineage specification, which gives rise to EMPs. Those are further differentiated into MYB-independent microglia precursors (Guttikonda et al. 2021; Haenseler et al. 2017; Takata et al. 2017). A common feature of all protocols is that they sequentially apply a cocktail of growth factors or small molecules to induce microglia differentiation (Abud

et al. 2017; Douvaras et al. 2017; Guttikonda et al. 2021; Haenseler et al. 2017; Konttinen et al. 2019; McQuade et al. 2018; Muffat et al. 2016; Pandya et al. 2017; Takata et al. 2017).

Growth factors

The protocols differ in the initiation of the differentiation, which affects the requirement of growth factors, the duration of the culture periods, the necessity of enriching intermediate progenitors, and the overall yield (see **Table 1**). Each protocol is based on a unique combination and timing of growth factors. However, a common growth factor is the bone morphogenetic protein 4 (BMP4), which is applied to mimic mesodermal lineage induction (Abud et al. 2017; Douvaras et al. 2017; Guttikonda et al. 2021; Konttinen et al. 2019; McQuade et al. 2018; Pandya et al. 2017; Takata et al. 2017). BMPs regulate multiple aspects of embryonic development and progenitor fate decisions: *E.g.* they are critical for the formation of the body plan (Heisenberg and Solnica-Krezel 2008), early hematopoiesis (Larsson and Karlsson 2005), and neuronal development (Liu and Niswander 2005). Therefore, the timing and duration of BMP4 treatment is critical: while short-term treatment (~24 hours) promotes early mesoderm induction, which can subsequently differentiate into *e.g.,* hematopoietic lineages (Feng et al. 2016); long-term treatment for more than two days leads to trophoblast and extraembryonic endoderm formation (P. Zhang et al., 2008). In addition to BMP4, some protocols use stem cell factor (SCF) and/ or vascular endothelial growth factor (VEGF) to promote further mesodermal specification (Abud et al. 2017; Douvaras et al. 2017; Guttikonda et al. 2021; Haenseler et al. 2017; Konttinen et al. 2019; McQuade et al. 2018; Muffat et al. 2016; Pandya et al. 2017; Takata et al. 2017).

Once the mesodermal lineage is induced, these protocols supplement the media with macrophage colony stimulating factor (MCSF/ CSF1), granulocyte-macrophage colony stimulating factor (GMCSF) and interleukin 34 (IL34), which bind to the colony stimulating factor 1 receptor (CSF1R) to promote microglia precursors specification (Abud et al. 2017; Douvaras et al. 2017; Guttikonda et al. 2021; Haenseler et al. 2017; Konttinen et al. 2019; McQuade et al. 2018; Muffat et al. 2016; Pandya et al. 2017; Takata et al. 2017). CSF1R signaling is essential for microglia colonization, proliferation, differentiation, and survival (Easley-Neal et al. 2019; Ginhoux et al. 2010; Greter et al. 2012).

For maintenance and maturation of microglia-like cells (iMG), precursor cells are either co-cultured with neurons or astrocytes (Guttikonda et al. 2021; Haenseler et al. 2017; Pandya et al. 2017; Takata et al. 2017), or the medium is supplemented with growth factors such as transforming growth factor beta (TGFb) to mimic a neuronal microenvironment (Abud et al. 2017; Douvaras et al. 2017; Konttinen et al. 2019; McQuade et al. 2018).

Table 1 – Comparison of protocols differentiating microglia-like cells. BMP4: bone morphogenic protein 4. C1QA: Complement C1q A chain. CD11B: Integrin subunit alpha M. CD11C: Integrin subunit alpha X.CD14: monocyte differentiation antigen CD14. CD34:CD43: Hematopoietic progenitor cell antigen CD34. CD43: Leukosialin. CD45: Protein tyrosine phosphatase receptor type C. CD163: Scavenger receptor cysteine-rich type 1 protein M130. CD200: CD200 antigen. CHIR9902: GSK3 inhibitor. CX3CL1: C-X3-C motif chemokine ligand 1. CX3CR1: C-X3-C motif chemokine receptor 1. EB: embryoid body. FGF: fibroblast growth factor. FLT3: Fms related receptor tyrosine kinase 3. GMCSF: granulocyte-macrophage colony stimulating factor. GPR34**:** G protein-coupled receptor 34**.** hIPSC: human induced pluripotent stem cells. HLA-DR: Major histocompatibility complex, class II, DR beta 1. IBA1: Ionized calcium-binding adapter molecule 1. IL: interleukin. IWP: Nodal signaling activator. LiCl: lithium chloride. MCSF: macrophage colony stimulating factor. P2RY12**:** Purinergic receptor P2Y, G-protein coupled, 12**.** PU.1: Hematopoietic transcription factor PU.1/ Spi-1 proto-oncogene. SCF: stem cell factor. TGFb: transforming growth factor β. TMEM119: Transmembrane protein 119**.** TPO: thioperoxides. TREM2: Triggering receptor expressed on myeloid cells 2**.** VEGF: vascular endothelial growth factor.

	Muffat *et al.* 2016	Pandya *et al.* 2016	Abud *et al.* 2017	Douvaras *et al.* 2017	Haenseler *et al.* 2017	Takata *et al.* 2017	Konttinen *et al.* 2018	McQuade *et al.* 2018	Gutti-konada *et al.* 2021
Starting condition	EBs	hIPSC	IPSC	hIPSC	EBs	hIPSC	hIPSC	hIPSC	hIPSC
Factors for mesoderm specification		BMP4, VEGF, SCF, ActivinA (Hypoxia until D10)	BMP4, VEGF, FGF2, ActivinA, LiCl (Hypoxia until D4)	BMP4, VEGF, SCF, bFGF	BMP4, VEGF, SCF	BMP4, VEGF, bFGF, CHIR99021 (Hypoxia until D10)	BMP4, CHIR99021 ActivinA Rock inhibitor (Hypoxia until D4)	Medium A Supp-lement A	CHIR9902 BMP-4, ActivinA, IWP2
Factors for progenitor expansion	IL34, MCSF	IL3, IL6, G-CSF, SCF, BMP4, Flt3L	SCF, FGF2, TPO, IL3, IL6	IL3, TPO, FLT3 MCSF, SCF,	IL3, M-CSF	IL3, IL6, SCF, VEGF, bFGF, DKK1	VEGF, FGF2, SB431512, IL3, IL6, SCF, TPO	Medium B Supp-lement B	VEGF, FGF2, SCF, IL6, IL3, TPO
Progenitor maturation	IL34, MCSF	IL3, MCSF, GMCSF	IL34, MCSF, TGFb	IL34, GMCSF, FLT3	IL34, MCSF	MCSF	IL34, MCSF	IL34, MCSF, TGFb	IL34, MCSF
Terminal different-iation into iMG		Astrocytes + IL3, MCSF, GMCSF	Rat neurons IL34, MCSF, TGF, CD200, CX3CL1	GMCSF, IL34	Cortical neurons	Cortical neurons		IL34, MCSF, TGFb, CD200, CX3CL1	Cortical neurons + IL34. MCSF

Table continued on next page…

	Muffat *et al.* 2016	Pandya *et al.* 2016	Abud *et al.* 2017	Douvaras *et al.* 2017	Haenseler *et al.* 2017	Takata *et al.* 2017	Konttinen *et al.* 2018	McQuade *et al.* 2018	Gutti-konada *et al.* 2021
Harvest of progenitors	Ultra-low attach-ment plates	$CD34^+$ $CD45^+$ $CD43^+$	$CD43^+$	$CD14^+$ $CX3CR1^+$	Non-adherent cells from super-natant	$CD45^+$ $CD11b^+$ $CD163^+$ $CD14^+$ $CX3CR1^+$	Non-adherent cells from super-natant	Non-adherent cells from super-natant	Non-adherent cells from super-natant
Harvest	Single harvest	Single harvest	Single harvest	Multiple harvests	Multiple harvests	Single harvest	Single harvest	Single harvest	Single harvest
Tested microglia markers	TMEM119, P2RY12, IBA1, CD45, PU.1, CD11B	CD11B, IBA1, CD45, CX3CR1, TREM2, HLA-DR	CD11B, CD45, TREM2, PU.1, CX3CR1, P2RY12	IBA1, CD11C, TMEM119, CD11B, CX3CR1	CD11B, CD14, CD45, TMEM119, P2RY12	IBA1, CX3CR1	IBA1, CX3CR1, TMEM119, P2RY12, TREM2 PU.1,	P2RY12, TREM2, CD45	IBA1, PU.1, CX3CR1, TMEM119, C1QA, P2RY12, GPR34
Functional assays	Phago-cytosis	Migration, phago-cytosis	Phago-cytosis	Phago-cytosis, inflamm-atory response	Migration, phago-cytosis, inflamm-atory response	Phago-cytosis		Phago-cytosis	Phago-cytosis, Inflamm-atory response

Alternative strategies

Alternatively, forward programming has been applied to generate iMG. This approach rapidly directs hIPSCs to differentiate into a distinct somatic cell by transiently overexpressing key transcription factors characteristic for the specific cell type. To induce iMG-differentiation, studies use two or a combination of up to six transcription factors highly expressed by microglia (**Table 2**) (Chen et al. 2021; Dräger et al. 2022; Speicher et al. 2022). PU.1 overexpression is a common feature, as it is highly expressed throughout embryonic development of microglia (Ginhoux et al. 2010; Hagemeyer et al. 2016) Depending on the protocol, iMG are generated within 8 to 16 days and resemble other hIPSC-derived iMGs in their identity and functionality.

Table 2 – Overview forward programming approaches to generate microglia like cells.
C1QA**:** Complement C1q A chain**.** $Ca2^{+}$: calcium ion. CD11B: Integrin subunit alpha M. CEBPα: CCAAT enhancer binding protein alpha. CEBPβ: CCAAT enhancer binding protein beta. CX3CR1: C-X3-C motif chemokine receptor 1. GAS6: Growth arrest specific 6. GPR34: G protein-coupled receptor 34. IBA1: Ionized calcium-binding adapter molecule 1. IRF5: Interferon regulatory factor 5. IRF8: Interferon regulatory factor 8. MAFB: MAF BZIP transcription factor B. MERTK: MER receptor tyrosine kinase. P2RY12: Purinergic receptor P2Y, G-protein coupled, 12. PROS1: Protein S.PU.1: Hematopoietic transcription factor PU.1/ Spi-1 proto-oncogene. ROS: reactive oxygen species. TMEM119: Transmembrane protein 119. TREM2: Triggering receptor expressed on myeloid cells 2.

Protocol	Transcription factors used	Days required until analysis	Tested microglia markers	Functional assays
Chen *et al.* 2021	• PU.1 • (CEBPα)	10 days	CD11B, C1QA, CX3CR1, IBA1, PU.1, P2RY12, TMEM119, TREM2 RNA sequencing	$Ca2^{+}$-activity, phagocytosis, inflammatory response
Dräger *et al.* 2022	• PU.1 • MAFB • CEBPα • CEBPβ • IRF5 • IRF8	8 days	IBA1, GPR34 RNA sequencing	Phagocytosis, inflammatory response
Speicher *et al.* 2022	• PU.1 • CEBPβ	16 days	IBA1, P2RY12, GAS6, MERTK, C1QA, PROS1, GPR34, CX3CR1, TMEM119 RNA sequencing	$Ca2^{+}$-activity, phagocytosis, inflammatory response, ROS production

Validation

HIPSC-derived iMG are characterized using various combinations of several methods including immunohistochemistry, gene expression profiling and functional analysis (**Table 1-2**). To verify their microglia-like identity, studies performed immunofluorescent staining, florescent activated cell sorting (FACS) or real-time quantitative polymerase chain reaction (rt-qPCR) to assess the expression of general macrophage markers including CD45, CX3CR1, IBA1 and microglia-specific markers TMEM119 and P2RY12(Abud et al. 2017; Chen et al. 2021; Douvaras et al. 2017; Dräger et al. 2022; Guttikonda et al. 2021; Haenseler et al. 2017; Hübschmann, Korkut-Demirbaş, and

Siegert 2022; Konttinen et al. 2019; McQuade et al. 2018; Muffat et al. 2016; Pandya et al. 2017; Speicher et al. 2022; Takata et al. 2017). To confirm that iMG exhibit functional activity similar to their *in vivo* counterparts, these studies performed calcium activity-, phagocytosis-, migration or inflammatory response assays. RNA sequencing revealed that hIPSC-derived iMG more closely resemble human fetal than adult microglia or monocytes (Abud et al. 2017; Douvaras et al. 2017; Konttinen et al. 2019; McQuade et al. 2018).

1.4.3. Generation of hPSC-derived brain organoids

Beyond the differentiation of individual cell types, hPSCs including hESC and hIPSC can also generate self-organizing three-dimensional structures known as organoids. They typically consist of multiple cell types, which mimic certain aspects of the development, the anatomical arrangement and function of the respective organ (Bagley et al., 2017; Camp et al., 2015; Renner et al., 2017; Sloan et al., 2018; Zhong et al., 2014). 3D-organoids provide a better representation of cell-cell interactions and tissue architecture observed *in vivo* compared to 2D models, in which cells are grown as a flat monolayer (Cowan et al. 2020; Lancaster et al. 2013).

Unguided/ minimally guided brain organoid approaches

Unguided or minimally guided protocols rely on intrinsic signaling and self-patterning capacities resulting in the parallel formation of a heterogenous mixture of various brain regions including fore-, mid- and hindbrain, retina, choroid plexus and mesodermal cells (Qian et al. 2019). Typical minimally guided approaches include protocols to generate cerebral- (Lancaster et al. 2013; Renner et al. 2017) and retinal organoids (Zhong et al. 2014). While these protocols mimic tissue interactions between different brain regions and rely on minimal interference, the disadvantage of this strategy is the unpredictable heterogeneous mix of tissue identities and a higher degree of variability.

Guided brain organoid approaches

Alternatively, guided differentiation protocols rely on the timed application of small molecules and growth factors to direct cell fate towards a desired tissue (Qian et al. 2019) like cerebral cortex (Pasca et al. 2015), midbrain- (Kim et al. 2019; Smits et al. 2019), thalamic- (Xiang et al. 2019) or choroid plexus organoids (Pellegrini et al. 2020). For these protocols, it is necessary to evaluate the optimal timing, concentration and combination of factors to induce the desired tissue fate (Amin et al. 2024). The advantage is the reproducibility of cell type proportions, while their cyto-architecture and cell-cell interactions are less representative compared to unguided approaches (Qian et al. 2019; Sloan et al. 2018).

Retinal organoids mimic structural and functional properties of the *in vivo* retina

My thesis focuses on retinal organoids ($_{3D}$RO), one of the first established brain organoid models (Eiraku et al. 2011). 3D-organoids recapitulate several key features compared to the *in vivo* tissue (Cowan et al. 2020; Zhong et al. 2014), concurrently their limitations need to be considered.

First, $_{3D}$ROs mimic retinal morphogenesis by forming optic-cup like structures and follow the developmental trajectories of ectodermal-derived retinal cell types in a specific and temporal order (Cowan et al. 2020; Hoshino et al. 2017; Sridhar et al. 2020): Initially, retinal ganglion cells are born, followed by amacrine cells, horizontal cells and cone photoreceptors. Later during development, bipolar cells, rod photoreceptors and Mueller glia cells emerge. Consequently, $_{3D}$RO exhibit a comparable neuronal cellular composition that closely resembles that of the human fetal retina at equivalent developmental stages (Cowan et al. 2020; Hoshino et al. 2017; Sridhar et al. 2020). However, some cell types which are not derived from the ectoderm including blood vessels and immune cells are lacking (Collin et al. 2019; Cowan et al. 2020; S. Kim et al. 2019).

$_{3D}$ROs also mimic the retinal cyto-architecture. In early stages, the organoid consists of a neuroblastic layer (NbL) with retinal progenitors and a retinal ganglion cell layer (Hoshino et al. 2017; Zhong et al. 2014). As development progresses, retinal cell bodies arrange in a five layered structure as described in **Figure 1** (Cowan et al. 2020; Hoshino et al. 2017; Sridhar et al. 2020). Thus, they also represent certain cell-cell interactions. It has been shown that $_{3D}$RO develop ribbon synapses between photoreceptors and bipolar cells (Cora et al. 2019). In contrast, the retinal pigment epithelium which should grow adjacent to the developing photoreceptors is generated but misplaced (Kolb et al. 1995; Zhong et al. 2014).

Finally, $_{3D}$ROs show some functional properties of the respective organ: In late-stages, $_{3D}$RO, photoreceptors develop rudimentary outer segment-like structures facing the surface of the organoid (Wahlin et al. 2017). These specialized structures are involved in capturing light and initiating the visual transduction process (Gupta et al., 2016; Kolb et al., 1995). While some photoreceptors show a response to light flashes, $_{3D}$ROs exhibit a limited functional maturation compared to *in vivo* (Cowan et al., 2020; Hallam et al., 2018; Saha et al., 2022; Zhong et al., 2014). Moreover, long term cultures result in the degeneration of ganglion cells and cells of the INL (Capowski et al. 2019; Cowan et al. 2020; Fligor et al. 2021; Wagstaff et al. 2021).

Overall, $_{3D}$RO provide a powerful tool to study human development (Cowan et al. 2020; Hoshino et al. 2017; Sridhar et al. 2020), to model diseases (Ashworth et al. 2024), to screen potential drugs (Spirig et al. 2023) and to develop cell replacement therapies (Hirami et al. 2023)

1.5. Outline of the thesis and research question

Viral infection-induced inflammation during pregnancy has been associated to malformations of the fetal brain (Auriti et al. 2021; Meyer 2019). Microglia respond to inflammatory signals (Bsibsi et al. 2002; Hickman et al. 2013) and at the same time actively modify neuronal development on the cellular- and synaptic level (Cunningham et al. 2013, 2013; Guizzetti et al. 2014; Schafer et al. 2012; Squarzoni et al. 2014). We know surprisingly little about how microglia balance the different demands during human embryonic development and which functional consequences an inflammatory environment has on neuronal organization and connectivity.

Brain organoids provide a unique opportunity to investigate this relationship. However, they commonly lack mesodermal-derived microglia (Camp et al. 2015; Collin et al. 2019; Cowan et al. 2020; Ginhoux and Prinz 2015; S. Kim et al. 2019). Brain organoid protocols favor the formation of neuroectodermal-derived cell types, including neurons and astrocytes (Noctor et al. 2002), and dampen endo- and mesoderm formation (Lancaster et al. 2013; Renner et al. 2017). Interestingly, some unguided brain organoid protocols have reported the presence of innately developing microglia-like cells (Gabriel et al. 2021; Ormel et al. 2018; Shiraki et al. 2022).

In my thesis, I aimed to assess human microglia-neuron interaction during embryonic development in a well-defined brain region, namely the retina. Due to their early presence in fetal brain tissue, including the retina (Hu et al., 2019; Mellough et al., 2019; Monier et al., 2006) and their reported neurodevelopmental role (Cunningham et al. 2013, 2013; Guizzetti et al. 2014; Schafer et al. 2012; Squarzoni et al. 2014), **I propose that microglia presence impacts neuronal patterning and activity during retinal development.**

In rodent models, prenatal immune activation has been reported to modulate microglia properties (He et al. 2021; Loayza et al. 2022; Ozaki et al. 2020; Pratt et al. 2013; Squarzoni et al. 2014) and to interfere with developmental processes, including neurogenesis, neuronal differentiation, axonal outgrowth, synaptogenesis, which are known to be influenced by microglia (Andoh et al. 2019; Ben-Reuven and Reiner 2019; Coiro et al. 2015; Cunningham et al. 2013; Forrest et al. 2012; Giovanoli et al. 2016; Squarzoni et al. 2014). Thus, I postulate that microglia **are involved in translating viral-mediated stimulation into neuronal consequences**. Finally, I was interested if the application of the **anti-inflammatory drug *ibuprofen* can modulate viral-mediated developmental** abnormalities.

In my thesis I investigated the following questions and aims:

1. Do **microglia like-cells innately develop** during retinal organoid differentiation and do they populate retinal structures?
2. **Characterizing the identity and function** of hIPSC-derived microglia precursors.
3. Assessing the **neuro-developmental role of human microglia** during retinal organoid development.
4. Modeling prenatal immune activation to determine the **immune-modulatory function of microglia and consequences** on retinal development
5. Does an anti-inflammatory treatment using ***ibuprofen*** **rescue or ameliorate viral-mediated** developmental abnormalities?

To address these questions, we applied an unguided differentiation protocol to generate retinal organoids (Cowan et al. 2020; Zhong et al. 2014) and characterized whether IBA1^{+}-microglia innately develop within the differentiation. As microglia did not populate the retinal cup, instead occupied mesenchymal structures, we established a protocol to enrich for microglia precursors using a BMP4-guided protocol (**chapter 1**).
Next, I integrated these microglia precursors into retinal structures to investigate microglia-neuron interaction during retinal development, upon viral stimulation and following anti-inflammatory treatment (**chapter 2**).

2. CHAPTER 1 | A systematic characterization of microglia-like cell occurrence during retinal organoid differentiation.

Chapter 1 is based on the following publication:

Bartalska, K.*, **Hübschmann, V**.*, Korkut-Demirbaş, M.*, Cubero, R.J.A., Venturino, A., Rössler, K., Czech, T., and Siegert, S. (2022). A systematic characterization of microglia-like cell occurrence during retinal organoid differentiation. iScience 25, 104580. https://doi.org/10.1016/j.isci.2022.104580.
* shared authorship

2.1. Keywords

Human induced pluripotent stem cells (hIPSC), microglia, IBA1, retinal organoids, BMP4, mesenchymal, CD163

2.2. Introduction

The human brain consists of billions of neurons, glial and endothelial cells that self-organize during development into cellular networks, which perform distinct functions (Barresi 2020). Microglia, the brain parenchymal immune cells, fine-tune neuronal circuits at the cellular and synaptic level (Cunningham et al. 2013; Guizzetti et al. 2014; Schafer et al. 2012; Squarzoni et al. 2014). They derive from a primitive macrophage population, which develops within the yolk sac in both mouse (Ginhoux et al. 2010) and humans (Bian et al. 2020). Therefore, they represent a distinct macrophage population as they occur prior to the onset of hepatic and bone marrow hematopoiesis (Juul and Christensen 2018; Menassa and Gomez-Nicola 2018). Immunostaining of human embryonic brain tissue indicates that microglia enter the cerebral wall from the ventricular lumen and the leptomeninges at 4.5 gestation weeks and gradually colonize the cortex (Monier et al. 2007; Rezaie et al. 2005). The critical role of microglia in early human brain development has been further supported by hereditary mutations in macrophage-selective genes that cause numerous structural brain malformations in pediatric leukoencephalopathy (Oosterhof et al. 2019) A current bottleneck is the lack of accessible models that accurately recapitulate human microglia development, distribution and action during circuit formation. So far, our knowledge is mostly limited to observations from post-mortem fetal brain studies or non-human model systems like mice.

Human induced pluripotent stem cells (hIPSC) have revolutionized the field of tissue engineering and allow exploring aspects of embryonic brain (Bagley et al. 2017; Camp et al. 2015; Renner et al. 2017; Sloan et al. 2018). However, mesoderm-derived microglia are commonly lacking within cerebral organoids (Collin et al. 2019; Cowan et al. 2020; S. Kim et al. 2019). One likely explanation for this is that differentiation protocols often use supplements to direct hIPSC-formed embryoid bodies (EB) towards the neuroectodermal lineage to obtain cerebral organoids (Chambers et al. 2009; Pasca et al. 2015). To obtain human microglia-like cells, several groups have established guided protocols with BMP4 as a common nominator (Abud et al. 2017; Douvaras et al. 2017; Guttikonda et al. 2021; Haenseler et al. 2017; Konttinen et al. 2019; McQuade et al. 2018; Muffat et al. 2016; Pandya et al. 2017; Takata et al. 2017). Thus, several groups have assembled the

hIPSC-derived microglia-like cells with separately-derived cerebral organoids to analyze microglia function and interaction with neurons (Abud et al. 2017; Song et al. 2019; Xu et al. 2021) but this does not capture the natural progression of microglial appearance and distribution within brain tissue.

Unguided cerebral organoid differentiation provides an alternative strategy to capture various cell types. Here, EBs are cultured with minimal external interference and self-organize to a variety of cell lineage identities from fore-, mid- and hindbrain (Qian et al. 2019). The hIPSC differentiation towards retinal organoids has been one of the first brain region-specific protocols (Eiraku et al. 2011; Nakano et al. 2012). This method reliably recapitulates the typical optical cup structure, expresses markers of well-defined cell types, and shows a light-sensitive response (Cowan et al. 2020; Zhong et al. 2014). In contrast, data are controversial regarding microglia occurrence in organoids. Whereas protocols report that microglia innately developed within cerebral organoids (Ormel et al. 2018), or single-cell RNA-sequencing identified a glial cluster expressing microglia-specific markers (Gabriel et al. 2021), other studies do not show, or the provided data do not support, their presence in retinal organoids (Collin et al. 2019; Cowan et al. 2020; S. Kim et al. 2019). On the other hand, microglia appear early in human embryonic retinal tissue at gestation week 5 as indicated by a microglial transcriptional signature (Hu et al. 2019; Mellough et al. 2019), and their localization within the human retinal layers by gestation week 10 (Diaz-Araya et al. 1995). To clarify whether microglia develop in unguided retinal organoid differentiation protocol (referred from now on as unguided protocol), we implemented the protocol from (Zhong et al. 2014) and stained with the pan-macrophage marker IBA1/AIF1 (ionized calcium binding adaptor molecule 1/ allograft inflammatory factor 1), which identifies brain parenchymal- (microglia), blood-derived- (MΦ), and border-associated- (perivascular pvMΦ, leptomeningeal mMΦ, choroid plexus cpMΦ) macrophages (Imai et al. 1996; Ito et al. 2001; Kierdorf et al. 2019; Prinz and Priller 2014). In 2.5D cultures, we consistently found $IBA1^+$-cells in parallel to developing retinal organoids by differentiation week 3 to 4. However, these $IBA1^+$-cells rarely occupied the retinal or cerebral compartment and preferentially occurred in non-pigmented, cystic compartments that are commonly overlooked in organoid-focused studies.

Such cystic structures have also been mentioned in other microglia differentiation protocols (Haenseler et al. 2017; Muffat et al. 2016; Vaughan-Jackson et al. 2021). One common factor that is frequently used to enhance for microglia is BMP4. Therefore, we applied a low-dosed BMP4 to the otherwise unchanged protocol to verify whether we can enrich for these 3D-cysts. We identified that these cysts highly express the mesenchymal and epithelial markers vimentin and E-Cadherin, respectively, and we confirmed a similar expression pattern in the cystic compartments in our unguided protocol. Finally, we found a strong overlap between IBA1 and CD163 expression, a marker for border-associated macrophages (BAMs) that reside either at perivascular structures, meninges, or choroid plexus, all of mesenchymal nature (Lun, Monuki, and Lehtinen 2015; MacCord 2012; Pill et al. 2015). The expression is turned on between week 5 and 6 in 2.5D culture.

In summary, our results confirm that IBA1^{+}-cells exist in our unguided protocol, and we map their presence to cystic mesenchymal-like compartments, which co-developed alongside to 3D-retinal organoids. This work offers a model for exploring microglia integration during early development, and provides a foundation for future studies to dissect the molecular signaling mechanisms that attract microglia and foster their incorporation into cerebral organoids.

Materials and Methods

Ethical approval

The IST Austria Ethics Officer and Ethics Committee approved the use of human induced pluripotent stem cells (hIPSC). The use of human brain samples was approved by the Ethics Committee of the Medical University Vienna.

Primary human tissue samples

Human brain samples were explanted from the temporal cortex (T1) of patients undergoing temporal lobe surgery for epilepsy treatment. Immediately after the surgical explant, the samples were transferred into saline solution (0.9% (v/v) NaCl (Braun 3570160) in H_2O). The tissue was immersed in 4% (w/v) PFA within 5 minutes and post-fixed on an orbital shaker at 4ºC overnight.

Cell lines

This study used two human induced pluripotent stem cell lines: SC 102A-1 GVO-SBI Human Fibroblast-derived (feeder-free) iPSC cell line (BioCat; male; hPSCreg.eu: SBLi006-A; in this study referred to SC102A). NCRM-5 (aka NL-5; human umbilical cord blood $CD34^+$ cells derived; RUCDR Infinite Biologicals, Cell line ID: CR0000005, NHCDR ID: ND5003; male; hPSCreg.eu: CRMi001-A; in this study referred to CR05). For more details, see (**Table 3**).

Table 3 – Overview of human induced pluripotent stem lines included in chapter 1.
hPSCreg.eu, human pluripotent stem cell registry. MYC, MYC proto-oncogene. KLF4, kruppel like factor 4. Large T antigen, large tumor antigen. LIN28, zinc finger CCHC domain-containing protein. OCT4, octamer-binding protein 4. POU5F1, POU domain, class 5, transcription factor 1. SOX2, sex determining region Y-box 2. SV40, simian-virus 40.

Cell line	SC 102A-1	CRMi001-A, CR0000005, NCRM-5, NL-5
hPSCreg.eu	SBLi006-A	CRMi001-A
Company	BioCat	RUCDR Infinite Biologics
Generator	SYSTEM BIOSCIENCES	National Institutes of Health - Center for Regenerative Medicine
Abbreviation within manuscript	SC102A	CR05
Source	Fibroblast (dermis)	Umbilical cord blood $CD34^+$ cells
Vector	Retrovirus (integrating)	Episomal (non-integrating)
Genes for reprogramming	MYC, KLF4, SOX2, OCT4/POU5F1	KLF4, MYC, SOX2, OCT4/POU5F1, LIN28, SV40, Large T antigen
Health status	Healthy	
Race	Caucasian	
Sex	Male	Male
Donor age	60-64	Fetal

Cell culture and unguided (retinal organoid differentiation) protocol

Matrigel-coating. Matrigel (Corning® Matrigel® hESC-Qualified Matrix, *LDEV-Free, (Corning, #354277) was used according to the manufacturer instructions with the following modifications: Matrigel aliquots were dissolved in ice-cold X-Vivo 10 chemically defined, serum-free hematopoietic cell medium (Lonza, #BE04-380Q) prior coating the plates. 6-cm dishes (VWR, #734-0007) were coated for unguided retinal organoid or BMP4-guided differentiation protocols and 2-well chambered coverslips (Ibidi, #80286) for 2.5D culture.

Maintenance of human induced pluripotent stem cells. hIPSCs were cultured at 37ºC and 5% CO_2 in a humidified incubator (BINDER C150) in mTeSR1 medium (STEMCELL Technologies, #85850) on Matrigel (Corning, #354277) coated 6-well plates (Corning, #3516). Cells were passaged in small aggregates every 3-4 days and were dissociated before reaching 80% confluency using EDTA dissociation buffer (0.5M EDTA (ethylenediaminetetraacetic acid, K.D. Biomedical, #RGF 3130), 0.9 g (w/v) NaCl (Sigma, #5886) in PBS (phosphate buffered saline, calcium/magnesium-free, Invitrogen, #14190), sterile filtered, stored at 4ºC) according to (Chen 2014). Cells were tested on regular basis for mycoplasma using MycoAlert Mycoplasma Detection Kit (Lonza, #LT07-518). For iPSC differentiation, two wells of a 6-well plate were used for SC102A and four wells for CR05 as starting material.

Unguided (retinal organoid differentiation) protocol. 3D-retinal organoids were generated as described before (Zhong et al. 2014) with the following modifications: On day 0 of differentiation, iPSC colonies were dissociated into evenly sized aggregates using a cell-passaging tool (Thermo Fisher Scientific, #23181-010). After mechanical scraping, floating aggregates were transferred with a 1250µl wide orifice pipette (VWR, #613-0737) onto one 10 cm Petri dish (Sarstedt, #82.1473), and cultured in mTeSR1 medium supplemented with 10 µM blebbistatin (Sigma, #B0560-5MG). On day 1, 2 and 3, the medium was gradually replaced with ¼, ½, and 1, respectively, of NIM (neural induction medium: DMEM/F12 (Gibco, #31331- 028), 1x N2 supplement (Gibco, #17502-48), 1% (v/v) NEAA Solution (Sigma, #M7145), 2 µg/ml heparin (Sigma, #H3149-50KU). From day 4 onwards, 10 ml medium was exchanged daily with NIM. On day 8, the floating embryoid bodies (EB) were collected, equally distributed onto 8 Matrigel-coated 6-cm dishes (approximately 20-40 number of EBs/cm^2) and cultured in 3 mL NIM. From day 16 onwards, NIM was exchanged daily for 3:1-DMEM/F12-medium (3 parts DMEM (Thermo Fisher Scientific, #31966047) and one-part F12 medium (Ham's F-12 Nutrient Mix, Thermo Fisher Scientific, #31765-027), supplemented with 2% (v/v) B27 without vitamin A (Thermo Fisher Scientific, #121587-10), 1% (v/v) NEAA solution (Sigma, #M7145), 1% (v/v) penicillin-streptomycin (Thermo Fisher Scientific, #15140122). On day 28-32, optic-cup structures were manually micro-dissected from the 6-cm plate and transferred into a 3.5-cm Petri dish (Corning, #351008) containing 2.5 mL 3:1-DMEM/F12-medium. 3:1-DMEM/F12-medium was exchanged twice per week. From day 42 onwards, 3:1-DMEM/F12-medium was supplemented with 10% (v/v) heat-inactivated FBS (Thermo Fisher Scientific, #10270-106) and 100 µM taurine (Sigma, #T0625- 25G). At week 10, the 3:1-DMEM/F12-medium was supplemented with 10 µM retinoic acid (Sigma, #R2625), and the medium was daily exchanged. At week 14, B27 supplement in the 3:1-DMEM/F12-medium was replaced with 1x N2 supplement (Gibco, #17502-48), 10% (v/v) heat-inactivated FBS (Thermo Fisher Scientific, #10270-106), 100 µM taurine (Sigma, #T0625-25G) and the retinoic acid concentration was reduced to 5 µM.

***Unguided (retinal organoid differentiation) protocol – Maintenance beyond day 28-32 in 2.5D culture*.** The differentiation protocol is identical to the "retinal organoid differentiation" section with the following modifications: On day 8, EBs within a volume of 1.5 mL were transferred on Matrigel-coated 2-well chambered coverslip. After the change to the 3:1-DMEM/F12-medium on day 16, 2.5D cultures were exclusively maintained in this media with daily media changes without any additional supplements that are typically added at later differentiation time points in the "retinal organoid differentiation".

BMP4-guided cystic compartment and microglial-like cell differentiation protocol. The differentiation protocol is identical to the "Unguided (retinal organoid differentiation) protocol – Maintenance beyond day 28-32 in 2.5D culture" section with the following differences: On day 1, 12.5 ng/mL (final concentration) of recombinant human BMP4 (Peprotech, #120-05) was added as a single shot. From D8 onwards, medium was exchanged twice per week.

Harvesting microglia-like cells after BMP4 application*.* From D40 onwards, microglia-like cells released into the supernatant were harvested. For this, the supernatant was collected and centrifuged (VWR, Mega Star 3.0R) at 200g for 4 minutes. Cells were resuspended in 3:1-DMEM/F12-medium, and transferred into 8-well chambers (IBIDI, #80826) for immunostaining.

Harvesting cystic structure after BMP4 application*.* At D18, D21, D28, D35 floating cystic structures were transferred into a new 3.5 cm petri dish (Corning, #351008) using a 1250µL wide orifice pipette tip and cultured in 2 mL 3:1-DMEM/F12-medium in parallel to not-transferred cysts, which were further cultured in the original differentiation dish until D45. The medium was exchanged twice per week until D45 when all time points were fixed as described in the result section.

Culturing 3D-retinal organoids within BMP4-guided cystic compartments*.* At D118, eight retinal organoids were transferred into a dish containing BMP4-guided cystic compartment and microglia-like cells and cultured for 10 days. The medium was exchanged to 3:1-DMEM/F12-medium supplemented with 1x N2 Supplement, 10% (v/v) heat-inactivated FBS, and 100 µM taurine (Sigma, #T0625- 25G). 3 mL medium was exchanged twice per week and 5 µM retinoic acid was added daily.

Supplementing 3D-retinal organoids with microglia-like cells*.* At D118, eight retinal organoids were transferred into a 24 well plate. Microglia-like cells were harvested as described "Harvesting microglia-like cells after BMP4 application" from two 6 cm dishes and added to the organoids once. The medium was exchanged to 3:1-DMEM/F12-medium supplemented with 1x N2 Supplement, 10% (v/v) heat-inactivated FBS, and 100 µM taurine (Sigma, #T0625- 25G). 3D-retinal organoids and microglia-like cells were cultured for 10 days. 2 mL medium was exchanged twice per week and 5 µM retinoic acid was added daily.

Functional assays for microglia-like cells

Phagocytosis bead assay*.* Microglia-like cells were generated with the BMP4-guided protocol, harvested between D40 and D50 from the culture supernatant of a 6-cm dish, and transferred into one well of an 8-well chamber (IBIDI, #80826). Microglia-like cells were cultured in 3:1-DMEM/F12-medium for 24 h. Before imaging, cells were washed once with 1x DPBS (Thermo Fisher Scientific, #14190-250) and stained with Tomato-Lectin (Szabo-Scandic, #VECDL-1174, 1:1000 in 1x DPBS) for 20 minutes at 37°C. Then, cells were washed with 1x DBPS, and L15 medium (Thermo Fisher Scientific, #21083027) was added. Images were acquired with a Zeiss

LSM880 inverted microscope and a Plan-Apochromat 20x/NA 0.8 Air objective in a temperature-controlled chamber (37°C). Z-stacked images of the 488 and 568 channel were captured simultaneously every minute. After 20 minutes baseline recording, sonicated pH-sensitive fluorescent beads (Thermo Fisher Scientific, #P35361, 1:40) diluted in L15 medium were added, and cells were imaged for the following 60 minutes. For analysis, surface renderings were generated of z-stacks of the entire image using the surface rendering function in Imaris 9.3 with the surface detail setting of 0.2 µm. Next, the intensity mean of the 568 channel was determined within the microglia-like cell created surfaces.

Real-time quantitative PCR (RT-qPCR) for inflammatory markers. Microglia-like cells were generated with the BMP4-guided protocol, harvested between D40 and D50 from the supernatant of eight 6-cm dishes, and seeded into a 24-well plate to reach a confluency of 60-80% per well. Cells were incubated overnight at 37°C, 5% CO_2. Microglia-like cells were treated with human IFN-γ (Sigma-Aldrich, #SRP3058-100UG) and IL1-β (Thermo Scientific, #RIL1BI) or both with a final concentration of 10ng/ml of each cytokine per well, with LPS (Sigma-Aldrich, #L5886-10MG) with a final concentration of 100ng/ml per well and with poly I:C (Tocris, #4287) with a final concentration of 50 µg/ml per well. Untreated controls received 3:1-DMEM/F12-medium. After 6h of incubation (37°C, 5% CO_2), RNA was isolated with innuPREP RNA Mini Kit 2.0 (Analytik-Jena, #845-KS-2040050) as described in the manufacturer's instructions. cDNA synthesis was performed with LunaScript RT SuperMix Kit (New England Biolabs, #E3010L) with a total RNA amount of 200-800ng (same amount for each condition within experimental repetition) and stored at -20°C. RT-qPCR was performed according to (Schulz et al. 2021). For data visualization, ddCq values from log2-scale were calculated to describe fold changes between the treated and untreated group.

Real-time quantitative PCR (RT-qPCR) for microglia markers. Microglia-like cells were harvested between D40 and D50 and cDNA synthesis was performed as described under "*Real-time quantitative PCR (RT-qPCR) for inflammatory markers*" with following adaptations: RNA was isolated 24h after microglia-like cells were seeded. PCR was performed using the following primers. IBA1: FW 5'-3': CAGGGATTTACAGGGAGGAA, REV 5'-3': CTCTTTGAAGCCTTCCAGTTTG. CX3CR1: FW 5'-3': GGCAGACTTGGATTTCAGGA, REV 5'-3': GCCTCAGCCAAATCATCGTA. P2RY12: FW 5'-3' AATACCAGATGCCACTCTGC, REV 5'-3': GCTTGCATTTCTTGTTGGTTAC. PU1: FW 5'-3': GTATTACCCCTATCTCAGCAGTG, REV 5'-3': AGCTCCGTGAAGTTGTTCTC.

***Ca^{2+} imaging*.** Microglia-like cells were generated with the BMP4-guided protocol, harvested between D40 and D50 from the supernatant of two 6-cm dishes, and were transferred into two wells of an 8-well chamber. Microglia-like cells were cultured in 3:1-DMEM/F12-medium for 24 h. Cells were labeled with Fluo-4 (Invitrogen, F10471; reconstituted at 1X in supplied buffer) for 30 minutes at 37°C and 5% CO2. Afterwards, cells were further incubated at room temperature (light-protected) and atmospheric CO_2 for another 30 minutes. Labeling solution was aspirated and L15 medium was added. Single-plane 16-bit images were acquired with a frame rate of 500 ms for a total duration of 360 seconds with LSM880 inverted microscope and a 20x air objective. After 180 seconds of baseline recording, 1 mM ATP (final concentration) or L15 medium was applied. Fluorescent intensity levels of Ca^{2+} events occurring in $IBA1^{+}$-cells were recorded for the following 180 seconds minutes. The data was visualized by normalizing the intensity of each cell to its average intensity throughout the entire 360 seconds recording. Ca^{2+} events were detected with the software PeakCaller (Artimovich et al. 2017) as described in (Schulz et al. 2021).

Histology

Histology - human brain samples. After PFA fixation, the samples were washed with PBS at least for 15 minutes three times. The samples were embedded in 3% (w/v) agarose (Sigma, #A9539) and sliced with a vibratome (Leica VT 1200) at a thickness of 100 µm. The vibratome slices were then cryoprotected with 30% (w/v) sucrose (Sigma, #84097, sterile filtered) until they sunk in the solution. The samples were stored at -80ºC until further use.

Fixation of 3D-retinal organoids/cystic structures (=aggregates). Aggregates were fixed in 4% (w/v) PFA in PBS for 20 minutes at room temperature, then washed three times with PBS at room temperature and cryopreserved in 30% (w/v) sucrose in PBS overnight at 4 ºC.

***Cryostat sectioning*.** Cryopreserved aggregates were transferred to a cryomold (PolyScience, #18985) using a 1250µL wide orifice pipette tip and embedded in Tissue-Tek O.C.T. compound (TTEK, A. Hartenstein) on dry ice. Samples were stored at -80ºC until further use. Cryosections (20-30 µm) of aggregates were generated using a cryostat (MICROM, NX70 CRYOSTAR, Thermo Scientific). Sections were mounted onto Superfrost Plus glass slides (Lactan, #H867.1), dried at room temperature overnight and stored at -80ºC until further use. For immunostaining, slides were dried for 1 h at room temperature. Sections on glass slices were encircled with an engraving, hydrophobic pen (Sigma-Aldrich, #Z225568).

Immunostaining of cryostat sections. Cryostat sections were incubated in "blocking solution" containing 1% (w/v) bovine serum albumin (Sigma, #A9418), 5% (v/v) Triton X-100 (Sigma, #T8787), 0.5% (w/v) sodium azide (VWR, #786-299), and 10% (v/v) serum (either goat, Millipore, #S26, or donkey, Millipore, #S30) for two hours in a humidified chamber protected from light at room temperature. Afterwards, the samples were immunostained with primary antibodies diluted in antibody solution containing 1% (w/v) bovine serum albumin, 5% (v/v) triton X-100, 0.5% (v/v) sodium azide, 3% (v/v) goat or donkey serum, and incubated overnight in a humidified chamber at room temperature. For the list of primary antibodies: **Table 4**. The sections were washed three times with PBS and incubated in a light-protected humidified chamber for 2 hours at room temperature, with the secondary antibodies diluted in antibody solution. The secondary antibodies raised in goat or donkey were purchased from Thermo Fisher Scientific (Alexa Fluor 488, Alexa Fluor 568, Alexa Fluor 647, 1:2000). The sections were washed three times with PBS. The nuclei were labeled with Hoechst 33342 (Thermo Fisher Scientific, Cat#H3570, 1:5000 diluted in PBS) for 8 minutes, and after a final two times PBS wash embedded using an antifade solution [10% (v/v) mowiol (Sigma, #81381), 26% (v/v) glycerol (Sigma, #G7757), 0.2M tris buffer pH 8, 2.5% (w/v) Dabco (Sigma, #D27802)] with microscope cover glass slips (Menzel-Glaser #0). Samples were stored at 4 ºC until imaging.

Immunostaining for human brain slices. The staining was performed as described under "Immunostaining for cryostat sections" with following adaptations: Floating brain slices were stained in a 24-well plate and the primary antibody was incubated for 48 hours on a shaker. After immunostaining, the slices were mounted on glass microscope slides (Assistant, #42406020) and embedded with antifade solution.

Table 4 – List of primary antibodies chapter 1.

Antibody	Host	Vendor	Catalogue #	Lot #	Dilution factor	RRID number
BRN3	Goat	Santa Cruz Biotechnology	sc-6026	K0215	100	AB_673441
CD31	Rabbit	Abcam	ab28364	GR3247742-26	50	AB_726362
CD45	Rabbit	Cell Signaling Technology	13917P	1	200	AB_2750898
CD163	Mouse	Bio-Rad AbD Serotec GmbH	MCA1853	157288	100	AB_2074540
CHAT	Goat	EMD Millipore	AB144P	3182642	400	AB_2079751
CRALBP	Mouse	Abcam	ab15051	GR229880-2	200	AB_2269474
CtBP2	Mouse	BD Biosciences	612044	5301880	200	AB_399431
CTIP2	Rat	Abcam	ab18465	GR3272266-5	100	AB_2064130
CX3CR1	Mouse	BioLegend	B355702	B194773	50	AB_2561726
E-Cadherin	Mouse	BD Biosciences	610182	9315423	100	AB_397581
IBA1	Rabbit	GeneTex	GTX100042	44200	750	AB_1240434
IBA1	Goat	Abcam	ab5076	GR3374909-1	250	AB_2224402
KI67	Mouse	BD Biosciences	550609	5267542	100	AB_393778
myb	Rabbit	Acris	AP31223PU-N	27931	100	AB_10976997
OTX2	Goat	R&D Sysytems	AF1979	KNO0920111	150	AB_2157172
P2RY12	Rabbit	Sigma-Aldrich	HPA014518	F119293	100	AB_2669027
PAX6	Mouse	Acris Antibodies/ EuBIO Koeck	AM50305PU-N	5080-1P160119	400	AB_2895216
PHOSPHO HISTONE H3 (PHH3)	Rabbit	Merck	06-570	3256620	300	AB_310177
PU.1	Rabbit	Cell Signaling Technology	2266S	1	500	AB_10692379
RECVN	Rabbit	EMD Millipore	AB5585	2691407	400	AB_2253622
RUNX.1	Mouse	BioLegend	659302	B276756	50	AB_2563194
VIMENTIN	Mouse	Santa Cruz Biotechnology	sc-6260	A1521	100	AB_628437

Immunostaining for whole mount aggregates. The staining was performed as described under "Immunostaining for cryostat sections" with the following adaptations: The primary antibody was incubated for 48 hours on a shaker at room temperature, and washed at least for two hours.
Immunostaining for whole mount organoids*.* The staining was performed as described under "Immunostaining for cryostat sections" with the following adaptations: Organoids were incubated in blocking solution for 2 days on a shaker at 4 ºC. The primary antibody concentration was doubled and organoids were incubated for 10 days on a shaker at 4 ºC, and washed three times in PBS at least for one day. Then the organoids were incubated with secondary antibodies (1:500) and Hoechst (1:1000) diluted in antibody solution simultaneously for 3 days on a shaker at 4ºC. After washing the organoids three times in PBS for one day, organoids were mounted with low gelling agarose followed by a glycerol gradient as described in "Immunostaining for whole mount aggregates".
Mounting of whole mount aggregates. For whole mount aggregates, the tissue was mounted on 8-well chambers (IBIDI, #80826) using 3% (w/v) low gelling temperature agarose (Sigma-Aldrich, #A9414-25G). Then a glycerol gradient was performed starting with 50% (v/v) glycerol (Sigma-Aldrich, G7757-1L) in H_2O followed by 75% (v/v) glycerol in H_2O. Afterwards, the whole mount aggregate was imaged.

Imaging

Brightfield. Differentiation was monitored with a bright-field microscope (Olympus CKX41) with 5x, 10x and 20x objectives (Olympus) and a lens marker (Nikon), and an EVOS microscope (Thermo Fisher Scientific) with 2x, 4x, 10x, 20x, 40x objectives (Thermo Fisher Scientific).
Confocal microscopy. Images were acquired with a Zeiss LSM880 Airyscan upright or inverted or with a Zeiss LSM800 upright. Ibidi plates were exclusively imaged using an inverted microscope. For overview images Plan-Apochromat 10x air objective NA 0.45 (WD=2.1mm) or Plan-Apochromat 20x Air objective NA 0.8 were used and tile-scan z-stacks were acquired. For detailed images Plan-Apochromat 40x oil immersion objective NA 1.3 was used.
Image analysis. Confocal images were converted to .ims files using the Imaris converter and imported to Imaris 9.3 (Bitplane Imaris 3/4D Image Visualization and Analysis Software).
Surface rendering were generated using the surface rendering module with the surface detail set to 0.2 µm.
Determining the volume of organoids. The Hoechst channel was processed using the normalize layer function of Imaris. Then, a surface rendering was performed and the total volume of the Hoechst channel was determined.
Determining the number of IBA1$^+$-cells. The spot function of Imaris was used to analyze the number of IBA1$^+$-cells. The estimated XY diameter was set to 15 µm.
Quantification of types of aggregates. Bright field images of aggregates were acquired and then classified into the four types as outlined in **Figure 2a** (retinal cup only, retinal cup with cerebral compartment, retinal cup with cystic compartment, cyst only). Then the percent ratio of each of the four types was determined.
Graphics. All graphics were generated using R (version 4.1.0). Excel files were loaded into R via the xlsx package (version 0.6.1) (Dragulescu 2014). Plots were made using ggplot2 (version 3.0.0) (Wickham 2016). Linear regression was performed using the lme4 package (version 1.1-17) (Bates et al. 2015).

Mass spectrometry

10 cystic structures were harvested at D28 and D45, washed once in DPBS (Thermo Fisher Scientific, # 14190-250) and snap frozen in liquid nitrogen. Samples were stored at -80°C until further analysis. For Liquid chromatography - mass spectrometry (LCMS) analysis, pelleted cystic structures were denatured, reduced, alkylated with iodoacetamide and trypsin-digested into peptides using a commercial in-Stage Tips kit (P.O.00001, Preomics), following exactly the manufacturer's instructions. Cleaned-up, reconstituted peptides were then analyzed by Liquid chromatography – tandem mass spectrometry (LC-MS/MS) on an Ultimate High-performance liquid chromatography (HPLC) (ThermoFisher Scientific) coupled to a Q-Exactive HF (ThermoFisher Scientific). Each sample was concentrated over an Acclaim PepMap C18 pre-column (5 µm particle size, 0.3 mm ID x 5 mm length, ThermoFisher Scientific) then bound to a 50 cm EasySpray C18 analytical column (2 µm particle size, 75 µm ID x 500 mm length, ThermoFisher Scientific) and eluted over the following 180 min gradient: solvent A, water + 0.1% formic acid; solvent B, 80% acetonitrile in water + 0.08% formic acid; constant 300 nL/min flow; B percentage: start, 2%; 155 min, 31%; 180 min, 44%. Mass spectra were acquired in positive mode with a Data Dependent Acquisition method: FWHM 20s, lock mass 445.12003 m/z; MS1: profile mode, 120,000 resolving power, AGC target 3e6, 50 ms maximum IT, 380 to 1,500 m/z; MS2: top 20, centroid mode, 1.4 m/z isolation window (no offset), 1 microscan, 15,000 resolving power, AGC target 1e5 (minimum 1e3), 20 ms maximum IT, 200 to 2,000 m/z scan range, NCE 28, excluding charges 1 and 8 or higher, 60s dynamic exclusion.

Raw files were searched in MaxQuant 1.6.5.0 against the reference *Homo sapiens* proteome downloaded from UniProtKB. Fixed cysteine modification was set to Carbamidomethyl. Variable modifications were Oxidation (M), Acetyl (Protein N-term), Deamidation (NQ), Gln->pyro-Glu and Phospho (STY). Match between runs, dependent peptides and second peptides were active. All FDRs were set to 1%.

Tissue enrichment analysis. To determine human tissues that resemble the highly expressed protein profile in the cystic structure, we performed a tissue enrichment analysis similar to previous approaches (Angeles-Albores et al. 2016; Jain and Tuteja 2019). Proteins specific to a given tissue (or *tissue-specific proteins*) were downloaded from the Human Protein Atlas (HPA, http://www.proteinatlas.org) (Uhlén et al. 2015) which has curated the expression profiles of human genes both on the mRNA and protein level in 44 normal human tissue types (corresponding to 62 tissue samples). In particular, tissue-specific proteins were defined as proteins that were highly detected, i.e., a strong immunohistochemical staining intensity in 25-75% of cells as annotated in HPA. Cystic-specific proteins in either D28 or D45, on the other hand, were obtained by taking proteins whose expressions are within the 98^{th} percentile of the protein expression distribution in the mass spectroscopy data. The overlap between the 3D-cyst specific proteins and the tissue-specific proteins were calculated and the hypergeometric test was used to calculate the enrichment of this overlap as

$$P(X \geq k) = \sum_{i \geq k} \frac{\binom{M}{i}\binom{N-M}{n-i}}{\binom{N}{n}} P(X \geq k) = \sum_{i \geq k} \frac{\binom{M}{i}\binom{N-M}{n-i}}{\binom{N}{n}} P(X \geq k) = \sum_{i \geq k} \frac{\binom{M}{i}\binom{N-M}{n-i}}{\binom{N}{n}}$$
$$P(X \geq k) = \sum_{i \geq k} \frac{\binom{M}{i}\binom{N-M}{n-i}}{\binom{N}{n}} P(X \geq k) = \sum_{i \geq k} \frac{\binom{M}{i}\binom{N-M}{n-i}}{\binom{N}{n}} P(X \geq k) = \sum_{i \geq k} \frac{\binom{M}{i}\binom{N-M}{n-i}}{\binom{N}{n}}$$

with *n* as the number of 3D-cyst specific proteins from the *N* total number of detected proteins with mass spectrometry, *M* as the number of tissue-specific proteins and *k* is the size of their overlap. The obtained *p*-values were Bonferroni-corrected for multiple comparisons implemented through the multitest function of statsmodels (Seabold and Perktold 2010). For the peptide sequence data please refer to *Supplementary Table 1* published in (Bartalska et al., 2022). A similar analysis was conducted for proteins found in previous mass spectrometry analyses of human iris, ciliary body, RPE/choroid (Zhang, Kirby, et al., 2016), optic nerve, sclera (Zhang, Karani, et al., 2016), retina (Zhang et al., 2015) and meninges (Dunn et al. 2019). Tissue-specific protein profiles were defined as the proteins that are present in the 80th percentile of the protein expression distribution. Tissue-specific proteins that are in at most two tissues were discarded to account for possible non-specific expression. Note that while the tissue enrichment p-values change with the percentile cut-off, the qualitative results remain the same. For the peptide sequence data please refer to *Supplementary Table 4* published in (Bartalska et al., 2022).

Heatmap of mesenchymal stem cell markers. The list of markers of epithelial and mesenchymal markers was obtained from (Andrzejewska et al. 2019; Owusu-Akyaw et al. 2019; Scanlon et al. 2013). Protein expression in 3D cysts for these markers was plotted as a heatmap for week 4 and 7. Fold-change was determined by dividing the intensity at D45 with the intensity at D28. Upregulated proteins are those with fold-change greater than or equal to 2.0 while downregulated proteins are those with fold-change less than or equal to 0.5. For the raw data refer to *Supplementary Table 2-3* published in (Bartalska et al., 2022).

Statistical analysis

All statistical tests were performed using R. Models were generated by changing the default contrast for unordered variables to “contr.sum” to apply type III ANOVA to the model to evaluate the overall contribution of the response variable. Post-hoc tests were performed via the “dplyr” package (version 1.0.7) (Wickham et al. 2021) and the “multcomp” package and were corrected for multiple testing using the single-step method (Hothorn et al. 2008). Pearson correlation was performed using the “ggpubr” package (version 0.4.0) (Kassambara 2017).

Inflammation assay. A one-sample t-test was performed to compare the stimulated condition with its untreated control (**Figure 18**).

3D cyst occupation and isolation. We performed a Pearson correlation test to the correlation between IBA1^{+}-cell density and age of differentiation (**Figure 20b**, **d**).

Co-expression of IBA and CD163. We performed two-way ANOVA to examine changes in expression over time by using an interaction of these two predictors. A random effect (cyst ID) was included to account for the dependency of the data which results from repeated counting of the same sections. As a significant effect ($p < 0.05$) was observed for the interaction we performed a post-hoc analysis for pair-wise comparison using the Tukey-Test and p-values were adjusted using the method set to “BH” (**Figure 23b**).

Integration of IBA1^{+}-cells into 3D-retinal organoids. A Shapiro-Wilk test determined that the data was not normally distributed. Therefore, we performed a Wilcoxon-test to test differences between experimental conditions (**Figure 29b**).

Repetition. All experiments were performed by at least two experimentalists independently for both cell lines with exceptions of the mass spectrometry (**Figure 22-23**) and (**Figure 28-29**). In total, we performed for the hIPSC lines SC102A 18x and CR05 10x retinal organoid differentiations and for SC102A 10x and CR05 8x BMP4-guided differentiation.

2.3. Results

IBA1^{+}-microglia-like cells appear in the unguided protocol.

To identify whether 3D-retinal organoids contain microglia-like cells, we applied an established unguided retinal organoid differentiation protocol (Zhong et al. 2014) to two hIPSC lines of different origins (**Figure 5a-b**) One hIPSC line was derived from a 60^{+}-old skin fibroblast donor (SC102A) and the other from fetal umbilical cord blood cells (CR05, **Table 3**). Both hIPSC lines behaved similarly and formed typical optic cup structures within four weeks in 2.5D culture. They developed further into anatomically comparable 3D-retinal cups (**Figure 5c**) expressing cell type-specific markers for photoreceptor-, bipolar-, amacrine-, ganglion and Müller glial cells by week 18 (**Figure 5d**) (Hoshino et al. 2017; Luo et al. 2019; Zhang et al. 2019).

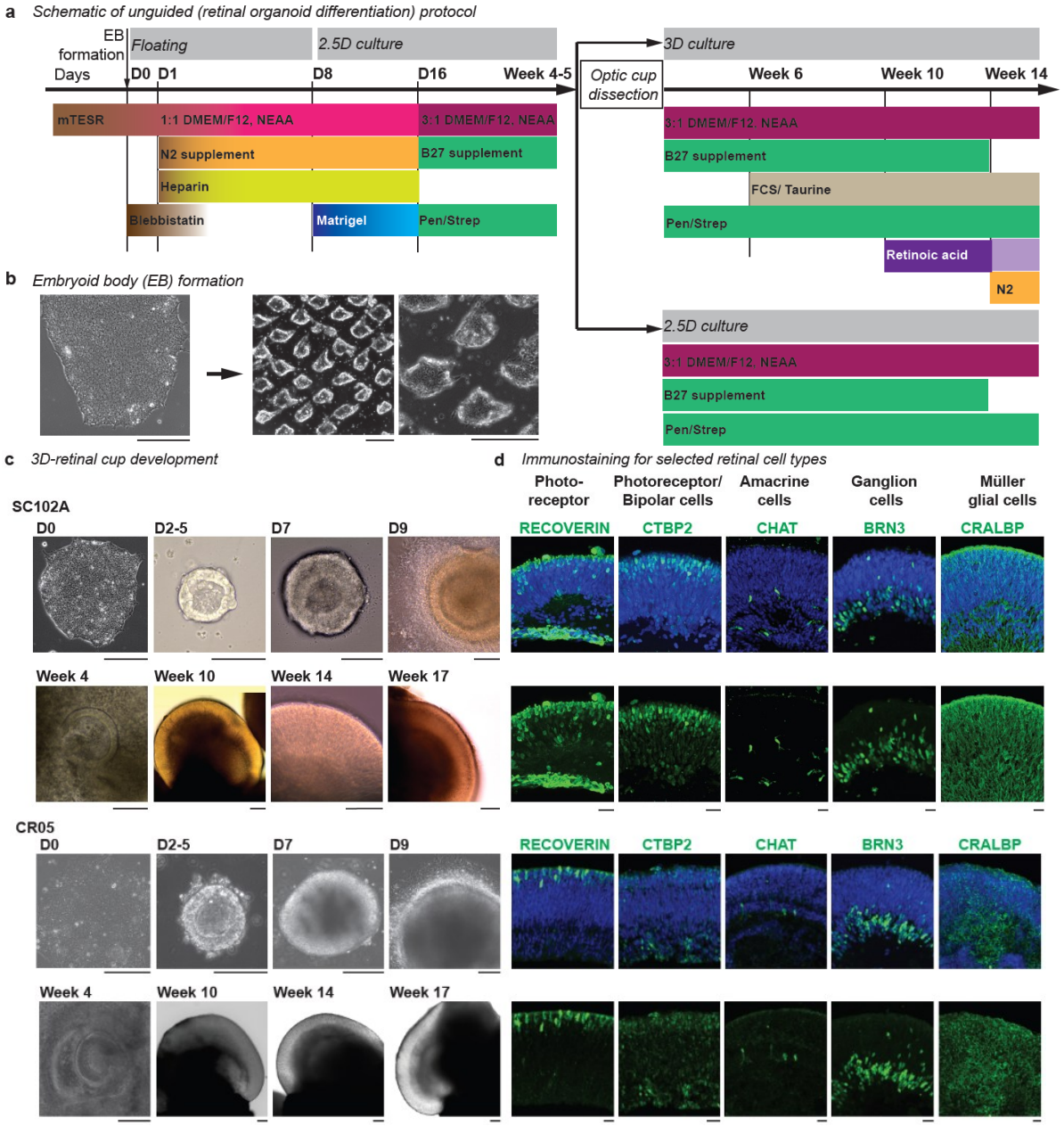

Figure 5 – Figure legend on next page.

Figure 5 – Differentiation of hIPSC lines SC102A and CR05 into 3D-retinal organoids.
a-b, Schematic of unguided (retinal organoid differentiation) protocol for 2.5D and 3D culture. After reaching 80% confluency, human induced pluripotent stem cells (hIPSC) were cut into evenly sized aggregates to form embryoid bodies (EBs) (b, Scale bar: 100 µm). EBs were cultured in suspension and were seeded on D8 on Matrigel-coated plates. At D30-32, optic-cup structures were manually micro-dissected and cultured in suspension. D, days after induced differentiation. FCS, fetal calf serum. NEAA, Non-Essential Amino Acid. Pen/Strep, penicillin and streptomycin. **c**, Brightfield images at selected days and weeks after induced differentiation (D) for SC102A (top) and CR05 (bottom). Scale bar: 100 µm. **d**, Immunostaining of cryostat sections for selected retinal cell type marker (green) and the nuclear dye Hoechst (blue) with focus on the retinal-cup for SC102A (top) and CR05 (bottom) between week 18-20 with exception of BRN3 for SC102A at week 9. CTBP2, C-Terminal-Binding Protein 2. CHAT, choline acetyltransferase. BRN3, brain-specific Homeobox/POU Domain Protein 3. CRALBP, cellular retinaldehyde-binding protein. Scale bar: 20 µm.

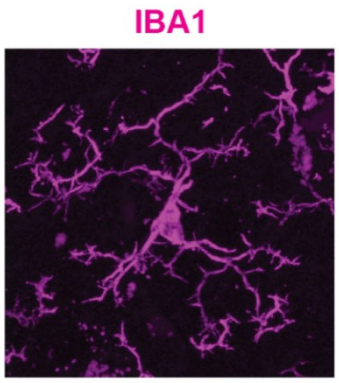

We used IBA1 as a marker for microglia and confirmed the antibody functionality in human temporal lobe brain tissue, where IBA1 labeled parenchymal microglia and pvMΦ (**Figure 6**).

Figure 6 – Validation of antibody specificity in human brain tissue.
Vibratome sections of adult human temporal lobe immunostained for IBA1 (ionized calcium-binding adapter molecule 1, magenta). Scale bar: 20 µm.

When we immunostained our 3D-retinal organoids, we commonly observed no cell-defined IBA1 staining (**Figure 7a**). Occasionally, we found a few IBA1^{+}-cells close to the retinal cup (**Figure 7b**) but the cells were not numerous or as deeply integrated as described for the human embryo retina at similar age (Diaz-Araya et al. 1995).

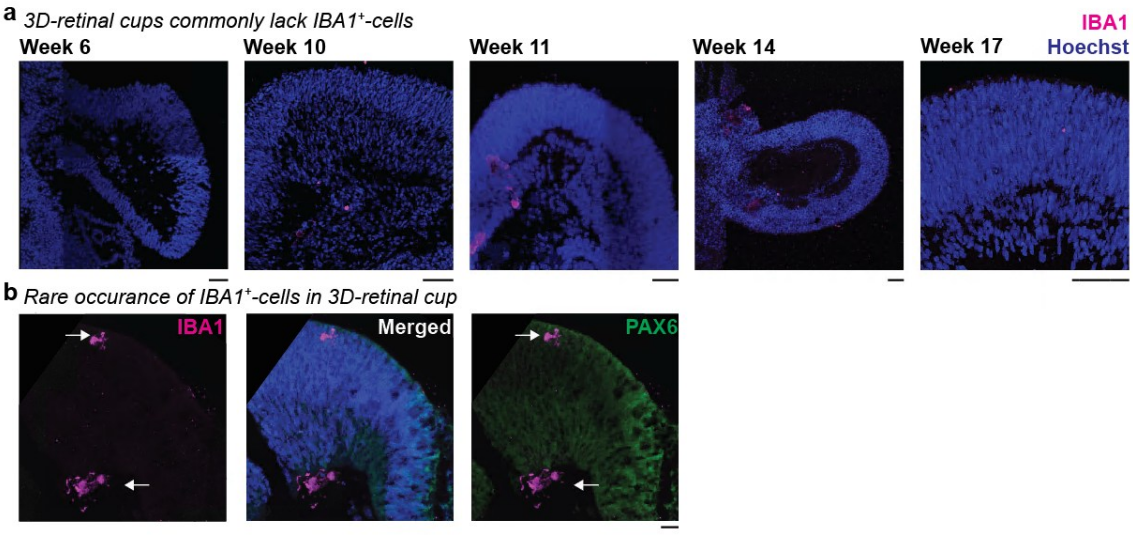

Figure 7 – Retinal cups widely lack IBA1^{+}-microglia.
a-b, Immunostaining cryostat section of 3D-retinal organoids with focus on retinal cups for SC102A for IBA1 (ionized calcium-binding adapter molecule 1, magenta) with Hoechst to highlight nuclei (blue) **a**, at week 6, 10, 11, 14, and 17. Note: IBA1 staining occasionally occurred as a layered or dotted structure, which did not resolve in distinct cell morphologies. We excluded such staining patterns from further interpretations. Scale bar: 50 µm. **b**, at week 9 with focus on retinal cup stained with PAX6 (Paired Box 6, green). White arrow, examples of overlap. Scale bar: 20 µm.

Based on this rare microglia presence, we hypothesized that IBA1^{+}-cells might be enriched in a compartment other than the retinal cup. Thus, we revisited the 2.5D culture prior to dissection of optic cups at week 4 (**Figure 5a**). Between week 3 and 4, we found clusters of IBA1^{+}-cells (**Figure 8a**), which started to spread within the culture by week 4 and occupy distinct compartments by week 7 (**Figure 4b**). These compartments were commonly less nuclei-dense (**Figure 8c**). To investigate whether these compartments contained cortical cell types, we stained the 2.5D culture with CTIP2/BCL11b (BAF chromatin remodeling complex subunit), a marker expressed in the neocortex from early embryonic stages (Qian et al. 2016). Remarkably, the majority of IBA1^{+}-cells were distinct from the CTIP2^{+}-region (**Figure 8d**), and if they were present, they mostly localized to the surface of these structures.

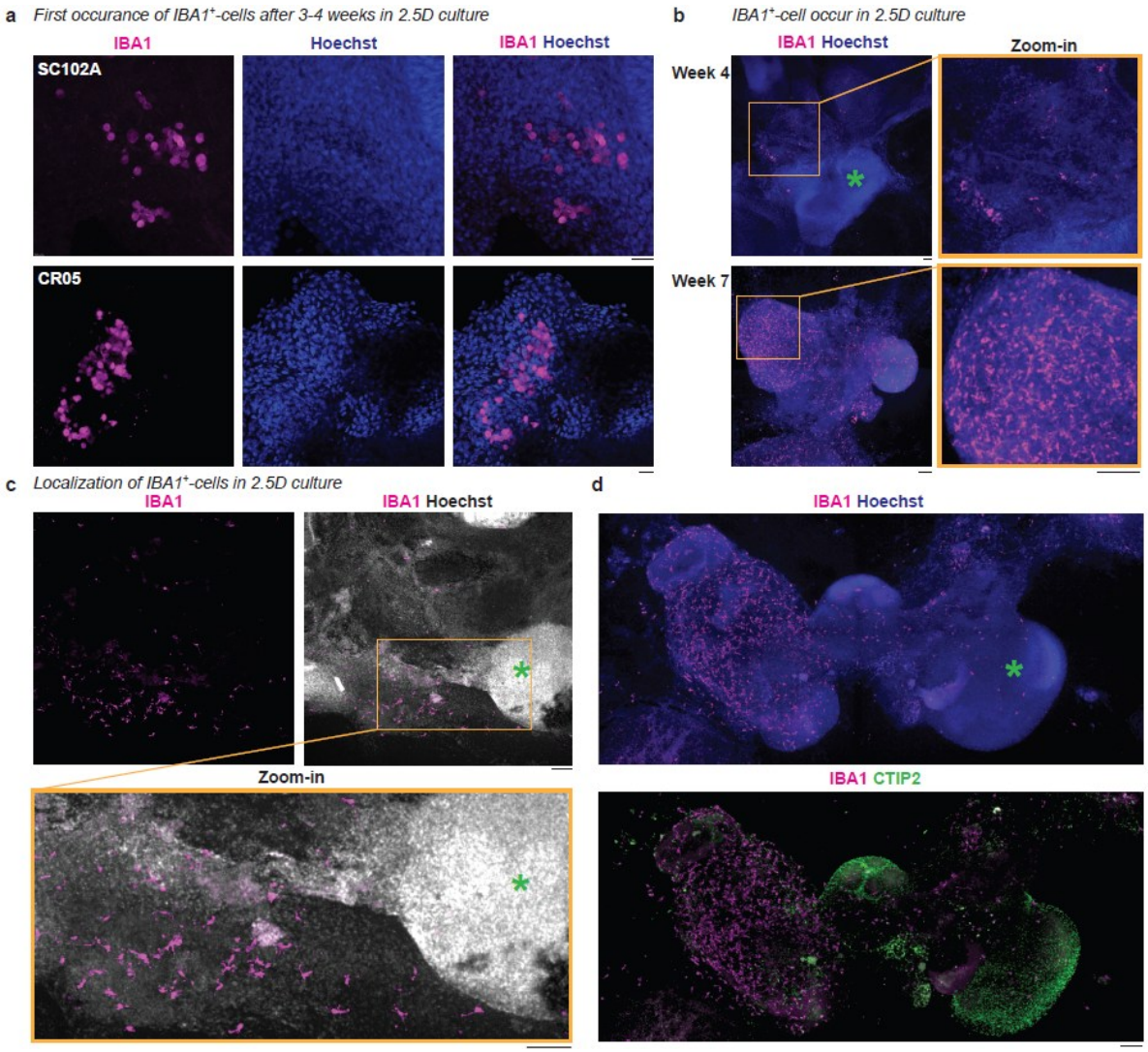

Figure 8 – IBA1$^+$-microglia-like cells develop during retinal organoid differentiation.
a-d, Immunostaining for IBA1 (ionized calcium-binding adapter molecule 1, magenta) with Hoechst to highlight nuclei (blue, except white in e) of 2.5D culture. **a**, First occurrence of IBA1$^+$-cells in SC102A (top) and CR05 (bottom) between week 3 and 4. Scale bar: 20 µm. **b**, SC102A at week 4 (top) and 7 (bottom). Scale bar: 100 µm. **c**, SC102A at week 9. Scale bar: 100 µm. **d**, SC102A at week 7. Green *, cell-dense area. Immunostaining for CTIP2 (COUP-TF-Interacting-Protein 2, green). Scale bar: 150 µm.

To confirm that IBA1$^+$-cells were microglia-like, we immunostained the 2.5D cultures between week 4 and 5 for the hematopoietic lineage-specific markers RUNX1 (Ginhoux et al. 2010), PU.1 (Kierdorf et al., 2013), and MYB (Schulz et al. 2012). As expected, all IBA1$^+$-cells were positive for RUNX1 and PU.1 and negative for MYB (**Figure 9a-c**). The IBA1$^+$-cells also expressed the mononucleate hematopoietic cell marker CD45 (Monier et al. 2007) (**Figure 9d**), the fractalkine receptor CX3CR1 (Hulshof et al. 2003) (**Figure 9e**), the purinergic receptor P2Y12 (Mildner et al. 2017) (**Figure 9f**) and did not express the monocytic marker CD14 (Geissmann, Jung, and Littman 2003) (**Figure 9g).**

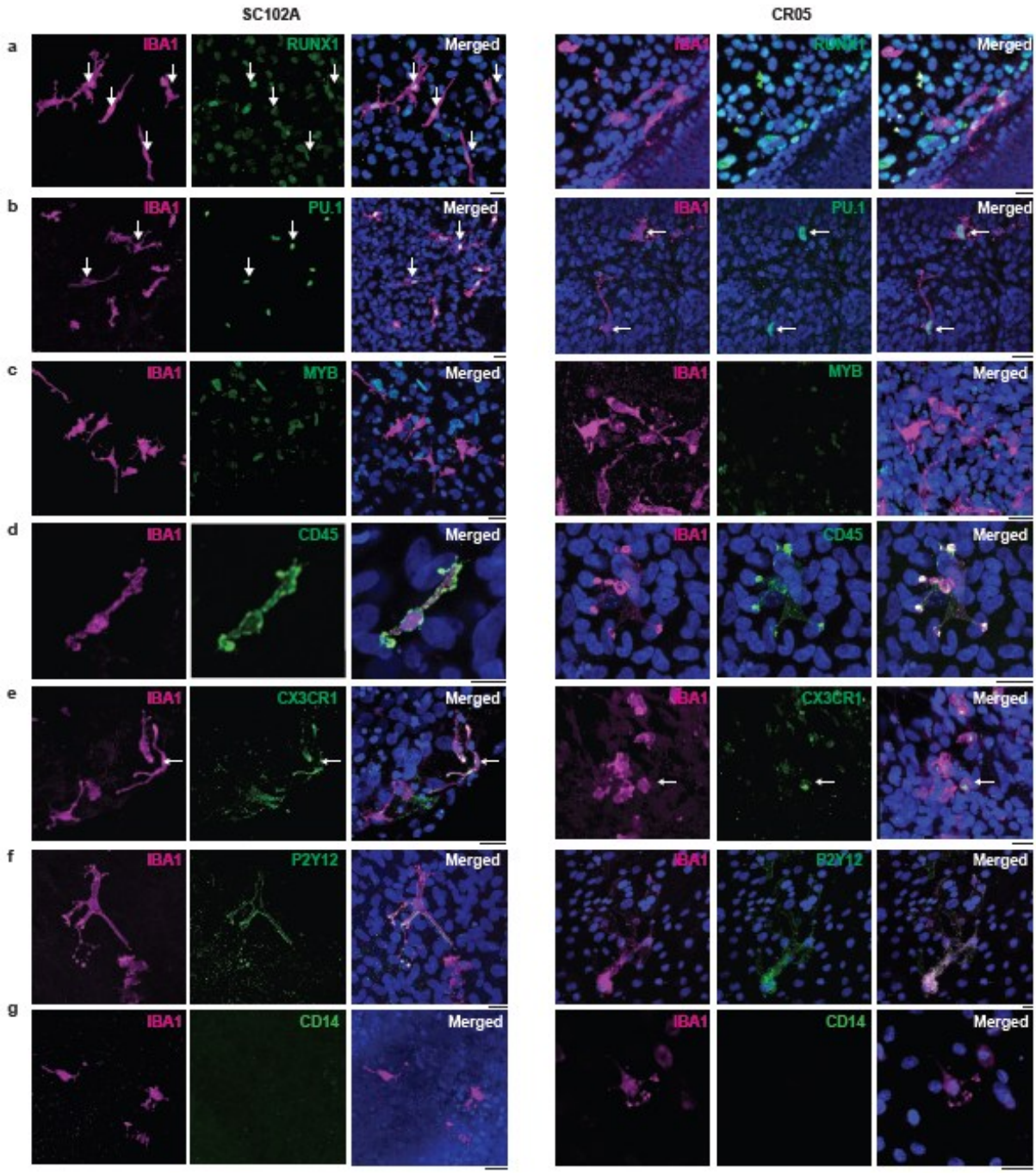

Figure 9 – Marker expression of IBA1^{+}-microglia-like cells.
Immunostaining for IBA1 (ionized calcium-binding adapter molecule 1, magenta) with Hoechst to highlight nuclei (blue) and the macrophage/ microglia marker **(**green) in SC102A (left) and CR05 (right) at week 4-5 in 2.5D culture: **a**, RUNX1 (runt-related transcription factor 1). **b**, PU.1 (hematopoietic transcription factor PU.1) in CR05. **c**, MYB (MYB Proto-Oncogene). **d**, CD45 (cluster of differentiation 45/ protein tyrosine phosphatase receptor). **e**, CX3CR1 (C-X3-C motif chemokine receptor 1). **f**, P2RY12 (purinergic receptor P2Y G-protein-coupled 12). **g**, CD14 (cluster of differentiation 14/ monocyte differentiation antigen CD14). Scale bar: 20 µm.

Importantly, all markers were cross-validated for their specificity in human brain tissue (**Figure 10**).

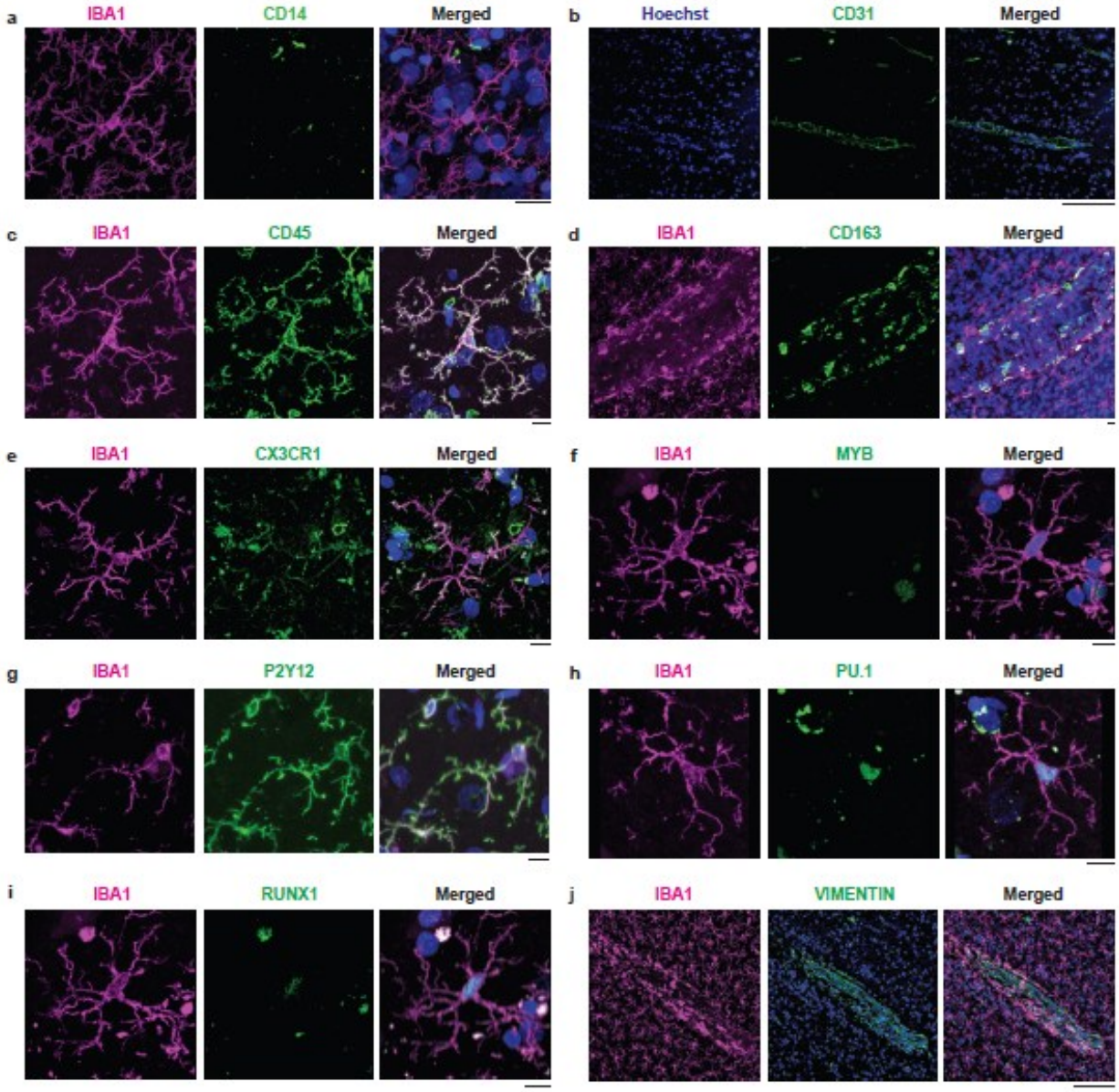

Figure 10 – Validation of antibody specificity in human brain tissue.
Vibratome sections of adult human temporal lobe immunostained for IBA1 (ionized calcium-binding adapter molecule 1, magenta), nuclei dye Hoechst (blue), and antibodies used throughout this study (green): **a**, CD14, cluster of differentiation 14/ monocyte differentiation antigen CD14. **b**, CD31, platelet endothelial cell adhesion molecule (PECAM-1). **c**, CD45, cluster of differentiation 45/ protein tyrosine phosphatase receptor. **d**, CD163, cluster of differentiation 163/ scavenger receptor cysteine-rich type 1 protein M130. **e**, CX3CR1, Chemokine (C-X3-C) Receptor 1. **f**, MYB, MYB Proto-Oncogene. **g**, P2Y12, Purinergic receptor P2Y G-protein-coupled 12. **h**, PU.1, Hematopoietic transcription factor PU.1. **i**, RUNX1, Runt-related transcription factor 1. **j**, VIMENTIN. Scale bar: 20 µm.

The IBA1^{+}-cells were morphologically branched and frequently presented phagocytic cups (**Figure 11a**). 47.9 % +/- 5.7 % of the IBA1^{+}-cells co-expressed KI67 indicating that they are in a proliferative state (Gerdes et al. 1984) (**Figure 11b**). The cells also expressed the mitotic marker

phosphorylated histone H3 (PHH3) (Hirata et al. 2004) (**Figure 11c**). This characterization suggests that IBA1$^+$-cells represent microglia-like cells that emerge within the unguided protocol in 2.5D culture by week 4 and, notably, do not extensively populate retinal cups or cerebral compartments.

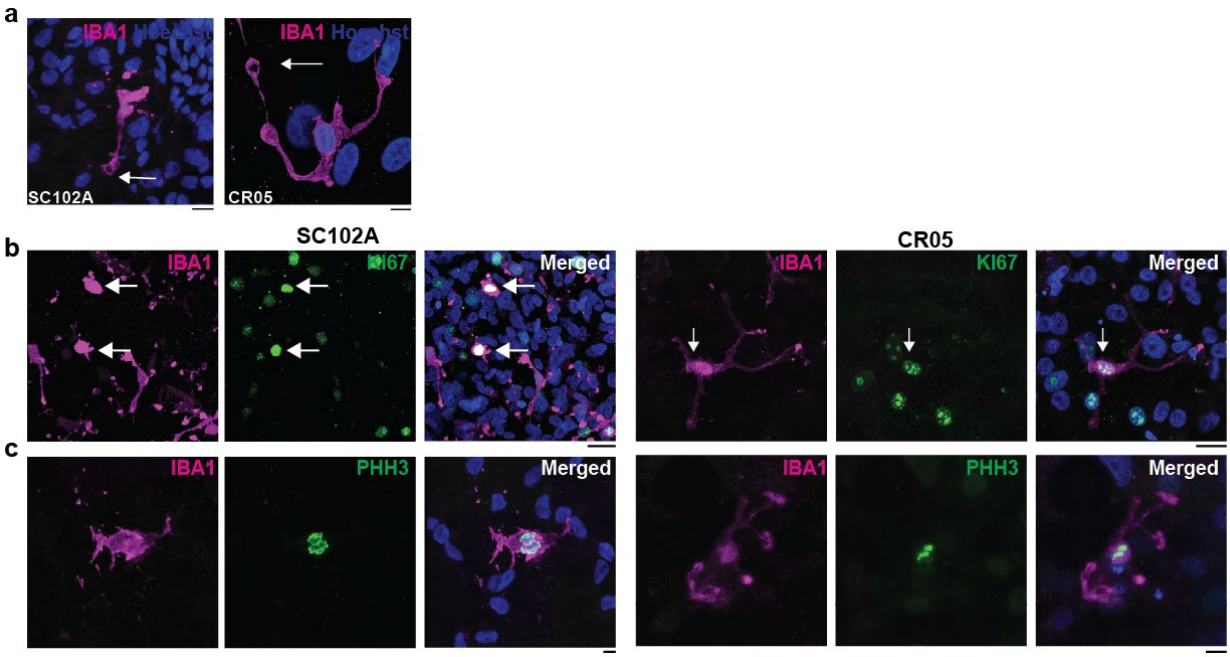

Figure 11 – Characterization of IBA1$^+$-microglia-like cells.
Immunostaining for IBA1 (ionized calcium-binding adapter molecule 1, magenta) and the nuclei dye Hoechst (blue) in 2.5D culture. **a**, Examples of IBA1+-cell forming phagocytic cups (arrow) in aggregates from SC102A (left) and CR05 (right) at week 8. Scale bar: 10 µm. **b-c**, Proliferation marker between in 2.5D cultures from SC102A (left) and CR05 (right) at week 8-10 in green: KI67 (**b**) PHH3 (phosphohistone H3, **c**). White arrow indicates overlap. Scale bar: 20 µm.

IBA1$^+$-cells enrich in cystic compartments of 3D-aggregates

The presence of IBA1$^+$-cells in less nuclear-dense structures in 2.5D culture inspired us to revisit our 3D culture. We found that the unguided protocol results in two groups of aggregates: either with or without retinal cups (**Figure 12a**). The aggregates with retinal cups, summarized as 3D-retinal organoids, can represent either a retinal cup only (**Figure 12a**, i), a retinal cup with a cerebral compartment (**Figure 12a**, ii) that can be characterized with OTX2 (Orthodenticle Homeobox 2) and CTIP2 (**Figure 12b**), respectively (Hoshino et al. 2017; Qian et al. 2016), or a retinal cup with cystic compartment (**Figure 12a**, iii). We named an aggregate without a retinal cup a 3D-cyst (**Figure 12a**, iv). These cysts were semi-transparent, contained various-sized lumens, and occasionally developed pigmentation or a cuboidal-shaped epithelial surface. We found approximately 10% of the aggregates to be non-retinal (**Figure 12c**), which is in line with previously reported studies (Cowan et al. 2020; Zhong et al. 2014). IBA1$^+$-cells enriched and distributed in the 3D-cysts (**Figure 12d**) and the cystic compartment of retinal organoids (**Figure 12e**). Cystic compartments that were pigmented tended to lack IBA1$^+$-cells (**Figure 12f**). This suggests that IBA1$^+$-cells occurring with the unguided protocol preferentially occupy non-pigmented cystic compartments.

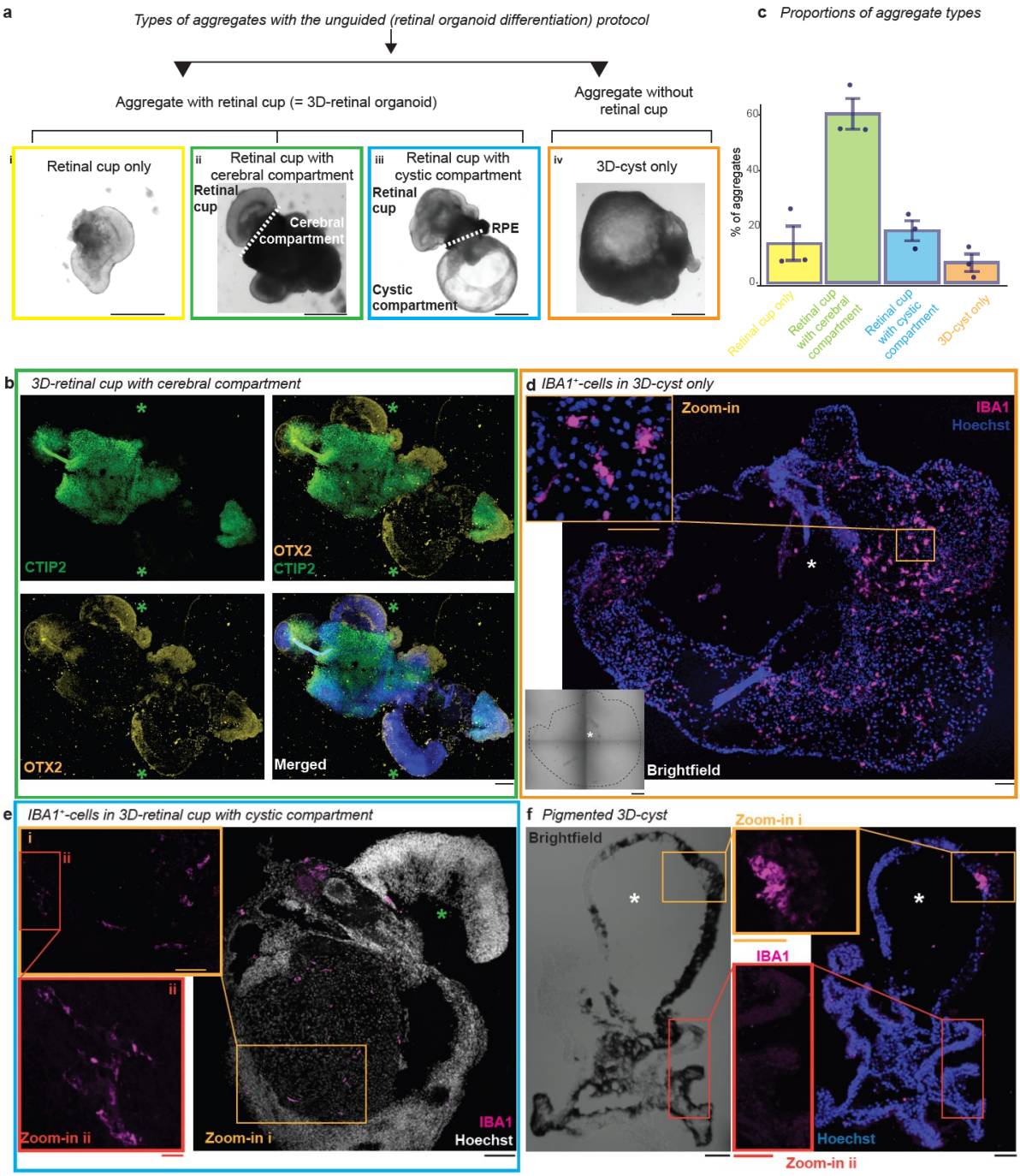

Figure 12 – Figure legend on next page.

Figure 12 – IBA1^{+}-cells occupy 3D-cystic compartments.
a, Representative bright field images of typical aggregates generated within unguided (retinal organoid differentiation) protocol at week 5 for SC102A. RPE: retinal pigment epithelium. Scale bar: 1000 µm. **b**, Immunostaining of cryostat section of 3D-retinal cup with cerebral compartment (week 8-9) from SC102A stained for OTX2 (orthodenticle homeobox 2, orange) and CTIP2 (COUP-TF-Interacting-Protein 2, green) and nuclei stained with Hoechst (blue). Green *, retinal cup. Scale bar: 150 µm. **c**, Mean percentage of aggregate type proportions with standard error of the mean. Each dot represents one differentiation. **d-f**, Immunostaining of cryostat sections for IBA1 (ionized calcium-binding adapter molecule 1, magenta), nuclei stained with Hoechst (blue, except e in white). **d**, 3D-cyst from SC102A (week 8-9) with brightfield image. Dashed-line, cyst surrounding. White *, cystic lumen. Scale bar: 100 µm. Zoom-in to IBA1^{+}-cells. Scale bar: 50 µm. **e**, 3D-retinal organoid with cystic compartment for SC102A (9-10 weeks). Scale bar: 100 µm. Zoom-in: Scale bar: 50 µm (i), 10 µm (ii). **f**, Pigmented 3D-cyst (week 8-9) from SC102A with bright field image. White *, cystic lumen. Scale bar: 100 µm, zoom-in: 50 µm.

Low dosed BMP4 application enhances 3D-cysts and IBA1^{+}-cells

Recent hIPSC-derived microglia-like protocols have reported that bone morphogenetic protein 4 (BMP4) promotes microglia generation *in vitro* (Abud et al. 2017; Douvaras et al. 2017; Guttikonda et al. 2021; Haenseler et al. 2017; Pandya et al. 2017; Takata et al. 2017) with some studies mentioning the development of cystic structures (Abud et al. 2017; Haenseler et al. 2017). Since we sought insight into the tissue identity of the IBA1^{+}-cell enriched cystic compartments and we were confronted with the heterogeneity of our unguided protocol culture, we decided to enrich for the cystic compartments with a low-dosed BMP4 application one day after EB formation to the otherwise unchanged protocol (**Figure 13a**). After BMP4 exposure, EBs formed an irregular shape and developed non-pigmented 3D-cysts that started to float by week 3 (**Figure 13b**). These 3D-cysts were the only aggregates formed by the BMP4-guided protocol in both hIPSC lines (**Figure 13c**).

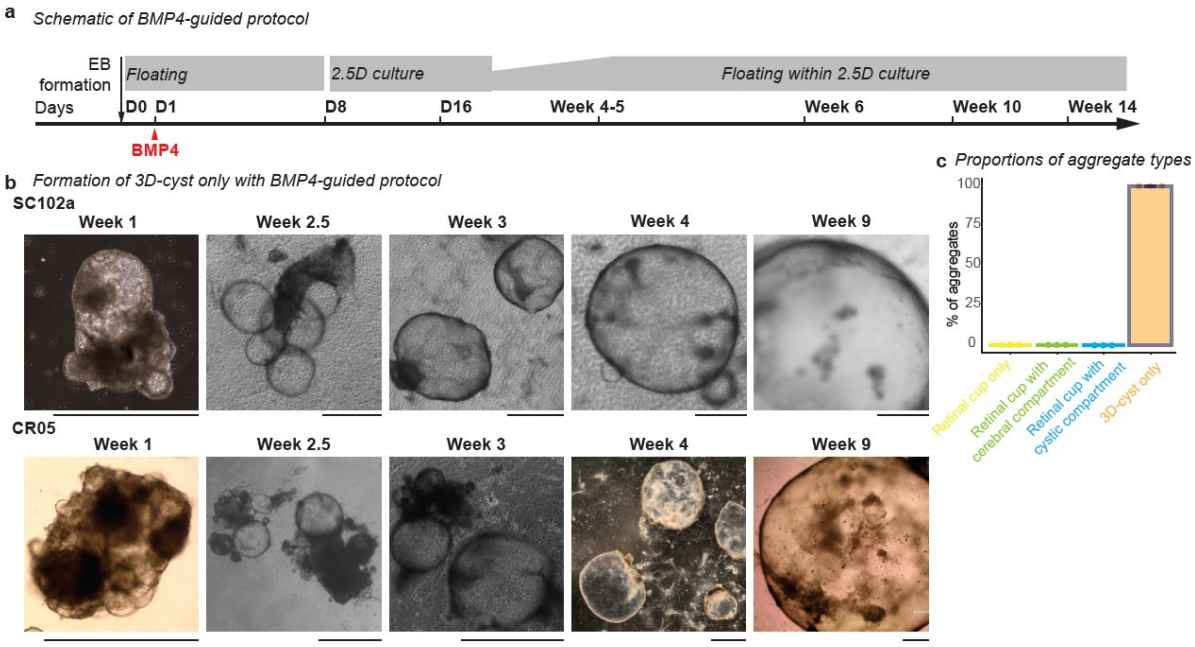

Figure 13 – Figure legend on next page.

Figure 13 – BMP4 induces 3D-cyst development.
a, Schematic of guided differentiation protocol with a single BMP4 (bone morphogenetic protein 4) application on Day (D) 1 after induced differentiation. EB, embryoid bodies. **b**, Brightfield images of developing 3D-cysts generated with BMP4-guided differentiation for SC102A (top) and CR05 (bottom). Scale bar: 1000 µm. **c**, Mean percentage of aggregate type proportions generated using BMP4-guided protocol with standard error. Each dot represents one differentiation.

They neither expressed Recoverin nor BRN3 for labeling photoreceptors and retinal ganglion cells, respectively (**Figure 14a-b**) nor the neuronal marker beta-III-tubulin (**Figure 14c**). OTX2 was expressed by week 9 but did not show an overlap with recoverin, both labeling photoreceptors (**Figure 14a**).

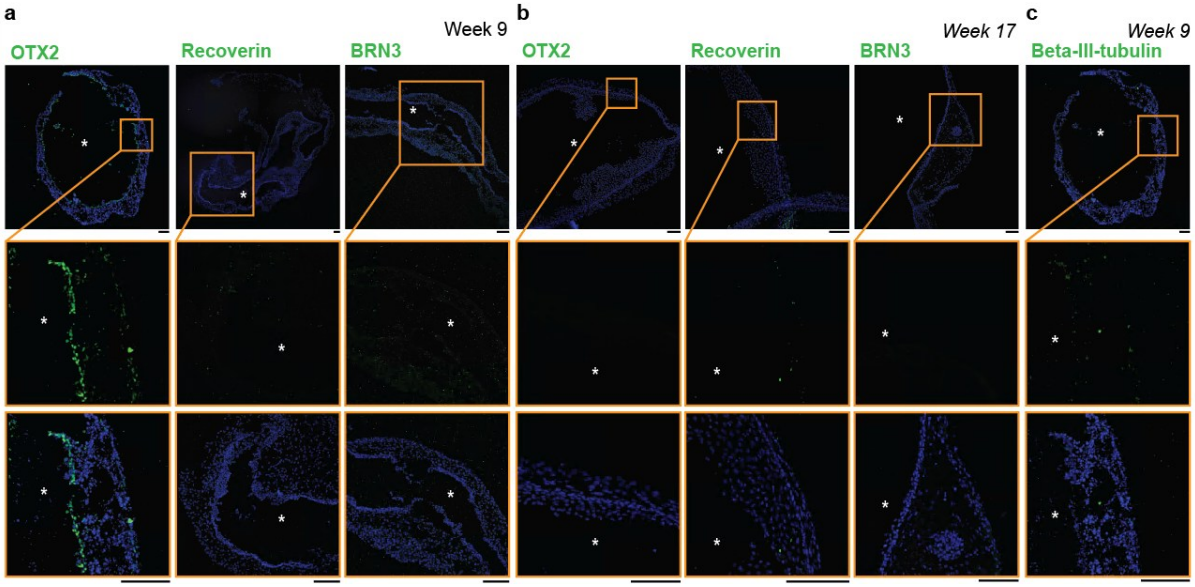

Figure 14 – Retinal cell types in 3D-cysts from BMP4-guided protocol.
Immunostaining of cryostat sections of 3D-cysts at week 9 (**a, c**) and week 17 (**b**) generated with BMP4-guided protocol from SC102A. Green: OTX2 (orthodenticle homeobox 2) for photoreceptors and bipolar cells. Recoverin for photoreceptors. BRN3 (brain-specific Homeobox/POU Domain Protein 3) for ganglion cells (**a-b**). Neuronal marker beta-III-tubulin (**c**). Blue: nuclei-dye Hoechst. BRN3, brain-specific Homeobox/POU Domain Protein 3 for ganglion cells. Orange frame, zoom in. *, lumen. Scale bar: 100 µm.

This supports previous observation with BMP4 to induce mesoderm (Faial et al. 2015; Pengbo Zhang et al. 2008). The lack of neuroectoderm is already prevalent at Day 12, when the formation of neuronal filaments is absent upon BMP4 application (**Figure 15a-b**). These 3D-cysts gradually grew in diameter and expanded their inner wall thickness (**Figure 15c-d**).

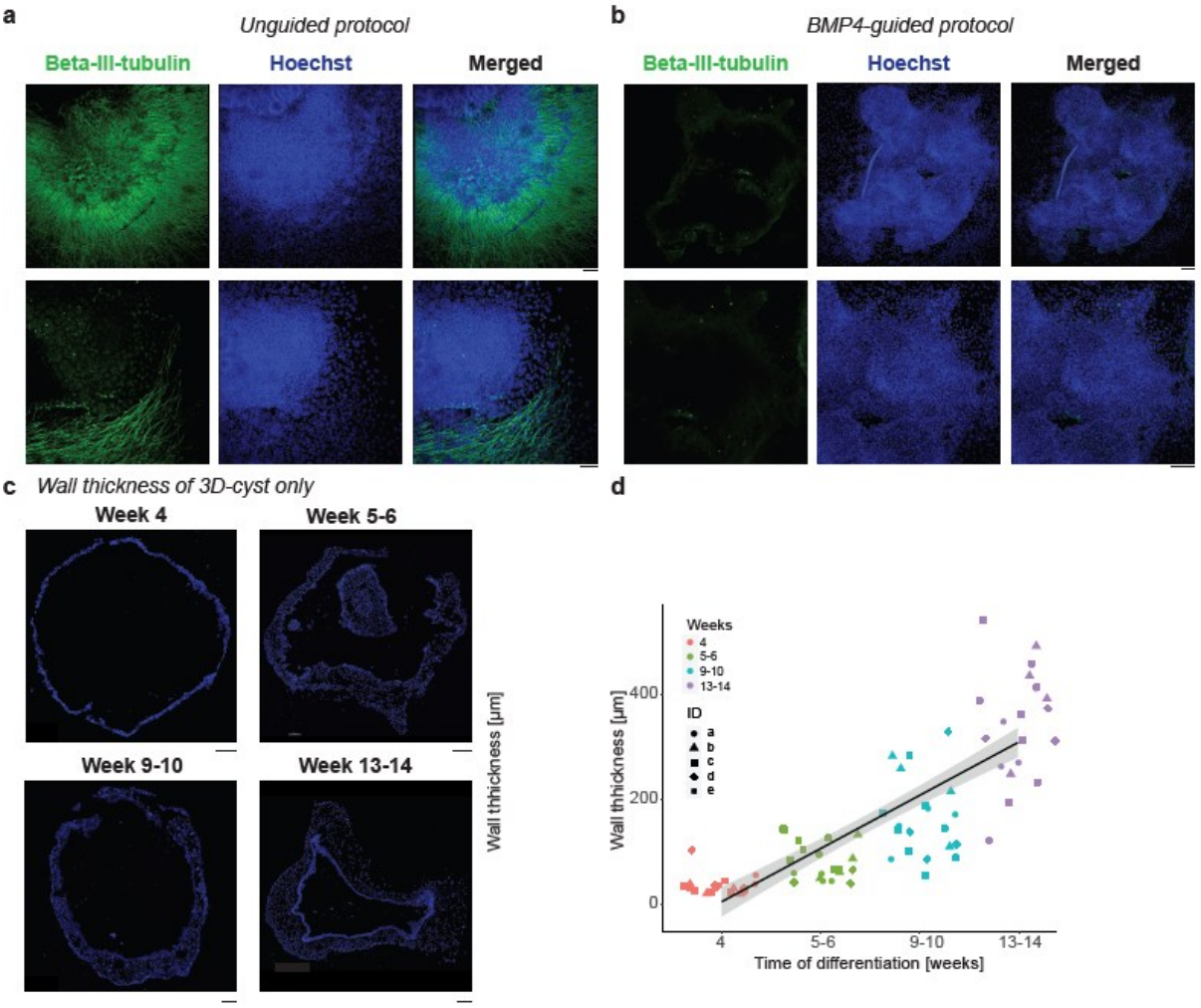

Figure 15 – Comparison unguided versus guided protocol.
a-b, Immunostaining of 2.5D culture from SC102A at day 12 from unguided protocol (**a**) and BMP4-guided protocol (**b**) for the neuronal marker beta-III-tubulin (green) and the nuclei dye Hoechst (blue). Scale bar: 100 µm. **c**, Cryostat sections of 3D-cysts generated with BMP4-guided protocol at four different time points counter-stained with nuclei-dye Hoechst (blue). Scale bar: 100 µm. **d**, Scatter plot of wall thickness. Each symbol (a-e) represents a 3D-cyst with four data points for the measured wall thickness on opposing sides. 5 cysts per time point with trend curve and 95% confidence level interval.

From week 4 onwards, small branched cells started to float in the supernatant (**Figure12 a**), which have previously been described as microglia-like cells (Haenseler et al. 2017). To verify this cell identity, we either collected and seeded these cells or directly labeled them on 2.5D culture plates. In both cases, the IBA1^{+}-cells expressed RUNX1, PU.1, CD45, and P2Y12 but not CD14 (**Figure 12b-i**). Moreover, we confirmed their mRNA expression for PU.1, IBA1, P2Y12, and CX3CR1 with real-time quantitative PCR (RT-qPCR, **Figure 12j**) suggesting that they are microglia-like cells similar to the microglia obtained with the unguided protocol (**Figure 9**).

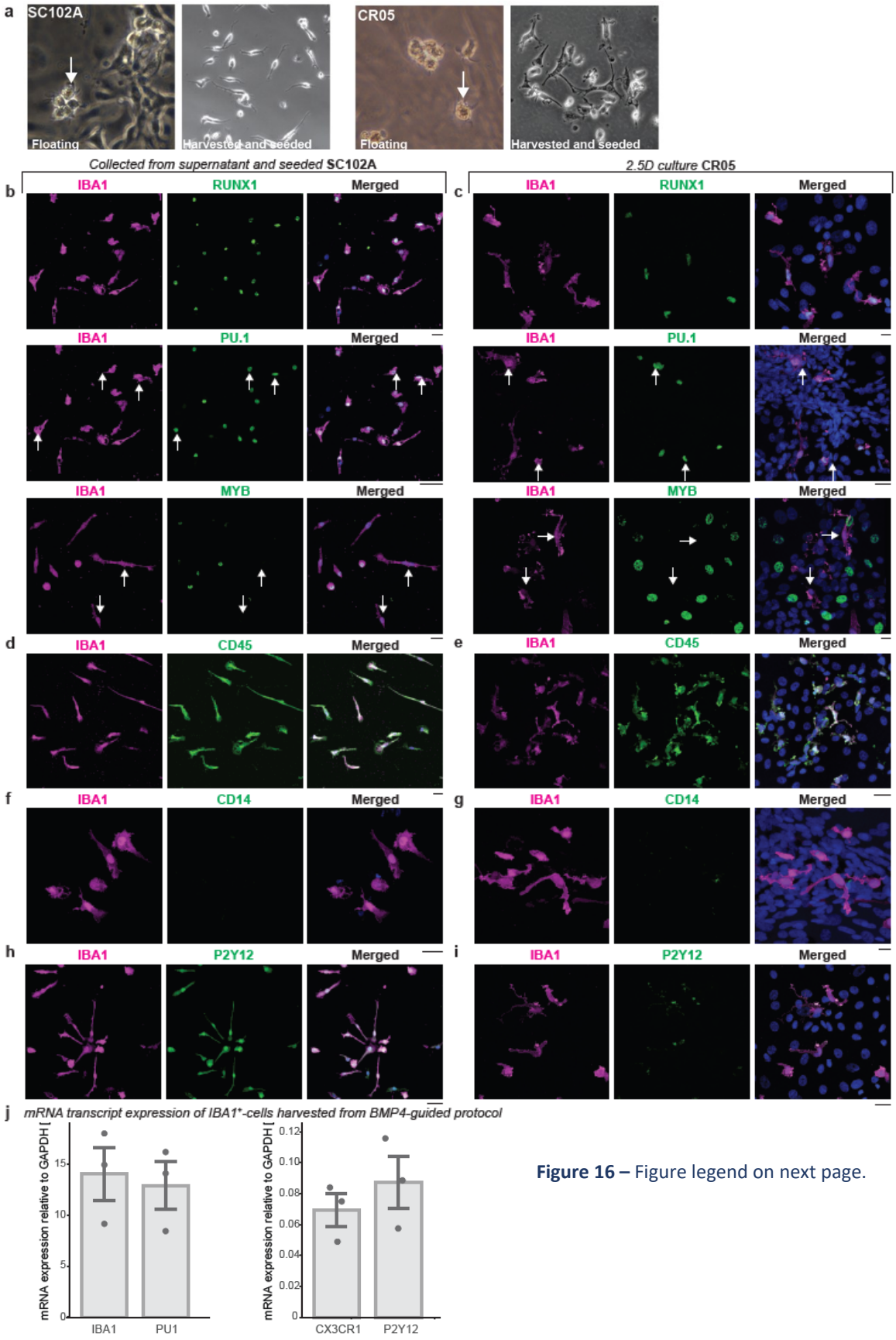

Figure 16 – Figure legend on next page.

Figure 16 – IBA1^{+}-cells occur with BMP4-guided protocol.
a, Brightfield images of branched cells in the supernatant for SC102A (left) and CR05 (right). Left, focus on floating cells in the original plate (week 6-7). Arrow, branching. Right, harvested supernatant and seeded on a new plate (week 5-6). Scale bar: 100 µm. **b-i**, Immunostaining for IBA1 (ionized calcium-binding adapter molecule 1, magenta) and nuclei dye Hoechst (blue) obtained from the BMP4-guided protocol either collected and seeded at week 6 from the supernatant of SC102A (**b, d, f, h**), or directly labeled on 2.5D culture plates of CR05 between week 4 and 6 (**c, e, g, i**). In green: Immunostaining for **b-c**, RUNX1 (runt-related transcription factor 1), PU1 (hematopoietic transcription factor PU.1), and MYB (MYB Proto-Oncogene). White arrow, examples of non-overlap. **d-e**, CD45 (cluster of differentiation 45/ protein tyrosine phosphatase receptor). **f-g**, CD14 (cluster of differentiation 14/ monocyte Differentiation Antigen CD14). **h-i**, P2Y12 (purinergic receptor P2Y G-protein-coupled 12). Scale bar: 20 µm. **j**, mRNA transcript expression of IBA1, PU1, CX3CR1 and P2Y12 relative to the housekeeping gene GAPDH with mean standard error of IBA1+-cells harvested from the supernatant of BMP4-guided protocol. Each dot represents an independent differentiation.

To further validate a microglia-like activity, we first measured the capability of IBA1^{+}-cells to phagocytose. We immunostained the IBA1^{+}-cells with tomato-lectin and live imaged the uptake of pH-sensitive fluorescent beads. The beads accumulated overtime within the IBA1^{+}-cells indicating phagocytic active cells (**Figure 17a-b**).

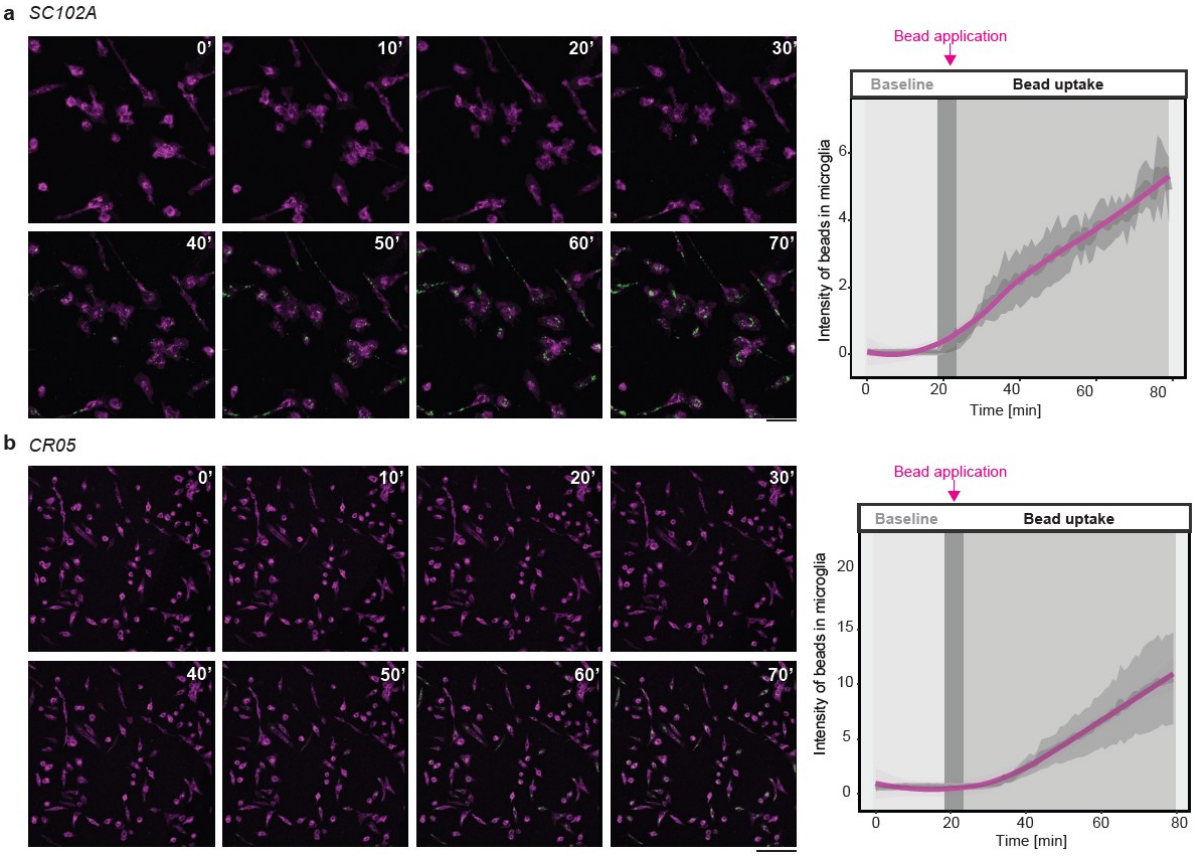

Figure 17 – Phagocytosis assay.
a-b, Left: Consecutive snapshots of live imaged tomato-lectin-labeled microglia-like cells (magenta) collected from the supernatant of the BMP4-guided protocol for **a**, SC102A and **b**, CR05 and their uptake of fluorescent beads (green) week 6-7. Scale bar: 100 µm. Mean intensity increase of beads within IBA1^{+}-cells and 95% confidence interval band during 80 minutes of recording of three biological replications. Dark grey bar: bead application after 20 minutes of baseline recording.

Next, we investigated whether the IBA1^{+}-cells trigger an upregulation of inflammatory signature genes IL6, TNF and IL1β (Smith et al. 2012) upon stimulation with either interferon γ (IFNγ), interleukin 1β (IL1β) or both, bacterial lipopolysaccharide (LPS) or POLY(I:C). For all stimulations, we confirmed the upregulation of these inflammatory genes in IBA1^{+}-cells (**Figure 18**).

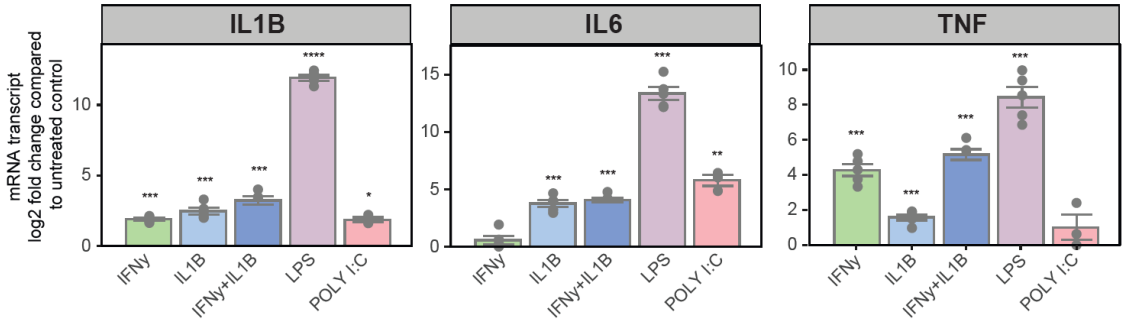

Figure 18 – Inflammatory response.
Real-time quantitative PCR (RT-qPCR) for interleukin 1β (IL1β, left), interleukin 6 (IL6, middle), and tumor necrosis factor (TNF, right). HIPSC-derived microglia from BMP4-guided protocol were treated with either recombinant interferon γ (IFNγ), IL1β, or both, bacterial lipopolysaccharide (LPS), or polyinosinic:polycytidylic acid (POLY(I:C)) at week 6-7. Bar chart: mRNA transcript log-2 fold changes compared to untreated control cells with standard error of the mean. Each dot represents an independent differentiation. One sample t-test. $^{*}p < 0.05$, $^{**}p < 0.01$, $^{**}p < 0.001$ and $^{****}p < 0.0001$.

Finally, to test, whether hIPSC-derived IBA1^{+}-cells display Ca^{2+}-events upon extracellular ATP administration (Palomba et al. 2021), we labeled IBA1^{+}-cells with the Ca^{2+}-sensitive fluorescent dye Fluo-4 and imaged the fluorescent intensity after ATP administration. IBA1^{+}-cells displayed rapid and synchronized accumulation of Ca^{2+}-events (**Figure19 –** Figure legend on next page.

Figure 19a-b), which was not observed with medium-treated IBA1^{+}-cell (**Figure 15c-d**).

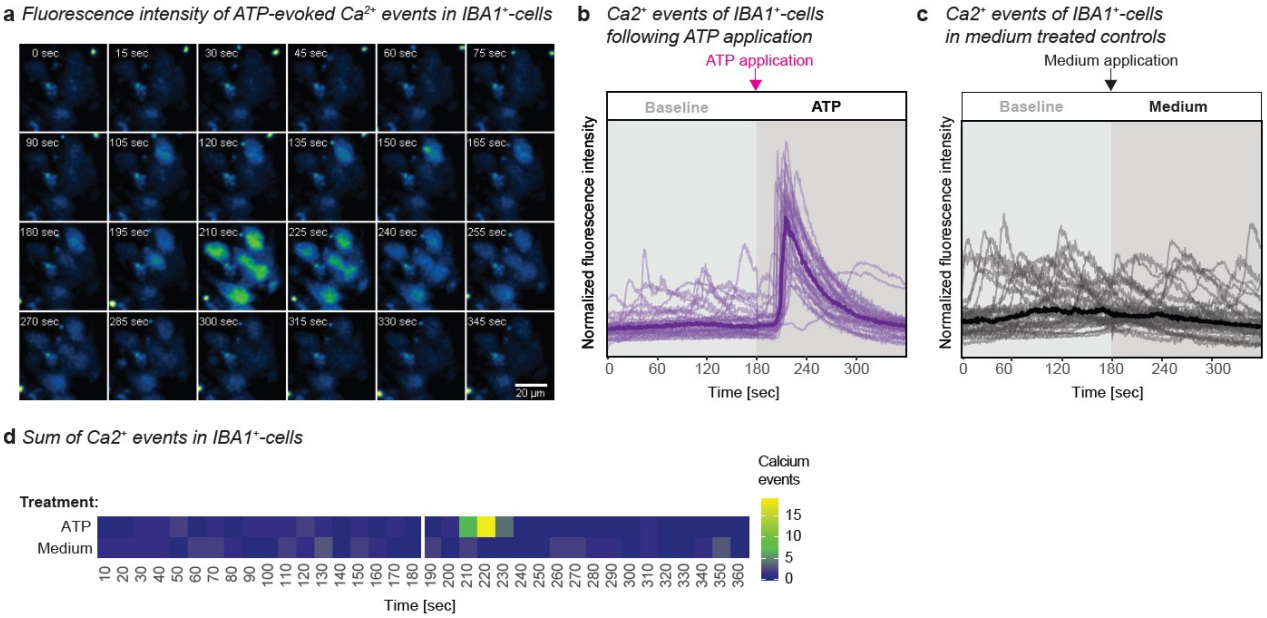

Figure19 – Figure legend on next page.

Figure 19 – Calcium events.
ATP-evoked $Ca2^+$ transients in $IBA1^+$-cells derived from BMP4-guided protocol for SC102A week 6-7. **a**, Consecutive snapshots of live imaged cells exposed to $Ca2^+$-sensitive fluorescent dye Fluo-4. Scale bar: 20µm. **b-c**, Graph shows Ca2+-dependent fluorescence intensity normalized to the mean intensity of the cells throughout 360 seconds of recording. After 180 seconds of baseline measurement (light grey area) **b**, ATP (1mM final concentration) was applied or **c**, L15 medium was applied and recording was continued up to 360 seconds (dark grey area). $Ca2^+$-events are detected by PeakCaller software. Each curve shows the $Ca2^+$-events of an individual cell. Thick line: Median of 32 cells from three independent differentiations. **d**, Graph shows sum of software-detected $Ca2^+$ events from all cells of ATP- and medium treated conditions across time in 10 second bins. $Ca2^+$-dependent fluorescence is displayed through an intensity-based color code (blue-green-yellow). White vertical line indicates drug application time point.

$IBA1^+$-cells populate but do not originate in 3D-cysts in BMP4-guided protocol

To identify whether $IBA1^+$-cells, similarly to the unguided protocol, occupied 3D-cysts in BMP4-guided protocol, we collected 3D-cysts at several time points after differentiation and performed wholemount immunostaining. Starting at week 5.5, $IBA1^+$-cells populated the 3D-cysts and increased in number over time (**Figure 16a**-**b**). To identify whether 3D-cysts might be the source of $IBA1^+$-cells, we collected 3D-cysts from a 2.5D culture plate at week 2.5, 3, 4, and 5 and cultured these separately, in parallel to the left-over 3D-cysts. These 3D-cyst cultures were developed until week 7.5 and then immunostained for IBA1 (**Figure 16c**). Unexpectedly, the 3D-cysts isolated at week 2.5 to 4 contained only a few $IBA1^+$-cells (**Figure 16d**).

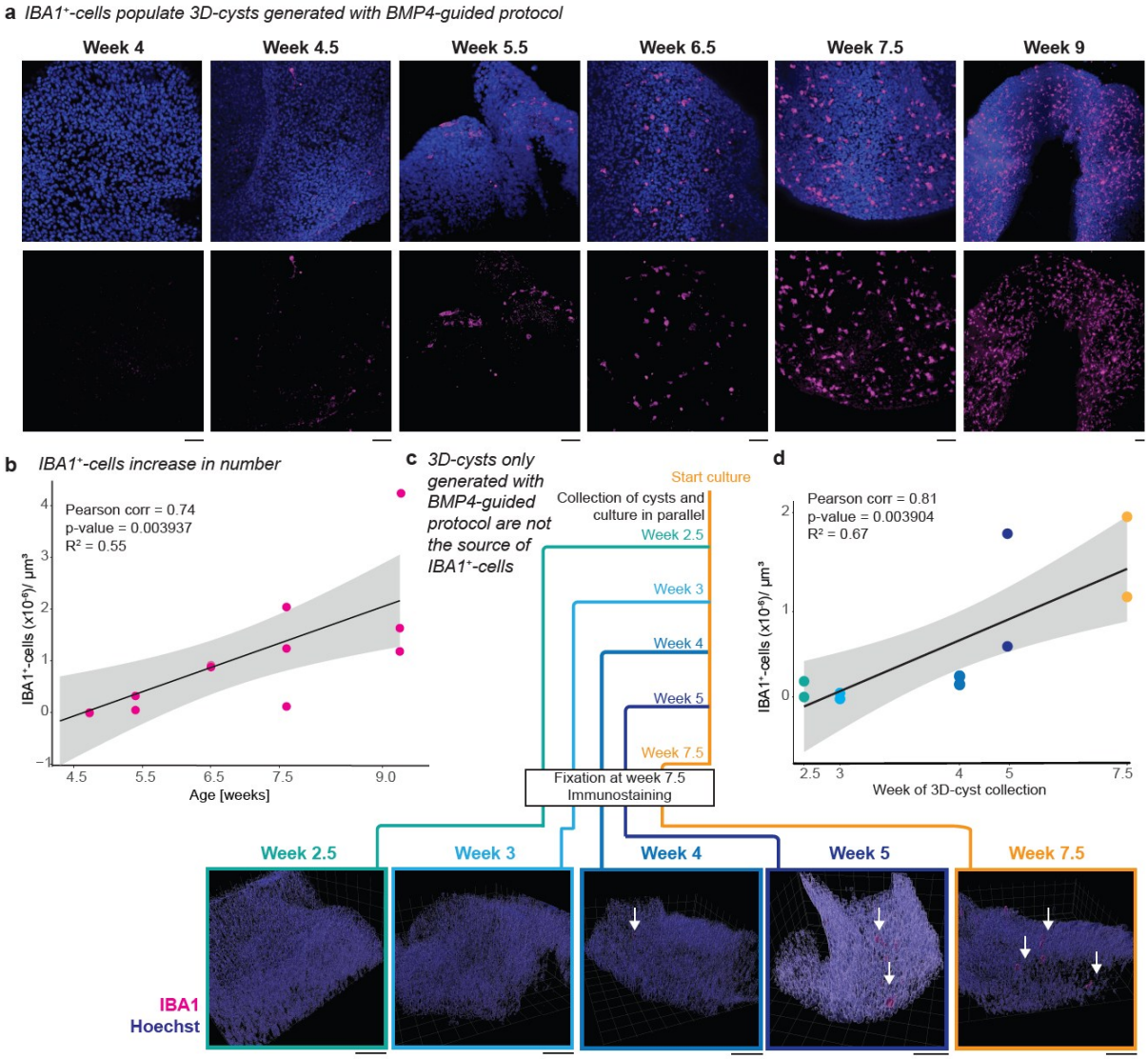

Figure 20 – IBA1⁺- populate but do not originate in 3D-cysts in BMP4-guided culture.
Immunostaining for IBA1 (ionized calcium-binding adapter molecule 1, magenta) and Hoechst (blue) in SC102A for BMP4-guided protocol. **a**, Timeline of the presence of IBA1⁺-cells in 3D-cysts from week 2.5 to week 9. Scale bar: 50 µm. **b**, Scatter plot of IBA1⁺-cells occupying 3D-cyst with trend curve and 95% confidence level interval. Pearson correlation showing a significant correlation between age of differentiation and number of IBA1⁺-cells occupying the cyst (Pearson's correlation = 0.738518 and p-value = 0.003937, R2 = 0.5454089). **c**, 3D-cysts collected and separated from the 2.5D culture at week 2.5, 3, 4, 5 and cultured until week 7.5, immunostained (wholemount) together with 3D-cysts which were kept in the original 2.5D culture until week 7.5 (orange frame). Representative images of 3D volume rendering to visualize the 3D-cyst with IBA1⁺-cells. White arrow, IBA1⁺-cells. Scale bar: 100 µm. **d**, Scatter plot of IBA1⁺-cells occupying isolated 3D-cyst with trend curve and 95% confidence level interval. Pearson correlation showing a significant correlation between age when 3D cysts were isolated and IBA1⁺-cells density (R = 0.81707 and p-value = 0.0039, R2 = 0.6676).

In contrast, 3D-cysts isolated at week 5 had a similarly high number of IBA1⁺-cells to the 3D-cysts cultured on the original plate excluding these structures as the source of IBA1⁺-cells. Indeed, we found IBA1⁺-cells already on the culture plate between week 2 and 3 (**Figure 21**) indicating that they are not derived from the 3D-cysts.

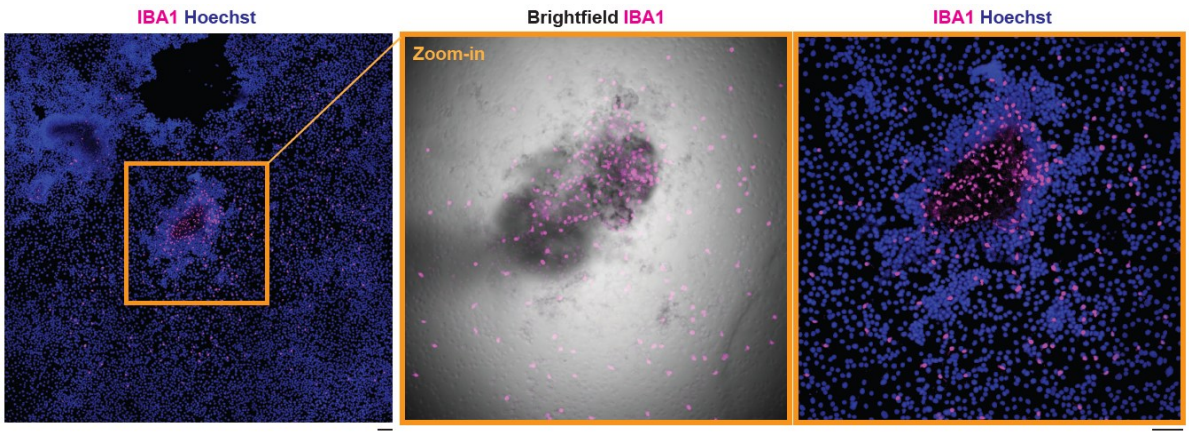

Figure 21 – First occurrence of IBA1⁺-cells in 2.5D culture by week 2.5D in BMP4-guided protocol.
Immunostaining for IBA1 (ionized calcium-binding adapter molecule 1, magenta) and Hoechst (blue) in SC102A for BMP4-guided protocol. Orange frame, zoom-in with brightfield image. Scale bar: 100 µm.

IBA1⁺-cells associate with the mesenchymal/vimentin⁺-region

To obtain insights into the cyst composition, we performed mass spectrometry of 3D-cysts from the BMP4-guided protocol with either sparse or high IBA1⁺-cell population at week 4 and 7, respectively (

Figure 22a). We obtained the peptide sequence data and compared the highly expressed proteins with 44 tissues from the human proteome atlas that have previously been characterized (Uhlén et al. 2015). At week 4, highly abundant proteins suggest that cells in the 3D-cysts have various fate potentials. Interestingly, at week 7, the protein composition was specific to tissues of partial or full mesodermal origin such as soft tissue, bone marrow and smooth muscles, which is consistent with BMP4 application and indicates a mesenchymal identity (**Figure 22b**).

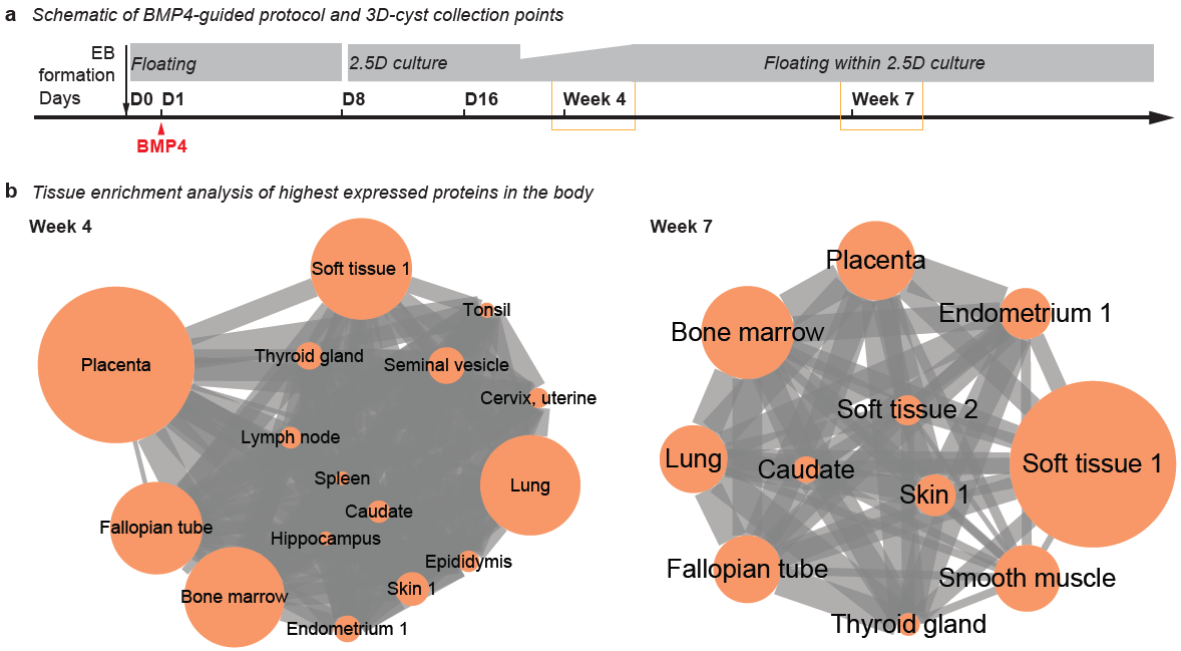

Figure 22 – Figure legend on next page.

Figure 22 – Tissue enrichment analysis.
a, Schematic of experimental design. For mass spectrometry, ten 3D-cysts generated with BMP4-guided protocol were collected at week 4 and week 7. **b**, Tissue enrichment analysis shown as a network. Nodes, tissue. Edges, connecting the tissues that share highly expressed proteins in the 98th percentile. The node size reflects the enrichment p-value and the thickness of the edge reflects the size of the shared proteins.

Similarly, when we performed tissue enrichment analysis of proteins related to human eye tissue (Dunn et al. 2019; Zhang et al. 2015; Zhang, Kirby, et al. 2016), we found a significant overlap of highly abundant proteins for meninges and sclera, both of which have mesenchymal origin. In contrast, proteins enriched in ectodermal retina and optic nerve were underrepresented (**Figure 23a**).

To validate whether the 3D-cysts are enriched for mesenchyme, we compared our mass spectrometry data with mesenchymal markers including transcription factors, cytoskeletal-, cell surface and extracellular matrix proteins (Andrzejewska et al. 2019; Owusu-Akyaw et al. 2019; Scanlon et al. 2013). We found that vimentin (VIM), laminin β1 (LAMB1), and fibronectin (FN1) were enriched with VIM among the most abundantly expressed mesenchymal proteins at week 7 (**Figure 23b**). Since one characteristic of mesenchyme is close interaction with the epithelium (MacCord 2012), we also investigated the presence of epithelial proteins in our dataset and found several to be upregulated from week 4 to 7 (**Figure 23c**).

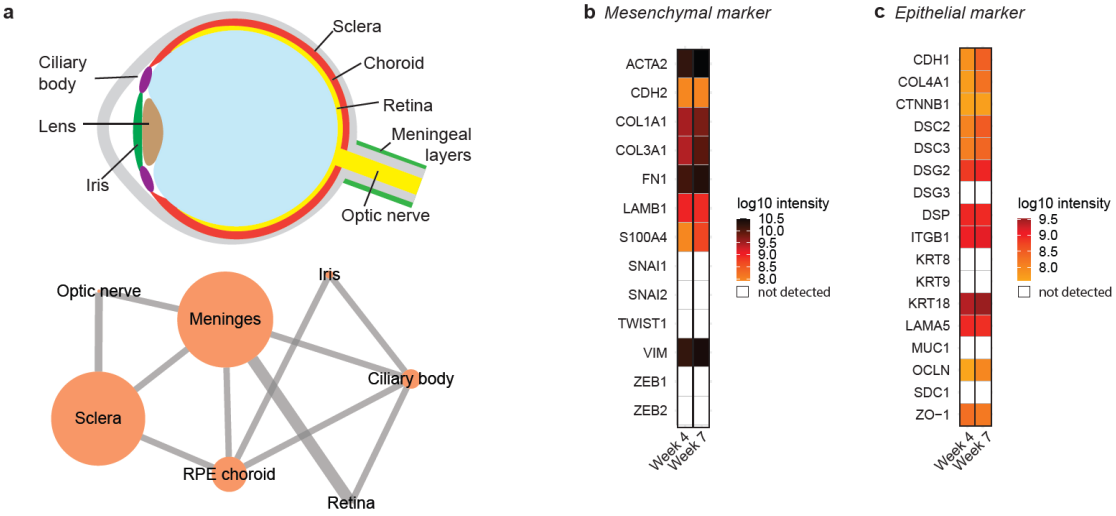

Figure 23 – Tissue enrichment analysis of highest expressed proteins in the eye.
a, Top: eye schematic. Bottom: tissue enrichment analysis of the week 7 dataset. RPE, retinal pigment epithelium. **b-c**, Heatmap of protein expression level in log10 (intensity) for week 4 and week 7 cystic compartments for **b**, mesenchymal marker; **c**, epithelial marker.

One of these epithelial markers is E-Cadherin (CDH1), which is commonly described together with the mesenchymal marker VIM in the epithelial-mesenchymal transition during development and cancer (Hay 2005; Thiery et al. 2009; Yamashita et al. 2018). Therefore, we validated the expression of both markers in 3D-cysts derived with the BMP4-guided protocol. VIM expression was strong in the cell layers facing the surface of the 3D-cyst wall (**Figure 24a**). In contrast, E-Cadherin marked a defined layer next to the cystic lumen and complemented VIM expression **Figure 24b**).

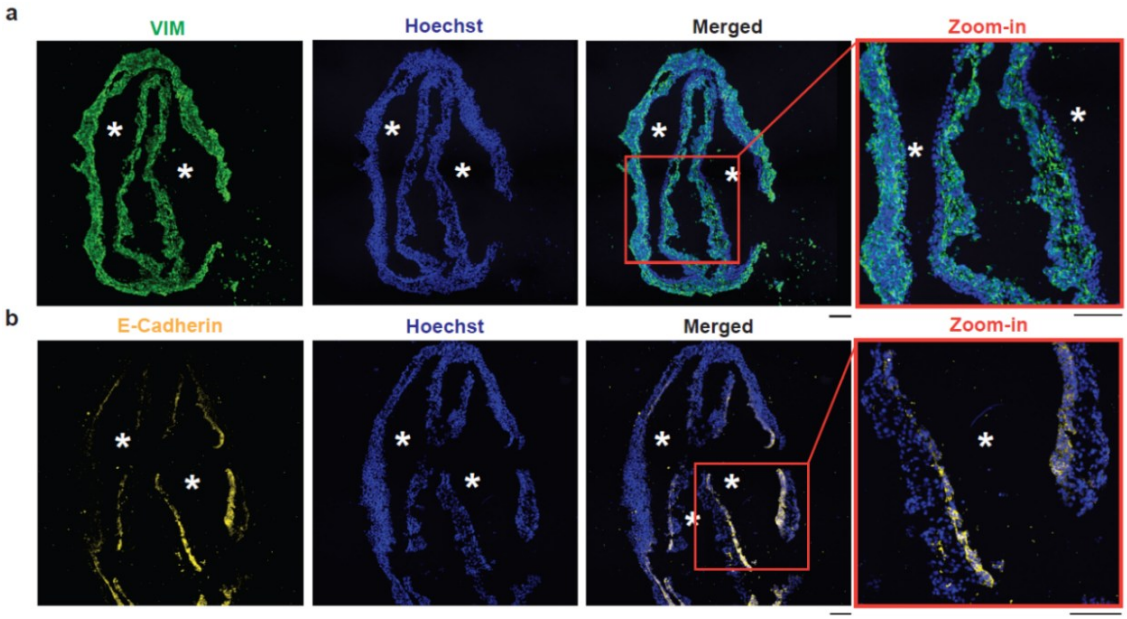

Figure 24 – Confirmation of mass spectrometry candidate proteins in 3D-cysts from BMP4-guided protocol.
Immunostaining of sequential cryostat sections of 3D-cysts from BMP4-guided differentiation at week 7 for VIM (vimentin, green, **a**), E-Cadherin (yellow, **b**) and counter-stained with the nuclei-dye Hoechst (blue). *: lumen. Zoom-in (red frame). Scale bar: 100 µm.

When we investigated the location of IBA1$^+$-cells, they mostly occupied the VIM$^+$-region (**Figure 25a**) and stayed distinct from the E-Cadherin$^+$-layer (**Figure 25b**). Only occasionally IBA1$^+$-cells intermingled with the E-Cadherin$^+$-cells (**Figure 25c**).

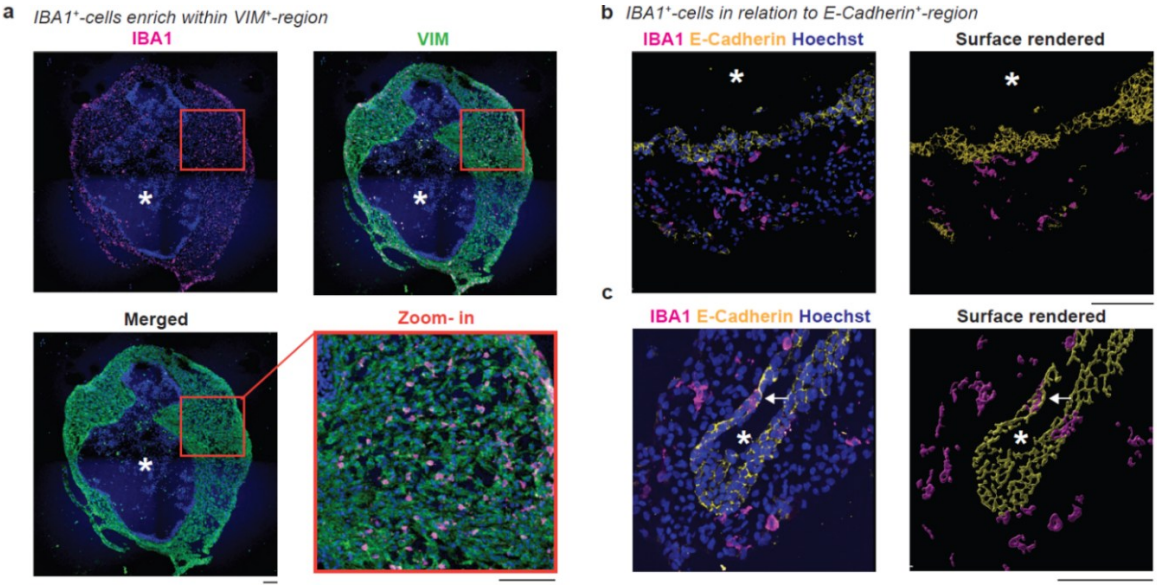

Figure 25 – IBA1$^+$-cells localize within VIM$^+$-region in cystic compartment.
Immunostaining of cryostat sections of 3D-cysts from BMP4-guided differentiation for IBA1 (ionized calcium-binding adapter molecule 1, magenta) and counter-stained with the nuclei-dye Hoechst (blue). **a**, Co-staining with VIM (vimentin, green, week 12, red frame: zoom-in) or **b-c**, E-Cadherin (yellow, week 10, with 3D-surface rendering for CR05 cysts). White arrow: IBA1$^+$-cells within E-Cadherin layer. *, lumen. Scale bar: 100 µm.

To verify whether the IBA1^{+}-cells prefer the mesenchymal-like VIM^{+}-region also in 3D-cysts obtained from the unguided protocol (**Figure 5a**), we repeated the above-described staining. VIM labeled a similar defined region in the 3D-cysts with E-Cadherin expression localized in a defined layer around the cystic lumen (**Figure 26a-d**).

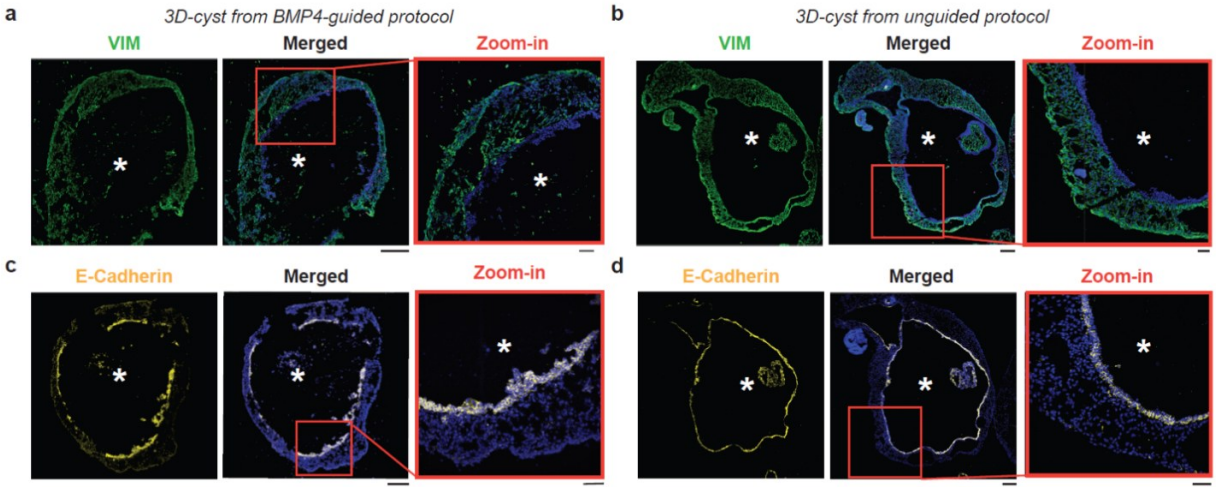

Figure 26 – Comparison of 3D-cysts from BMP4-guided or unguided protocols.
Immunostaining of VIM (vimentin, green, **a-b**) and E-Cadherin (yellow, **c-d**) for SC102A at week 8 for 3D-cysts from BMP4-guided (**a, c**) and unguided (**b, d**) protocol, counter-stained with the nuclei-dye Hoechst (blue). *: lumen. Red frame: zoom-in. Scale bar: 200 µm. Zoom in, Scale bar: 50 µm.

In addition, we found E-Cadherin^{+}-expression at regions facing the surface (**Figure 27a**). IBA1^{+}-cells rarely intermingled with the E-Cadherin^{+}-layer facing the lumen or the surface of the 3D-cyst (**Figure 27a-b**) and mostly localized within the VIM^{+}-region (**Figure 27c**) suggesting that IBA1^{+}-cells prefer the mesenchymal region.

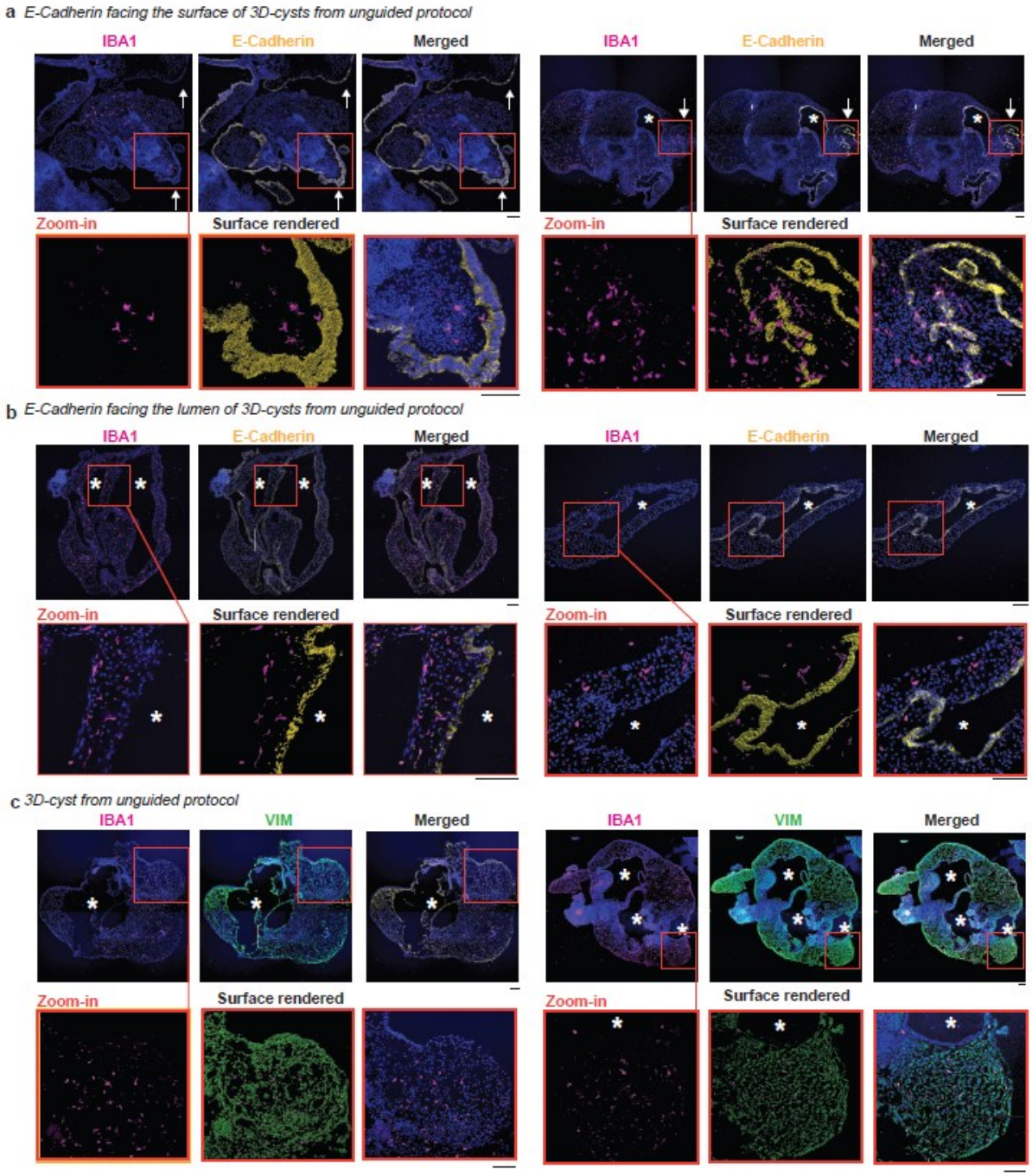

Figure 27 – IBA1⁺-cells preferentially localize within VIM⁺-regions in 3D-cysts.
Immunostaining of cryostat sections of 3D-cysts from unguided protocol for IBA1 (ionized calcium-binding adapter molecule 1, magenta), E-Cadherin (yellow, a-b), VIM (vimentin, green, c), and the nuclei-dye Hoechst (blue) for SC102A at week 8. *, lumen within the cystic compartment. a, Arrow, E-Cadherin staining on 3D-cyst surface. Red frame, zoom-in with surface rendering in the middle. Scale bar: 100 µm.

Mesenchymal stem cells can have immunomodulatory capabilities (Andrzejewska et al. 2019) and could sequester IBA1⁺-cells away from infiltrating into the retinal cups. To test this, we added 17-week-old retinal organoids without a cystic compartment (**Figure 12a**, i/ii) from the unguided protocol to the culture of BMP4-guided protocol, which contains both floating IBA1⁺-cells and

3D-cysts in the supernatant (**Figure 28a**). IBA1^{+}-cells did not integrate into the retinal cup or the cerebral compartment (**Figure 28b**).

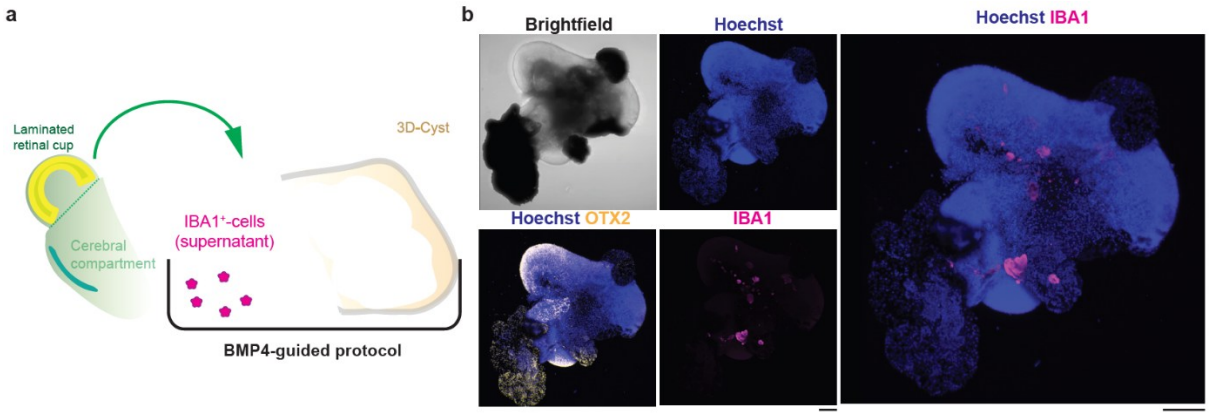

Figure 28 – Adding 3D-retinal organoids without cystic compartment to 2.5D culture of BMP4-guided protocol. **a**, Experimental schematic (condition 1). **b**, Whole mount 3D-retinal organoid without cystic compartment from SC102A immunostained for IBA1 (ionized calcium-binding adapter molecule 1, magenta), OTX2 (orthodenticle homeobox 2, yellow), the nuclei-dye Hoechst (blue) and brightfield image at week 18. Scale bar: 100 µm.

In contrast, if we harvested IBA1^{+}-cells from the BMP4-guided protocol and applied them to 3D-retinal organoids without a cystic compartment (**Figure 29a**), IBA1^{+}-cells successfully integrated into both retinal cup and cerebral compartment (**Figure 29b-c**). These data show that when there is no cystic compartment, IBA1^{+}-cells start to occupy the retinal cup. Otherwise, they are preferentially enriched in the mesenchymal, cystic region.

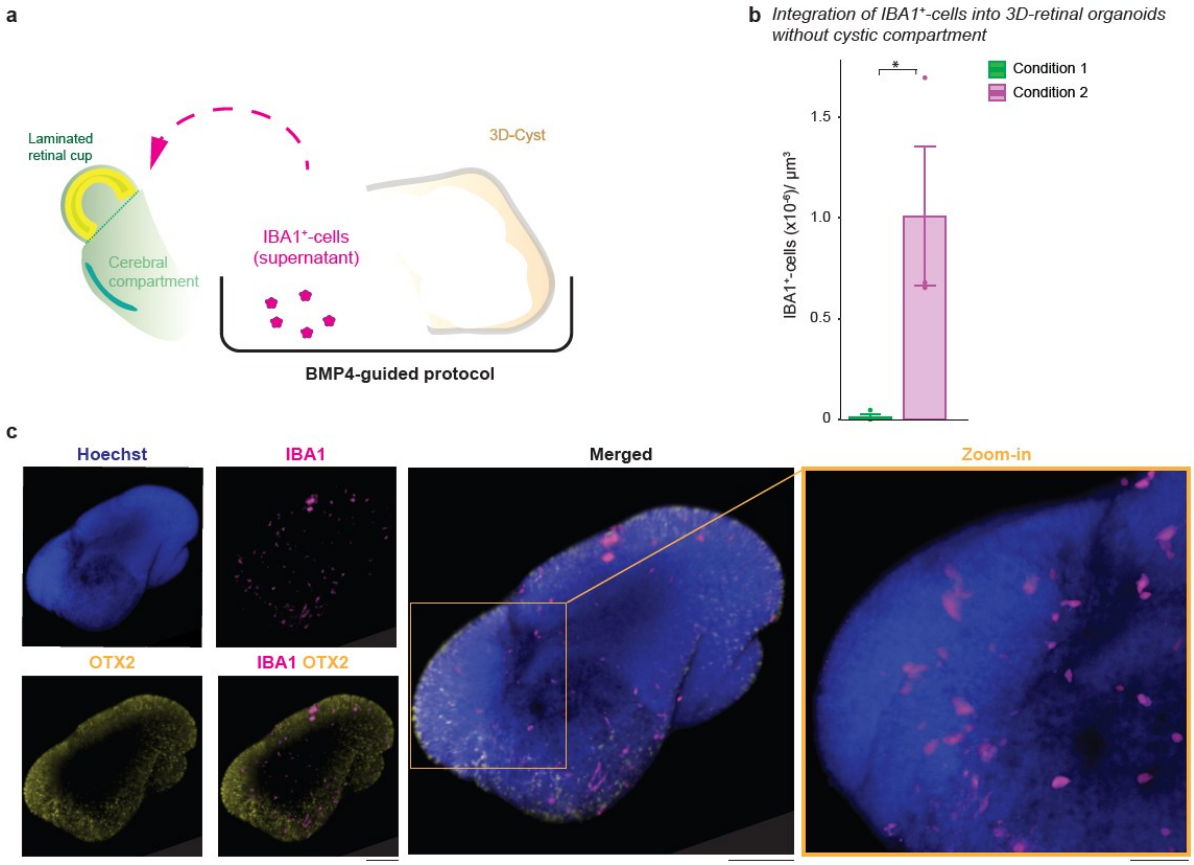

Figure 29 – Adding IBA1$^+$-cells from BMP4-guided protocol to 3D-retinal organoids without cystic compartment. **a**, Experimental schematic (condition 2). **b**, Bar chart of number of IBA1$^+$-cells integrating into the structure and standard error at week 17 after 10 days of adding IBA1$^+$-cells. Each dot represents a 3D-retinal organoid. Green, condition 1 related to **Figure 22a-b**. Magenta, condition 2 related to **Figure 23a, c**. Wilcox test p-value = 0.0436. *p < 0.05. **c**, Whole mount 3D-retinal organoid without cystic compartment from SC102A immunostained for IBA1 (ionized calcium-binding adapter molecule 1, magenta), OTX2 (orthodenticle homeobox 2, yellow), the nuclei-dye Hoechst (blue) and brightfield image at week 18. Scale bar: 100 µm.

IBA1$^+$-cells adopt a BAM signature in the mesenchymal environment

Border-associated macrophages (BAMs) are non-parenchymal macrophages that reside either at perivascular structures, meninges, or choroid plexus, all of mesenchymal nature (Lun et al. 2015; MacCord 2012; Pill et al. 2015). Transcriptional profiling of macrophage populations in embryonic mouse brain identified CD163 as a potential marker for BAMs (Utz et al. 2020), which also labels human perivascular macrophages (Fabriek et al. 2005), mononuclear phagocytes in the choroid plexus, and cells in the meningeal- and subpial granular layer (Rezaie and Male 2003). Indeed, we found that 99% of IBA1$^+$-cells co-expressed CD163 by week 10 in the 3D-cyst (**Figure 30a-b**).

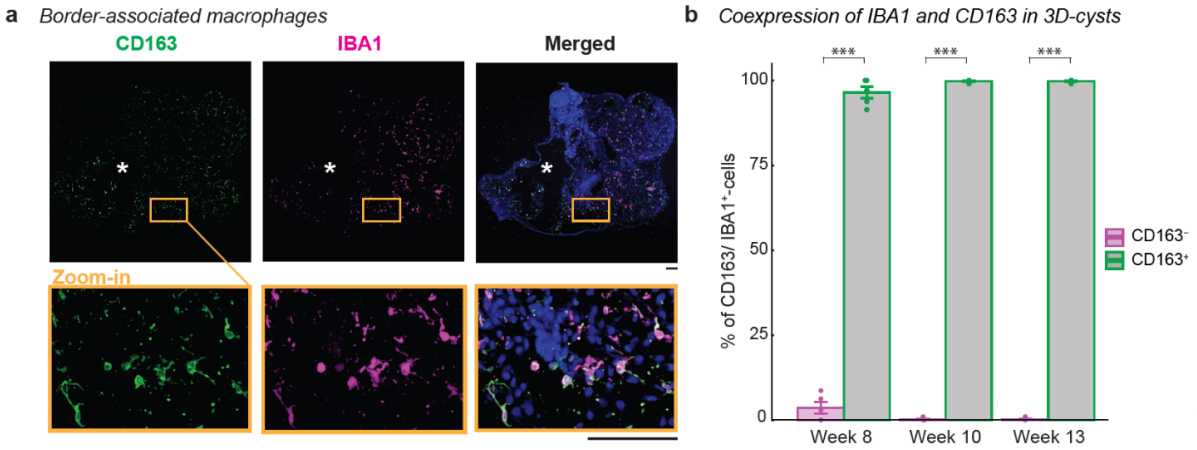

Figure 30 – IBA1$^+$-cells express CD163, a marker for border-associated macrophages.
a, Immunostaining of cryostat sections of SC102A 3D-cysts from unguided protocol week 8 for IBA1 (ionized calcium-binding adapter molecule 1, magenta), CD163 (cluster of differentiation 163/ protein tyrosine phosphatase receptor type C, green) and the nuclei-dye Hoechst (blue). Orange frame: zoom-in. *: lumen within the cystic compartment. Scale bar: 100 µm. **b**, Bar chart of % of CD163$^+$/IBA1$^+$-cells and % of CD163$^-$/IBA1$^+$-cells per time point with standard error. Each dot represents one section of individual 3D-cyst. Two-way ANOVA p-value = < 2.2e-16 with selected post hoc-test. ***p < 0.001.

Interestingly, the onset of CD163 expression occurs in a defined window. At week 5, IBA1$^+$-cells were still negative for CD163 in the 2.5D culture (**Figure 31a**). Within one week, IBA1$^+$-cells co-expressed CD163, as they started to distribute within the 2.5D culture and occupy compartments that were sparse in nuclei (**Figure 31b**).

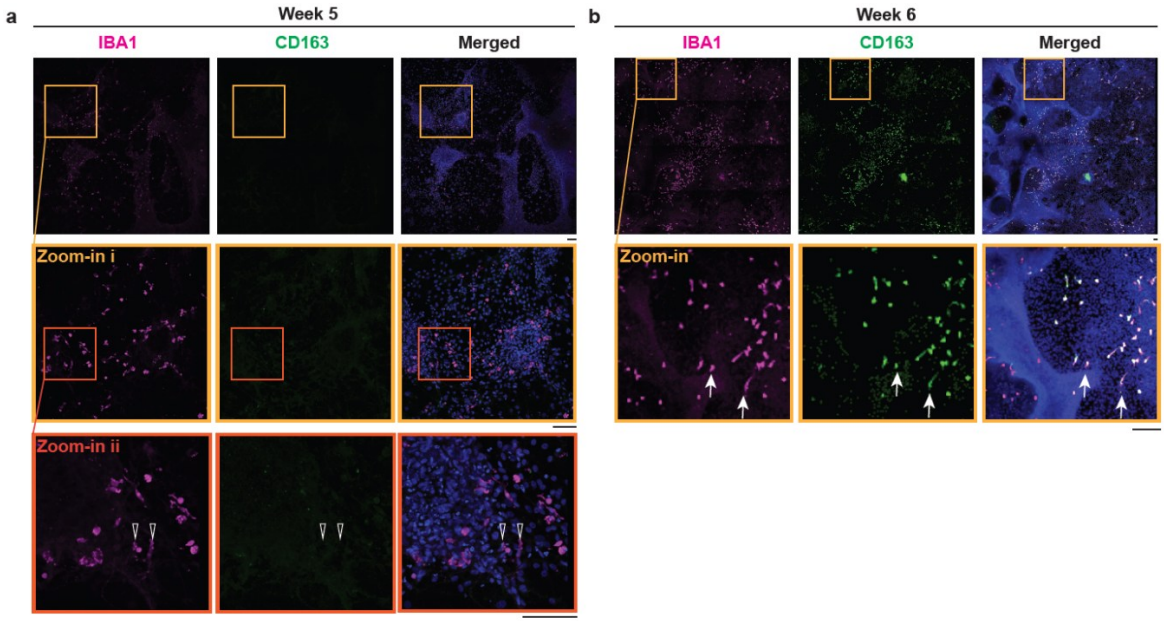

Figure 31 – Onset of CD163 expression in unguided protocol.
Immunostaining of 2.5D-culture from unguided protocol of CR05 for IBA1 (ionized calcium-binding adapter molecule 1, magenta), CD163 (cluster of differentiation 163/ protein tyrosine phosphatase receptor type C, green) and the nuclei-dye Hoechst (blue) at week 5 (**a**) and week 6 (**b**). Open arrow: CD163$^-$/IBA1$^+$. Arrow: CD163$^+$/IBA1$^+$. Orange and red frame: zoom in. Scale bar: 100 µm.

To identify whether the 3D-cysts expressed a blood vessel endothelium, we stained for CD31. Only occasionally, we observed CD31 in the VIM$^+$-region (**Figure 32**) suggesting that IBA1$^+$-cells occupy the 3D-cyst even without blood vessel system. In contrast to mice that require the blood vessel system (Ginhoux et al. 2010), human microglia infiltrate the cortex from the ventricular lumen and the leptomeninges (Monier et al. 2007; Rezaie et al. 2005) thus, the strong preference of IBA1$^+$-cells to the mesenchyme might explain the preferential location of IBA1$^+$-cells to infiltrate the brain tissue.

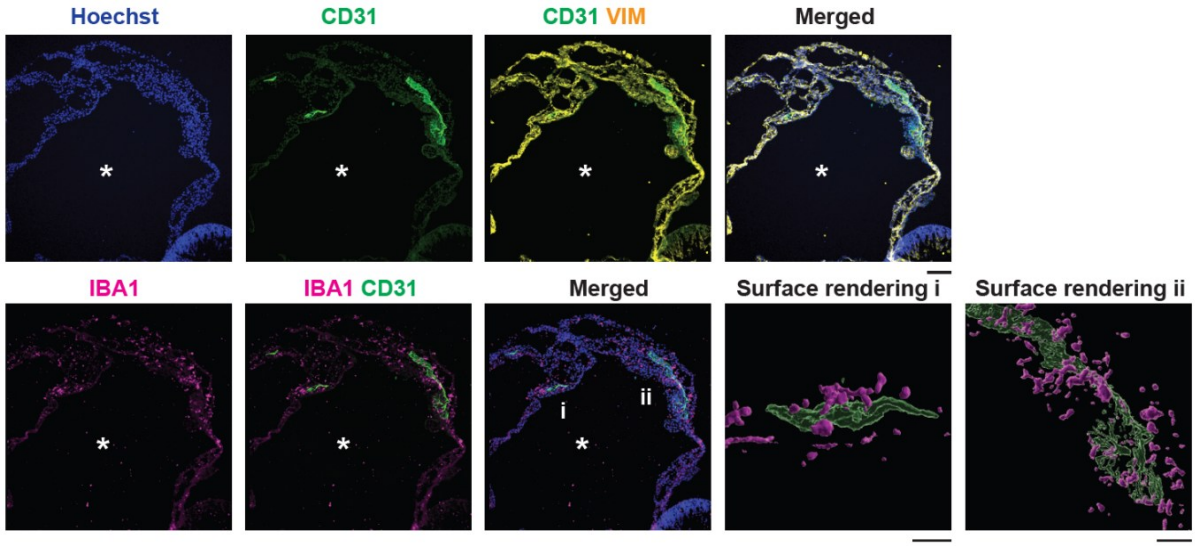

Figure 32 – CD31$^+$-endothelial cells within VIM$^+$-region.
Immunostaining of cryostat-sections of 3D-cyst from unguided protocol for SC102A at week 8 for IBA1 (ionized calcium-binding adapter molecule 1, magenta), CD31 (platelet and endothelial cell adhesion molecule 1, green), VIM (vimentin, yellow) and counter-stained for the nuclei-dye Hoechst (blue). *: lumen within the cystic compartment. Scale bar: 100 µm. (i, ii) Zoom in and 3D-surface rendering. Scale bar: 20 µm.

2.4. Discussion

IBA1$^+$-cells innately develop within retinal organoid differentiation protocol

In this study, we demonstrate that microglia-like cells emerge between week 3 to 4 in 2.5D culture (**Figure 8a**) in an unguided retinal organoid differentiation protocol (Zhong et al. 2014). At this time point, the 2.5D culture is highly heterogeneous and reflects an unperturbed self-organized environment. The properties of EBs in our unguided protocol allow the formation of retinal cell types derived from the neuroectodermal lineage (**Figure 5d**) and mesenchymal cells that are mainly derived from the mesoderm (**Figure 26b, d, Figure 27**). This environment and the time frame is similar to when IBA1$^+$-cells have been reported to appear in human embryonic development (Bloom and Bartelmez 1940; Kelemen and Jánossa 1980; Monier et al. 2007; Rezaie et al. 2005). Our results also support a recent study that identified a cluster of microglial cells using RNA-sequencing of cerebral organoids with bilateral optic vesicles (Gabriel et al. 2021). However, in contrast to human embryonic retinal development (Hu et al. 2019; Mellough et al. 2019) , we rarely observed microglia-like cells in the hIPSC-derived retinal cups at 5 weeks or later (**Figure 7**). Instead, IBA1$^+$-cells strongly preferred the mesenchymal-like cystic- over the neuronal compartment (**Figure 12b-f**).

The ambiguity of TMEM119 expression

A recent study by Shiraki *et al.* reports the occurrence of PAX6-positive microglia-like cells evolved in hIPSC-derived ocular organoids (Shiraki et al. 2022). Their 'SEAM' (self-formed ectodermal autonomous multizone) protocol, which provides the potential to differentiate hiPSCs into anlages of different ocular lineages such as neuroectoderm (zone 1), neural crest (zone 2), ocular-surface ectoderm (zone 3), or non-ocular surface ectoderm (zone 4) (Hayashi et al. 2016, 2017). They found microglia-like cells between zone 2-3 as early as day 10 after the hIPSC differentiation (Shiraki et al. 2022).

The authors have used TMEM119-staining to identify microglia-like cells. However, we are not convinced that the shown TMEM119-positive cells indeed reflect microglia due to their morphology, size, and the ambiguity of TMEM119 also having a role in osteoblast differentiation and bone development (Jiang et al. 2017; Kanamoto et al. 2009; Mizuhashi et al. 2012; Tanaka et al. 2014): When we compared the images of the TMEM119-positive microglia-like population to our IBA1$^+$-cells, we were surprised about the size of more than 200 µm and their highly branched morphology at week 4. Both parameters are rather unusual: First, in the adult human brain tissue, the average size of TMEM119$^+$/IBA1$^+$-immunostained microglia is around 50 µm (**Figure 33a**). Second, in human embryonic brain tissue, the average size of microglia stained with either CD68, IBA1, or CD45 is around 20 µm (Monier et al. 2007; Rezaie and Male 2003). Similarly, our hIPSCs-derived microglia cell diameter ranges from 20 to 100 µm (**Figure 9**, **Figures 16**), which is in line with previous studies (Abud et al. 2017; Douvaras et al. 2017; Haenseler et al. 2017; McQuade et al. 2018; Muffat et al. 2016; Ormel et al. 2018; Pandya et al. 2017; Takata et al. 2017). Finally, we and others identified microglia to typically reflect a more amoeboid or bipolar-shaped morphology during human embryonic development (Cunningham et al. 2013; Diaz-Araya et al. 1995; Monier et al. 2007; Rezaie et al. 2005). We are not aware of another study that shows a similar highly branched microglia-like cell network starting from week 2 as described by Shiraki

et al. 2022. Even in adulthood, individual microglia rarely overlap with their processes (**Figure 10**).

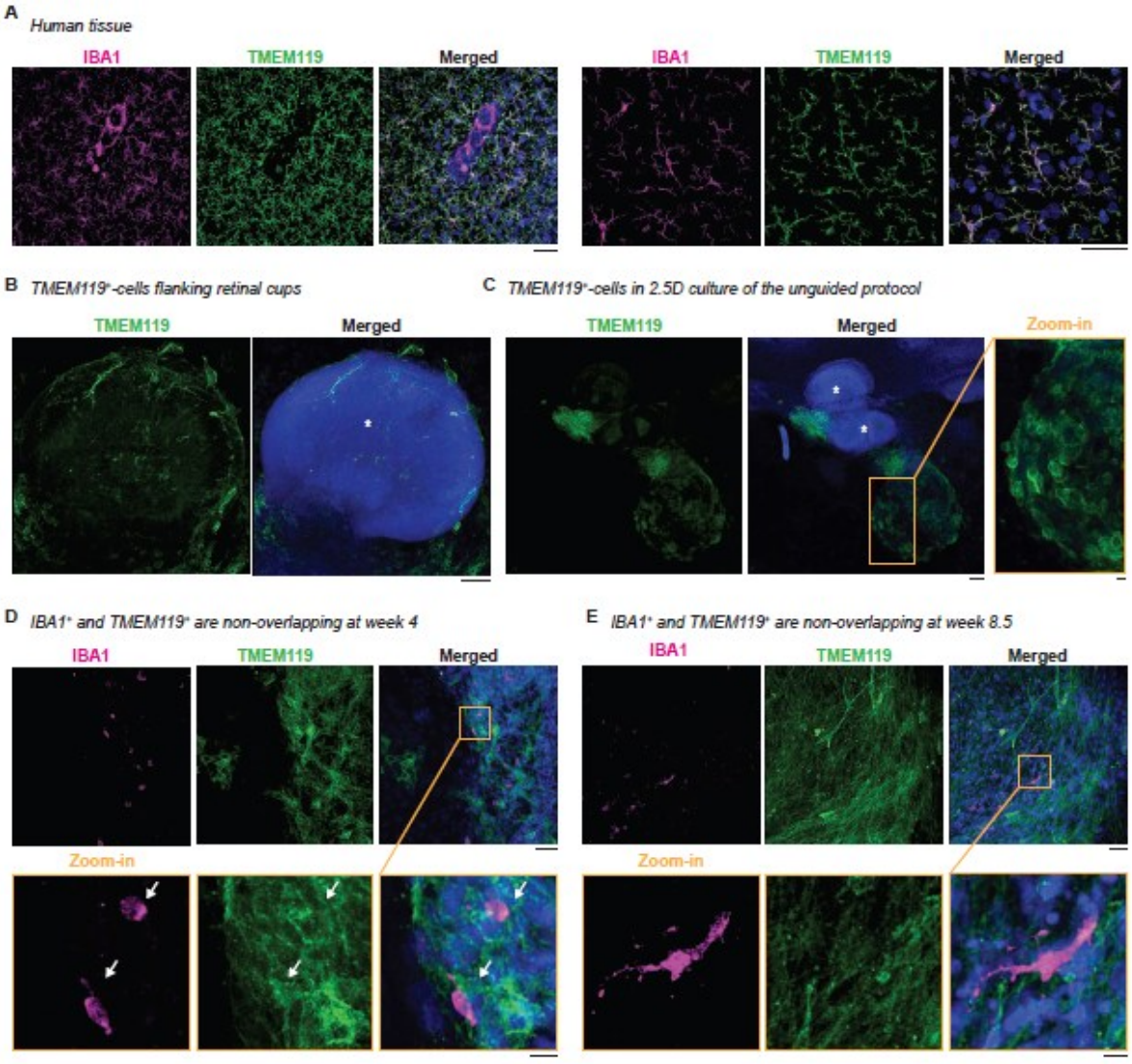

Figure 33 – TMEM119 expression.
Immunostaining for TMEM119 (Transmembrane Protein 119, green), IBA1 (ionized calcium-binding adapter molecule 1, magenta) and the nuclei dye Hoechst (blue). A, Two examples of vibratome sections of adult human temporal lobe. Left example with a blood vessel in a center that does not express TMEM119. Scale bar: 50 µm. B-E, 2.5D culture of unguided protocol from SC102A at week 4.5 (B-D) and week 8.5 (E). White *, cell-dense area. Scale bar: 50 µm. Orange frame: zoom-in with scale bar: 10 µm. Arrows: IBA1+-cell embedded within TMEM119 side but not overlapping.

Therefore, we decided to stain our 2.5D culture for TMEM119 at week 4 to compare the expression pattern with Shiraki *et al.* 2022. TMEM119 accumulated similarly around the retinal cup and the cells showed a radial distribution (**Figure 33b**). The approximate size of TMEM119^{+}-cells is around 200 µm as described in Shiraki *et al.* and rather be atypical for microglia. Moreover, we found that cell type-specific TMEM119 staining also occurred at the 3D-cyst (**Figure 33c**).

In contrast to Shiraki *et al.* 2022, we identified microglia-like cells with IBA1 which is a well-established marker commonly used for hIPSC-derived microglia-like cells (Abud et al. 2017; Douvaras et al. 2017; Haenseler et al. 2017; McQuade et al. 2018; Muffat et al. 2016; Pandya et al. 2017) and has not been used for immunostaining by Shiraki *et al.* 2022. Furthermore, IBA1 has been shown to be highly specific in human embryonic tissue at gestation week 4.5 (Monier et al. 2007). We found the earliest expression of IBA1$^+$-cells between week 3-4 in our 2.5D culture (**Figure 8c**), which is in the line with observations from Ormel *et al.* 2018, who describes the first IBA1$^+$-cells at day 24 (Ormel et al. 2018). Since we have shown that IBA1$^+$-cells specifically enrich at the 3D-cyst, we stained for IBA1. Surprisingly, IBA1$^+$-cells do not overlap with TMEM119 neither at week 4.5 (**Figure 33d**) nor at week 8.5 (**Figure 33e**). Instead TMEM119 and IBA1 labeled distinct cells which were located next to each other. We validated two TMEM119 antibodies (Abcam, ab185333, poly-clonal, binding at the C-terminus, and Novus Biologicals, NBP2-30551, poly-clonal) with the Abcam antibody overlapping the antibody peptide sequence from the Sigma HPA051870 poly-clonal antibody used by Shiraki *et al.* 2022. For both antibodies, we observed the same picture.

TMEM119 has been described as a selective marker for both human and mouse parenchymal microglia/IBA1$^+$-cells (Bennett et al. 2016). However, this assumption has been recently challenged: For example, studies have shown that TMEM119 is neither exclusive to microglia nor does it label all microglia (Satoh et al. 2016; Vankriekelsvenne et al. 2022). Also, the specificity of TMEM119 to microglia-precursors during development is unclear. TMEM119 (type IA single-pass transmembrane protein) is also known as osteoblast induction factor Obif, which has a reported role in osteoblast differentiation and bone development (Jiang et al. 2017; Kanamoto et al. 2009; Mizuhashi et al. 2012; Tanaka et al. 2014). Thus, the observed TMEM119 staining might not necessarily reflect microglia. To validate their microglia-like cells, they represented CD11b (ITGAM) and CX3CR1 which are commonly used for labeling microglia, but both have been also associated to regulate bone homeostasis and osteoblasts (Hoshino et al. 2013; Koizumi et al. 2009; Park-Min et al. 2013), which could potentially explain their TMEM119 co-expression.

The performed qRT-PCR for other microglia markers by Shiraki *et al.* 2022 shows a high standard deviation in the first 2-3 weeks and an overall low expression value suggesting low abundance. Only by week 4, they start to see a stronger signal, which is also the time point where they enrich for CD11b$^+$/CD45$^+$-cells for single-cell RNA sequencing. The switch to enrich for CD11b$^+$/CD45$^+$ and not TMEM119$^+$-cells at week 4 will likely explain their success to find microglia-like transcriptional signature. Week 4 is also the time point when we reliably observed IBA1$^+$-cells (**Figure 8**) and Ormel *et al.* 2018 showed that their microglia express CD11b and CD45.

Thus, we are convinced that the TMEM119 staining in Shiraki *et al.* 2022 does not represent microglia-like cells based on the above outlined discrepancy about the microglia phenotypes, our independently performed TMEM119 staining, and a potential alternative explanation of the role of TMEM119 during development, that might have been overshadowed by the preferential association of TMEM119 being a microglia-selective marker. Future studies will have to investigate whether TMEM119 reflects a human developmental signature gene for early microglia precursor cells.

IBA1^{+}-cells express BAM signature and are enriched in mesenchymal structures

In humans, microglia first enter the embryonic cortical regions via the ventricular lumen, choroid plexus, and leptomeninges (David A. Menassa and Gomez-Nicola 2018; Rezaie and Male 2003) all tissues originating from the mesenchyme (Catala 2019; Lopes 2009; O'Rahilly and Müller 1986). As mesenchymal structures develop *in vivo* around the neuronal retina with the choroid close to the photoreceptors and meninges wrapping the optic nerve (Forrester et al. 2010; Sturrock 1987), the preferential location of our IBA1^{+}-cells in the mesenchymal region potentially recapitulates how microglia enter the retina. The CD163 expression of IBA1^{+}-cells further supports a perivascular-associated role. Initially, parenchymal microglia and border-associated macrophages are derived *in vivo* from the same primitive macrophage (Goldmann, Wieghofer, Prutek, et al. 2016) and then adapt their transcriptional landscape to their local environment at early developmental stages (Gosselin et al. 2017; Masuda et al. 2019; Utz et al. 2020). CD163 is one example of a human border-associated- (perivascular, leptomeningeal, choroid plexus) macrophage marker (Fabriek et al. 2005; Rezaie and Male 2003), and its expression is upregulated during mouse embryonic development (Utz et al. 2020). Indeed, our IBA1^{+}-cells in the 2.5D culture arose as CD163 negative and express CD163 after one week (**Figure 30**).

However, it remains unclear why IBA1^{+}-cells do not further infiltrate the neuronal compartment especially when 3D-aggregates contain both retinal cups and cystic compartments (**Figure 12a**/iii, **12e**). Even if we transferred 3D-retinal organoids to 2.5D cultures of BMP4-guided protocol, IBA1^{+}-cells favor the cystic- over the neuronal compartment (**Figure 28-29**). It is possible that the cystic compartment releases guidance signals that attract IBA1^{+}-cells. These cues are likely to be similar to those that recruit macrophages to the epithelial-mesenchymal transition sides in glioma (Song et al. 2017). There is limited knowledge about developmental guidance cues that attract microglia to the neuronal compartment and more specifically to the retina. Further investigation will be required to answer these questions.

2.5. Conclusion

In summary, our study confirms that microglia-like cells occur within the unguided retinal organoid differentiation protocol and preferentially occupy mesenchymal region. These findings will allow future analysis of microglial migration in complex tissue environments and facilitate identification of mechanistic cues that attract microglia in complex tissue structures.

2.6. Limitation

A possible limitation in our study is that we employed two hIPSC lines from different origins and both resulted in a similar phenotype. We cannot exclude that the qualitative outcome could be different for other hIPSC lines due to properties related to genetic origin, epigenetic landscape, or transcriptional state at the time of the differentiation (Kilpinen et al. 2017; Ortmann and Vallier 2017). Such factors might prevent the generation of cystic compartments and therefore the appearance of microglia-like cells.

3. CHAPTER 2 | Microglia determine an immune-challenged environment and facilitate ibuprofen action in human retinal organoids.

Chapter 2 is based on the following publication:

Schmied, V., Korkut-Demirbaş, M., Venturino, A., Maya-Arteaga, J.P., and Siegert, S. (2025). Microglia determine an immune-challenged environment and facilitate ibuprofen action in human retinal organoids. J Neuroinflammation *22*, 98. https://doi.org/10.1186/s12974-025-03366-x.

3.1. Keywords

Human induced pluripotent stem cells, retinal organoid, microglia, prenatal, neuro-immune challenge, POLY(I:C), ibuprofen, prostaglandin, COX1, PTGS1, TORCH

3.2. Introduction

Prenatal exposure to infections can be detrimental to human embryonic development (Auriti et al. 2021; Meyer 2019). Certain infectious diseases like rubella belonging to the TORCH complex (Toxoplasmosis, Others, Rubella, Cytomegalovirus, Herpes) can be vertically transmitted from pregnant women to their fetus, resulting in malformations of the fetal brain and eye (Campos et al. 2020; Dudgeon 1967; Thompson et al. 2016; Töndury and Smith 1966). Medication is recommended to a certain degree to treat inflammatory symptoms during pregnancy, but there are significant knowledge gaps on the effects of anti-inflammatory drugs on embryonic development (Stock and Norman 2019).

Brain organoids derived from human induced pluripotent stem cells (hIPSCs) provide a unique strategy to investigate the consequences of prenatal inflammation, which we refer to as neuro-immune challenge, and drug exposure to this environment. Specifically, retinal organoids are one of the first established brain region-specific models (Eiraku et al. 2011). Their developmental trajectories and cytoarchitecture are well-defined (Cowan et al. 2020; Zhong et al. 2014) and match anatomical observations in human fetal retinal development, like the formation of the ganglion cell layer and the outer plexiform layer (OPL) (Gupta et al. 2016). At the same time, neuroectodermal-derived organoids commonly lack mesodermal-derived brain-resident macrophages (Bian et al. 2020), which colonize the human fetal brain and eye between gestation week (GW) 4.5 and 5 (Hu et al. 2019; Monier et al. 2007). Once in the neuronal environment, these microglia have multifunctional developmental tasks demonstrated in the rodent nervous system. They regulate, amongst others, the number of neural precursor cells (Cunningham et al. 2013; Loayza et al. 2022), axonal outgrowth and neuronal wiring (Squarzoni et al. 2014), as well as synaptogenesis and pruning (Paolicelli et al. 2011; Schafer et al. 2012) across various brain regions (Anderson et al. 2019; Burger et al. 2020; Kuse et al. 2018; Miyamoto et al. 2016). Microglia maintenance and survival depend on the colony-stimulating factor 1 receptor (CSF1R) (Elmore et al. 2014; Greter et al. 2012; Wang et al. 2012) , which, when inhibited, affects the total number of neurons and the macroglia cell populations consisting of astrocytes, oligodendrocytes and also their migration, distribution, and the functional connectivity (Anderson et al. 2019; Arnò

et al. 2014; Erblich et al. 2011; Marsters et al. 2020; Rosin et al. 2021; Squarzoni et al. 2014). Embryonic death and brain malformation have been reported in humans harboring homozygous mutations within the CSF1R genome (Guo et al. 2019; Oosterhof et al. 2019).

In recent years, protocols have been developed to generate hIPSC-derived microglia precursor cells (preMG), which acquire microglia-like cell (iMG) properties once integrated into neuroectodermal tissue and exposed to the environmental cues (Abud et al. 2017; Bartalska et al. 2022; Guttikonda et al. 2021; Haenseler et al. 2017; Park et al. 2023; Takata et al. 2017). Recent studies demonstrate that iMG promote brain organoid maturation (Park et al. 2023) and fine-tune their neuronal environment at the cellular and synaptic levels (Chichagova et al. 2023; Gao et al. 2022; Usui-Ouchi et al. 2023) Thus, microglia integration seems relevant to mimic *in vivo* human brain development.

Human cerebral organoids have been used to model the consequences of TORCH viruses such as Zika, and a reduction in neuronal progenitor numbers (Dang et al. 2016; Garcez et al. 2016; Krenn et al. 2021; Su et al. 2021; Xu et al. 2019). However, due to the lack of microglia in these studies, our insights into the inflammatory response and its consequences on human embryonic development are limited. Microglia are susceptible to environmental cues beyond pathogens (Bsibsi et al. 2002), including inflammatory mediators such as cytokines and chemokines (Chhor et al. 2013; Hanisch and Kettenmann 2007; Lively and Schlichter 2018). In rodent models, prenatal neuro-immune challenges induce microglia to express receptors to sense pathogens and inflammatory mediators (Ostrem et al. 2024) and affect microglia properties such as morphology, motility, and their actual number (He et al. 2021; Loayza et al. 2022; Ozaki et al. 2020; Pratt et al. 2013; Squarzoni et al. 2014). In parallel, these immune challenges also affect neurogenesis (Cunningham et al. 2013; Kuse et al. 2018; Loayza et al. 2022), neuronal differentiation (Ben-Reuven and Reiner 2019), synaptogenesis (Forrest et al. 2012; Giovanoli et al. 2016), and synaptic pruning (Andoh et al. 2019; Coiro et al. 2015), to which microglia regularly contribute. Although microglia are critical to sense and adopt a response against infectious agents (Hanisch & Kettenmann, 2007) their impact on the neuronal organization and connectivity in an inflammatory environment and the consequences of an anti-inflammatory treatment are poorly understood.

Here, we mimicked a prenatal neuro-immune challenged environment and subsequent treatment with the non-steroidal anti-inflammatory drug (NSAID) ibuprofen in microglia-assembled retinal organoids (iMG-$_{3D}$RO). After we identified the optimal time-point to investigate microglia-neuron interaction in the hIPSC-derived 3D-retinal organoid ($_{3D}$RO) [60], we developed a 2D-model system ($_{diss}$RO) that mimics the retinal development the closest (Diaz-Araya et al. 1995) and counteracts the previously reported ganglion cell loss in $_{3D}$RO (Cowan et al. 2020; Fligor et al. 2021; Wagstaff et al. 2021). This model also circumvents known challenges of organoid-to-organoid variability in size, shape, and cell type composition (Capowski et al. 2019; Cowan et al. 2020; Hallam et al. 2018), as well as diffusion biases of drugs. In this iMG-$_{diss}$RO model, iMG actively interact with and phagocytose retinal ganglion cells as anticipated (Cowan et al. 2020; Fligor et al. 2021; Wagstaff et al. 2021).

We then modeled a prenatal neuro-immune challenge by exposing the culture to the immunostimulant *polyinosinic: polycytidylic acid* (POLY(I:C)), which mimics a viral-mediated

response and activates the toll-like receptor 3 (TLR3) (Alexopoulou et al. 2001). TLR3 stimulation induces a downstream signaling cascade involving NFkB- and interferon pathways, resulting in cytokines and chemokines release (Bsibsi et al. 2002; Kawai and Akira 2010; Matsumoto and Seya 2008).

Furthermore, POLY(I:C) directly acts on microglia as they upregulate TLR3 mRNA expression (Town et al. 2006). We investigated the consequences of POLY(I:C)-mediated immune challenge in our iMG-$_{diss}$RO model and identified a microglia-dependent inflammatory signature and increased retinal cell proliferation. To evaluate the effects of anti-inflammatory drugs on the identified consequences, we focused on the NSAID ibuprofen, which can be taken cautiously during the first half of the pregnancy (Schaefer et al. 2012). Ibuprofen targets cyclooxygenase 1 and 2 (*PTGS1*/COX1, *PTGS2*/COX2, respectively) and prevents arachidonic acid conversion into prostaglandins like PGE2 (Griswold and Adams 1996; Kato et al. 2010). In the presence of ibuprofen, POLY(I:C)-mediated effects on microglia were dampened, and the neuronal phenotypes were restored. Yet, this beneficial effect depended on *PTGS1* expressed by iMG since ibuprofen did not show this rescue in cultures without iMG.

Our study highlights the interplay of human microglia with neurons during normal development, under prenatal neuro-immune challenges, and after anti-inflammatory drug exposure. Across all three conditions, we identified microglia-dependent phenotypes, emphasizing their significance. In light of future clinical drug tests in organoid models and known species-specific differences in microglial gene signature associated with immune response and neurodegenerative diseases (Geirsdottir et al. 2019; Sabogal-Guáqueta et al. 2023), microglia contribution cannot be excluded from experiments.

3.3. Material and Methods

Ethical approval

The ISTA Ethics Officer and Ethics Committee approved the usage of human induced pluripotent stem cells (hIPSC).

Cell lines

We used two human induced pluripotent stem cell lines (hIPSC): SC 102A-1 GVO-SBI Human Fibroblast-derived (feeder-free) IPSC line (BioCat; hPSCreg.eu: SBLi006-A; in this study referred to SC102A) and the human fibroblast-derived IPSC line 01F49i-N-B7 (Renner lab (Cowan et al. 2020), in this study referred to F49B7). For more details, see (**Table 5**).

Table 5 – Overview of human induced pluripotent stem lines included in chapter 2.
hPSCreg.eu, human pluripotent stem cell registry. MYC, MYC proto-oncogene. KLF4, kruppel-like factor 4. Large T antigen, large tumor antigen. LIN28, zinc finger CCHC domain-containing protein. OCT4 (octamer-Binding Protein 4)/ POU5F1 (POU domain, class 5, transcription factor 1). SOX2, sex-determining region Y-box 2. SV40, simian-virus 40.

Cell line	SC 102A-1	01F49i-N-B7
hPSCreg.eu	SBLi006-A	
Company	BioCat	
Generator	SYSTEM BIOSCIENCES	Institute of Molecular and Clinical Ophthalmology Basel; Cowan et al 2020, Cell
Abbreviation within manuscript	SC102A	F49B7
Source	Fibroblast (dermis)	Fibroblast
Vector	Retrovirus (integrating)	Sendai virus
Genes for reprogramming	MYC, KLF4, SOX2, OCT4/POU5F1	Oct3/4, Sox2, Klf4, and cMyc
Health status	Healthy	unknown
Race	Caucasian	unknown
Sex	Male	Female
Donor age	60-64	

Cell culture and human induced pluripotent stem cells

Matrigel coating. Matrigel (Corning® Matrigel® hESC-Qualified Matrix, *LDEV-Free, Corning, #354277) was used according to the manufacturer protocol with the following modifications: Matrigel aliquots were dissolved in ice-cold X-Vivo 10 chemically defined, serum-free hematopoietic cell medium (Lonza, #BE04-380Q). Dishes were coated for 1 hour at room temperature.

Maintenance of human induced pluripotent stem cells (hIPSCs). hIPSCs were maintained in mTeSR1 medium (STEMCELL Technologies, #85850) on Matrigel-(Corning, #354277) coated 6-well plates (Corning, #3516) cultured at 37ºC and 5% CO_2 in a humidified incubator (BINDER C150). Before reaching 80% confluency, hIPSCs were passaged as small aggregates every 3-4 days using EDTA dissociation buffer composed of 0.5M EDTA (ethylenediaminetetraacetic acid, K.D. Biomedical, #RGF 3130), 0.9 g (w/v) NaCl (Sigma, #5886) in PBS (phosphate buffered saline, calcium/magnesium-free, Invitrogen, #14190), sterile filtered and stored at 4ºC according to

(Chen 2014). The ISTA Molecular Biology Facility regularly tested hIPSCs for mycoplasma using the Multiplex qPCR assay – 16S DNA-according to (Janetzko et al. 2014).

Freezing and thawing of hIPSCs. For freezing, hIPSCs were washed once with DPBS (Thermo Fisher Scientific, #14190250), incubated in EDTA dissociation buffer for 2.5 minutes, detached as small aggregates using mFReezer (STEMCELL Technologies, #05854), and frozen at -80°C. For long-term storage, hIPSCs aliquots were transferred to liquid nitrogen. For thawing, hIPSCs were removed from liquid nitrogen and quickly thawed in a bead bath at 37°C. hIPSCs were transferred into a falcon tube containing mTesR1 medium. The cells were centrifuged (VWR, Mega Star 3.0R) at 200×g for 3 minutes, then resuspended in mTesR1 medium and transferred into one well of a Matrigel-coated 6-well plate.

Generation of tdTomato expressing hIPSC lines. To generate ubiquitous tdTomato expressing hIPSC lines, a reporter construct encoding tdTomato under the constitutive enhancer/β-actin (CAG) promoter (2xCHS4-CAG-tdTomato-SV40-2xCHS4, gift from the Knoblich lab (Bagley et al. 2017) was inserted into the safe-harbor AAVS1 locus. A CRISPR/CAS9 approach was used, as previously described (Oceguera-Yanez et al. 2016). For nucleofection, 80% confluent hIPSCs were dissociated into single-cell suspension using Accutase (Merck, #SCR005) treatment for 4 minutes. Cells were collected, centrifuged (VWR, Mega Star 3.0R) at 200×g for 3 minutes, and resuspended in mTeSR1 medium supplemented with 10 µM ROCK inhibitor (Y-27632, STEMCELL Technologies #72307). The Human Stem Cell NucleofectorTM Kit 1 (Lonza, #VPH-5012) was applied using 1 million hIPSCs, 3 µg donor plasmid DNA, and 1 ug CRISPR/CAS9 guideRNA (pXAT2 plasmid, Addgene: #80494). After nucleofection, hIPSCs were distributed on six wells of a Matrigel-coated 6-well plate. Colonies from single cells were grown for 5-6 days in mTeSR1 medium. Then, tdTomato expressing hIPSCs were isolated using fluorescent activated cell sorting (FACS, Sony, SH800SFP). Therefore, transfected hIPSCs were collected using Accutase treatment for 4 minutes, centrifuged at 200g for 3 minutes, and resuspended in mTesR1 medium supplemented with 10 µM ROCK inhibitor. Using a 100 µm nozzle, 10.000 hIPSCs were sorted and distributed on three wells of a Matrigel-coated 6-well plate. After 4-5 days, 20 to 30 colonies, which were well separated from one another and evenly expressed tdTomato, were identified using an EVOS imaging system (Thermo Fisher Scientific). Identified colonies were manually picked with a 200 µL tip, transferred into a Matrigel-coated 96-well plate, and cultured in mTesR1 medium. The colonies were expanded into 24- (Corning, #3527), 12- (Corning, #3512), and 6-well plates (Corning, #3516). For passaging, refer to "*Maintenance of human induced pluripotent stem cells (hIPSCs)".*

Validation of tdTomato expressing hIPSC lines. Half of the hIPSCs were collected for genotyping when splitting colonies from a 24-well plate to a 12-well plate. DNA was extracted using the DNeasy Blood and Tissue kit (QIAGEN, #69504). All reactions were performed using Q5 Hot Start High Fidelity 2x Master Mix (NEB, #M0494S) with 50 -100 ng of template DNA per reaction. PCR was performed using the following primers to identify whether the insertion was heterozygous or homozygous: AAVS1_FWD: 5'-TCGACTTCCCCTCTTCCGATG-3', AAVS1_WT_REV 5'-CTCAGGTTCTGGGAGAGGGTAG-3' and AAVS1_Insert_REV 5'-GAGCCTAGGGCCGGGATTCTC -3'as described previously (Oceguera-Yanez et al. 2016). The size of PCR products was analyzed by gel electrophoresis (wildtype allele 1.4 kbp and target allele 1.2 kbp). Clones with correctly targeted homozygous insertions were expanded.

Differentiation of retinal organoids, astrocytes, and microglia precursor cells

***Retinal organoid differentiation*.** 3D-retinal organoids were generated as described with the following modifications (Cowan et al. 2020; Zhong et al. 2014): On day 0 of the differentiation, colonies of the hIPSC line F49B7 from two wells of a 6-well plate were cut into evenly sized aggregates using a cell-passaging tool (Thermo Fisher Scientific, #23181-010). After detaching, floating aggregates were transferred with a 1250 µL wide orifice pipette (VWR, #613-0737) into one 9-cm Petri dish (Sarstedt, #82.1473), and cultured in mTeSR1 medium supplemented with 10 µM blebbistatin (Sigma, #B0560-5MG). On day 1, 2, and 3, the medium was gradually exchanged with ¼, ½, and 1, respectively, to NIM (neural induction medium: DMEM/F12 (Gibco, #31331-028), 1×N2-supplement (Gibco, #17502-48), 1% (v/v) NEAA Solution (Sigma, #M7145), 2 µg/mL heparin (Sigma, #H3149-50KU)). From day 4 onwards, 10 mL NIM was changed daily. On day 8, embryoid bodies (EB) were equally distributed onto 8 Matrigel-coated 6-cm dish plates (Corning, #3516) (approximately 20-40 number of EBs/cm^2) and cultured in 3 mL NIM. From day 16 onwards, NIM was replaced to 3:1-medium consisting of 3 parts DMEM (Thermo Fisher Scientific, #31966047) and one-part F12 medium (Ham's F-12 Nutrient Mix, Thermo Fisher Scientific, #31765-027) supplemented with 2% (v/v) B27 without vitamin A (Thermo Fisher Scientific, #121587-10), 1% (v/v) NEAA solution (Sigma, #M7145), 1% (v/v) penicillin-streptomycin (Thermo Fisher Scientific, #15140122). Media was changed daily. On day 30, optic-cup structures were detached from the 6-cm plate by checkerboard scraping using a 200 µL pipette tip and transferred into a 9-cm Petri dish containing 10 mL 3:1-medium. The medium was changed twice per week. Between D36 and D42, retinal structures displaying a bright stratified neuroepithelium were manually picked using an EVOS imaging system (Thermo Fisher Scientific). 3D-retinal organoids were not dissected to remove non-retinal tissue. From day 42 onwards, 3:1-medium was supplemented with 10% (v/v) heat-inactivated FBS (Thermo Fisher Scientific, #10270-106) and 100 µM taurine (Sigma, #T0625- 25G). The medium was changed twice per week. From week 10, 1 µM retinoic acid was added daily (Sigma, #R2625) while the medium was changed twice per week. From week 14, 3D-retinal organoids were cultured in N2-medium consisting of 3 parts DMEM (Thermo Fisher Scientific, #31966047) and one-part F12 medium (Ham's F-12 Nutrient Mix, Thermo Fisher Scientific, #31765-027) supplemented with 1×N2 supplement (Gibco, #17502-48), 1% (v/v) NEAA solution (Sigma, #M7145), 1% (v/v) penicillin-streptomycin (Thermo Fisher Scientific, #15140122), 10% (v/v) heat-inactivated FBS (Thermo Fisher Scientific, #10270-106), and 100 µM taurine (Sigma, #T0625- 25G). The retinoic acid concentration was reduced to 0.5 µM and added daily. Organoids were cultured at 37ºC and 5% CO_2 in a humidified incubator (BINDER C150).

Microglia precursor cell differentiation. The differentiation protocol is identical to the "*Retinal organoid differentiation*" section with the following modifications: 2 wells of the hIPSC line tdTomato-SC102A were used to start the differentiation. On day 1, a final concentration of 12.5 ng/mL recombinant human BMP4 (Bone Morphogenetic Protein 4, Peprotech, #120-05) was added to the medium. From day 8 onwards, NIM was changed twice per week. From day 16 until the termination of the differentiation, cultures were maintained in 3:1-medium, with the medium changed twice per week.

Harvesting microglia precursor cells (preMG). From day 36 onwards, preMG were harvested from the supernatant. For this, the supernatant was passed through a 100 µm cell strainer (Corning, ##352360) and collected in a falcon. After centrifugation (VWR, Mega Star 3.0R) at 200g

for 3 minutes, the medium was aspirated, and preMG were resuspended in 3:1-medium supplemented with 50 ng/mL recombinant human MCSF (Macrophage Colony Stimulating Factor, BioLegend, #574804). Cells were counted using an automated cell counter (Bio-Rad, #1450102).

***Neural Progenitor cell (NPC) differentiation*.** According to the manufacturer's instructions, neuronal progenitor cells (NPCs) were generated using the STEMdiff™ SMADi Neural Induction Kit (STEMCELL Technologies, #08581). NPCs were expanded in STEMdiff™ Neural Progenitor Medium (STEMCELL Technologies, #05833) and frozen in STEMdiff™ Neural Progenitor Freezing Medium (STEMCELL Technologies, #05838). NPCs were passaged at 1.25×10^5 cells/cm^2 weekly with Accutase™ (STEMCELL Technologies, #07920).

***Astrocyte differentiation*.** Astrocytes were differentiated as described previously (TCW et al. 2017) with minor modifications. For astrocyte differentiation, NPCs were dissociated into single cells using Accutase™ (STEMCELL Technologies, #07920) treatment for 5-10 minutes. Cells were centrifuged at 400×g for 5 minutes (VWR, Mega Star 3.0R), and the medium was aspirated. Cells were resuspended in complete astrocyte-medium composed of astrocyte medium (Sciencell, #1801-b), 2% (v/v) heat-inactivated FBS (Thermo Fisher Scientific, #10270-106), 1% (v/v) astrocyte growth supplement (Sciencell, #1852) and 1% (v/v) penicillin-streptomycin (Thermo Fisher Scientific, #15140122). 1.5×10^5 cells were seeded per well of Matrigel-coated 6-well plates (Corning, #3516). Cells were cultured for 30 days for astrocyte maturation, and the medium was changed every second day. Cells were passaged before reaching 80-90% confluency once per week. Following the initial 30-day differentiation period, astrocytes were maintained in serum-free astrocytes-medium. Before stimulation, the astrocyte medium was changed gradually to N2-medium over four days.

Generating microglia-assembled retinal organoids (iMG-$_{3D}$RO). 3D-retinal organoids ($_{3D}$RO) were individually placed into 1.5 mL tubes (Roth, #1KP0.1), each containing 500 µL medium (either supplemented 3:1-medium or N2-medium depending on the age of the differentiation). preMG were collected as described in "Harvesting microglia precursor cells (preMG)," and 6×10^4 cells were added to each organoid. After 72 hours, 6-8 organoids were pooled into one well of a 24-well plate (Corning, #3527) and cultured in the respective medium supplemented with 50 ng/mL MCSF for three weeks. Media was exchanged twice per week, and retinoic acid was added daily. Cultures were maintained at 37ºC and 5% CO_2 in a humidified incubator (BINDER C150).

Generation of dissociated retinal organoid cultures

Retinal cup dissociation and 2D plating. At day 105, four 3D-retinal organoids were dissected to remove non-retinal tissue using a scalpel (Fisher Scientific, #11798343), transferred into a 1.5 mL tube, and washed twice in DPBS (Thermo Fisher Scientific, #14190250) (**Table 6**). Organoids were incubated in Accutase (STEMCELL Technologies, #07920) for 30 minutes at 37°C. Then, an equal volume of HBSS (Thermo Fisher Scientific, #14175-129) supplemented with 10% (v/v) heat-inactivated FBS (Thermo Fisher Scientific #10270106) was added, and organoids were dissociated by pipetting up and down ten times using a 200 µL tip. Cells were centrifuged at 3.2×g (VWR, Micro Star 17) for 2 minutes, the medium aspirated, and cells resuspended in N2-medium. Following another centrifugation at 3.2×g for 2 minutes, cells were resuspended in N2-medium supplemented with 20 ng/mL BDNF (Brain-Derived Neurotrophic Factor, Biolegend, #788904), passed through a 70 µm cell strainer (Corning, #352350), and distributed in 6 wells of a Matrigel-

coated 8-well chamber (IBIDI, #80826). N2-medium supplemented with 20 ng/mL BDNF was changed every 3-4 days. 0.5 µM retinoic acid was added daily.

***Integrating microglia precursor cells into dissociated retinal organoids*.** At day 130, preMG were harvested as described in "Harvesting microglia precursor cells (preMG)," and 6×10^4 cells were added per well of an 8-well chamber (**Table 6**). Cultures with and without microglia were maintained in N2-medium supplemented with 20 ng/mL BDNF and 50 ng/mL MCSF. Medium was exchanged every 3-4 days, and 0.5 µM retinoic acid was added daily.

Table 6 – Important numbers depending on plate-format.

Plate	Surface area	Retinal cups/ well	preMG/ well
8 well IBIDI	1 cm^2	0.75	60.000
24 well	1.9 cm^2	1.5	125.000
12 well	3.5 cm^2	3	250.000

Stimulation paradigms

POLY(I:C) (Tocris, #4287) was diluted in fresh medium with a final concentration of 50 µg/mL and then applied to the cells as indicated in the experiments. For POLY(I:C), POLY(I:C)+IBU, or POLY(I:C) and SC-560, 50 µg/mL POLY(I:C) was mixed with 400 µM of the active enantiomere S(+)-ibuprofen (Sigma-Aldrich, #375160-1G) or with 20nM SC-560 (Abcam, # ab120649) in fresh medium and applied to the cells.

***For microglia precursor cells to assay gene expression*.** preMG were harvested as described "Harvesting microglia precursor cells (preMG)," and 2×10^5 cells were transferred into one well of a 24-well (Corning, #3527) containing 3:1-medium supplemented with 50 ng/mL MCSF. After 24h, the medium was replaced, and preMG were treated as described above. Untreated controls received 3:1-medium supplemented with 50 ng/mL MCSF. preMG were incubated for 24 hours at 37°C and 5% CO_2. Four distinct cultures of independent differentiations were analyzed per condition.

For differentiated astrocytes. 80% confluent astrocyte cultures were stimulated as described above. Three distinct cultures of independent differentiations were analyzed per condition.

For assembled dissociated retinal organoids ($_{diss}$RO) with and without microglia. At week 20 (D139), N2-medium supplemented with 50 ng/mL MCSF was changed. We omitted the BDNF application because it has been shown to have anti-inflammatory effects [17,18]. The withdrawal did not significantly alter ganglion cell survival (data not shown).

For each condition, one well of $_{diss}$RO and iMG-$_{diss}$RO were treated for 24 hours as described above. Untreated controls received medium supplemented with 50 ng/mL MCSF. Five distinct cultures of independent differentiations were analyzed per condition.

***For retinal organoids*.** At week 20 (D139), three 3D-retinal organoids were transferred into one well of a 24-well plate per condition and cultured in N2-medium supplemented with 50 ng/mL MCSF. $_{3D}$ROs in parallel to iMG-$_{3D}$ROs were treated as described above. Untreated controls received N2-medium supplemented with 50 ng/mL MCSF. Organoids were incubated for 24 hours at 37°C and 5% CO_2. Five distinct cultures of independent differentiations were analyzed per condition.

For CCL2 stimulation. At week 20 (D139), N2-medium supplemented with 50 ng/mL MCSF was changed, and BDNF was withdrawn from the medium. For each condition, one well of $_{diss}$RO and iMG-$_{diss}$RO were treated with recombinant human CCL2 (C-C Motif Chemokine Ligand 2, Peprotech, #300-04) at a final concentration of 10 ng/mL, 20 ng/mL, or 50 ng/mL. Untreated controls received N2-medium supplemented with 50 ng/mL MCSF. Five distinct cultures of independent differentiations were analyzed per condition.

Gene expression profile of microglia marker and inflammatory cytokines

Cultures to determine iMG marker. Cultures were prepared as described in the sections "Retinal cup dissociation and 2D plating" and "Integrating microglia precursor cells into dissociated retinal organoids" with the following modification: Samples were grown in 24-well plates. The number of integrated iMG was constant between 1 and 10 days of co-culture (data not shown).

***RNA isolation*.** Samples were washed with DPBS (Thermo Fisher Scientific, #14190250) before RNA isolation using the innuPREP RNA Mini Kit 2.0 (Analytik-Jena, #845-KS-2040050) as described in the manufacturer's instructions. cDNA synthesis was performed with LunaScript RT SuperMix Kit (New England Biolabs, #E3010L) with a total RNA amount of 200-800 ng (same amount for each condition within experimental repetition) and stored at -20°C.

Gene expression analysis. RT-qPCR (Luna Universal qPCR Master Mix, New England BioLabs, #M3003L) was performed in 384-well plates (Bio-Rad; HSR4805) using the Roche Lightcycler 480 applying the device's "Second Derivative Maximum Method." The total reaction volume was 10 µL containing 1 µL of 1:10 diluted cDNA. The final concentration for each primer was 0.25 µM. The primer pairs are listed in **Table 7**. Cycle conditions were 60 s at 95 °C for initial denaturation, followed by 40 cycles of denaturation (15 s; 95 °C) and annealing/extension (30 s; 60 °C). Each run was completed with a melting curve analysis to confirm the amplification of only one amplicon. Each PCR reaction was run in triplicates, from which a mean Cq value was calculated and used for further analysis. dCq values were obtained by normalizing mean Cq values to the geometric mean of four reference genes (GAPDH, ACTB, OAZ1, RPL27) measured within the same sample [equation 1]. ddCq values were then calculated by normalizing dCq values to the respective control condition (untreated cells/organoids) within each experimental repetition [equation2]. Fold changes were obtained by transforming ddCq values from log2 to linear scale [equation 3].

Equations for consecutive RT-qPCR normalization:

$$_{d}Cq = \text{geometric mean}_{\text{reference genes}} - Cq \quad (1)$$

$$_{dd}Cq = {}_{d}Cq - {}_{d}Cq_{control} \quad (2)$$

$$\text{Fold change} = 2^{ddCq} \quad (3)$$

To analyze the mRNA expression relative to GAPDH, dCq values were normalized to GAPDH dCq values in the respective conditions.

Table 7 – Primer sequences used for chapter 2.

Target	Gene	Primer pair	Primer sequence 5'-3'
House keeping genes	**OAZ1**	Forward	AGGACAGCTTTGCAGTTCTC
		Reverse	CGGTTCTTGTGGAAGCAAATG
	GAPDH	Forward	GTCTCCTCTGACTTCAACAGCG
		Reverse	ACCACCCTGTTGCTGTAGCCAA
	ACTB	Forward	CACCATTGGCAATGAGCGGTTC
		Reverse	AGGTCTTTGCGGATGTCCACGT
	RPL27	Forward	ATCGCCAAGAGATCAAAGATAA
		Reverse	TCTGAAGACATCCTTATTGACG
Gene of interest	**PTGS1**	Forward	GATGAGCAGCTTTTCCAGACGAC
		Reverse	AACTGGACACCGAACAGCAGCT
	PTGS2	Forward	CCCTTCTGCCTGACACCTTT
		Reverse	TTCTGTACTGCGGGTGGAAC
	TLR3	Forward	CCTTTTGCCCTTTGGGATGC
		Reverse	TGAAGTTGGCGGCTGGTAAT
	C1Qa	Forward	GTGACACATGCTCTAAGAAG
		Reverse	GACTCTTAAGCACTGGATTG
	CX3CR1	Forward	CTTACGATGGCACCCAGTGA
		Reverse	CAAGGCAGTCCAGGAGAGTT
	HEXB	Forward	TTAGCTCGGCTCCTCGCTTC
		Reverse	TCGGGAGCTTCGACTAGAGG
	MERTK	Forward	AGGACTTCCTCACTTTACTAAG
		Reverse	TGAACCCAGAAAATGTTGAC
	P2RY12	Forward	GATGCCACTCTGCAGGTTG
		Reverse	GTGCACAGACTGGTGTTACC
	SALL1	Forward	ACCTTCTCCTCATCGAGTGC
		Reverse	GCTATTCCACATGTGAGTGCC
	TMEM119	Forward	CACGGACTCTCTCTTCCAG
		Reverse	GCAGCAACAGAAGGATGAGG

Proteome profiler array

Cultures were prepared as described in the sections “Retinal cup dissociation and 2D plating” and “Integrating microglia precursor cells into dissociated retinal organoids” with the following modification: Since samples were grown in 12-well plates, three retinal cups were dissociated per well, and 2.5×10^5 preMG were added per well. Cultures were stimulated as described in “Stimulating microglia assembled dissociated retinal organoids”.

Human cytokine array. After two, four, or 24h of stimulation, the supernatant was harvested, snap-frozen on dry ice, and stored at -80°C. The Proteome Profiler Human Cytokine Array Kit (R&D Systems, #ARY005B) was performed following the manufacturer’s instructions. The membranes were imaged using the luminescent image analyzer Amersham Imager 600 (GE Healthcare Bio-Science). For the 24-hour time point, the supernatant from three distinct cultures of independent differentiations was assayed. Only one supernatant from one differentiation was screened for the two and four-hour time points.

Analysis of proteome profiler array. Pixel densities for positive signals were extracted using the ImageJ plugin ‘Protein Array Analyzer’ (https://imagej.nih.gov/ij/macros/toolsets/Protein%20Array%20Analyzer.txt). For each experimental condition, the average signals were determined per protein-of-interest, background signal subtracted, and signals normalized to the mean of six reference spots per membrane. Hierarchical clustering of the median (24h time point) of normalized pixel values was carried out using the *pheatmap* package (version 1.0.12, RRID: SCR_016418) in R (version version 4.2.2). Fold changes were obtained by normalizing relative pixel values to the control condition.

ELISA

Cultures were stimulated as described in “Stimulating microglia assembled dissociated retinal organoids” or “*Stimulating retinal organoids*.” After 24 hours of stimulation, the supernatant was harvested, snap-frozen on dry ice, and stored at -80°C. PGE2 ELISA (Enzo Life Sciences, #ADI-900-001) was performed according to the manufacturer’s instructions. Samples were analyzed in duplicates, and PGE2 concentration was determined based on the standard curve. The supernatant from three distinct cultures of independent differentiations was assayed.

Histology

Fixation of 3D-retinal organoids. 3D-retinal organoids were fixed in 4% (w/v) PFA (Paraformaldehyde, Thermo Fisher Scientific, #28908) in PBS for 25 minutes at room temperature on an orbital shaker in the dark. Then, organoids were washed three times with PBS at room temperature and cryopreserved in 30% (w/v) sucrose (Sigma-Aldrich, #84097) in PBS overnight at 4ºC or stored in PBS at 4ºC until further use.

Fixation of microglia precursor cells and dissociated retinal organoids. Cells were fixed in 4% (w/v) PFA in PBS for 20 minutes at room temperature in the dark, then washed three times with PBS at room temperature and stored in PBS at 4ºC.

Cryostat sectioning**.** Cryopreserved 3D-retinal organoids were transferred to a cryomold (PolyScience, #18985) using a 1250 µL wide orifice pipette tip and embedded in Tissue-Tek O.C.T. compound (TTEK, A. Hartenstein) on dry ice. Samples were stored at -80ºC until further use. Organoids were cut into 50 µm sections using a cryostat (MICROM, NX70 CRYOSTAR, Thermo Scientific). Sections were mounted onto glass slides Superfrost Plus (Lactan, #H867.1), dried at room temperature overnight, and stored at -80ºC until further use. For immunostainings, slides were thawed and dried for 1 hour at room temperature. Sections on glass slices were encircled with an engraving, hydrophobic pen (Sigma-Aldrich, #Z225568).

Immunostaining of cryostat sections, microglia precursor cells, and dissociated retinal organoid cultures. Samples were incubated in a "blocking solution" containing 1% (w/v) bovine serum albumin (Sigma, #A9418), 5% (v/v) Triton X-100 (Sigma, #T8787), 0.5% (w/v) sodium azide (VWR, #786-299), and 10% (v/v) serum (either goat, Millipore, #S26, or donkey, Millipore, #S30) for two hours in a humidified chamber protected from light at room temperature. Afterward, the samples were immunostained with primary antibodies diluted in antibody solution containing 1% (w/v) bovine serum albumin, 5% (v/v) triton X-100, 0.5% (v/v) sodium azide, 3% (v/v) goat or donkey serum. They incubated overnight in a humidified chamber at room temperature. For the list of primary antibodies, see **Table 7.** After washing the samples three times with PBS, the samples were incubated light-protected in a humidified chamber for 2 hours at room temperature, with the secondary antibodies diluted in antibody solution. The secondary antibodies raised in goat or donkey were purchased from Thermo Fisher Scientific (Alexa Fluor 488, Alexa Fluor 568, Alexa Fluor 647, 1:2000). The sections were washed three times with PBS. The nuclei were labeled with Hoechst 33342 (Thermo Fisher Scientific, Cat#H3570, 1:5000 diluted in PBS) for 15 minutes and then washed two times in PBS. After immunostaining, antifade solution [10% (v/v) mowiol (Sigma, #81381), 26% (v/v) glycerol (Sigma, #G7757), 0.2M tris buffer pH 8, 2.5% (w/v) Dabco (Sigma, #D27802)] was dropped on the cryostat sections and covered with microscope coverslips (Menzel-Glaser #0). Slides were dried at room temperature overnight. 8-well chambers were maintained in PBS. Samples were kept at 4ºC for long-term storage.

Immunostaining of entire 3D-retinal organoids. The staining was performed as described under "*Immunostaining of cryostat sections, microglia precursor cells and dissociated retinal organoid cultures*" with the following adaptations: 3D-organoids were incubated in blocking for 24 hours on an orbital shaker at 4ºC in the dark. The primary antibody concentration was doubled (**Table 8**), and organoids were incubated for ten days on an orbital shaker at 4ºC in the dark. After washing the organoids three times in PBS for 30 minutes each, secondary antibodies (Thermo Fisher Scientific, Alexa Fluor 488, and Alexa Fluor 647, 1:500) and Hoechst 33342 (1:1000) diluted

in antibody solution were added for three days on an orbital shaker at 4ºC in the dark. Finally, the organoids were washed three times in PBS for 30 minutes each. 4-5 3D-organoids were placed into one well of an 8-well chamber (IBIDI, #80826) and covered with 3% (w/v) low gelling temperature agarose (Sigma-Aldrich, #A9414-25G). The samples were stored in glycerol (Sigma-Aldrich, G7757) overnight at 4ºC in the dark.

Table 8 – List of antibodies used for chapter 2.

Antibody	Host	Vendor	Catalogue #	Lot #	Dilution factor	RRID number
BRN3B	Goat	Santa Cruz Biotechnology	sc-6026	K0215	100	AB_673441
Cleaved Caspase3	Rabbit	Cell Signaling Technology	9661	47	100	AB_2341188
CALB2	Mouse	Swant	6B3		100	AB_10000320
CALB1	Guinea pig	Synaptic Systems	214 004	1-15	200	AB_10550535
CD45	Rabbit	Cell Signaling Technology	13917P	1	200	AB_2750898
ChAT	Goat	EMD Millipore	AB144P	3182642	400	AB_2079751
CX3CR1	Mouse	BioLegend	B355702	B194773	50	AB_2561726
GFAP	Rat	STEMCELL Technologies	60048.1	1000079097	100	AB_3095092
IBA1	Rabbit	GeneTex	GTX100042	44200	750	AB_1240434
IBA1	Goat	Abcam	ab5076	GR3374909-1	250	AB_2224402
ITGAM	Chicken	Acris Antibodies	AP31807PU-N	MAC7967984	100	AB_11146887
KI67	Mouse	BD Biosciences	550609	5267542	100	AB_393778
MAP2	Chicken	EMD Millipore	AB5543	4045792	250	AB_571049
myb	Rabbit	Acris	AP31223PU-N	27931	100	AB_10976997
NANOG	Rabbit	Proteintech/ THP medical product	#14295-1-AP	00019675	200	AB_1607719
OCT3/4	Mouse	BD Biosciences	#611202	4052889	100	AB_398736
OTX2	Goat	R&D Systems	AF1979	KNO0920111	150	AB_2157172
P2Y12	Rabbit	Sigma-Aldrich	HPA014518	F119293	100	AB_2669027
PRKCA	Mouse	BD Biosciences	610107	K1315	100	AB_397513
PSD95	Rabbit	Cell Signaling Technology	3450	5	200	AB_2292883
PU.1	Rabbit	Cell Signaling Technology	2266S	1	500	AB_10692379
RCRVN	Rabbit	EMD Millipore	AB5585	2691407	400	AB_2253622
RIBEYE	Mouse	EMD Millipore	MABN804	Q2583290	100	AB_3271577
RLBP1	Mouse	Abcam	ab15051	GR229880-2	200	AB_2269474
RUNX.1	Mouse	BioLegend	659302	B276756	50	AB_2563194
TREM2	Goat	R&D Systems	AF1828	JWF0719111	100	AB_2208689
VGLUT1	Guinea pig	Synaptic Systems	135304	4-73	100	AB_887878

Imaging and image analysis

Brightfield. The differentiation was monitored using a bright-field microscope (Olympus CKX41) with 5×, 10× and 20× objectives (Olympus) and a lens marker (Nikon), and an EVOS imaging system (Thermo Fisher Scientific) with 2×, 4×, 10×, 20×, 40× objectives (Thermo Fisher Scientific).
Confocal microscopy. Images were acquired with a Zeiss LSM880 Airyscan or LSM800 inverted. For overview images, Plan-Apochromat 10× air objective NA 0.45 (WD=2.1mm) or Plan-Apochromat 20× Air objective NA 0.8 were used, and z-stacks were acquired. For detailed images, Plan-Apochromat 40× oil immersion objective NA 1.3 was used. For synaptic puncta analysis, images were acquired on Zeiss LSM900 microscope using a Plan-Apochromat 40X objective NA 1.4 using 'confocal' mode.
Imaging of dissociated retinal organoids. Three regions-of-interests were acquired per condition and biological replicate using the Plan-Apochromat 20× Air objective NA 0.8 with a zoom of 0.8.
***Imaging of 3D retinal organoid sections*.** Based on the nuclei staining, one cryostat section per 3D retinal organoid displaying a retinal cup with a lumen was identified and imaged using the Plan-Apochromat 20×Air objective per condition and biological replicate.
***Imaging of entire 3D-retinal organoids*.** The embedded organoids were imaged using Plan-Apochromat 10×Air objective NA 0.45 (WD=2.1mm).
Live cell imaging of dissociated microglia assembled retinal organoids. Microglia-assembled dissociated retinal organoids were generated as described in "Incorporating microglia-like cells into dissociated retinal organoids". The cells were stimulated as described in "Stimulating microglia assembled dissociated retinal organoids". Images were acquired with a Zeiss LSM880 inverted microscope and a Plan-Apochromat 20×/NA 0.8 Air objective in a temperature-controlled chamber (37°C). Z-stacked images of the Alexa 568 channel were captured every minute for 20 minutes.

Image analysis. Confocal images were converted to .ims files using the Imaris File Converter 9.9.1 and imported to Imaris 9.9 (Bitplane Imaris 3/4D Image Visualization and Analysis Software). Images were cropped and processed using background subtraction.
iMG positioning within layers. Cryostat sections with a focus on retinal cups were used for the analysis. Since we focused on retinal cups displaying a laminated structure, Hoechst-staining was used to identify the formation of layers. Microglia positioning was based on the location of the microglial cell soma. Each data point represents the percentage of microglia within a respective layer relative to the total number per section.
Determining the number of microglia in entire 3D-retinal organoids. Z-stack images of entire organoids were cropped to focus on the retinal cup. The number of microglia-like cells (iMG) were determined using the spot function of Imaris. The estimated XY diameter was set to 15 µm.
Determining cell numbers: The spot function of Imaris was used to analyze cells of interest and Hoechst^{+}-cells. For nuclear stainings such as Hoechst, OTX2, BRN3, and KI67, the estimated XY diameter was set to 7 µm. For CALB2, CALB1, and RCVRN-labeling, the estimated XY diameter was set to 10 µm. To analyze the number of tdTomato^{+}-iMG, the estimated XY diameter was set to 15 µm. The spots were manually edited. For cryostat sections of retinal organoids, we focused on the retinal cup.
For analysis, each data point represents the percentage of the respective marker relative to the total number of Hoechst^{+}-cells, or the total number of microglia was determined for each region

of interest. To calculate the proliferation rate of retinal cell types, the number of KI67$^+$/iMG was subtracted from the total number of KI67$^+$-cells, and the number of iMG were subtracted from the total number of Hoechst$^+$-cells.
Fold change was determined by normalizing the median of three regions of interest per biological replicate to the respective control condition (untreated cells).
Determining Hoechst$^+$-fragments: Hoechst$^+$-fragments with a 2-5 µm diameter were manually counted using Imaris software. In the plot, each data point represents the number of Hoechst$^+$-fragments per mm^2.
Microglia surveillance. Time-lapse videos were binarized in ImageJ using the method 'Li.' The Matlab script determined the surveillance index (Madry et al. 2018), normalized to the total number of microglia imaged per video. Fold changes were calculated by normalizing to untreated control within each experimental repetition.
Microglia morphology. To determine the area, we generated the microglia surface with the surface rendering module with the surface detail set to 0.2 µm in Imaris. Incomplete iMG morphologies at the image border were manually removed and not included in the analysis. We excluded surfaces if multiple microglia were summarized as one surface. The exported Imaris file shows the surface area for each detected surface. To extract the number of end points and the total branch length, images were preprocessed using a Python script. The iMG channel was extracted and the image converted to an 8-bit format. After equalizing the images, a 'Top-hat filter' (disk size = 15) and 'unsharp mask' (sigma = 3) were applied. The mean threshold function was used to generate binary images. Individual cells were identified, and the morphometric features were calculated from the skeletonized representation using a Python script as described in (Maya-Arteaga, Martínez-Orozco, and Diaz-Cintra 2024).
Microglia engulfing BRN3$^+$-cells. Surface rendering was performed for iMG and BRN3$^+$-cells with the surface detail set to 0.2 µm. The surface-surface co-localization function in Imaris was used to visualize co-localization. The total number of iMG and the number of iMG engulfing BRN3$^+$-cells were determined using the spot function. In the plot, each data point represents the percentage of iMG engulfing a BRN3$^+$-cell relative to the total number of microglia per field of view.
Distance from spot to surface. First, all BRN3$^+$-cells were determined using the spot function of Imaris (XY diameter = 7 µm). Second, the iMG surface was generated using the surface rendering module with the surface detail set to 0.2µm. Finally, the function 'spot to surface' with a distance of 5 µm was used to determine the number of BRN3$^+$-cells close to the iMG surface. In the plot, each data point represents the percentage of BRN3$^+$-cells close to iMG relative to the total number of BRN3$^+$-cells per field of view.
Synaptic puncta quantification. Images were processed using background subtraction and median filter. MAP2 (405/420nm), VGLUT1 (488/520 nm), and PSD95 (633/650 nm) channels were deconvolved in Imaris using the default parameter settings for oil objectives. For the analysis, we focused on MAP2$^+$-cells, cropped one branch (25-35µm) close to the soma, and measured its length. Then, the MAP2 surface was generated using the surface rendering module with the surface detail set to 0.2µm. With the Spot function in Imaris, we detected all VGLUT1$^+$ (XY diameter = 0.19µm) and all PSD95$^+$ puncta (XY diameter = 0.18µm) in the field of view. Using the function 'spot to surface' with a distance of 0.3 µm, we determined VGLUT$^+$-spots or PSD95$^+$-spots close to the rendered MAP2-surface and extracted the statistics. Finally, we analyzed the

number of active synapses. Therefore, we focused on the puncta close to the MAP2 surface. Using the function 'colocalization' with a distance of 0.3 µm, we determined $VGLUT^+$-puncta in close proximity to $PSD95^+$-puncta. We analyzed three cells per field of view. In the plot, each data point represents the number of $VGLUT1^+/PSD95^+$-puncta per 10µm $MAP2^+$-process.
Graphics: All graphics were generated using R (version 4.2.2). Excel files were loaded into R via the *xlsx* package (version 0.6.5) (Dragulescu 2014). Plots were made using ggplot2 (version 3.4.1) (Wickham 2016).

Calcium imaging of dissociated cultures

AAV production and titration.
The ISTA Molecular Biology Facility generated the virus. Human embryonic kidney (HEK) 293T cells were maintained at 37°C in 5% (v/v) CO_2 in complete medium (DMEM medium (Thermo Fisher Scientific, #31966047), 10% (v/v) fetal bovine serum (Thermo Fisher Scientific, #10270106], 1% (v/v) penicillin/streptomycin (Thermo Fisher Scientific, #15140122), 1% (v/v) non-essential amino acids (Sigma-Aldrich, #M7145-100ML). Ten 15-cm culture dishes with 80% confluency were transfected using 6.8 µM polyethyleneimine (Polysciences, #24765-1), 70 µg AAV transgene plasmid (pAAV-EF1a-GCaMP6s-WPRE-pGHpA, Addgene, #67526), 70 µg 7M8 Cap-encoding plasmid (7M8, Addgene, #64839), 200 µg pHGT1-Adeno1 helper plasmid. Sixty hours post-transfection, cells were harvested with a cell scraper and pelleted at 4000 rpm for 15 minutes at 4°C. The pellet was resuspended in lysis buffer (200 mM NaCl, PBS, 0.001% pluronic F68, sterile filtered). Cell-lysis was obtained by three rounds of freezing-thawing cycles between dry ice/ethanol and a 37°C water bath, followed by sonication for 1 minute at 37kHz. Next, Benzonase (50 U/mL, Sigma Aldrich, #E1014-25KU) was added, and the solution was incubated at 37°C for 45 minutes. Afterward, the solution was centrifuged at 2415×g for 10 minutes at 4°C. The AAV particles in the supernatant were purified by discontinuous iodixanol gradient ultracentrifugation. Optiseal tubes (Beckman Coulter, 361625) were filled with a density gradient of 60%, 40%, 25%, and 17% iodixanol solutions (Optiprep Iodixanol, Progen Biotechnik, 1114542). The virus lysate was loaded on the top layer, and the tubes were centrifuged at 350000 g (Beckman Optima XPN-100 ultracentrifuge Sorvall T-850 rotor) for 90 minutes at 10°C. The AAV particles were harvested from the intersection of 60% and 40% gradients and concentrated using 100kDa Vivaspin 20 Centrifugal Concentrator. Aliquots were stored at -80°C.
For titration by qPCR, AAV particles were denatured with DNase I (Fisher Scientific, #10103533) and the viral DNA quantification was performed with Universal SYBR Master Mix 2X (Thermo Fisher Scientific, #4309155) using the following primers: forward primer: 5'-GGAACCCCTAGTGATGGAGTT; reverse primer: 5'-CGGCCTCAGTGAGCGA. The final titer measured 1.1×10^{13} viral genome copy number per milliliter (GC/mL).
AAV infection of dissociated cultures. At week 17 (D120), dissociated retinal organoid cultures were infected with 5×10^{10} GC of AAV2/7m8- EF1α- GCAMP6s (Cowan et al. 2020; Garita-Hernandez et al. 2020) cultured in 100 µL 3:1-medium. After 24 hours, 100 µL fresh 3:1-medium was added. The next day, the medium was changed to N2-medium supplemented with 20 ng/mL BDNF. The medium was changed every 3 to 4 days, and 0.5 µM retinoic acid was added daily.
***Calcium imaging*.** Four days before calcium imaging at day 138, dissociated retinal organoids were gradually transferred to BrainPhys medium (StemCell Technologies, #05791) supplemented with 1×N2 supplement, 100 µM taurine supplemented with 20 ng/mL BDNF, 50 ng/mL MCSF and

0.5 µM retinoic acid. Twenty-four hours before imaging, the medium was changed, and BDNF was withdrawn. Cultures were treated as described in "Stimulating microglia assembled dissociated retinal organoids", except that the samples were cultured in a supplemented BrainPhys medium. Live imaging was performed using the Dragonfly microscope (Andor Dragonfly 505, Oxford Instruments) equipped with a heated chamber at 37°C and CFI P Apochromat 20× NA 0.95/ WD 0.95 mm water objective (Nikon, MRD77200). The Andor iXon Ultra 888Ultra EMCCD camera (13 µm pixel size) was used to acquire the 488 nm channel using a pinhole size of 25 µm. The following parameters were used for acquisition: exposure time of 40 ms, EM gain of 100, Laser 7.0%, and an AOI of 1024×1024. Baseline activity was acquired for five minutes using a time series at 12.16 Hz. Baseline calcium dynamics were recorded for 5 minutes from five distinct cultures of independent differentiations.

***Pharmacological manipulation*.** First, baseline calcium activity was recorded for 2.5 minutes. For pharmacological manipulation, either 1 µM Tetrodotoxin (Abcam, # ab120054) to block voltage-gated sodium channels was applied or a mixture of 10 µM NBQX (2,3-dioxo-6-nitro-7-sulfamoyl-benzo[f]quinoxaline; Tocris Bioscience, #1044), 10 µM DL-AP4 (DL-2-amino-4-phosphonobutyric acid, Tocris Bioscience, #0101), 10 µM (±)-CPP (3-[(R)-2-carboxypiperazin-4-yl]-propyl-1-phosphonic acid; Abcam, #ab144495) to inhibit glutamatergic synaptic transmission was applied. After 5 minutes of incubation, calcium activity was recorded for another 2.5 minutes.

To chelate extracellular calcium, 5mM EGTA (ethylene glycol-bis(β-aminoethyl ether)-N,N,N',N'-tetraacetic acid) was applied and recording immediately continued for another 2 minutes.

***Pharmacological manipulation following POLY(I:C) stimulation*.** For the stimulation of iMG-$_{diss}$RO, see '*Stimulating microglia assembled dissociated retinal organoids'.* Otherwise, following 24h stimulation, calcium activity was recorded for 5 minutes. Then, a mixture of 10 µM NBQX (2,3-dioxo-6-nitro-7-sulfamoyl-benzo[f]quinoxaline; Tocris Bioscience, #1044), 10 µM DL-AP4 (DL-2-amino-4-phosphonobutyric acid, Tocris Bioscience, #0101), and 10 µM (±)-CPP (3-[(R)-2-carboxypiperazin-4-yl]-propyl-1-phosphonic acid; Abcam, #ab144495) was applied to inhibit glutamatergic synaptic transmission. After 5 minutes of incubation, calcium activity was recorded for another 5 minutes.

***Calcium imaging analysis*.** Cells showing calcium transients were identified manually as regions of interest using ImageJ, and mean grey values were extracted. We focused on cells where the cell soma and the primary branches were clearly visible. Transients in the background were not included in the analysis. Fluorescent signal time series (F/ΔF: change in fluorescence divided by the mean baseline fluorescence) were calculated for each region of interest. Calcium events were detected in Matlab 2017 using the script 'PeakCaller' (Artimovich et al. 2017) using the following parameters: required rise = 9% absolute; max. lookback =100 pts; required fall = 5% absolute; max. lookahead = 100 pts; no trend control; trend smoothness = 100; interpolate across closed shutters = true. For each cell, waveform parameters such as number of events and peak amplitude were extracted and plotted.

Statistical analysis

All statistics were performed using R (version 4.2.2). The linear regression model was calculated using the "lme4"-package. First, groups for comparison were tested for normal distribution and equal variances using the Shapiro-Wilk and Levene tests, respectively. No data was excluded for analysis. If the data was normally distributed and the groups had equal variances, Student's t-

test was used to compare the two groups. For multiple comparisons, the default contrast for unordered variables was set to 'contr.sum' to perform one-way ANOVA, followed by Tukey's post-hoc comparison. Welch's test was performed to compare normally distributed groups with unequal variances. A two-sided one-sample T-test was used to analyze if a normally distributed condition significantly differs from a value of 1 or 0.

If groups were not normally distributed, the Wilcoxon rank-sum test or Kruskal-Wallis test, followed by Dunn's test, was used to compare two or multiple groups, respectively. For multiple comparisons, p-values were adjusted using the "p.adjust" function, and the method was set to 'BH.' The following packages were used to perform the analysis: "FSA"-package (dunn-test); "multcomp"-package (Tukey'-test); "psych"-package (t-test, kruskal-wallis test); "stats"-package (wilcox-test, shapiro-wilk test), "dplyr"-package (levene-test).

Significance levels are indicated using the following notation: $^{n.s.}p > 0.05$; $^{*}p < 0.05$; $^{**}p < 0.01$; $^{***}p < 0.001$. Please refer to (Schmied et al. 2025) for details about the statistical analysis which are summarized in the publication's *Supplementary Table 4*, and the respective raw data in the publication's *Supplementary Table 5*.

3.4. Results

OPL formation aligns with successful iMG integration into retinal organoids.

To generate retinal organoids ($_{3D}$RO), we differentiated the human induced pluripotent stem cell (hIPSC) line F49B7, which has been recently analyzed for its transcriptional cell diversity across different time points of $_{3D}$RO differentiation (Cowan et al. 2020). We monitored the retinal cup formation under brightfield microscopy over 30 weeks (**Figure 34a**) and observed the formation of the outer plexiform layer (OPL) around week (WK) 20. When we performed immunostaining for the presynaptic markers VGLUT1 and the post-synaptic marker PSD95 at WK13, 17, and 20, the staining was confined to the OPL at WK20 (**Figure 34b-c**). By WK20, we also found the presynaptic marker RIBEYE limited to the OPL (**Figure 34d**).

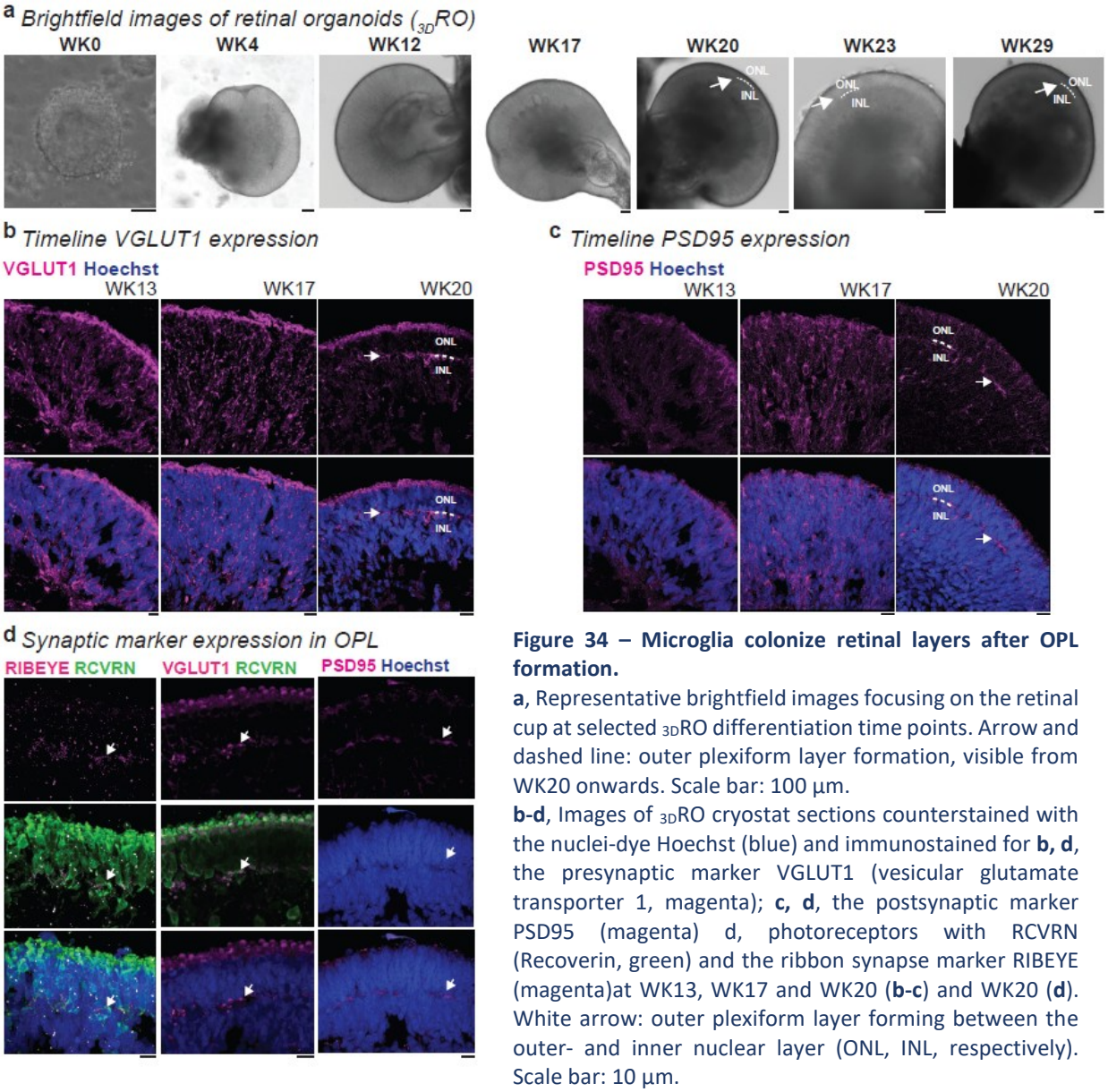

Figure 34 – Microglia colonize retinal layers after OPL formation.

a, Representative brightfield images focusing on the retinal cup at selected $_{3D}$RO differentiation time points. Arrow and dashed line: outer plexiform layer formation, visible from WK20 onwards. Scale bar: 100 µm.

b-d, Images of $_{3D}$RO cryostat sections counterstained with the nuclei-dye Hoechst (blue) and immunostained for **b, d**, the presynaptic marker VGLUT1 (vesicular glutamate transporter 1, magenta); **c, d**, the postsynaptic marker PSD95 (magenta) d, photoreceptors with RCVRN (Recoverin, green) and the ribbon synapse marker RIBEYE (magenta)at WK13, WK17 and WK20 (**b-c**) and WK20 (**d**). White arrow: outer plexiform layer forming between the outer- and inner nuclear layer (ONL, INL, respectively). Scale bar: 10 µm.

Furthermore, we confirmed the existence and the location of the different cell types within their expected nuclear layer at WK20, such as RCVRN$^+$-/ OTX2$^+$-/ CALB2$^+$-photoreceptors in the outer nuclear layer and OTX2$^+$/ CALB2$^+$-bipolar cells, CALB2$^+$-amacrine cells, CALB1$^+$-horizontal- and amacrine cells, and CHAT$^+$-amacrine cells in the inner nuclear layer (**Figure 35**). Few BRN3$^+$-ganglion cells localized close to the $_{3D}$RO lumen. RLBP1$^+$-Müller glial cells expanded their processes across all layers. OPL formation and cell type expression patterns matched the anticipated timeline observed in human fetal tissue studies (Hendrickson 2016; Hoshino et al. 2017; Nag and Wadhwa 2001).

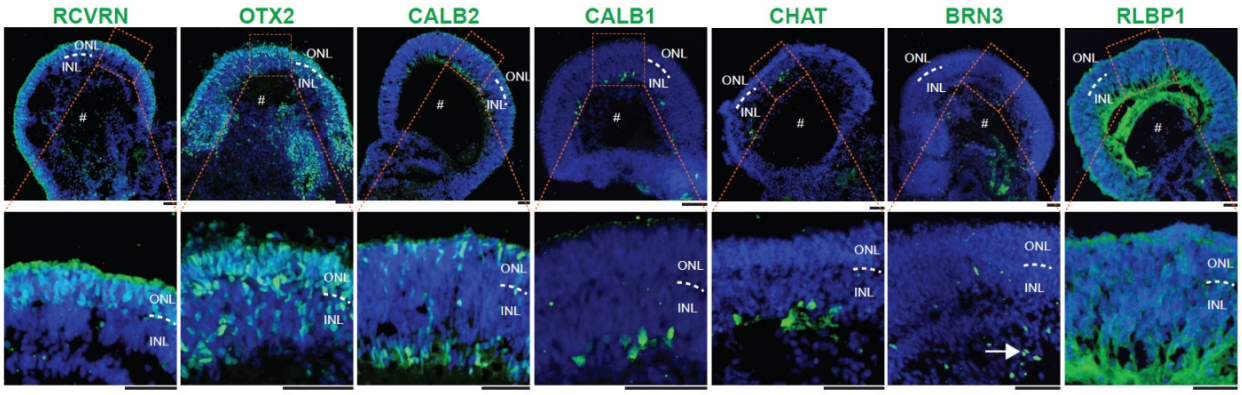

Figure 35 – Retinal cell types generated in $_{3D}$RO.
Representative cryostat section images of $_{3D}$RO counterstained with the nuclei-dye Hoechst (blue) and immunostained for retinal cell type-specific markers (green) and at WK20: RCVRN (recoverin; photoreceptors). OTX2 (orthodenticle homeobox 2; photoreceptors, bipolar cells). CALB2 (calretinin; photoreceptors, bipolar-, amacrine cells). CALB1 (calbindin; amacrine-, horizontal cells). CHAT (choline acetyltransferase; amacrine cells). BRN3 (brain-specific homeobox/POU domain protein 3B; ganglion cells). RLBP1 (cellular retinaldehyde-binding protein; Müller glia). ONL: outer nuclear layer. INL: inner nuclear layer. White dashed line: outer plexiform layer. #: retinal cup lumen. White arrow: BRN3$^+$-cells close to lumen. Scale bar: 50 µm.

Human microglia have been shown to accumulate at the optic disc between GW10-13 and then populate the OPL between GW20-25 (Diaz-Araya et al. 1995). When we stained $_{3D}$RO for the microglia-associated marker IBA1 (Ito et al. 1998), we did not find innately developing IBA1$^+$-microglia within the retinal cup at any collected time points (**Figure 36a**). This is in line with our previous observations (Bartalska et al. 2022) and confirms the sequencing data at weeks 30 and 38 by Cowan *et al.*, which failed to identify microglia signature gene transcripts like IBA1/AIF1, CX3CR1, PU.1/SPI1, and P2RY12 (**Figure 36b**) (Butovsky et al. 2014; Gosselin 2017; Kierdorf et al. 2013; Matcovitch-Natan et al. 2016).

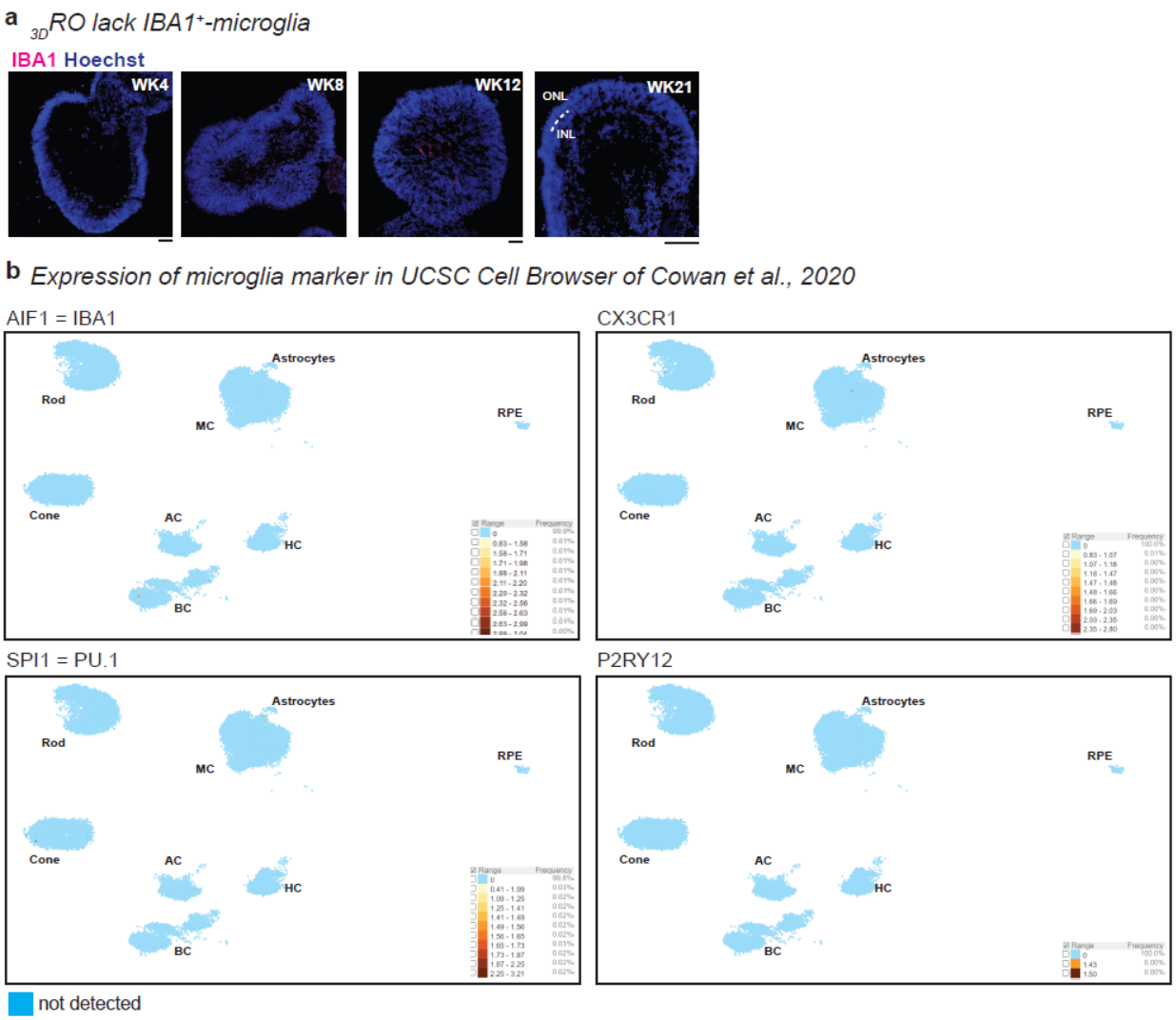

Figure 36 – 3DRO lack innately developing microglia-like cells.
a, Images of 3DRO cryostat sections counterstained with the nuclei-dye Hoechst (blue) and immunostained for the microglia marker IBA1 (ionized Calcium-Binding Adapter Molecule 1, magenta) at WK4, WK8, WK12, and WK21. Scale bar: 100 µm.
b, Expression of microglia transcript markers in USCS Cell Browser of Cowan et al., 2020: Dataset ID: 'Developed human retinal organoid.' Uniform manifold approximation and projection (UMAP) of transcript expression for AIF (also known as IBA1), CX3CR1 (C-X3-C motif chemokine receptor 1), SPI1 (also known as PU.1, Spi-1 proto-oncogene) and P2RY12 (purinergic receptor P2Y12) of 3D-retinal organoid at WK 32 and 38. AC: amacrine cell. BC: bipolar cell. Cone: cone photoreceptors. HC: horizontal cell. MC: Müller glia. RPE: retinal pigment epithelium. Rod: rod photoreceptors. Blue dot: not detected.

Therefore, we focused on a microglia-assembled retinal organoid (iMG-3DRO) model, for which we developed a hIPSC line expressing the red fluorescent protein from the AAVS1 locus (**Figure 37a-c**) (Oceguera-Yanez et al. 2016). First, we confirmed that the hIPSC line remained pluripotent (**Figure 37d**) and successfully differentiated into tdTomato+/IBA1+-microglia precursors (preMG) expressing the previously described and expected preMG-markers (Bartalska et al. 2022) (**Figures 37e-k**).

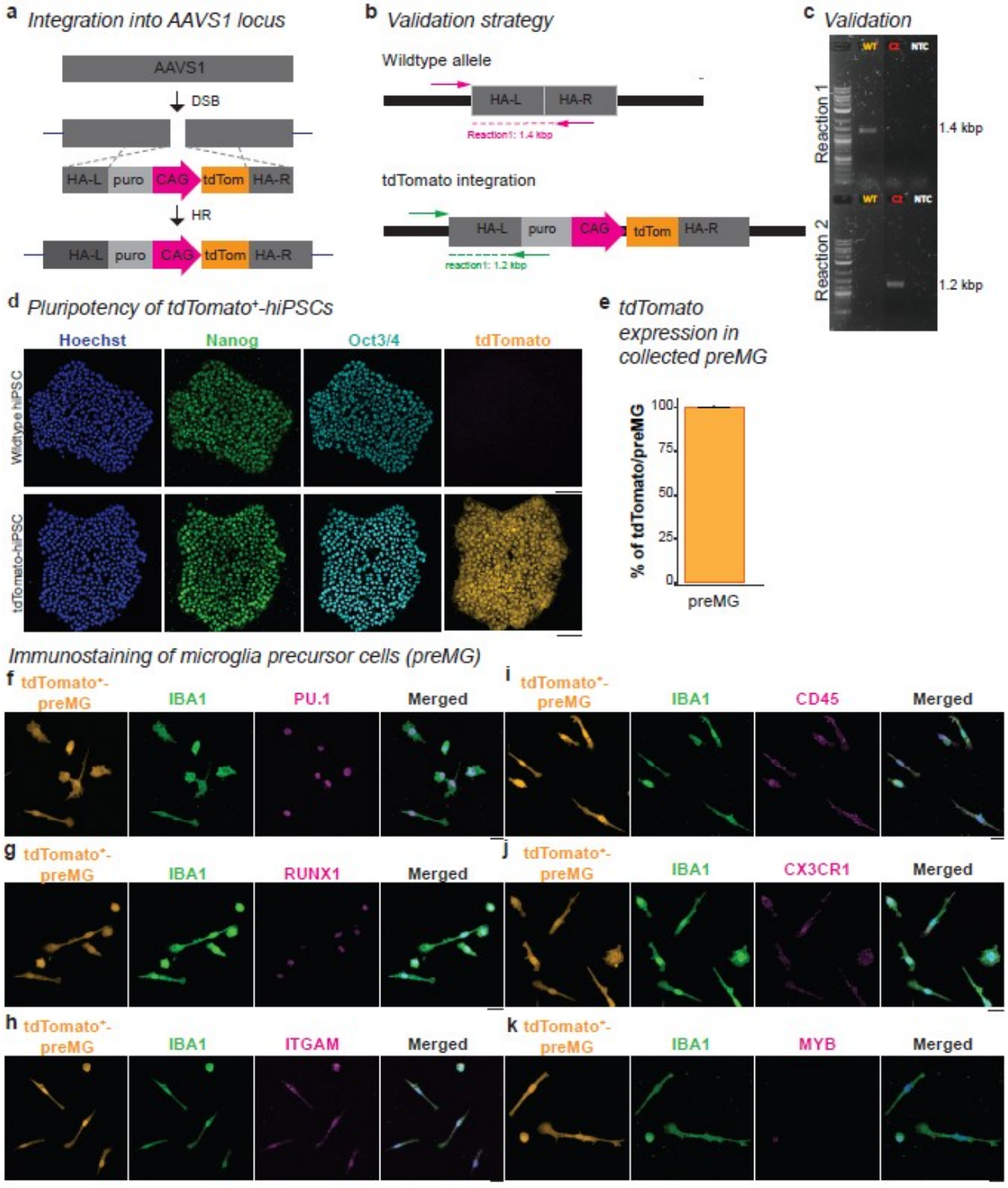

Figure 37 – Figure legend on next page.

Figure 37 – Generation of tdTomato$^+$-hIPSC cell line and characterization of differentiated tdTomato$^+$-microglia precursors (preMG).
a, Integration strategy into the adeno-associated virus integration site 1 (AAVS1) locus. DSB: double-strand break. CAG: CMV immediate enhancer/β-actin promoter. HA-L: homologous arm left. HA-R: homologous arm right. HR: homologous recombination. Puro: puromycin selection side. tdTom: tdTomato.
b-c, Validation strategy. Reaction 1: wildtype allele: PCR product 1.4 kbp. Reaction 2: tdTomato allele: PCR product 1.2 kbp. PCR: polymerase chain reaction.
c, PCR product size. Top: Reaction 1 - wildtype AAVS1 locus (1.4 kbp). Bottom: Reaction 2 - construct integrated into AAVS1 (1.2 kbp). Orange: wildtype clone. Red: clone with homozygous integration of the construct. NTC: non-template control. Kbp: kilobase pair.
d, Validating pluripotency for the wildtype human induced pluripotent stem cell (hIPSC) line SC102A (top) and the tdTomato$^+$-hIPSC line SC102A (bottom). Immunostaining of hIPSC colonies for NANOG (nanog homeobox, green), OCT3/4 (octamer-binding protein 3, cyan), and counterstaining for the nuclei-dye Hoechst (blue). Intrinsic tdTomato expression (orange). Scale bar: 100 µm.
e, Bar chart of tdTomato+/ IBA1+-preMG with standard error of the mean.
f-k, Representative images of tdTomato-expressing microglia precursor cells (preMG, orange) harvested from the supernatant and plated on a new dish. Cells counterstained for the nuclei-dye Hoechst (blue, merged image), immunostained for IBA1 (ionized calcium-binding adapter molecule 1, green) and the microglia/macrophage markers in magenta for f, PU.1 (hematopoietic transcription factor PU.1); g, RUNX1 (runt-related transcription factor 1); h, ITGAM (integrin subunit alpha m); i, CD45 (cluster of differentiation 45/ protein tyrosine phosphatase receptor); j, CX3CR1 (chemokine (C-X3-C) receptor 1); k, MYB (MYB proto-oncogene). Scale bar: 20µm.

Then, we added tdTomato$^+$-preMG to $_{3D}$ROs at WK 6, 13, 16, or 17 of $_{3D}$RO differentiation and followed their integration (**Figure 38a**). Independent of the differentiation week of the organoid, tdTomato$^+$-preMG attached to the developing outer nuclear layer within 24h (**Figure 38b**). After a few days, the initially roundly-shaped preMG infiltrated into the $_{3D}$RO and adapted their morphology into a bipolar profile, which spanned throughout the layers projecting towards the lumen of the retinal cup (**Figure 38c**).

Differences in the preMG integration pattern correlated

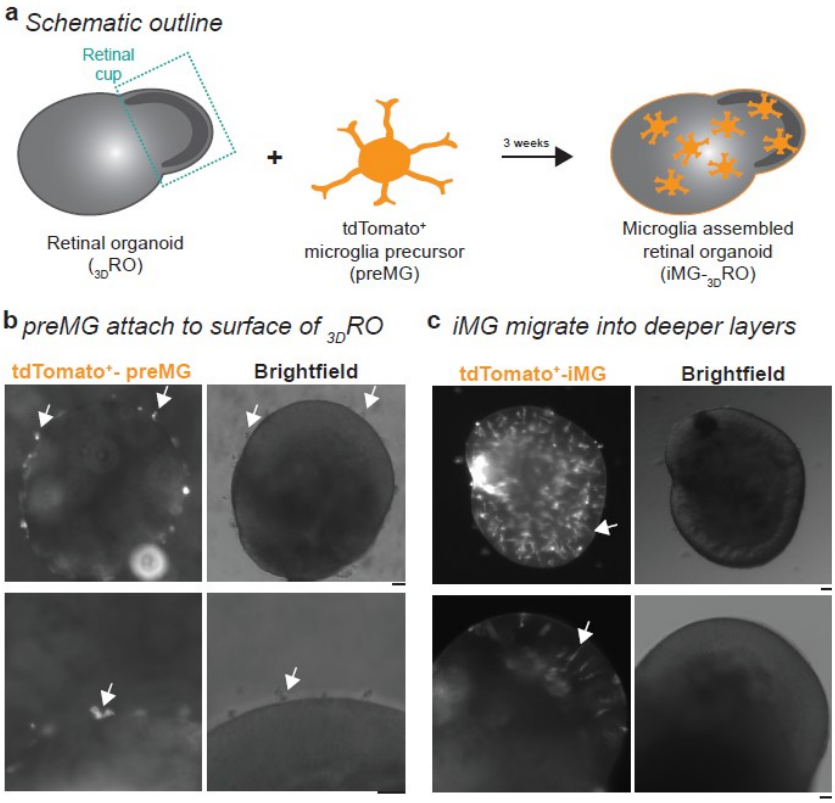

Figure 38 – Generation of microglia assembled 3D-retinal organoids.
a, Experimental schematic to generate iMG-3DRO.
b-c, Representative images of iMG-$_{3D}$RO. Left: fluorescence image, right: brightfield image. 4x magnification (top) and 10x magnification (bottom). Scale bar: 20µm.
b, tdTomato$^+$-microglia precursor cells (preMG, white arrow) attach on WK 17 at the surface of $_{3D}$RO.
c, tdTomato$^+$- microglia-like cells (iMG) integrate into the $_{3D}$ROs at WK 20, showing a bipolar shape (white arrow).

with the OPL formation. Before WK20, iMG preferentially accumulated in the lumen close to BRN3^{+}-ganglion cells and rarely interacted with the developing retinal cells (**Figure 39a**). After WK20, iMG integrated into the OPL (**Figure 39b-c**), or they extended their processes toward it (**Figure 39a**).

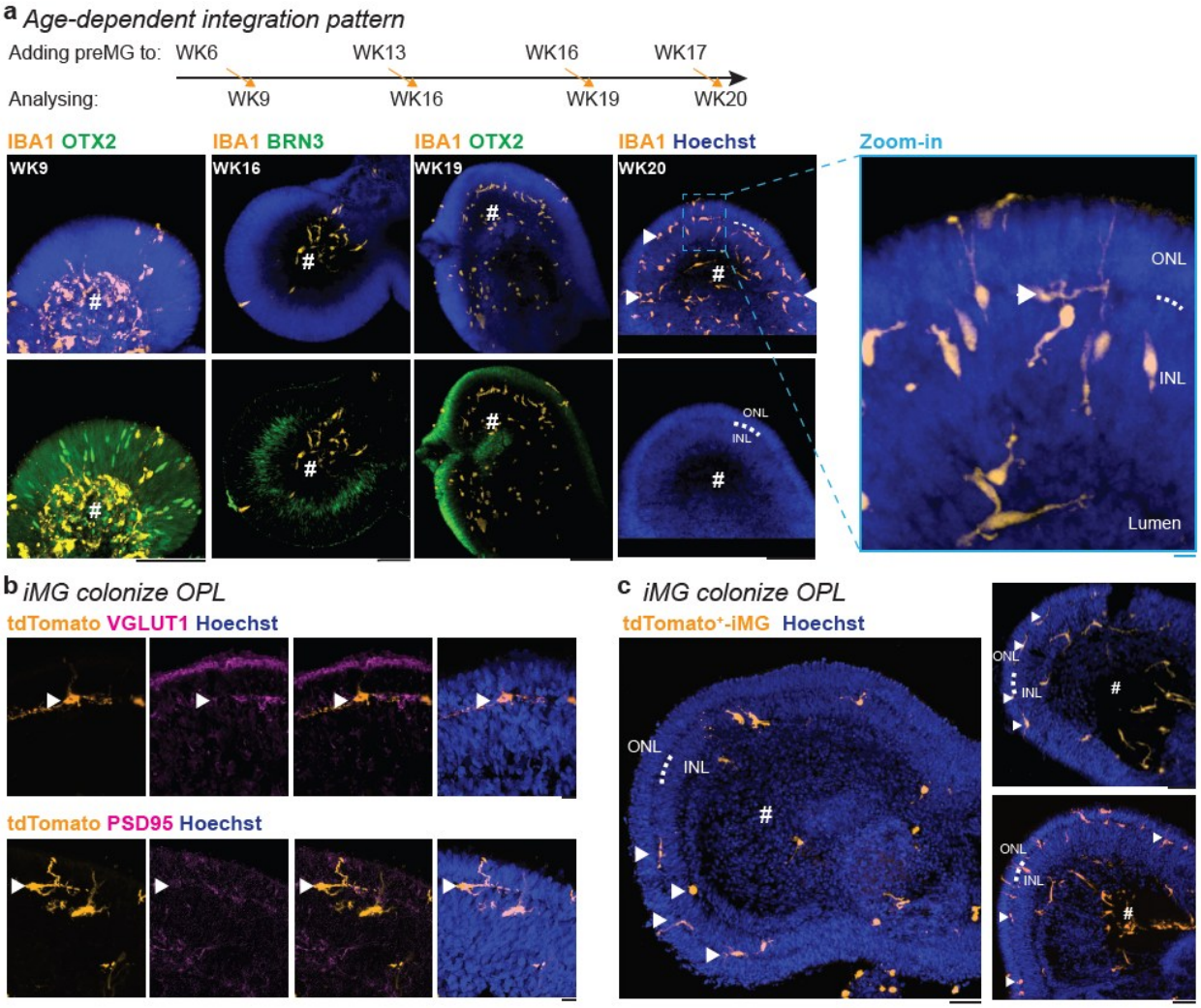

Figure 39 – Microglia colonize outer plexiform layer (OPL).

a, Maximum intensity projection image of entire iMG-$_{3D}$RO counterstained with the nuclei-dye Hoechst (blue) at different time points of preMG (microglia precursor cells) application and collection of iMG-$_{3D}$RO as outlined in the schematic (top). Immunostaining for IBA1 (ionized Calcium-Binding Adapter Molecule 1, orange), BRN3 (brain-specific homeobox/POU domain protein 3B, green, for WK16), and OTX2 (orthodenticle homolog 2, green, for WK9 and WK19). Scale bar: 100 µm. Zoom-in: 10 µm.

b, Images of iMG-$_{3D}$RO cryostat sections with tdTomato^{+}-iMG (orange) at WK20 immunostained for the presynaptic marker VGLUT1 (vesicular glutamate transporter 1, magenta, top) or the postsynaptic marker PSD95 (postsynaptic density protein 95, magenta, bottom). Blue: nuclei-dye Hoechst. White arrowhead: iMG located in OPL. Scale bar: 10 µm.

c, Images of iMG-$_{3D}$RO cryostat sections with tdTomato^{+}-iMG (orange) counterstained with the nuclei-dye Hoechst (blue) and at WK20. Scale bar: 50 µm.

White arrowhead: iMG positioned in the outer plexiform layer (OPL) forming between the outer- and inner nuclear layers (ONL, INL, respectively). White dashed line: OPL. #: retinal cup lumen. WK: weeks after differentiation started.

The position of the iMG soma indicated a spatial distribution across all retinal layers (**Figure 40a**), and the total number of iMG significantly increased from WK9 to WK20 (**Figure 40b**). Overall, we determined WK20 as the time point, which aligns with the microglia integration and spatial distribution pattern in human retinal development (Diaz-Araya et al. 1995).

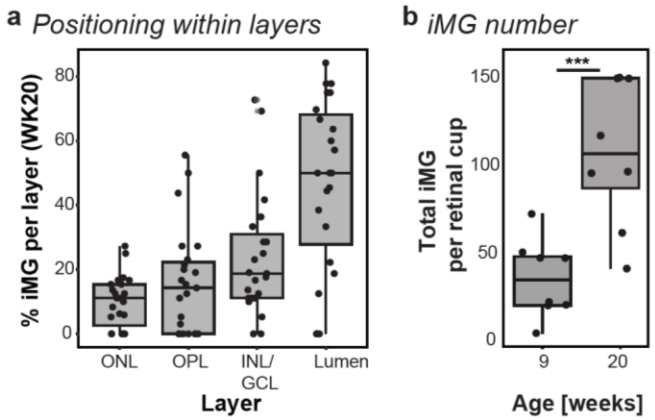

Figure 40 – Quantification.
a-b, Boxplot. **a**, Percent of iMG in the ONL (outer nuclear layer), OPL (outer plexiform layer), INL (inner nuclear layer), GCL (ganglion cell layer), and within the retinal cup lumen (#) at WK20. Each dot: one cryostat section of an independent retinal cup.
b, Total number of iMG integrated per retinal cup at WK9 and WK20. Each dot represents an entire retinal cup. Students's t-test. *** p<0.001.
iMG: microglia-like cells. WK: week after the start of the differentiation.

iMG control ganglion cell number in adapted 2D-RO model with improved ganglion cell survival.

In human fetal tissue, the ganglion cell layer fully forms by GW24 (Gupta et al. 2016), and its formation is accompanied by extensive cell loss peaking between GW16 and 21 (Provis 1987). Microglia have been shown to interact with newborn BRN3^{+}-ganglion cells and reduce their density in the rodent retina (Anderson et al. 2019). To recapitulate this phenotype in human $_{3D}$RO is challenging due to the gradual loss of retinal ganglion cells with increasing maturation (**Figure 41a-b**), a well-documented phenotype (Cowan et al. 2020; Fligor et al. 2021; Wagstaff et al. 2021).

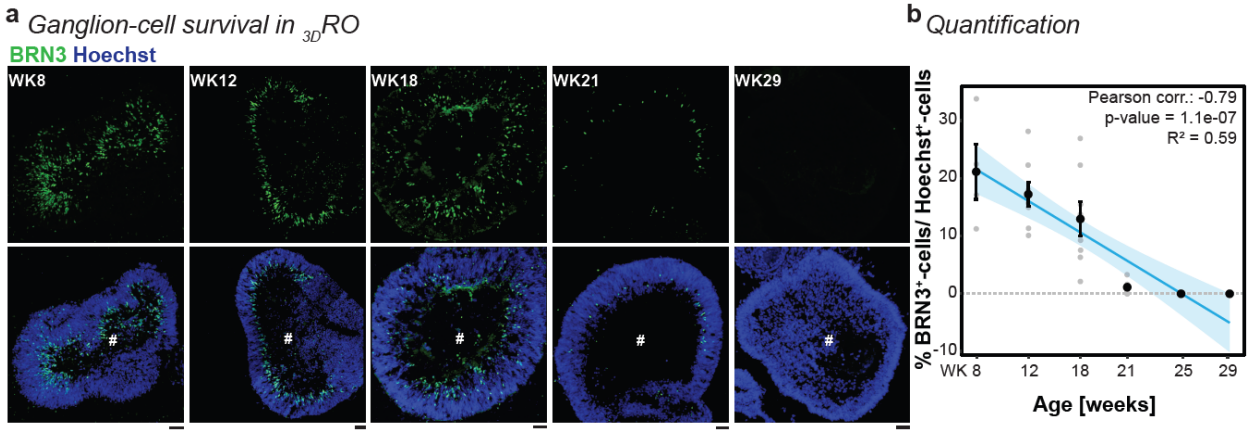

Figure 41 – Figure legend on next page.

Figure 41 – Gradual ganglion cell loss with $_{3D}$RO maturation.
a, Images of $_{3D}$RO cryostat sections counterstained with the nuclei-dye Hoechst (blue) collected at WK8, 12, 18, 21, 29 and immunostaining for BRN3 (brain-specific homeobox/POU domain protein 3B, green). Scale bar: 50 µm.
b, Scatterplot of BRN3$^+$-cells relative to Hoechst$^+$-cells per cryostat section with SEM and trend curve. Pearson correlation with a significant negative correlation between the differentiation age and the BRN3$^+$-cells number.
$_{3D}$RO: 3D-retinal organoid. SEM: standard error of the mean. WK: week after the start of the differentiation.

Therefore, we adapted recent protocols that dissociate 3D organoids, plated them as 2D cultures, and validated cortical network activity reestablishment (Sakaguchi et al. 2019; Victor et al. 2022). Dissociated retinal organoid culture ($_{diss}$RO) will allow us to minimize diffusion biases and compare treatment paradigms directly because the wells derive from the same pool of dissociated WK15 $_{3D}$ROs, circumventing organoid-to-organoid variability. Until WK20, retinal cells will have had sufficient time to successfully reform their synaptic connections (Ludwig et al. 2023). First, we compared the cell type composition and density to the age-matched $_{3D}$ROs (**Figure 42a-b**). We found that the percentage of each cell type was similar between $_{3D}$RO and $_{diss}$RO with the exceptions of CALB1 and BRN3, which both significantly increased in $_{diss}$RO (**Figure 42b**). Importantly, brain-derived neurotrophic factor (BDNF) in the culture medium supported BRN3$^+$-ganglion cell survival in $_{diss}$RO compared to $_{3D}$RO (**Figure 42c**).

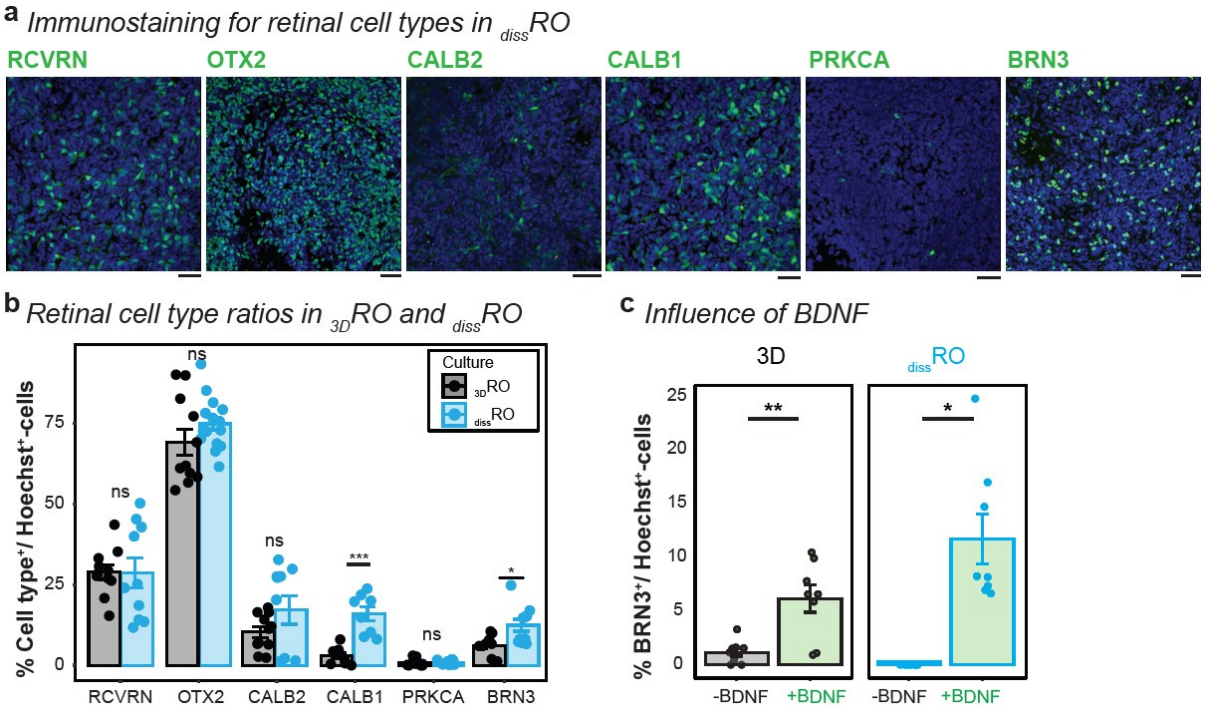

Figure 42 – Figure legend on next page.

Figure 42 – Retinal cell types in $_{diss}$RO.
a, Immunostaining for retinal markers (green) and nuclei-dye Hoechst (blue) at WK20. Scale bar: 50 µm. Retinal cell type markers: RCVRN (recoverin) for photoreceptors, OTX2 (orthodenticle homolog 2) for photoreceptors and bipolar cells, CALB2 (calretinin) for photoreceptors, bipolar- and amacrine cells, CALB1 (calbindin) for amacrine-, horizontal cells, PRKCA (protein kinase C alpha) for rod bipolar cells, and BRN3 (brain-specific homeobox/POU domain protein 3B) for ganglion cells.
b, Bar chart with SEM of retinal cell types relative to Hoechst$^+$-cells in $_{3D}$ROs (black) and $_{diss}$RO (blue). Each dot: cryostat section of individual $_{3D}$ROs (black) or a field of view in $_{diss}$RO (blue). Student's t-test except for CALB1 (Wilcoxon rank-sum test).
c, Impact of brain-derived neurotrophic factor (BDNF) on ganglion cell survival. Bar chart of percentage of BRN3$^+$-cells relative to Hoechst$^+$-cells with standard error of the mean in 3D-retinal organoids ($_{3D}$RO, left) and dissociated retinal organoid culture ($_{diss}$RO, right) cultured either in standard retinal organoid differentiation media without (-BDNF, grey) or supplemented with BDNF (+BDNF, green) from WK 15 to 20. $_{3D}$RO: Each dot is one cryostat section of independent retinal cups. Welch's t-test. $_{diss}$RO: Each dot is one region of interest. One-sample Wilcoxon signed rank test. ***p < 0.001. **p < 0.01. *p < 0.05. ^{ns}p > 0.05, not significant.
$_{3D}$RO: 3D-retinal organoid. SEM: standard error of the mean.

Next, we added tdTomato$^+$-preMG to $_{diss}$RO at WK18.5 (iMG-$_{diss}$RO, **Figure 43a**). After ten days in culture, iMG were distributed across the plate, representing 2.61% ±1.13 of the total Hoechst$^+$-nuclei number (**Figure 43b**).

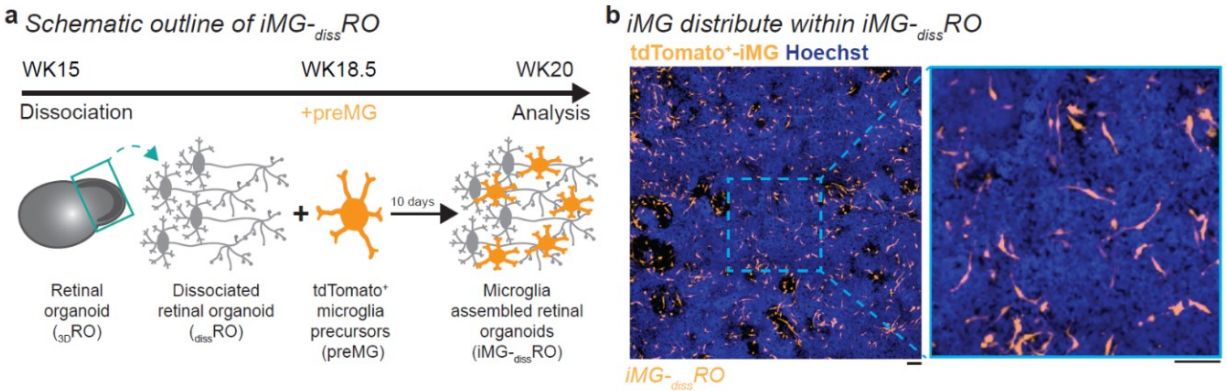

Figure 43 – Generation of microglia assembled dissociated retinal organoids (iMG-$_{diss}$RO).
a, Experimental timeline to generate iMG-$_{diss}$RO. At WK15, retinal cups were dissociated and plated as $_{diss}$RO. At WK18.5, independently differentiated tdTomato$^+$-preMG were added. iMG-$_{diss}$RO was analyzed ten days later at WK20.
b, Image of tdTomatro$^+$-iMG distribution within iMG-$_{diss}$RO (orange) at WK20, counterstained with the nuclei-dye Hoechst (blue). Scale bar: 100 µm.
$_{3D}$RO: 3D-retinal organoid. preM: microglia precursor cells. WK: week after the start of the differentiation.

To evaluate if the co-culture promotes iMG maturation (**Figure 44a**) (Butovsky et al. 2014; Guttikonda et al. 2021; Haenseler et al. 2017; Park et al. 2023, 2023; Schmid et al. 2002) we performed RT-qPCR of iMG-$_{diss}$RO. On day one, we observed the mRNA expression of microglia-associated markers such as C1QA, CX3CR1, P2RY12, and TMEM119 (**Figure 44b**) (Butovsky et al. 2014; Gosselin, et al. 2017), which were not detected in the absence of iMG (**Figure 36b**). Except for TMEM119, their mRNA expression significantly increased over 9 days, indicating that co-culturing with $_{diss}$RO promoted microglia marker expression on the mRNA level. On day 10, iMG expressed the transcription factors for primitive macrophage development PU.1 and RUNX1, and MYB was not present (**Figure 44c**) (Buchrieser, James, and Moore 2017). iMG also expressed IBA1, CD45 as well as more mature microglia marker TREM2 and P2RY12 (**Figure 44d-e**).

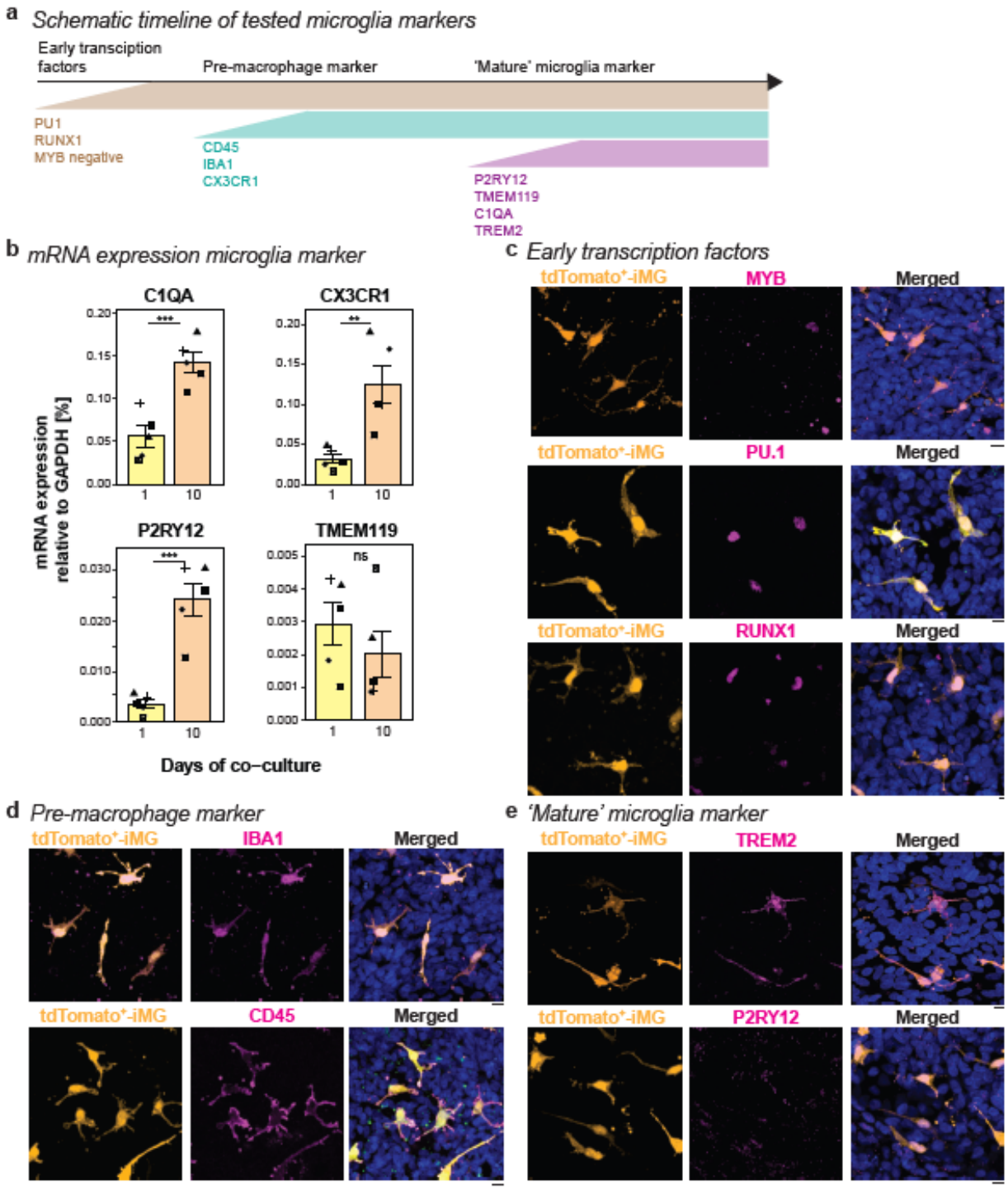

Figure 44 – Figure legend on next page.

Figure 44 – Microglia marker expression in iMG-$_{diss}$RO.
a, Schematic timeline of microglia marker expression during development.
b, RT-qPCR for the microglia marker C1QA (complement component C1q), CX3CR1 (C-X3-C motif chemokine receptor 1), P2RY12 (purinergic receptor P2Y G-protein-coupled 12) and TMEM119 (transmembrane protein 119) in iMG-$_{diss}$RO after 1 and 10 days of coculture. Bar chart with SEM of mean mRNA transcript expression relative to GAPDH (glyceraldehyde 3-phosphate dehydrogenase). Each symbol is one biological replicate. Student's t-test. ***$p < 0.001$. **$p < 0.01$. $^{ns}p > 0.05$, not significant.
c-e, Representative images of iMG-$_{diss}$RO with tdTomato$^+$-iMG (orange), counterstained for the nuclei-dye Hoechst (blue) and immunostained in magenta for **c**, early transcription factors PU.1 (hematopoietic transcription factor PU.1), RUNX1 (runt-related transcription factor 1) and MYB (MYB Proto-Oncogene); **d**, 'early' microglia marker IBA1 (ionized calcium-binding adapter molecule 1) and CD45 (cluster of differentiation 45/ protein tyrosine phosphatase receptor); and **e**, 'mature' microglia marker P2RY12 and TREM2 (Triggering Receptor Expressed On Myeloid Cells 2). Scale bar: 10 µm.
iMG-$_{diss}$RO: microglia assembled dissociated retinal organoid. mRNA: messenger ribonucleic acid. RT-qPCR: real-time quantitative polymerase chain reaction. SEM: standard error of the mean.

To understand the functional consequences of iMG integration, we investigated their phagocytic ability. Similar to rodent studies (Anderson et al. 2019), the number of BRN3$^+$-ganglion cells significantly reduced in iMG-$_{diss}$RO compared to $_{diss}$RO (**Figure 45a**). Furthermore, 22.53% ± 7.13 % of all BRN3$^+$-ganglion cells positioned within a 5 µm radius of iMG. An average of 1.72 ± 1.70 iMG engulfed BRN3$^+$-ganglion cell bodies (**Figure 45b**), indicating their role in regulating neuron number during development.

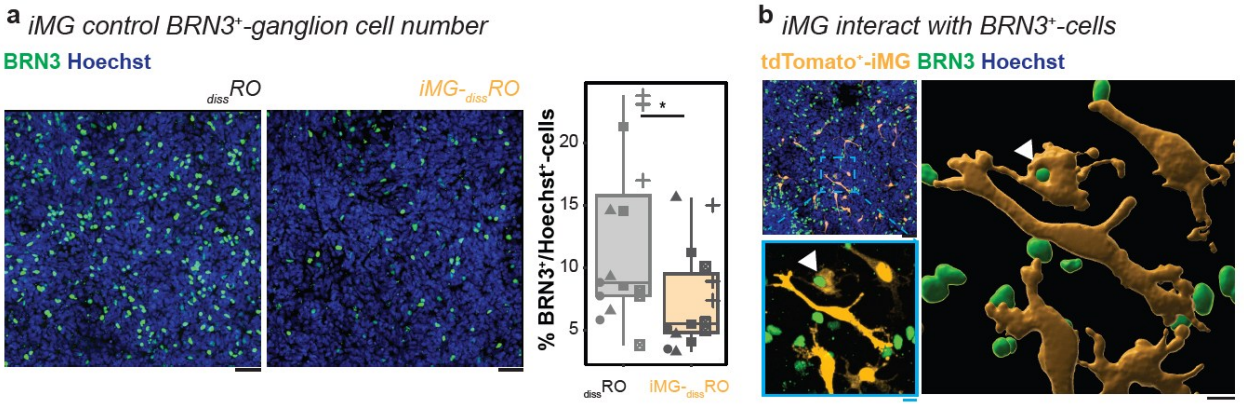

Figure 45 – Microglia control ganglion cell number in iMG-$_{diss}$RO.
a, Image of $_{diss}$RO (left) and iMG-$_{diss}$RO (right) at WK20 counterstained with the nuclei-dye Hoechst (blue) and immunostained for BRN3 (brain-specific homeobox/POU domain protein 3B, green). Scale bar: 50 µm. Next, boxplot of BRN3$^+$-ganglion cells relative to Hoechst$^+$-cells in $_{diss}$RO (grey) and iMG-$_{diss}$RO (orange). Symbols: single ROI of three biological replicates from five independent differentiation. Wilcoxon rank-sum test. *$p < 0.05$.
b, Representative images of BRN3$^+$-ganglion cells (green), tdTomato$^+$-iMG (orange) and the nuclei-dye Hoechst (blue) of iMG-$_{diss}$RO at WK20. Scale bar: 50 µm, zoom-in: 10 µm. Zoom-in: 3D-surface rendering of a region of interest. White arrowhead: iMG engulfing BRN3$^+$-cell.
$_{diss}$RO: dissociated retinal organoid. iMG: microglia-like cell. iMG-$_{diss}$RO: microglia assembled dissociated retinal organoid.

To determine if these engulfed cells are apoptotic ganglion cells, we co-labeled the culture with the apoptotic marker cleaved caspase-3 (CCAS3). CCAS3$^+$-cells were present (**Figure 46a**), but the total number was unaffected by iMG presence (**Figure 46b**). In line with previous observations in rodents (Anderson et al. 2019), iMG engulfed non-apoptotic ganglion cells (CCAS3$^-$/BRN3$^+$) (**Figure 46a**). At WK20, iMG selectively targeted ganglion cells as all phagocytosed Hoechst$^+$-

nuclei co-expressed BRN3$^+$. On a note, the number of Hoechst$^+$-cells or OTX2$^+$-photoreceptor/ bipolar cells remained unaffected at WK20 (**Figure 46c-d**).

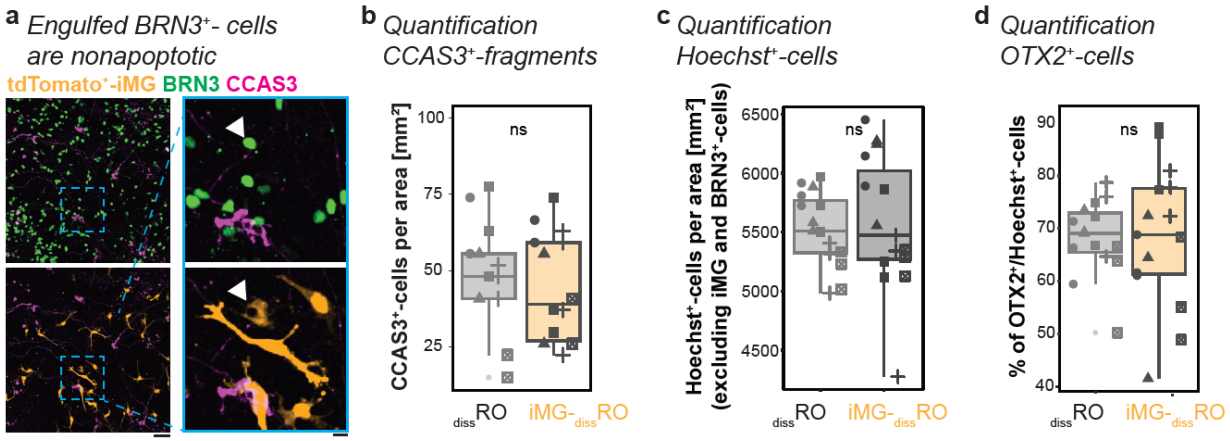

Figure 46 – Microglia specifically engulf non-apoptotic ganglion cells.
a, Representative images of BRN3$^+$-ganglion cells (brain-specific homeobox/POU domain protein 3B, green), tdTomato$^+$-iMG (orange), and the apoptotic marker CCAS3 (cleaved caspase-3, magenta) of iMG-$_{diss}$RO at WK20. Scale bar: 50 µm, zoom-in: 10 µm. White arrowhead: iMG engulfing BRN3$^+$/CCAS3$^-$-cell.
b-d, Boxplot of percent of **b**, CCAS3$^+$-cells per area; **c**, Hoechst$^+$-cells per area and **c**, OTX2$^+$-photoreceptor- and bipolar cells relative to Hoechst$^+$-cells in $_{diss}$RO (grey) and iMG-$_{diss}$RO (orange). Symbols: single ROI of three biological replicates from five independent differentiations. **b-c**, Student's t-test. **d**, Welch's t-test. $^{ns}p > 0.05$, not significant. $_{diss}$RO: dissociated retinal organoid. iMG: microglia-like cell. iMG-$_{diss}$RO: microglia assembled dissociated retinal organoid. OTX2: orthodenticle homolog 2. WK: Week after the start of the differentiation.

On a side note, the CCAS3 staining also highlighted that iMG removed cellular debris exemplified in their processes surrounding Hoechst$^+$/ CCAS3$^+$-nuclear fragments (**Figure 47a**). Consequently, iMG-$_{diss}$RO contained fewer Hoechst$^+$-nuclear fragments than cultures without iMG (**Figure 47b-c**). Also, in $_{3D}$ROs, iMG phagocytosed Hoechst$^+$-nuclear fragments (**Figure 47d**), emphasizing their phagocytic role in both models [20].

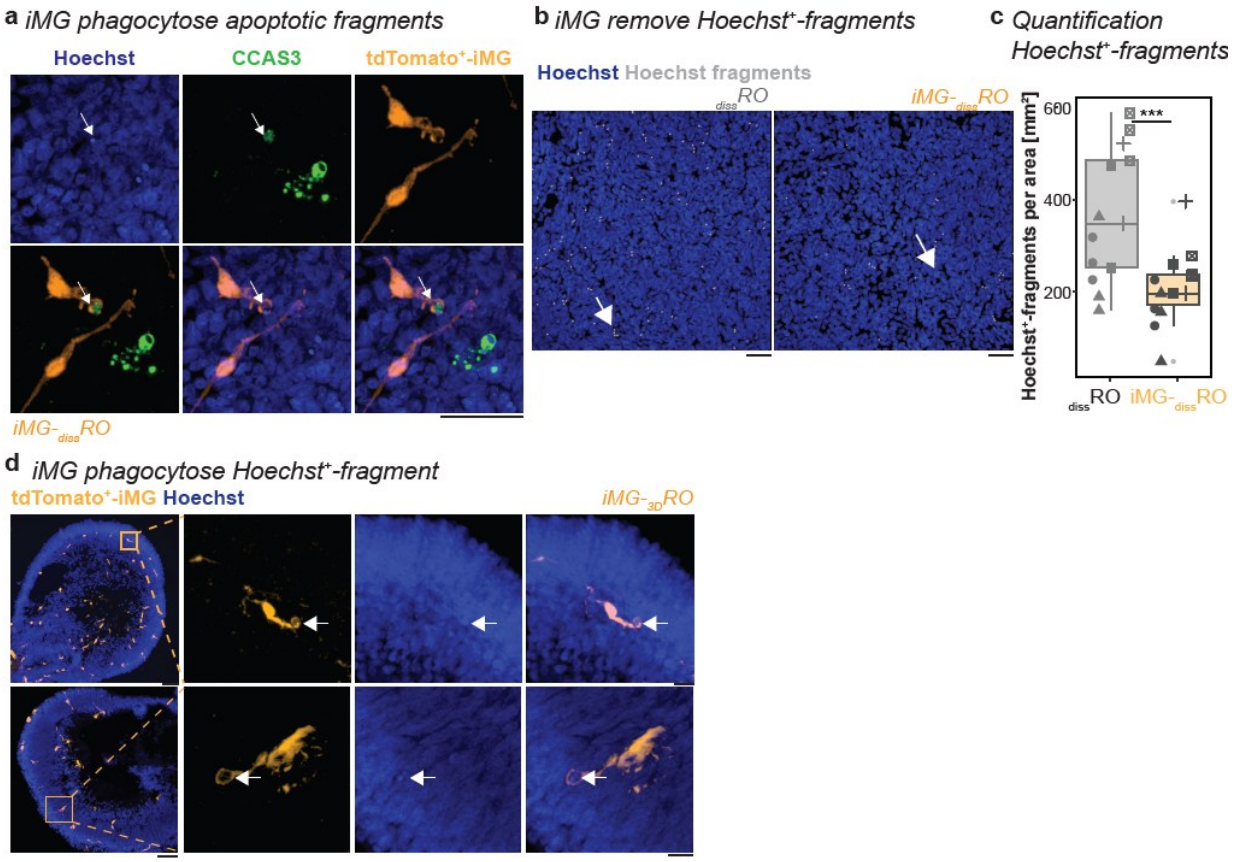

Figure 47 – Microglia remove Hoechst$^+$-fragments.
a, Representative images of iMG-$_{diss}$RO for tdTomato expression (orange), counterstained for the nuclei-dye Hoechst (blue) and immunostained for the apoptotic marker CCAS3 (cleaved caspase3, green). White arrowhead: iMG engulfing CCAS3$^+$-fragment. Scale bar: 50µm.
b, Hoechst$^+$-fragments (white) in $_{diss}$RO (left) and iMG-$_{diss}$RO (right). Scale bar: 50 µm.
c, Boxplot of the percent of Hoechst$^+$-fragments per area in $_{diss}$RO (grey) and iMG-$_{diss}$RO (orange). Symbols: single ROI of three biological replicates from five independent differentiations. Welch's t-test. ***p < 0.001.
d, Representative images of iMG-$_{3D}$RO cryostat sections counterstained with the nuclei-dye Hoechst (blue) and tdTomato$^+$-iMG (orange) at WK20. Arrow: iMG engulfing Hoechst$^+$-fragment. Scale bar: 50µm. Zoom in: Scale bar: 10µm.
$_{diss}$RO: dissociated retinal organoid. iMG: microglia-like cell. iMG-$_{diss}$RO: microglia assembled dissociated retinal organoid.

POLY(I:C) affects iMG phenotype without interfering with the ganglion cell interaction.

To mimic a prenatal neuro-immune challenge in our WK20 culture, we applied POLY(I:C) for 24h (**Figure 48a**). This immunostimulant activates a TLR3 response cascade, triggering downstream signaling pathways related to immune defense (Perales-Linares and Navas-Martin 2013; Sartorius et al. 2021). Indeed, *TLR3* mRNA level significantly increased after POLY(I:C) stimulation in preMG culture (**Figure 48b**), supporting a direct effect of POLY(I:C) on iMG. Next, we monitored iMG activity for 20 minutes in iMG-$_{diss}$RO. We found that iMG surveillance significantly increased compared to the control condition without POLY(I:C) (**Figure 48c**).

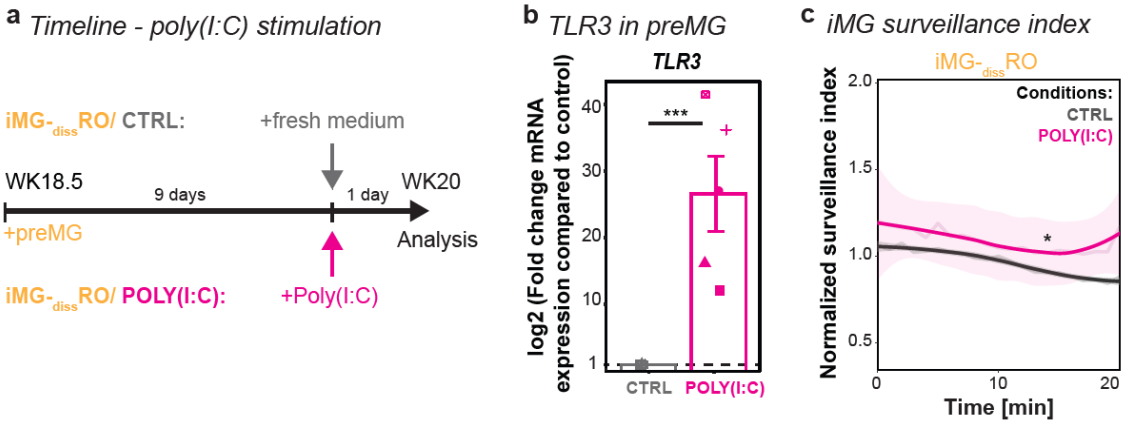

Figure 48 – Microglia respond to POLY(I:C) stimulation.
a, Experimental timeline. At WK18.5, preMG are added to dissRO. After nine days, the culture medium was replaced with fresh medium either containing POLY(I:C) (magenta) or without as a control (CTRL, grey). Analysis was performed 24 hours later on day 10.
b, RT-qPCR for TLR3 (toll-like receptor 3) of preMG after CTRL or POLY(I:C) stimulation. Bar chart with SEM: Mean mRNA transcript log2-fold changes compared to CTRL. Symbol: mean of technical triplicate from five independent differentiations. One sample t-test.
c, iMG-dissRO live imaging for 20 minutes for CTRL or POLY(I:C) stimulation after 24 hours. iMG surveillance index normalized to the mean surveillance of the cells in CTRL with a 95% confidence interval. Four independent differentiations. Wilcoxon rank-sum test. ***p < 0.001. * p < 0.05.
iMG: microglia-like cell. iMG-dissRO: microglia assembled dissociated retinal organoid. preMG: microglia precursors. POLY(I:C): polyinosinic:polycytidylic acid. WK: week after the start of the differentiation.

Furthermore, iMG significantly enlarged their surface area at 24h post-stimulation (**Figure 49a-b**), and they showed changes in other morphological features commonly found in reactive microglia (Fan et al. 2018; Montilla et al. 2020).

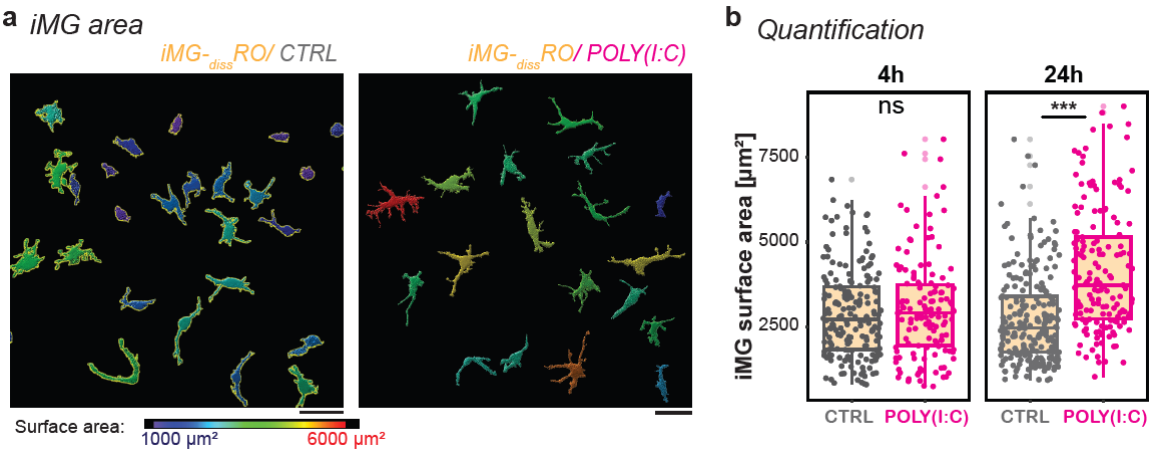

Figure 49– Figure legend on next page.

Figure 49 – Microglia change their morphology upon POLY(I:C) stimulation.
a, iMG surface rendering for CTRL (left) and POLY(I:C) (right) 4h and 24h following stimulation, color-coded based on surface area: blue = 1000 µm2 to red = 6000 µm2. Scale bar: 50 µm.
b, Boxplot of individual iMG surface areas in iMG-$_{diss}$RO for CTRL and POLY(I:C). iMG were collected from five independent differentiations. Kruskal-Wallis test with post-hoc Dunn's test. ***p < 0.001. ^{ns}p > 0.05, not significant. H: Hour. iMG: microglia-like cell. iMG-$_{diss}$RO: microglia assembled dissociated retinal organoid. POLY(I:C): polyinosinic:polycytidylic acid.

Based on these iMG phenotypes, we revisited the previously observed iMG-ganglion cell interaction (**Figure 45b**). iMG engulfed a comparable number of ganglion cells to age-matched, untreated control conditions (**Figure 50a**). When we analyzed the number of BRN3$^+$-ganglion cells, we observed a trend towards an increase in POLY(I:C)-treated culture, but this effect was insignificant (**Figure 50b**). We thus also investigated whether the iMG interaction with BRN3$^+$-ganglion cells is altered and determined the iMG position within a 5 µm radius of BRN3$^+$-labeling. The proximity measurement did not reveal an apparent difference between POLY(I:C) -stimulated and non-stimulated conditions (**Figure 50c-d**), suggesting that POLY(I:C) does not have an immediate effect on the iMG developmental task to regulate the ganglion cell number.

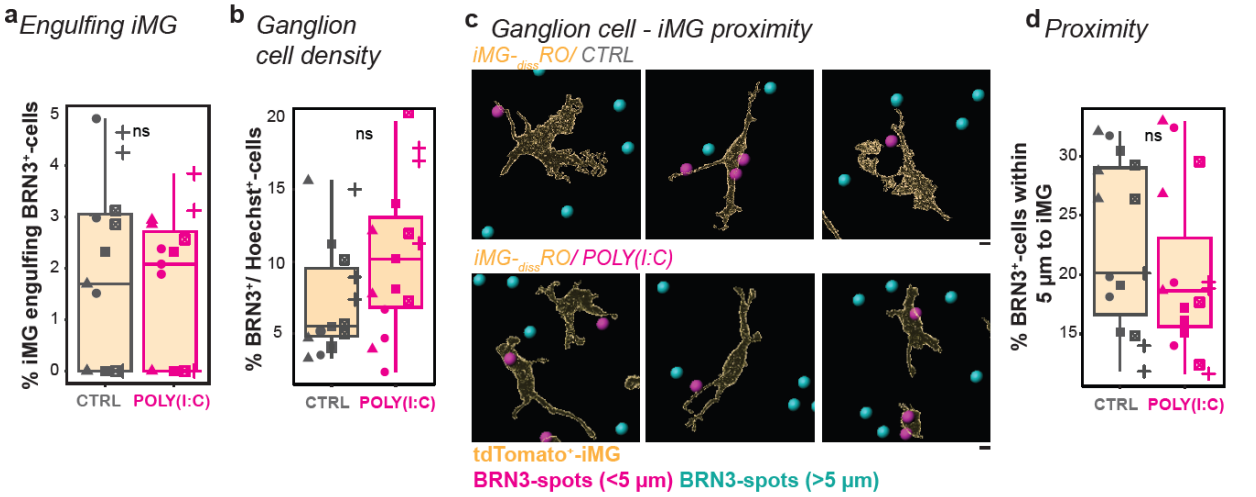

Figure 50 – Microglia still interact with ganglion cells following POLY(I:C) stimulation.
a, Boxplot quantifying the number of iMG engulfing BRN3$^+$-cells (brain-specific homeobox/POU domain protein 3B) in iMG-$_{diss}$RO for CTRL and POLY(I:C). Symbols: single ROI of three biological replicates from five independent differentiations. Wilcoxon rank-sum test.
b, Boxplot determines ganglion cell density based on BRN3$^+$-cells relative to Hoechst$^+$-cells in iMG-$_{diss}$RO for CTRL and POLY(I:C). Symbols: single ROI of three biological replicates from five independent differentiations. Wilcoxon rank-sum test.
c-d, Ganglion cell-iMG proximity in iMG-$_{diss}$RO. **c**, Surface rendering of iMG for CTRL (top) and POLY(I:C) (bottom). BRN3$^+$-spots color-coded based on the proximity to the iMG surface with spots < 5 µm (magenta) and spots > 5 µm (cyan). Scale bar: 10 µm. **d**, Boxplot of percent of magenta BRN3$^+$-spots. Symbols: single ROI of three biological replicates from five independent differentiations. Wilcoxon rank-sum test.
^{ns}p > 0.05, not significant.
iMG: microglia-like cell. iMG-$_{diss}$RO: microglia assembled dissociated retinal organoid. POLY(I:C): polyinosinic:polycytidylic acid. ROI: region of interest.

iMG presence influences POLY(I:C)-mediated inflammatory secretome signature and cell proliferation.

To obtain insights into how iMG presence affects the POLY(I:C)-mediated neuro-immune response, we analyzed the supernatant of $_{diss}$RO and iMG-$_{diss}$RO after 24h of POLY(I:C) stimulation and compared it to the untreated control (**Figure 48a**).

At baseline without POLY(I:C) stimulation, $_{diss}$RO with or without iMG were comparable, showing a similar set of secreted mediators, including MIF, CCL2, CXCL12, IL18, and SerpinE1 (**Figure 51a-b**).

$_{diss}$RO exposed to POLY(I:C) formed a separate cluster with only moderate differences from the controls. The additional detected cytokines CXCL10, CXCL11, CXCL1, and IL8 belong to the CXC family and are known to be secreted by astrocytes (Kim et al. 2022; Michael et al. 2020; Phares et al. 2013). Indeed, we verified the presence of GFAP$^+$-glia cells in $_{diss}$RO (**Figure 51c**).

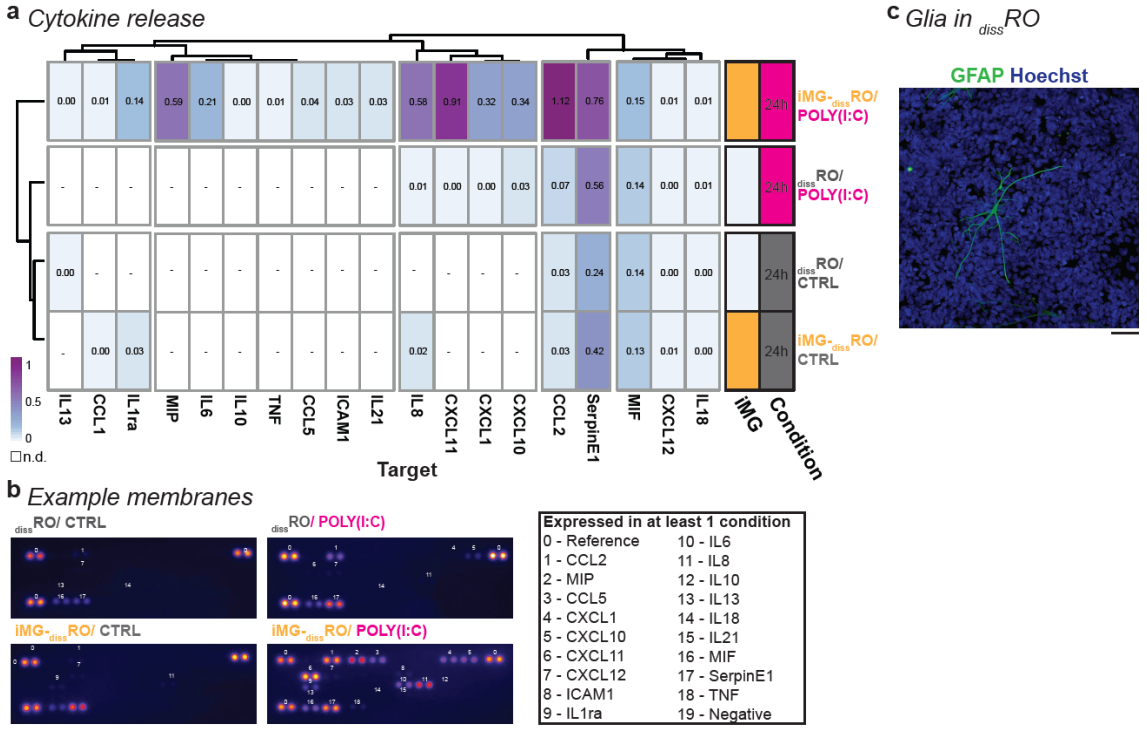

Figure 51 – Microglia dependent inflammatory response.

a, Release of inflammatory cytokines and chemokines into the supernatant based on the experimental paradigm described in **Figure 48a** for control (CTRL, grey) and POLY(I:C) (magenta) after 24-hour stimulation. Heatmap with color-coded mean pixel intensity relative to the reference of three independent differentiations. White: n.d. Side-bar: condition with iMG (iMG-$_{diss}$RO, orange) or without ($_{diss}$RO, white) or CTRL versus POLY(I:C).

b, Representative membranes for each condition. Numbers refer to the legend on the right.

c, Example images of $_{diss}$RO counterstained with the nuclei-dye Hoechst (blue) and immunostained for the glial marker GFAP (glial fibrillary acidic protein, green). Scale bar: 20 µm.

iMG-$_{diss}$RO: microglia assembled dissociated retinal organoid. POLY(I:C): polyinosinic:polycytidylic acid.

The most robust inflammatory secretome signature occurred when we stimulated iMG-$_{diss}$RO with POLY(I:C). The previous four factors were significantly higher released, and we detected an additional eight secreted inflammatory mediators such as TNFα, IL6, and MIP (**Figure 51a**, **Figure 52a**). Since those factors have already been partially upregulated in $_{diss}$RO, iMG seemed to amplify the signal. On a note, approximately half of the inflammatory mediators assayed were not secreted in any condition (**Figure 52b**).

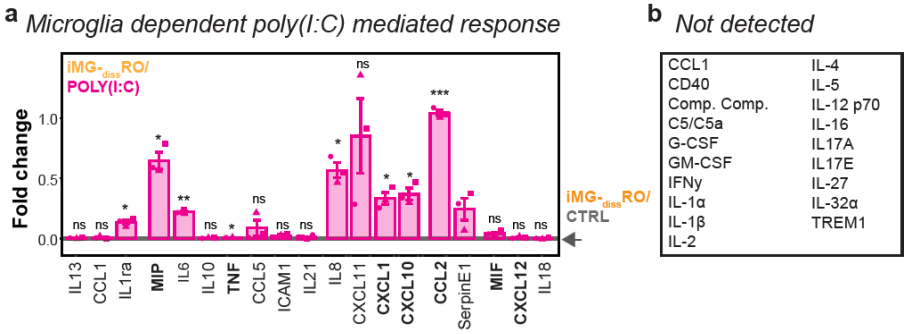

Figure 52 – POLY(I:C) mediated response.

a, Release of inflammatory cytokines and chemokines into the supernatant after 24-hour stimulation in iMG-$_{diss}$RO. Bar chart with SEM: Fold change of pixel intensity upon POLY(I:C) stimulation(magenta) relative to CTRL (grey). Each dot is an independent differentiation (n=3). Shapiro-Wilk normality test <0.05, Wilcoxon rank-sum test. Shapiro-Wilk normality test > 0.05, one sample t-test. ***p < 0.001. **p < 0.01. *p < 0.05. ^{ns}p > 0.05, not significant.

b, List of proteins assayed on the membrane but not detected in the supernatant of any condition.

iMG-$_{diss}$RO: microglia assembled dissociated retinal organoid. POLY(I:C): polyinosinic:polycytidylic acid. SEM: standard error of the mean.

These mediators were also not detected after only 2- or 4 hours of POLY(I:C) exposure in iMG-$_{diss}$RO (**Figure 53a**). In contrast, iMG morphology started already to adapt 4h post-stimulation (**Figure 49a-b**, **Figure 53b**), suggesting that iMG activation occurs before the release of inflammatory mediators.

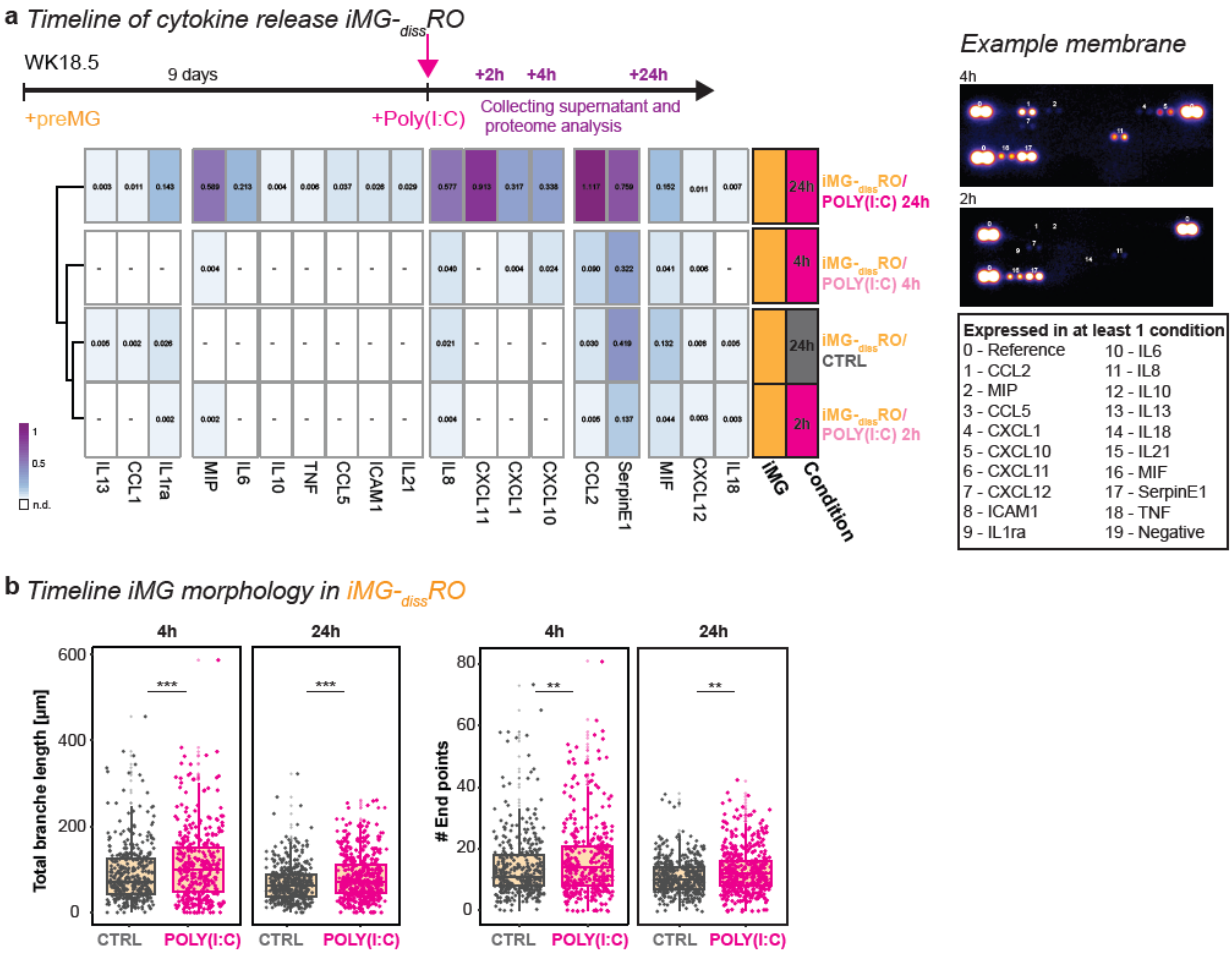

Figure 53 – Timeline POLY(I:C)-mediated response. (to be continued on next page)
a, Same assay as for in **Figure 51a** with additional measurement of cytokine and chemokine release after two and four hours compared to 24h in iMG-$_{diss}$RO with annotated example membranes.
b, Boxplot of the total branch length (left) and the number of endpoints (right) per iMG for CTRL (grey) and POLY(I:C) (magenta) following 4h and 24h stimulation in iMG-$_{diss}$RO. iMG-$_{diss}$RO were collected from five independent differentiations. Kruskal-Wallis test with post-hoc Dunn's test. ***p < 0.001.
H: hour. iMG: microglia-like cell. iMG-$_{diss}$RO: microglia assembled dissociated retinal organoid. POLY(I:C): polyinosinic:polycytidylic acid.

CCL2 (C-C Motif Chemokine Ligand 2) has been one of the strongest upregulated factors upon POLY(I:C) stimulation in iMG-$_{diss}$RO (**Figure 52a**). Besides being involved in the homing of monocytes and T-cells from the periphery (Bose and Cho 2013; Chen et al. 2003), CCL2 also contributes to neuronal proliferation in concert with the other upregulated secreted factors CXCL12, MIF, MIP, TNFα, CXCL1, and CXCL10 (Bernardino et al. 2008; Marsters et al. 2020; Rosin et al. 2021; Shang et al. 2019; Wu et al. 2009; Zhang et al. 2013) (**Figure 51a, Figure 52a**). To investigate the consequences on the number of proliferating cells, we immunostained for the proliferation marker KI67 (**Figure 54a-i**). In iMG-$_{diss}$RO, POLY(I:C) stimulation significantly reduced the number of KI67^{+}/iMG-cells compared to the control (**Figure 54a-b**), which supports data in rodents (Ben-Yehuda et al. 2019). Yet, the overall iMG density remained similar (**Figure 54c**), suggesting that iMG are less proliferative. In contrast, the overall number of proliferating retinal cells excluding iMG significantly increased upon POLY(I:C) stimulation in iMG-$_{diss}$RO (**Figure 54d-**

e). We observed the same effect in iMG-$_{3D}$ROs (**Figure 54f-g**) emphasizing that this effect is independent from $_{diss}$RO *versus* $_{3D}$RO. Overall, this consequence aligns with rodent studies after prenatal immune challenges (Baines et al. 2020; Kuse et al. 2018; Loayza et al. 2022). Since the secretion of proliferation-associated factors was only upregulated in the presence of iMG (**Figure 51a**), we determined the number of KI67$^+$/Hoechst$^+$-cell in $_{diss}$RO and $_{3D}$ROs lacking iMG. POLY(I:C) failed to increase KI67$^+$-cells in both conditions (**Figure 54h-i**), emphasizing an iMG-dependent effect on cell proliferation upon POLY(I:C) exposure.

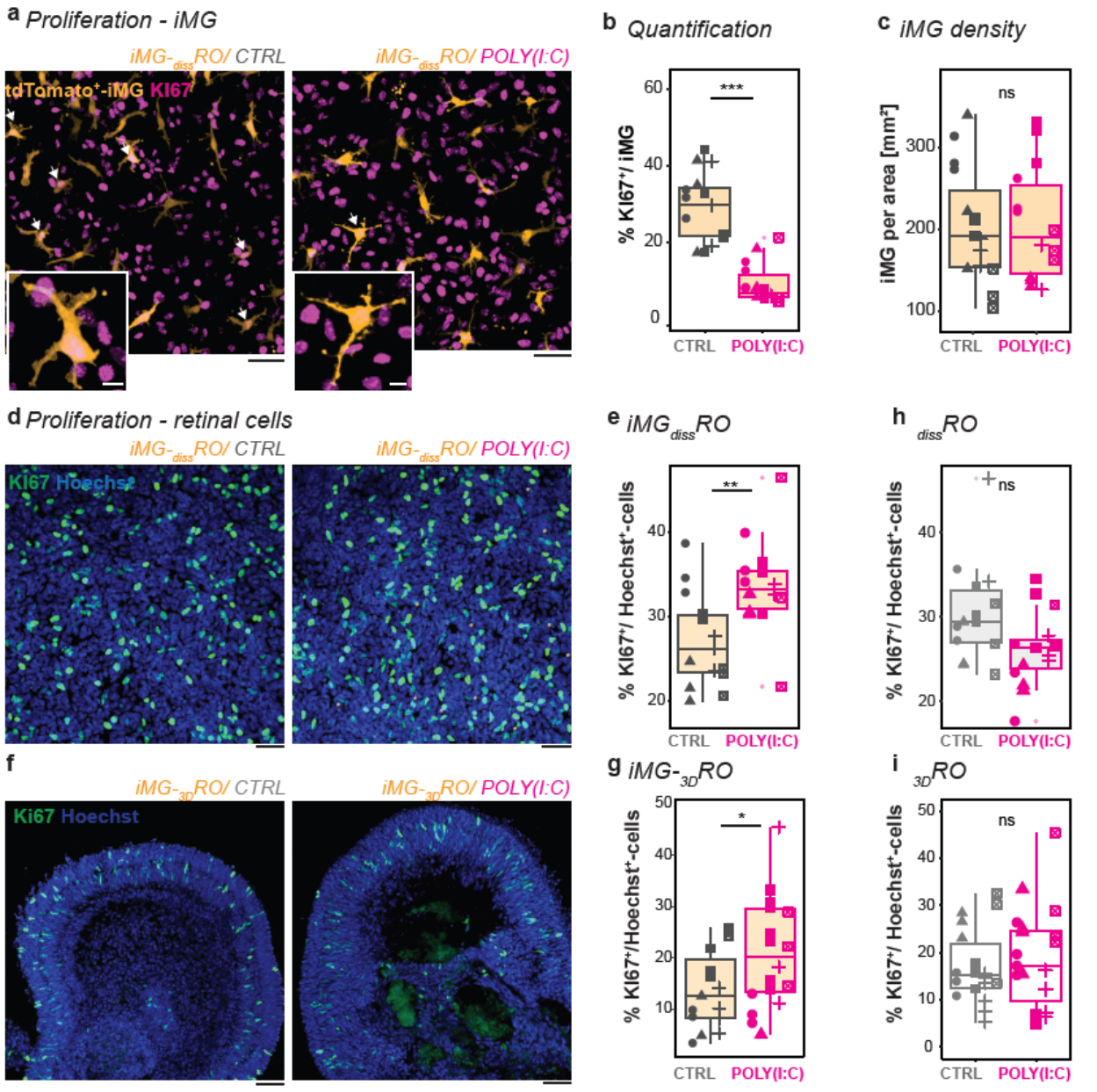

Figure 54 – Figure legend on next page.

Figure 54 – POLY(I:C)-mediated microglia-dependent consequences on the retinal environment.
a-c, iMG proliferation rate in iMG-$_{diss}$RO for CTRL (left) and POLY(I:C) (right). **a**, Example ROI image of tdTomato$^+$-iMG (orange) and immunostained for the proliferation marker KI67 (proliferation marker protein Ki-67, magenta). White arrow: KI67$^+$-expressing iMG. Scale bar: 50µm. Zoom-in: Scale bar: 10 µm. **b**, Boxplot of KI67$^+$/iMG percentage. Wilcoxon rank-sum test. **c**, Boxplot of iMG per area. Students' t-test. **b-c**, Symbols: single ROI of three biological replicates from five independent differentiations.
d-i, Proliferation of retinal cells. **d, f**, Example ROI images counterstained for the nuclei-dye Hoechst (blue) and immunostained for the proliferation marker KI67 (green) for CTRL (left) and POLY(I:C) stimulation (right) for iMG-$_{diss}$RO (**d**) and cryostat section with a focus on the retinal cup of iMG-3DRO (**f**). Scale bar: 50 µm. **e, g-i,** Boxplot percent of KI67$^+$-cells relative to Hoechst$^+$-cells, excluding KI67$^+$/iMG, for CTRL (grey) and POLY(I:C) (magenta) in iMG-$_{diss}$RO (**e**), iMG-$_{3D}$RO (**g**), $_{diss}$RO (**h**), and $_{3D}$RO (**i**). Symbols: single ROI of three biological replicates from five independent differentiations. Students' t-test. ***p < 0.001. **p < 0.01. *p < 0.05. ^{ns}p > 0.05, not significant.
CTRL: control. iMG: microglia-like cell. iMG-dissRO: microglia assembled dissociated retinal organoid. POLY(I:C): polyinosinic:polycytidylic acid. ROI: region of interest.

Next, to identify whether CCL2 is the primary mediator of this effect, we applied 10 ng/ml CCL2 to iMG-$_{diss}$RO cultures at WK20 and analyzed the consequences 24h later (**Figure 55a**). In contrast to POLY(I:C) stimulation (**Figure 54d-e**), CCL2 exposure did not increase the overall proliferation rate (**Figure 55b**). Even if we applied higher CCL2 concentrations, the ratio of KI67$^+$/Hoechst$^+$-cells remained the same. Unexpectedly, the ratio of KI67$^+$/iMG rose with 10 ng/ml CCL2 (**Figure 55c**), which is in contrast to the POLY(I:C) condition (**Figure 54a-b**). This suggests that CCL2 alone cannot drive the observed phenotypes and that the interplay with additional proliferation-associated factors is critical.

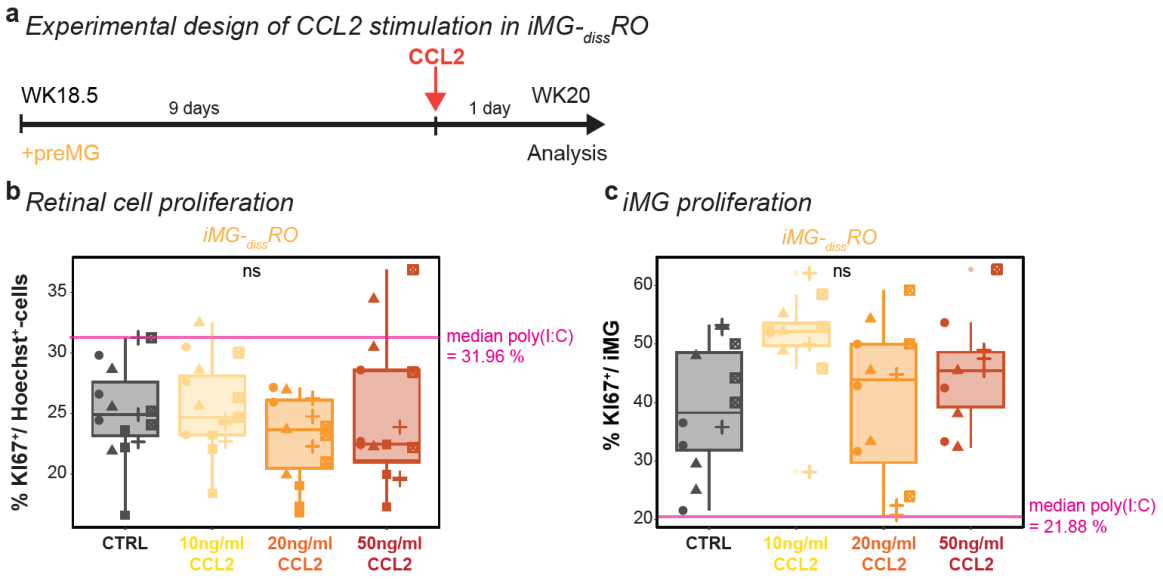

Figure 55 – Figure legend on next page.

Figure 55 – The POLY(I:C)-mediated proliferation rate increase cannot be replicated with CCL2 alone.
a, Experimental timeline. At WK18.5, preMG are added to $_{diss}$RO. After nine days, iMG-$_{diss}$RO received fresh medium for control or CCL2 (C-C motif chemokine ligand 2) stimulation for 24 hours.
b, Effect of CCL2 on retinal cell proliferation excluding iMG. Boxplot of percent KI67^{+}-cells relative to Hoechst^{+}-cells in iMG-$_{diss}$RO for CTRL (grey) and CCL2 stimulation at a final concentration of 10 ng/mL (yellow), 20 ng/mL (orange), and 50 ng/mL (red). Magenta line: Median proliferation rate in POLY(I:C) stimulation of iMG-$_{diss}$RO (**Figure 53e**). Symbols: three biological replicates from five independent differentiations. One-way ANOVA.
c, Effect of CCL2 on iMG proliferation. Boxplot of percent KI67^{+}/iMG for CTRL (grey) and CCL2 stimulation at a final concentration of 10 ng/mL (yellow), 20 ng/mL (orange), and 50 ng/mL (red). Magenta line: Median iMG-proliferation rate in POLY(I:C) stimulation of iMG-$_{diss}$RO (**Figure 53b**). Symbols: three biological replicates from five independent differentiations. Kruskal-Wallis test. $^{ns}p > 0.05$, not significant.
CTRL: control. preMG: microglia precursor. iMG: microglia-like cell. iMG-$_{diss}$RO: microglia assembled dissociated retinal organoid. POLY(I:C): polyinosinic:polycytidylic acid. WK: week after the start of the differentiation.

Ibuprofen dampens POLY(I:C)-induced iMG phenotypes and reduces cell proliferation.

Besides cytokines and chemokines, another hallmark of inflammation is the secretion of prostaglandins such as PGE2, which mediate classic symptoms of inflammation (Lima et al. 2012; Pecchi et al. 2009). Indeed, we found that iMG-$_{diss}$RO stimulated with POLY(I:C) for 24h showed increased PGE2 levels in the supernatant (**Figure 56a**-**b**). NSAIDs like ibuprofen target the enzymes cyclooxygenase 1 and 2 (*PTGS1*/COX1, *PTGS2*/COX2, respectively) and prevent arachidonic acid conversion into prostaglandins (Griswold and Adams 1996; Kato et al. 2010). Simultaneous exposure of POLY(I:C) with the active enantiomer S(+)-ibuprofen dampened PGE2 upregulation in iMG-$_{diss}$RO (**Figure 56b**) as well as in iMG-$_{3D}$RO (**Figure 56c**).

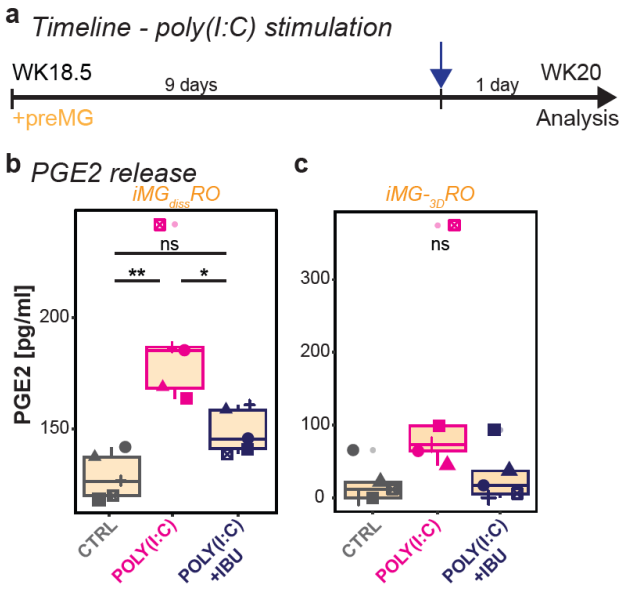

Figure 56 – Ibuprofen dampens PGE2 release.
a, Experimental timeline. At WK18.5, preMG are added to $_{diss}$RO. After nine days, cultures received fresh medium for untreated control (CTRL), POLY(I:C) or POLY(I:C) and S(+)-ibuprofen (POLY(I:C)+IBU) for 24 hours before analysis.
b-c, PGE2 (prostaglandin E2) is released into the supernatant of iMG-$_{diss}$RO (**b**) and iMG-$_{3D}$RO (**c**). Boxplot of PGE2 concentration [pg/ml] after CTRL (grey), POLY(I:C) (magenta), and POLY(I:C)+IBU (blue). Each symbol: an independent differentiation (n=5).
b, One-way ANOVA with post-hoc Tukey's test. **c**, Kruskal-Wallis test with post-hoc Dunn's test.
CTRL: control. preMG: microglia precursor. IBU: S(+)-ibuprofen. iMG-$_{diss}$RO: microglia assembled dissociated retinal organoid. POLY(I:C): polyinosinic:polycytidylic acid. WK: week after the start of the differentiation.

Next, we investigate the release of cytokine and chemokine into the supernatant during the POLY(I:C)-mediated neuro-immune challenge when we simultaneously applied S(+)-ibuprofen. Most inflammatory mediators remained unaffected upon exposure to S(+)-ibuprofen (**Figure 57**). Only TNF secretion increased, which aligns with a previous study identifying that PGE2 inhibits TNF expression in macrophage cell lines *in vitro* (Stafford and Marnett 2008).

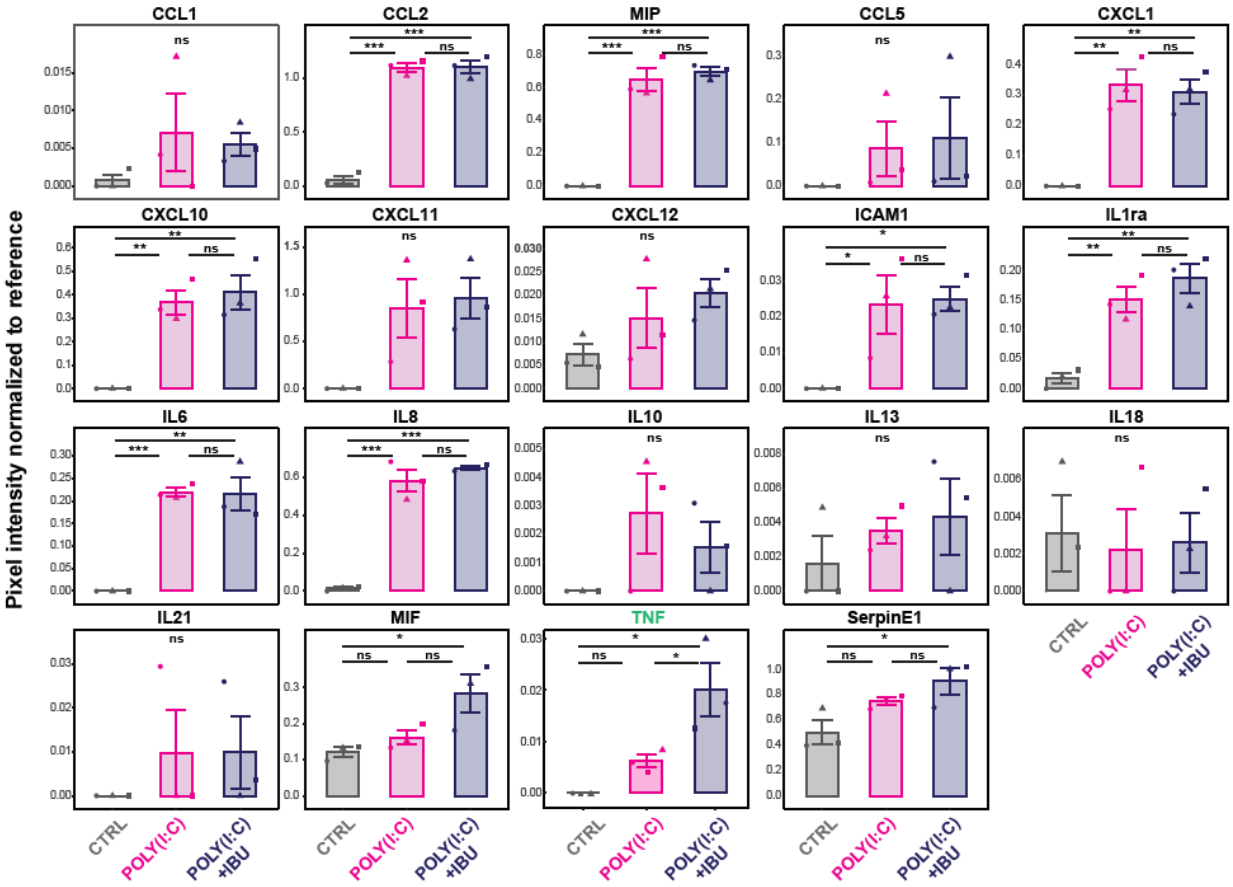

Figure 57 – Comparison of individual secreted inflammatory mediators after ibuprofen exposure.
a, Release of inflammatory cytokines and chemokines into the supernatant based on the experimental paradigm described in **Figure 51a** for untreated control (CTRL, grey), POLY(I:C) (magenta), and POLY(I:C) and S(+)-ibuprofen (POLY(I:C)+IBU, blue) stimulation in iMG-$_{diss}$RO. Bar chart of pixel intensity normalized to reference with standard error of the mean. Each symbol is an independent differentiation (n=3). One-way ANOVA with post-hoc Tukey's test, except IL13, IL18, IL21 Kruskal-Wallis test. ***p < 0.001. **p < 0.01. *p < 0.05. ^{ns}p > 0.05, not significant.
CTRL: control. IBU: S(+)-ibuprofen. POLY(I:C): polyinosinic:polycytidylic acid.

Since microglia have been shown to constitutively express PTGS1/COX1 (Deininger and Schluesener 1999) and ibuprofen targets PTGS1/COX1, we revisited iMG surveillance and monitored their activity**.** 24h following exposure of S(+)-ibuprofen simultaneously with POLY(I:C), iMG surveillance significantly reduced compared to just POLY(I:C) and even below the control level in $_{diss}$RO (**Figure 58a**). Morphologically, iMG remained confined, exhibiting less cell surface area than just POLY(I:C) exposure (**Figure 58b-c**), indicating a dampened activity and underlining a direct ibuprofen-mediated effect on iMG.

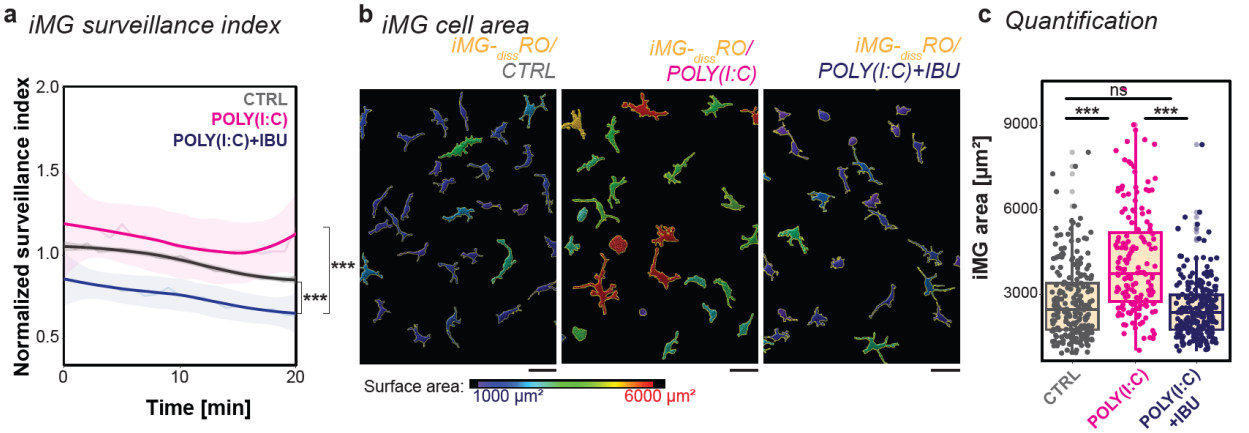

Figure 58 – Ibuprofen impacts POLY(I:C)-mediated consequences on iMG.

a, iMG-$_{diss}$RO live imaging for 20 minutes after 24h stimulation. iMG surveillance index normalized to the mean surveillance of the cells in CTRL with a 95% confidence interval. Data from five independent differentiations. Kruskal-Wallis test with post-hoc Dunn's test.

b-c, iMG surface area in iMG-$_{diss}$RO. **b**, iMG surface rendering for CTRL (left), POLY(I:C) (middle), and POLY(I:C)+IBU (right), color-coded based on surface area: blue = 1000 µm2 to red = 6000 µm2. Scale bar: 50 µm. **c**, Boxplot of individual iMG surface areas. iMG from five independent differentiations. Kruskal-Wallis test with post-hoc Dunn's test.

***$p < 0.001$. $^{ns}p > 0.05$, not significant.

CTRL: control. IBU: S(+)-ibuprofen. iMG-$_{diss}$RO: microglia assembled dissociated retinal organoid. POLY(I:C): polyinosinic:polycytidylic acid.

To further examine whether ibuprofen improves the consequences of the prenatal neuro-immune challenge, we revisited the increased proliferation phenotype upon POLY(I:C) exposure. Following simultaneous treatment with S(+)-ibuprofen, the ratio of KI67$^+$/Hoechst$^+$-cells reduced for four out of five differentiation in iMG-$_{diss}$RO compared to POLY(I:C) stimulation alone (**Figure 59a-c**). In iMG-$_{3D}$RO, we observed a similar beneficial effect (**Figure 59d-e**).

Since ibuprofen has been associated with anti-proliferative effects in cancer cell lines (Janssen et al. 2006; Yao et al. 2005), we evaluated S(+)-ibuprofen without POLY(I:C) exposure in iMG-$_{diss}$RO. The number of proliferating cells remained similar (**Figure 59f**).

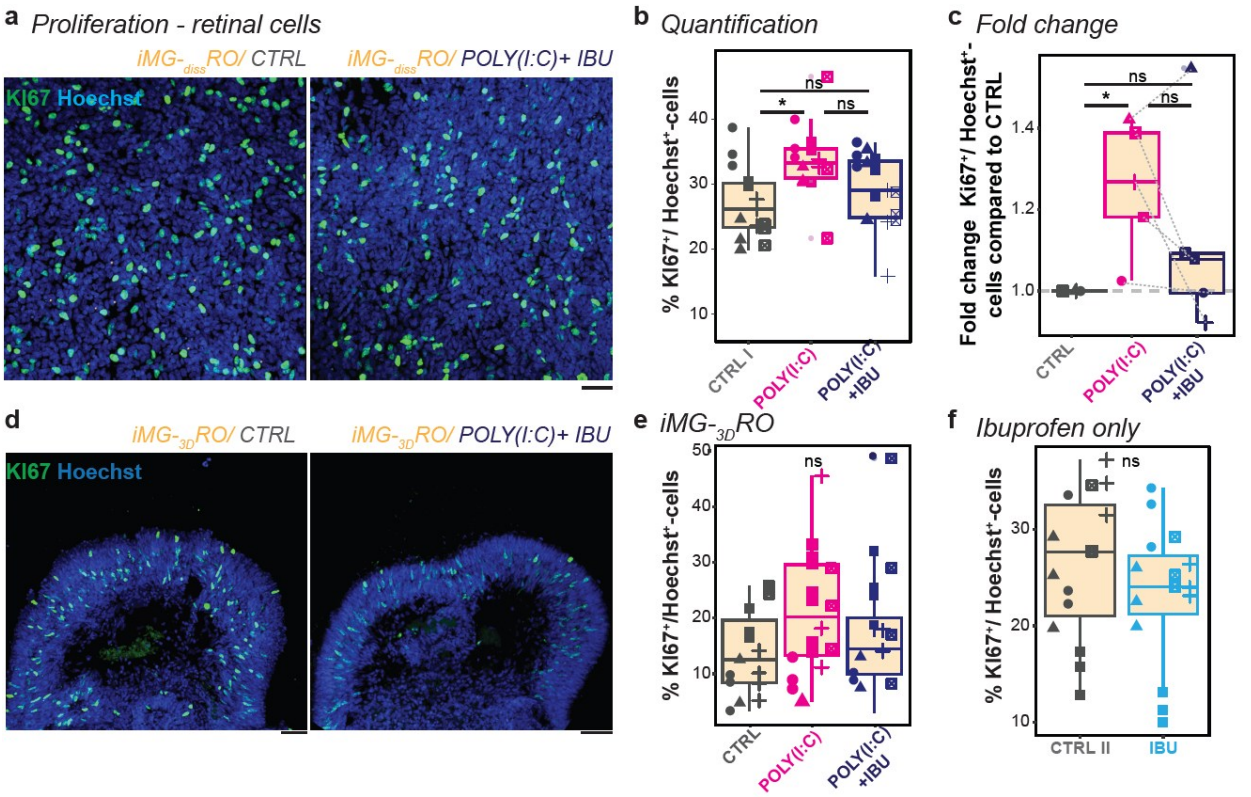

Figure 59 – Ibuprofen partially reverses POLY(I:C)-mediated consequences on retinal cell proliferation.
a and **d**, Example image of iMG-$_{diss}$RO (**a**) and cryostat sections focusing on retinal cup iMG-$_{3D}$RO (**d**) at WK20 counterstained with the nuclei-dye Hoechst (blue) and immunostained for KI67 (proliferation marker protein Ki-67, green) for CTRL (left) and POLY(I:C) +IBU (right). Scale bar: 50 µm.
b-c and e-f, Quantification proliferation rate of retinal cells in iMG-$_{diss}$RO (**b-c, f**) and iMG-$_{3D}$RO (**e**). Each symbol is an independent differentiation (n=5). Single ROI of three biological replicates. (**b, e**) Boxplot percent of KI67$^+$-cells relative to Hoechst$^+$-cells for CTRL (grey), POLY(I:C) (magenta), and POLY(I:C) +IBU (blue) excluding KI67$^+$/iMG.. **b**, One-way ANOVA with post-hoc Tukey's test. **e**, Kruskal-Wallis test. **c**, Fold change of median percent of KI67$^+$-cells relative to Hoechst$^+$-cells compared to CTRL. One sample t-test and Student's t-test. **f**, Boxplot percent of KI67$^+$-cells relative to Hoechst$^+$-cells for CTRL (grey) and only IBU exposure (light-blue) for 24 hours. Students's t-test.
*p < 0.05. nsp > 0.05, not significant.
CTRL: control. IBU: S(+)-ibuprofen. iMG-$_{diss}$RO: microglia assembled dissociated retinal organoid. POLY(I:C): polyinosinic:polycytidylic acid.

Ibuprofen depends on iMG to reverse POLY(I:C)-mediated effects on neuronal activity.

Initially, we described that the OPL formation aligned with iMG integration. Once the OPL is formed, spontaneous glutamatergic activity shapes neuronal circuits *in vivo* (Morgan and Wong 2007). Since iMG-$_{diss}$RO expressed synaptic markers (**Figure 60a**), we investigated the number of presynaptic VGLUT1$^+$-puncta and postsynaptic PSD95$^+$-puncta on MAP2$^+$-neurons, and their proximity as an indicator for functional synapses (VGLUT1$^+$/PSD95$^+$-puncta) in $_{diss}$RO and iMG-$_{diss}$RO. iMG presence affected neither of those parameters at WK20 (**Figure 60b-d**).

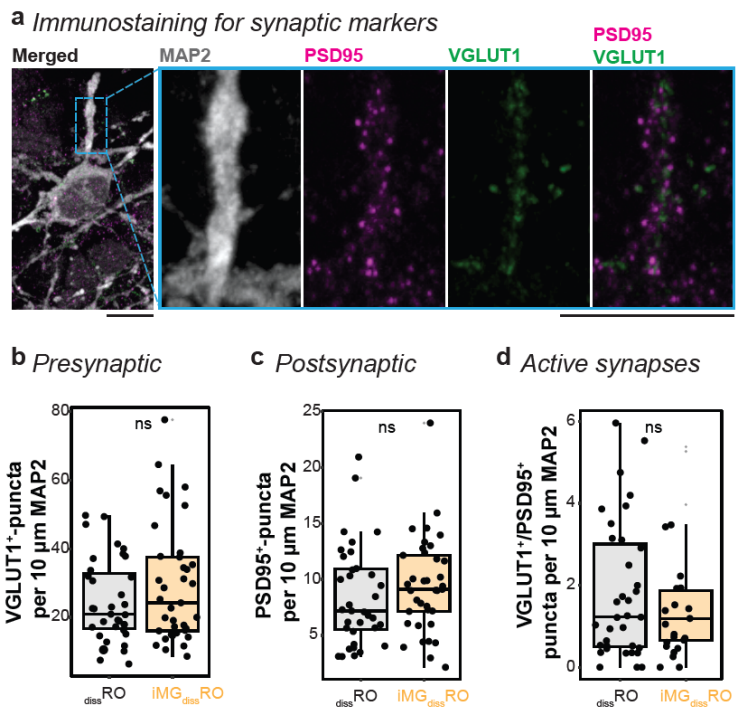

Figure 60 – Microglia do not influence the number of synaptic puncta.

a, Example image of iMG-$_{diss}$RO immunostained for the neuronal marker MAP2 (microtubule-associated protein 2, grey), the presynaptic marker VGLUT1 (vesicular glutamate transporter 1, green), and the postsynaptic marker PSD95 (postsynaptic density protein 95, magenta) with zoom-in. Scale bar: 10 µm.

b-d, Boxplots of synaptic puncta quantification in $_{diss}$RO (grey) and iMG-$_{diss}$RO (orange) for VGLUT1$^+$-puncta per 10µm MAP2 (**b**), PSD95$^+$-puncta per 10µm MAP2 (**c**) and VGLUT1$^+$/PSD95$^+$-puncta per 10µm MAP2 (**d**). Each dot represents one process close to the soma of a single cell. Five independent dissociations from three differentiations. Wilcox-test.

^{ns}p > 0.05, not significant. iMG-$_{diss}$RO: microglia assembled dissociated retinal organoid.

Next, we visualized spontaneous calcium transients as a correlate for neuronal activity. First, we transduced $_{diss}$RO with adeno-associated virus (AAV), which is independent of TLR3-signaling (Cao and Herzog 2008). The AAV encoded for the calcium sensor GCAMP6s under the control of the ubiquitous EF1α promoter (Cowan et al. 2020; Garita-Hernandez et al. 2020), resulting in a broad expression across retinal cell types (**Figure 61a-e**).

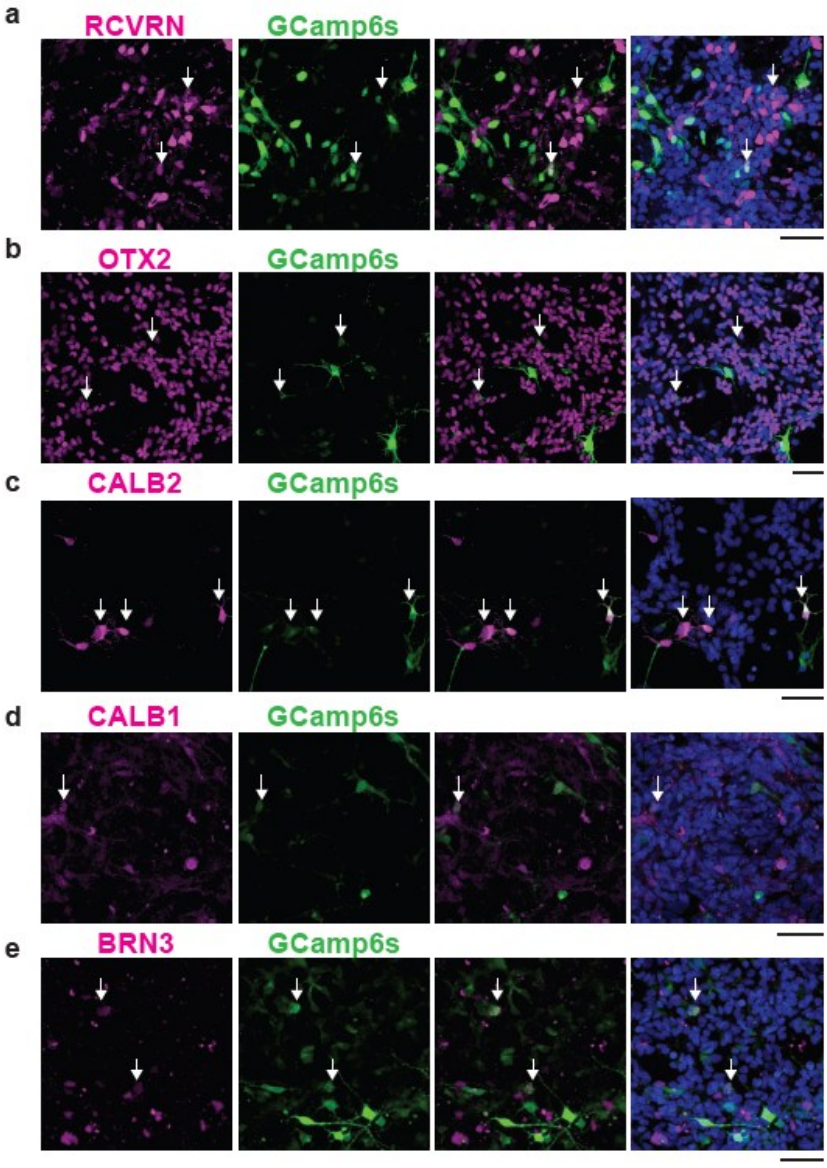

Figure 61 – GCAMP6s expression across retinal cell types.
a-e, Example ROI images of $_{diss}$RO infected with AAV2-GCAMP6s at WK17, analyzed at WK20, counterstained for the nuclei-dye Hoechst (blue) and the calcium sensor GCAMP6s (green), and immunostaining for retinal cell types (magenta): **a**, RCVRN (recoverin; photoreceptors). **b**, OTX2 (orthodenticle homeobox 2; photoreceptors, bipolar cells). **c**, CALB2 (calretinin; photoreceptors, bipolar-, amacrine cells). **d**, CALB1 (calbindin; amacrine-, horizontal cells). **e**, BRN3 (brain-specific homeobox/POU domain protein 3B; ganglion cells). Arrow: Co-expression of calcium sensor and retinal marker. Scale bar: 50µm.
ROI: region of interest. WK: Week after the start of the differentiation.

Importantly, to exclude any AAV-mediated microglia activation, we applied the virus to $_{diss}$RO at WK17 and 1.5 weeks before adding preMG (**Figure 62a**). At WK20, we analyzed the spontaneous calcium transients (**Figure 62b-c**). The calcium peak amplitude and the mean frequency remained similar in $_{diss}$RO and iMG-$_{diss}$RO (**Figure 62d**).

The calcium transients were either abolished after application of the voltage-gated sodium channel blocker tetrodotoxin (TTX) (**Figure 62e**) or significantly reduced after pharmacological blocking of glutamatergic synaptic transmission using a combination of CPP, NBQX, and APB (**Figure 62f**). Furthermore, the spontaneous calcium activity depended on extracellular calcium because the transients stopped when we applied the Ca^{2+}-chelator EGTA into the media (**Figure 62g**).

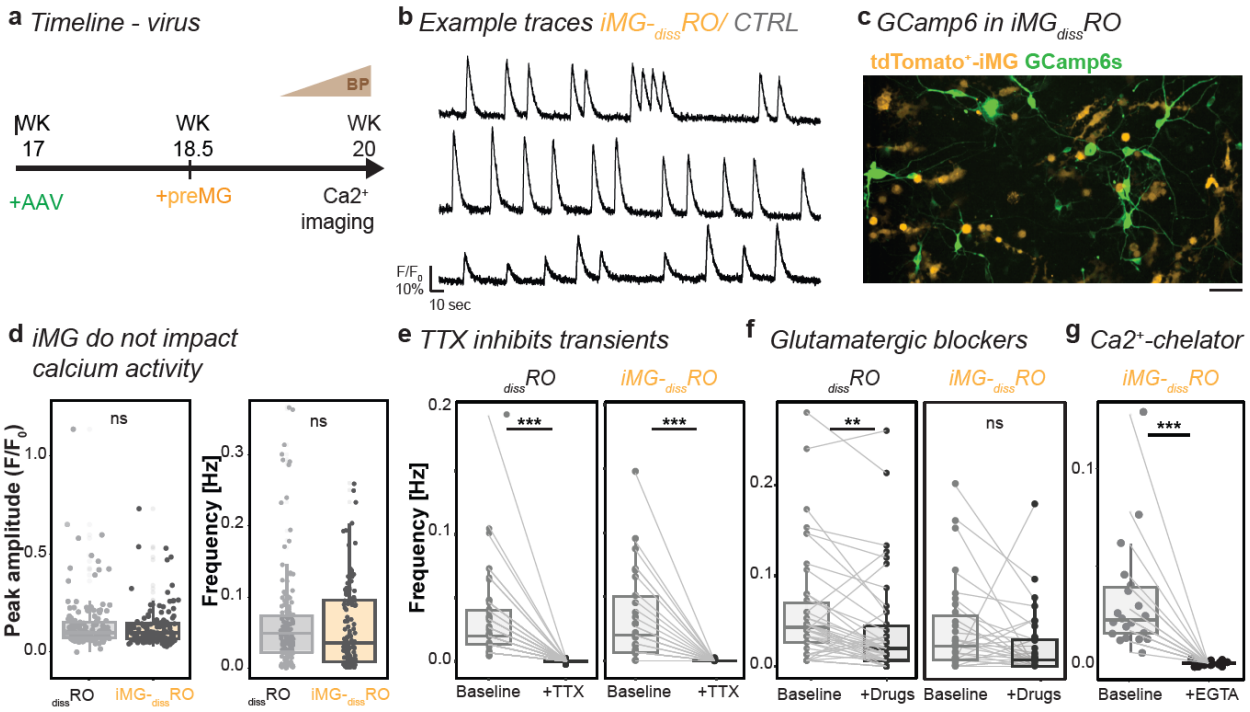

Figure 62 – Calcium dynamics of retinal cell types.

a, Experimental timeline. At WK17, $_{diss}$RO transduced with AAV2-GCAMP6s. preMG added at WK18.5. Four days before calcium imaging, gradual transition to Brain-Phys (BP) medium until WK20.

b, Three example traces of spontaneous calcium transients in iMG-$_{diss}$RO.

c, Example ROI image of iMG-$_{diss}$RO expression of the calcium sensor GCAMP6s (green) and tdTomato^{+}-iMG (orange). Scale bar: 50µm.

d, Spontaneous calcium dynamics during five minutes recording in $_{diss}$RO (grey) and iMG-$_{diss}$RO (orange). Boxplot of the mean peak amplitude [F/F_0] (left) and the mean frequency [Hz] (right). Wilcoxon rank-sum test.

e, TTX (Tetrodotoxin) abolishes calcium transients in $_{diss}$RO (left) and iMG-$_{diss}$sRO (right). Boxplot of mean frequency [Hz] during 150-sec baseline recording (baseline) and following TTX application for another 150 sec (+TTX). One-sample Wilcoxon signed rank test.

f, Boxplot of mean frequency [Hz] during 150-sec baseline recording (baseline) and following exposure to glutamatergic blockers CPP (4-(3-phosphonopropyl)piperazine-2-carboxylic acid), APB (2-aminoethoxydiphenyl borate), and NBQX (2,3-dioxo-6-nitro-7-sulfamoyl-benzo[f]quinoxaline) for 150 sec in $_{diss}$RO (left) and iMG-$_{diss}$RO (right). Wilcoxon rank-sum test.

g, Boxplot of mean frequency [Hz] during 150-sec baseline recording (baseline) and following Ca^{2+}-chelator EGTA (ethylene glycol tetraacetic acid) application for another 150 sec in iMG-$_{diss}$RO. One-sample Wilcoxon signed rank test.

***$p < 0.001$. **$p < 0.01$. $^{ns}p > 0.05$, not significant.

Ca^{2+}: calcium. $_{diss}$RO: dissociated retinal organoid. Hz: Hertz. iMG-$_{diss}$RO: microglia assembled dissociated retinal organoid. preMG: microglia precursor. Sec: seconds. WK: week after the start of the differentiation.

Inflammatory factors have been shown to modulate neuronal activity (Clarkson et al. 2017; Hayes et al. 2022; Vezzani and Viviani 2015; Zhu et al. 2006). Indeed, we found that POLY(I:C) exposure in both iMG-$_{diss}$RO and $_{diss}$RO significantly increased the calcium peak amplitude of individual cells (**Figure 63a-b**) and had no effect on the mean frequency (**Figure 63c-d**). To obtain insights into whether the increased calcium peak amplitude is mediated via glutamatergic synaptic transmission, we applied CPP, NBQX, and APB following 24h POLY(I:C) stimulation. Similar to the untreated control (**Figure 62f**), the frequency significantly decreased (**Figure 63e**). We found that

the amplitude was unaffected, suggesting that the increase in the calcium amplitude peak is independent of glutamatergic signaling and instead mediated through microglia-neuron signaling.

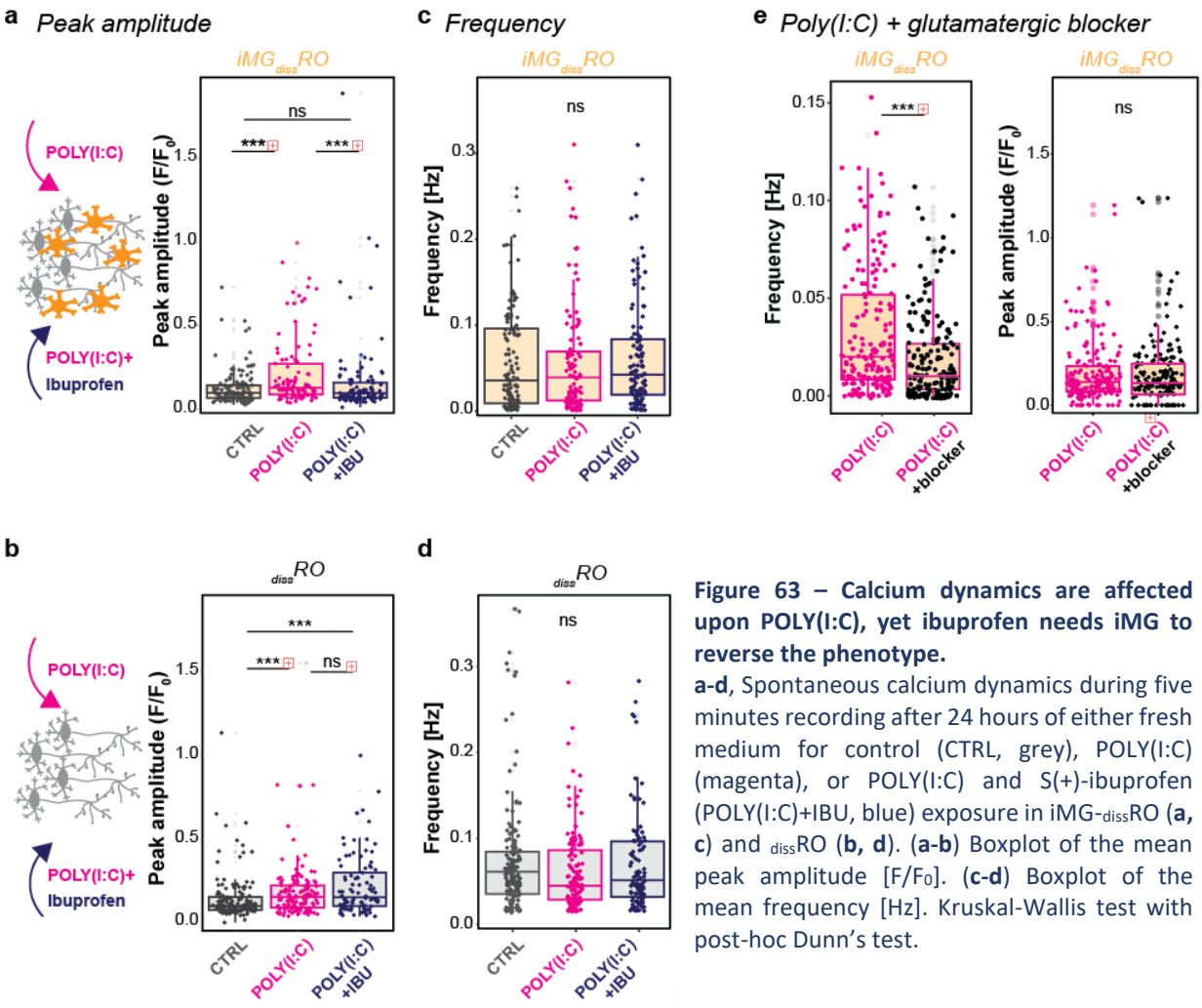

Figure 63 – Calcium dynamics are affected upon POLY(I:C), yet ibuprofen needs iMG to reverse the phenotype.

a-d, Spontaneous calcium dynamics during five minutes recording after 24 hours of either fresh medium for control (CTRL, grey), POLY(I:C) (magenta), or POLY(I:C) and S(+)-ibuprofen (POLY(I:C)+IBU, blue) exposure in iMG-$_{diss}$RO (**a, c**) and $_{diss}$RO (**b, d**). (**a-b**) Boxplot of the mean peak amplitude [F/F$_0$]. (**c-d**) Boxplot of the mean frequency [Hz]. Kruskal-Wallis test with post-hoc Dunn's test.

e, Spontaneous calcium dynamics in iMG-$_{diss}$RO after 24 hours POLY(I:C) stimulation and following exposure to glutamatergic blockers CPP, APB, and NBQX. Boxplot of the mean frequency [Hz] (left) and the mean peak amplitude [F/F$_0$] (right). Wilcoxon rank-sum test.

Each dot represents an active cell. Recordings from five independent differentiations. ***$p < 0.001$. $^{ns}p > 0.05$, not significant.

CTRL: control. $_{diss}$RO: dissociated retinal organoid. IBU: S(+)-ibuprofen. iMG-$_{diss}$RO: microglia assembled dissociated retinal organoid. POLY(I:C): polyinosinic:polycytidylic acid.

Finally, when we simultaneously applied POLY(I:C) and S(+)-ibuprofen, strikingly, the peak amplitude was only restored to the control condition in iMG-$_{diss}$RO (**Figure 63a**). In $_{diss}$RO, the peak amplitude remained elevated compared to the control (**Figure 63b**), and the frequency was unaltered (**Figure 63c-d**). This data suggests that iMG presence is critical for the effect of ibuprofen on restoring POLY(I:C)-induced changes in the calcium dynamics.

Both ibuprofen targets, PTGS1 in microglia and PTGS2, are required to rescue calcium dynamics.

To identify the mechanism behind the iMG-dependent response upon ibuprofen exposure, we revisited the two main targets of ibuprofen, *PTGS1* and *PTGS2*, at the transcriptional level. In the $_{3D}$RO sequencing data (Cowan et al. 2020), *PTGS2* transcripts occurred in Müller glial and horizontal cells, whereas *PTGS1* transcripts were absent (**Figure 64a**). Since this dataset lacks iMG, we collected $_{3D}$RO with and without iMG around WK20 and analyzed the mRNA transcript levels of both enzymes. *PTGS1* relative to *GAPDH* was significantly increased in iMG-$_{3D}$RO compared to $_{3D}$RO (**Figure 64b**), whereas the *PTGS2* levels remained similar (**Figure 64c**).

Microglia have been shown to express PTGS1 constitutively (Deininger and Schluesener 1999), and a common assumption is that PTGS2 is upregulated during inflammatory conditions (Font-Nieves et al. 2012). To validate these assumptions, we investigated the transcript level in $_{pre}$MG cultures. Indeed, the absolute expression of *PTGS1* compared to *GAPDH* was significantly higher than that of *PTGS2* (**Figure 64d**). Yet, neither PTGS1 nor PTGS2 levels increased upon POLY(I:C) exposure of $_{pre}$MG (**Figure 64e**). At the same time, we observed a trend for *PTGS1* and *PTGS2* increase in iMG-$_{3D}$RO follwoing POLY(I:C) stimulation (**Figure 64f**) which is absent in $_{3D}$RO (**Figure 64g**).

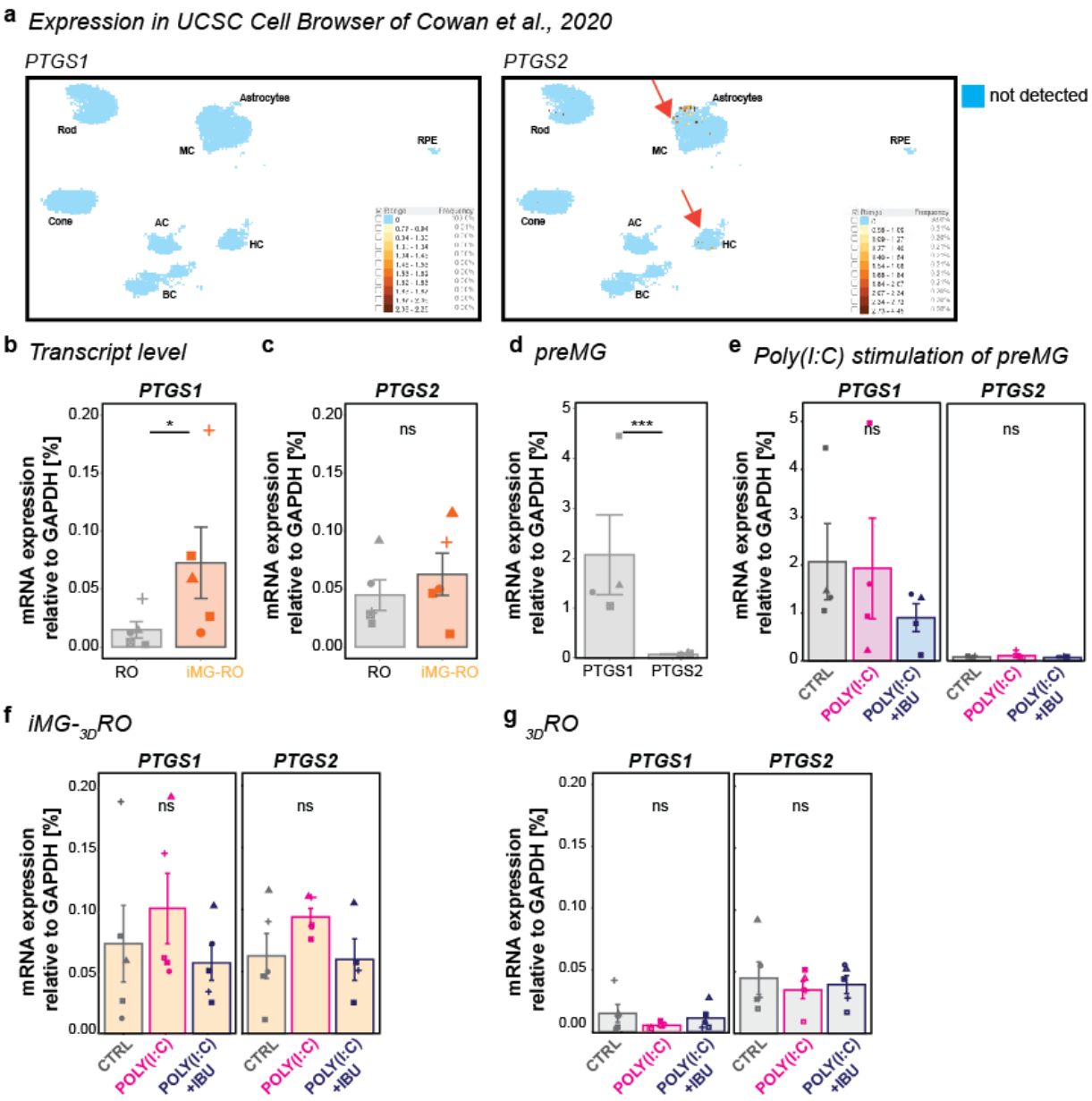

Figure 64 – Cell type-dependent transcriptional differences in PTGS1 and PTGS2.

a, Expression of PTGS1 and PTGS2 (prostaglandin-endoperoxide synthase 1 and 2) in USCS Cell Browser of Cowan et al., 2020. Cell Browser dataset ID: 'Developed human retinal organoid.' Uniform manifold approximation and projection (UMAP) of transcript expression. AC: amacrine cell. BC: bipolar cell. Cone: cone photoreceptors. HC: horizontal cell. MC: Müller glia. RPE: retinal pigment epithelium. Rod: rod photoreceptors. Red arrow: positive transcript expression. Blue dot: not detected.

b-g, Real-time quantitative polymerase chain reaction (RT-qPCR). Bar chart with SEM of mean mRNA transcript expression relative to GAPDH (glyceraldehyde 3-phosphate dehydrogenase) for PTGS1 (**b, d-g**) and PTGS2 (**b**-g) across untreated (**b-d**) and CTRL versus POLY(I:C) (magenta) or POLY(I:C) and S(+)-ibuprofen (POLY(I:C)+IBU, blue) (**e-g**) for $_{3D}$RO versus iMG-$_{3D}$RO (**b-c**), preMG (**d-e**), iMG-$_{3D}$RO (**f**), $_{3D}$RO (**g**). Students t-test (**b-d**). One-way ANOVA (**e-g**).

***$p < 0.001$. *$p < 0.05$. $^{ns}p > 0.05$, not significant.

CTRL: control. $_{3D}$RO: 3D-retinal organoid. IBU: S(+)-ibuprofen. iMG-$_{3D}$RO: microglia assembled 3D-retinal organoid. POLY(I:C): polyinosinic:polycytidylic acid. preMG: microglia precursor. SEM: Standard error of the mean.

When we analyzed the cytokine assay (**Figure 51a**), we observed several secreted factors known to be released by astrocytes. In $_{3D}$RO, astrocytes/Mueller-glia show a low expression level of TLR3 (**Figure 65a**). We confirmed this expression in hIPSC-derived astrocyte cultures (Bsibsi et al. 2006), which further upregulate *TLR3* transcripts upon POLY(I:C) exposure (**Figure 65b**). When we profiled *PTGS1* and *PTGS2*, we found that hIPSC-derived astrocytes significantly increased *PTGS2* transcripts (**Figure 65c**). This emphasizes that $_{pre}$MG and astrocytes differentially express the enzymes cyclooxygenase 1 and 2, respectively.

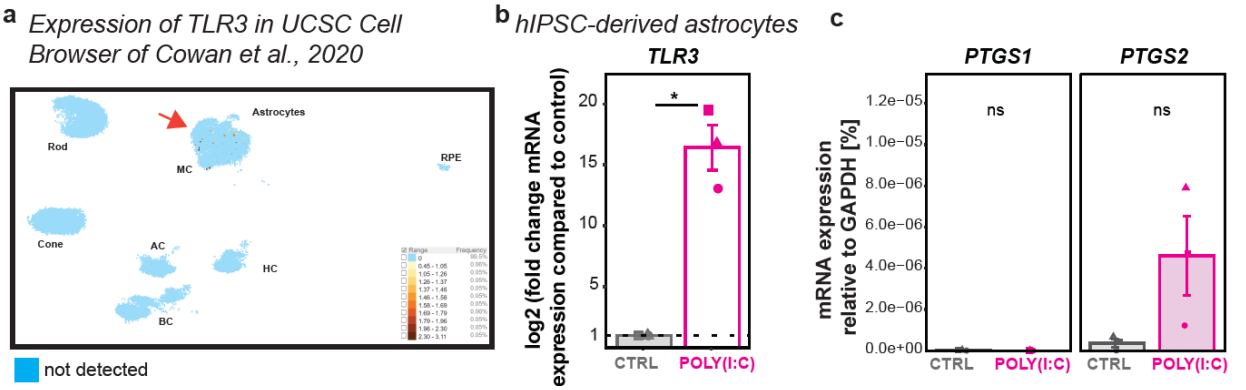

Figure 65 – The effect of POLY(I:C) on hIPSC-derived astrocytes.
a, Expression of TLR3 (toll-like receptor 3) in USCS Cell Browser of Cowan et al., 2020. Cell Browser dataset ID: 'Developed human retinal organoid.' Uniform manifold approximation and projection (UMAP) of transcript expression. AC: amacrine cell. BC: bipolar cell. Cone: cone photoreceptors. HC: horizontal cell. MC: Müller glia. RPE: retinal pigment epithelium. Rod: rod photoreceptors. Red arrow: positive transcript expression. Blue dot: not detected.
b-c, Real-time quantitative polymerase chain reaction (RT-qPCR) for (**b**) TLR3 as well as (**c**) PTGS1 and PTGS2 in hIPSC-derived astrocytes for untreated control (CTRL, grey) and POLY(I:C) (magenta) exposure. (**b**) Mean mRNA transcript log2-fold changes compared to untreated control cells with standard error of the mean. (**c**) Bar chart with SEM of mean mRNA transcript expression relative to GAPDH. Each symbol is an independent differentiation (n=3). (**b**) One sample t-test. (**c**) Students t-test.
*$p < 0.05$. $^{ns}p > 0.05$, not significant.
CTRL: control. $_{3D}$RO: 3D-retinal organoid. POLY(I:C): polyinosinic:polycytidylic acid. SEM: standard error of the mean.

Since ibuprofen targets both enzymes, we were interested in whether applying POLY(I:C) in combination with S(+)-ibuprofen results in an iMG-dependent effect on *PTGS1* and *PTGS2* expression. While the treatment reduced *PTGS1* mRNA expression in preMG (**Figure 64e**), it indicates a reversal of the POLY(I:C)-mediated increase to control levels in iMG-$_{3D}$RO (**Figure 64f**). In $_{3D}$ROs, S(+)-ibuprofen showed no trend (**Figure 64g**), suggesting that iMG are involved in a beneficial ibuprofen effect.

Ibuprofen did not rescue the calcium peak amplitude in the absence of iMG (**Figure 53b**), a condition in which PTGS1 is underrepresented (**Figure 64b**). Since S(+)-ibuprofen targets both enzymes simultaneously, we selectively blocked PTGS1 to understand if the beneficial effect depends on microglial PTGS1. To test this hypothesis, we took advantage of the inhibitor SC-560, which has a 700-fold selectivity for PTGS1 over PTGS2 (Hoozemans et al. 2002; Smith et al. 1998) and, therefore, will directly affect iMG in iMG-$_{diss}$RO. When we applied SC-560 together with POLY(I:C) for 24 hours (**Figure 66a**) and measured the calcium dynamics in iMG-$_{diss}$RO, the calcium peak amplitude was similarly upregulated as in $_{diss}$RO following ibuprofen treatment (**Figure 66b**).

The frequency remained unaffected (**Figure 66c**). This suggests that inhibition of functional PTGS1 or the simple lack of iMG prevents the positive effect of ibuprofen from restoring the calcium peak amplitude, highlighting a critical interplay between PTGS1-expressing iMG and PTGS2-mediated POLY(I:C) upregulation in other cells.

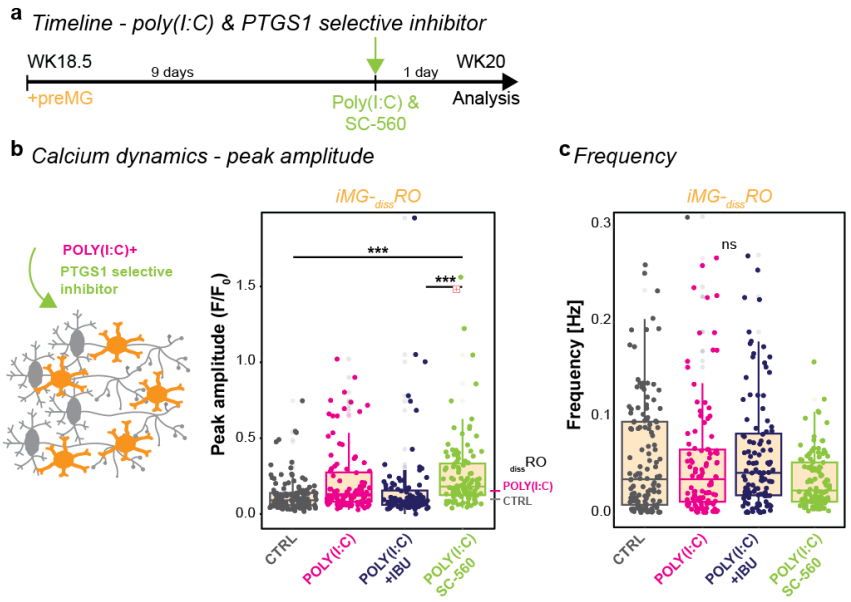

Figure 66 – PTGS1 selective inhibition.

a, Experimental timeline similar to **Figure 58a** with POLY(I:C) and SC-560 exposure for 24h in iMG-dissRO at WK20.

b-c, Spontaneous calcium dynamics in iMG-$_{diss}$RO during 5 minutes recording after 24 hours of either fresh medium for control (CTRL, grey), POLY(I:C) (magenta), POLY(I:C) and S(+)-ibuprofen (POLY(I:C)+IBU, blue), or POLY(I:C) and SC-560 (POLY(I:C)+SC-560, green) exposure. Boxplot of mean peak amplitude [F/F_0, **b**] and mean frequency [Hz, **c**]. Each dot represents an active cell from five independent differentiations. Peak amplitude: reference lines for the median of the control and POLY(I:C) stimulation in $_{diss}$RO from **Figure 60b.** Kruskal-Wallis test with post-hoc Dunn's test. ***$p < 0.001$. $^{ns}p > 0.05$, not significant.

CTRL: control. IBU: S(+)-ibuprofen. iMG-$_{diss}$RO: microglia assembled dissociated retinal organoid. POLY(I:C): polyinosinic:polycytidylic acid. preMG: microglia precursor. WK: week after the start of the differentiation.

3.5. Discussion

This study highlights the importance of including microglia in hIPSC-neuronal organoids to mimic fetal brain development and adequately model pathogen- and ibuprofen-mediated processes.

Prenatal neuro-immune challenge.

TORCH infection (Toxoplasmosis, Others, Rubella, Cytomegalovirus, Herpes) in a pregnant woman challenges her immune system and can severely threaten the fetus (Auriti et al. 2021; Campos et al. 2020). Through vertical transmission, TORCH can directly harm the developing fetus, inducing growth restrictions or birth defects such as blindness (Megli and Coyne 2021). For example, the Zika virus has been shown to target human fetal microglia (Lum et al. 2017) and to activate the innate immune receptor TLR3 (Dang et al. 2016; Plociennikowska et al. 2021). Thus, we mimicked the TLR3 signaling pathway using POLY(I:C) (Alexopoulou et al. 2001). *In vivo*, the receptor is expressed predominantly in microglia but also in astrocytes, endothelial cells, and pericytes, while only minimally in neurons and neuronal progenitors (Ostrem et al. 2024). We confirmed this expression pattern in preMG (**Figure 48b**) and hIPSC-derived astrocytes (**Figure 65b**). Furthermore, we demonstrated that 24 hours of POLY(I:C) exposure resulted in a robust iMG-dependent cytokine release (**Figure 51a**), accompanied by enhanced iMG surveillance (**Figure 48c**), elevated calcium peak amplitude in retinal cells (**Figure 63a-b**), and increased retinal cell proliferation (**Figure 54d-g**). Our observations in $_{diss}$RO lacking iMG showed a trend of reduced proliferation (**Figure 54h**). Overall, our observations align with rodent models. The proliferation rate remained unaffected if microglia were depleted and the pregnant females were exposed to an immune challenge during embryonic and early postnatal stages (Kuse et al. 2018). Contrarily, the proliferation increased in the presence of microglia (Baines et al. 2020; Kuse et al. 2018; Loayza et al. 2022), comparable to our data (**Figure 54d-g**). Microglia-dependent effects have also been reported on the transcriptional level after prenatal neuro-immune challenges, such as IFNɣ stimulation of brain organoids (Buonfiglioli et al. 2025) or three days of POLY(I:C) exposure on E15.5 rodent brain (Ostrem et al. 2024), emphasizing the microglia relevance in the inflammatory response and therefore, their integration into organoids should be standard procedure to capture developmental effects fully.

The presence of iMG determines ibuprofen's beneficial effect.

The observed POLY(I:C)-mediated consequences raise the question of how to treat infectious diseases during pregnancy to avoid adverse pregnancy outcomes (Mor and Cardenas 2010). NSAIDs act on prostaglandin G/H synthase 1 and 2 (PTGS1/COX1 and PTGS2/ COX2), resulting in anti-inflammatory, antipyretic, and analgesic properties (Adams, McCullough, and Nicholson 1969; Ajmone-Cat et al. 2010). We decided to use ibuprofen because Germany allows this medication during the first two trimesters of pregnancy (Schaefer et al. 2012). Ibuprofen crosses the placental barrier and accesses the developing fetus (X. Chen et al. 2024; Leverrier-Penna et al. 2018). We found that by applying ibuprofen simultaneously with POLY(I:C), we could ameliorate the increased cell proliferation (**Figure 59a-e**), restore the calcium peak amplitude (**Figure 63a-b**), and dampen the POLY(I:C)-mediated microglial response (**Figure 58a-c**). Surprisingly, ibuprofen did not reduce most of the secreted inflammatory mediators in iMG-$_{diss}$RO

(**Figure 57**), possibly due to the lack of infiltrating immune cells to resolve the inflammatory response.

iMG constitutively express PTGS1 over PTGS2 (**Figure 64d**) and the beneficial effect of ibuprofen depends on iMG. In iMG absence, ibuprofen mainly interferes with PTGS2 in $_{diss}$RO, which was insufficient to rescue the calcium peak amplitude (**Figure 63b**). On the other hand, calcium dynamics also did not recover when we selectively inhibited PTGS1 with SC-560 (**Figure 66a-b**). Since *PTGS2* seems to be preferentially expressed in astrocytes (**Figure 65c**) and iMG interact extensively with them, a potential astrocyte-microglia link exists and warrants follow-up studies.

The effects of microglia in retinal organoids.

Recently, three studies have been published focusing on iMG integration into retinal organoids (Chichagova et al. 2023; Gao et al. 2022; Usui-Ouchi et al. 2023).Both Usui-Ouchi *et al.* and Chichagova *et al.* performed their integration and investigation on a timeline similar to our study and compared $_{3D}$RO with and without iMG. Usui-Ouchi *et al.* confirmed iMG integration into the developing OPL (**Figure 39**) and shows that their presence temporarily increases the pro-inflammatory factors *IL1B*, *TNF,* and *IL6* using qRT-PCR. Our cytokine release assay did not detect differences in their secretion between $_{diss}$RO and iMG-$_{diss}$RO in untreated condition (**Figure 51**), instead only after POLY(I:C) stimulation, IL-6 and TNF were released in iMG-$_{diss}$RO. We also performed qRT-PCR for these three factors and observed a similar mRNA upregulation as the authors describe. However, POLY(I:C) stimulation exceeded at least 500-fold (data not shown). This indicates that translation from mRNA to an actual release into the supernatant might be tightly controlled. Chichagova *et al.* mimicked bacterial infection with lipopolysaccharide (LPS) and confirmed an iMG-dependent secretome using a different assay. We can observe differences in the response to LPS and POLY(I:C) as they, *e.g.,* don't observe an effect on CCL2/MCP-1, one of our strongest affected chemokines (**Figure 52a**). Due to the lack of control conditions, they might have missed changes due to iMG integration, as reported before by Usui-Ouchi *et al*. Finally, the study by Gao *et al.* compares mostly macrophages not integrated into a neuronal environment, which we named in our study preMG, after either LPS and POLY(I:C) stimulation. We consider this comparison suboptimal due to the known effects of LPS and POLY(I:C) on neuronal populations (Baines et al. 2020; Kuse et al. 2018; Loayza et al. 2022), also exemplified in the impact on the calcium peak amplitude (**Figure 63a-b**). The authors suggest a similar reduction in BRN3$^+$-cells in their D30-old iMG-$_{3D}$RO, as we have seen (**Figure 45a**). Yet, they do not show iMG-BRN3$^+$-interaction (**Figure 45b**) and only describe that they found a few microglia in the retina without insights into their positioning, making it challenging to derive further conclusions. In summary, the above studies are inconclusive regarding the ideal timing for studying microglia-neuron interaction, and our study closes this knowledge gap.

3.6. Conclusion

Our study provides a baseline for the neurodevelopmental role of microglia, the cross-talk with their neuron-glia environment, and how prenatal neuro-immune activation and anti-inflammatory drug treatment are affected. In light of replacing *in vivo* models for drug screening and validation for FDA drug approval (Rumsey et al. 2022) with *in vitro* models (Spirig et al. 2023),

integrating all relevant cell types becomes critical to achieving drug efficiency in screenings. The limitation of these models to replicate adequately an inflammatory response will severely affect the information regarding the safety of medications during pregnancy for both the pregnant woman and the fetus and will raise serious public health concerns. Specifically, our model can serve as a platform for follow-up investigations on drug tests or the interplay between inflammation and microglia activation leading to neurological phenotypes in adulthood. For example, a rubella infection during pregnancy is one of the risk factors for developing schizophrenia (Sullivan 2005).

3.7. Limitation

This study focuses on the acute response to an early-life neuro-immune challenge and how microglia contribute to the observed consequences (**Figure 48-66**). We did not further investigate potential long-term effects caused by, *e.g.*, the increased proliferation rate (**Figure 54d-g**), which could result in an imbalance of retinal cell type populations changing the cytoarchitecture, or the elevated calcium peak amplitude (**Figure 63a**) may lead to altered network activity. iMG might be able to sense and compensate for POLY(I:C)-mediated consequences over time. Also, a prolonged stimulation period might be interesting, as infections usually last longer than 24 hours. Furthermore, stimulation before WK20 or later could also result in different responses because the timing of an immune challenge contributes to differences in the outcomes (Meyer et al. 2006, 2008). Finally, future models must expand on the possibility of including the blood-brain barrier into the system. Identified factors such as MIP, CCL5, CXCL1, and CCL2 (**Figure 51a**) are known candidates for homing monocytes and T-cells from the periphery (Chen et al. 2003; Fife et al. 2001; Johnson et al. 2011; Romagnani and Crescioli 2012; Ubogu et al. 2006) and might be needed to downregulate the inflammatory signature once recruited.

4. Summary discussion

In my thesis, I verified that IBA1$^+$-cells develop parallel to retinal structures during retinal organoid differentiation and optimized a protocol to generate IBA1$^+$-microglia precursors (**chapter 1**). By integrating these cells into retinal organoids, I established an hIPSC-derived model to examine microglia-neuron interaction in a retinal environment. Beside investigating human microglia colonization patterns into the developing retina, this model also allowed me to study microglia-mediated effects on retinal development, in response to viral stimulation and following an anti-inflammatory treatment (**chapter 2**).

IBA1$^+$-cells innately develop during retinal organoid differentiation and predominantly populate mesenchymal structures

In chapter 1, we confirmed that IBA1$^+$-cells innately develop during unguided retinal organoid differentiation, similar as previously reported in some unguided brain organoid protocols **Table 9** (Gabriel et al. 2021; Ormel et al. 2018; Shiraki et al. 2022). We further characterized their preferential location and observed that IBA1$^+$-cells barely colonize retinal cups (**Figure 7**, **Figure 36**). Instead, they populate mesenchymal regions (**Figure 12, Figure 27**), where they acquire the expression of CD163 (**Figure 30**), a marker characteristic for brain-border associated macrophages (BAMs) (Utz et al. 2020). This study was published in *iScience* in 2022.

Characterization of hIPSC-derived microglia-precursors

In our *iScience* publication, we also established a protocol to generate IBA1$^+$-microglia precursors using a BMP4-guided differentiation protocol (**Figure 13, Figure 16**). First, we characterized their microglia-like identity (**Figure 16**). Next, we validated their functionality including their ability to phagocytose fluorescent beads as a proxy for their phagocytic capacity (**Figure 17**), their mRNA transcript upregulation to inflammatory stimuli using rt-qPCR to assess their immune-sensing properties (**Figure 18**), and their Ca^{2+}-response to extracellular ATP to mimic their reaction to damage signals released by injured neurons (**Figure 19**). We were later invited to write a detailed protocol outlining the methodology to characterize hIPSC-derived microglia-like cells (iMG), which was published in *Star-protocol* in 2022.

Microglia influence neuronal development in retinal organoids

In chapter 2, we incorporated these IBA1$^+$-microglia precursor cells into 3D-retinal organoids (**Figure 38**), since microglia properties, including morphology, function and transcriptional profile depend on their microenvironment (Bohlen et al. 2017; Butovsky et al. 2014; Gosselin et al. 2017). In recent years, several approaches have been published to generate microglia-assembled brain organoids as summarized in **Table 9**. HIPSC-derived EMPs or microglia precursors have been added to various brain organoid models such as cortical (Abud et al. 2017; Bejoy et al. 2019; Fagerlund et al. 2021; Park et al. 2023; Schafer et al. 2023; Song et al. 2019; Xu et al. 2021), midbrain (Sabate-Soler et al. 2022) or retinal organoids (Chichagova et al. 2023; Gao et al. 2022; Usui-Ouchi et al. 2023). Alternatively, iMG differentiation has been induced within brain organoids by overexpressing the microglial transcription factor PU1 in a subset of hIPSCs (Cakir

et al. 2022). Instead of integrating hIPSC-derived iMGs, early studies incorporated immortalized human microglia (Abreu et al. 2018; Ao et al. 2021) or human primary fetal microglia (Popova et al. 2021) into brain organoids

In our model, the integrated iMG mimicked retinal colonization (**Figure 39**) which allowed us to identify week 20 as the optimal timepoint to investigate how microglia influence retinal development. To validate our model, we examined whether iMGs perform development tasks previously observed in rodent models (Li et al. 2019; Nag and Wadhwa 2001; Santos et al. 2008). Indeed, iMG phagocytosed $BRN3^{+}$-ganglion cells (**Figure 45**) and engulfed apoptotic fragments (**Figure 47**).

Across various brain organoid models, studies have demonstrated that integrated iMG recapitulate developmental tasks (**Table 9**). First, iMGs phagocytose newborn or apoptotic cells. (Gao et al. 2022; Popova et al. 2021; Xu et al. 2021) Second, integrated iMG have also been implicated in synaptic remodeling (Cakir et al. 2022; Fagerlund et al. 2021; Popova et al. 2021; Sabate-Soler et al. 2022; Sun et al. 2022; Xu et al. 2021) and in promoting neuronal network activity and maturation within brain organoids (Chen et al. 2025; Fagerlund et al. 2021; Park et al. 2023; Sabate-Soler et al. 2022; Sun et al. 2022). However, iMG-dependent neuronal maturation has been shown to be timepoint- (Fagerlund et al. 2021) and brain region-dependent (Chichagova et al. 2023).

Modeling prenatal immune activation and assessing microglia-dependent effects

To characterize the immune-sensing properties of integrated iMG, microglia-assembled brain organoids have been exposed to viral and bacterial stimulation, Aβ42 oligomers or injury (**Table 9**) (Abreu et al. 2018; Abud et al. 2017; Ao et al. 2021; Buonfiglioli et al. 2025; Chichagova et al. 2023; Schafer et al. 2023; Song et al. 2019; Sun et al. 2022; Xu et al. 2021). While most studies perform these assays to validate the functionality of integrated iMG, we aimed to understand the acute effects of neuroinflammation on retinal development following 24h POLY(I:C) stimulation (**Figure 51, Figure 54, Figure 63**).

Human cerebral organoids lacking microglia have been used to model viral infections such as Zika virus (ZIKV), herpes simplex virus type 1 (HSV1), or SARS-CoV-2 to investigate viral tropism and identify anti-viral compounds (Jacob et al. 2020; McMahon et al. 2021; Song et al. 2021; Zhou et al. 2017). Some studies have also assessed neurodevelopmental consequences and found that ZIKV and HSV1 infections caused a reduction in neuronal progenitor numbers (Dang et al. 2016; Garcez et al. 2016; Krenn et al. 2021; Su et al. 2021; Xu et al. 2019) resulting in smaller organoids (Krenn et al. 2021).

Krenn *et al.* demonstrated that ZIKV and HSV1 do not induce type I interferon response in brain organoids lacking microglia (Krenn et al. 2021). Indeed, our results emphasize the necessity to incorporate microglia to elict an inflammatory response in brain organoids (**Figure 51**) - an observation that has recently been confirmed by other studies (Buonfiglioli et al. 2025; Chichagova et al. 2023). While our study focused on POLY(I:C)-mediated neuronal consequences, Buonfiglioli *et al.* assessed microglia-dependent effects following IFN-γ stimulation (Buonfiglioli et al. 2025). Between organoids with and without microglia, they observed differences on the

transcriptional and protein level including the dysregulation of genes associated to autism. This is in line with our observations that microglia contribute to viral-mediated consequences (**Figure 51, Figure 54, Figure 63-64**). Additionally, studies confirmed that ZIKV or SARS-CoV-2 influence microglia-neuron interaction in microglia-assembled brain organoids as they observed an increased phagocytosis of synapses by iMG (**Table 9**) (Samudyata et al. 2022; Xu et al. 2021). In general, it is essential to assess infections and neurodegenerative diseases in the presence of microglia, as inflammation is a hallmark of many neurological conditions (Adamu et al. 2024; Zhang et al. 2023). Thus, the impact of neuro-inflammation itself should be considered in brain organoid studies.

Anti-inflammatory treatment modulates POLY(I:C)-mediated developmental abnormalities

We still lack sufficient knowledge about the safe usage of drugs, including anti-inflammatory treatments, during pregnancy. The goal of medication during pregnancy is to minimize any harm to both the mother and the fetus while effectively managing health conditions.

In our study, we decided to use ibuprofen, since it is considered acceptable for use during the first two trimesters of pregnancy in Germany (Schaefer et al. 2012). Because ibuprofen crosses the placental barrier it can reach the fetus (X. Chen et al. 2024; Leverrier-Penna et al. 2018). Therefore, it is crucial to study its effects on embryonic development. We observed that ibuprofen treatment ameliorated and even rescued POLY(I:C)-mediated effects on iMG surveillance (**Figure 58a**) as well as neuronal consequences including the proliferation rate (**Figure 69a-e**) and calcium signaling (**Figure 63b**). Again, we determined microglia-dependent effects by comparing cultures with and without iMG (**Figure 63a-d, Figure 64f-g**). Our study is the first to investigate drug-mediated effects in microglia-assembled retinal organoids (**Table 9**) and was published in *Journal of Neuroinflammation* in 2025.

Table 9 – Example studies using microglia assembled brain organoids.
Aβ: beta-amyloid. ASD: autism spectrum disorder. $Ca2^{+}$: calcium. D: days of differentiation. EMPs: erythro-myeloid progenitors. hIPSC: human induced pluripotent stem cells. IFNα: interferon alpha. IFNγ: interferon gamma. IL6: interleukin 6. iMG: microglia-like cells. LPS: lipopolysaccharide. NEUN: neuronal nuclei antigen. NPC: neuronal progenitor cell. OTX2: orthodenticle homolog 2. POLY(I:C): polyinosinic:polycytidylic acid. WK: week after the start of differentiation. Green background: studies integrated into this thesis.

Study	Microglia	Organoid (timepoint of analysis)	Microglia properties	The effect of iMG on neuronal properties/ modelling
Innately developing microglia				
Ormel *et al.* 2018	Innate	Cerebral organoid	*Transcriptional profile *Immune-sensing properties upon LPS stimulation	-
Gabriel *et al.* 2021	Innate	Optic vesicle containing organoid	-	-
Shiraki *et al.* 2022	Innate	Ocular organoid	iMG identity	-
Bartalska *et al.* 2022	Innate	Retinal organoid differentiation	iMG identity	-
Samudyata *et al.* 2022	Innate (based on Ormel *et al.* 2018)	Cerebral Organoid Analysis: D56	-	**SARS-CoV-2 infection:** *Decreased post-synaptic density *Transcriptional profile: glia cells adopt neurodegenerative phenotype
Integrating microglia precursor cells				
Abud *et al.* 2017	hIPSC derived microglia precursor	Brain organoid Analysis: WK12	*iMG morphology Response to injury (needle)	-
Song *et al.* 2019	hIPSC derived microglia precursor	Dorsal/ ventral cortical organoids Analysis: D52	*Intracellular Ca^{2+} transients *Transcriptional profile 2D vs 3D *Immune-sensing properties to Aβ42 oligomers	-
Bejoy *et al.* 2019	hIPSC derived microglia precursor	Dorsal cortical organoids Analysis: D30	-	Transcriptional profile of organoid: metabolic shift to aerobic glycolysis
Sabate-Soler *et al.* 2022	hIPSC derived microglia precursor	Midbrain organoid Analysis: D35-85	*Cytokine release	*Transcriptional profile *Synaptic remodeling

				*Increase neuronal excitability
Gao *et al.* 2022	hIPSC derived microglia precursor	Retinal organoid Analysis: D25-77	Transcriptional profile	*Reduced ganglion cell number *Increased number of $OTX2^+$-cells
Chichagova *et al.* 2023	hIPSC derived microglia precursor	Retinal organoid Analysis: WK15-22	*Localization within organoid *Immune-sensing properties to LPS	*Transcriptional profile *No difference in neuronal activity
Wenzel *et al.* 2024	Innate versus microglia precursor	Brain organoid Analysis: D90	-	*Promote Aβ oligomerization
Chen *et al.* 2025	hIPSC derived microglia precursor	Sliced and attached brain organoids Analysis: Long term co-culture (up to 1 year)	-	*Promote synapse formation *Enhanced neuronal activity (Ca^{2+}) *Reduced p-Tau accumulation in neurons (sign of degeneration), apoptosis
Schmied *et al.* 2025	hIPSC derived microglia precursor	Retinal organoids Analysis: WK20	*Localization within organoid *Phagocytosis of ganglion cells *Immune-sensing properties to POLY(I:C)	**POLY(I:C)-stimulation:** *iMG-dependent increase in retinal proliferation rate **Ibuprofen treatment:** *iMG-dependent rescue of calcium activity
Integrating EMPs/ primitive macrophages				
Xu *et al.* 2021	hIPSC derived primitive macrophages	Dorsal and ventral forebrain organoids Analysis: D40-55	*Phagocytosis of newborn and apoptotic cells *Synaptic pruning of postsynaptic material	**Zika virus infection:** *Immune-sensing properties *Increase of synapse elimination upon
Fagerlund *et al.* 2021	hIPSC derived EMPs	Cerebral organoid Analysis: D66-213	Synaptic pruning of postsynaptic material	iMG promote neuronal maturation
Park *et al.* 2023	hIPSC derived primitive macrophages	Cerebral organoid Analysis: D42-45	Transcriptional profile	*iMG promote neuronal maturation *Limited NPC proliferation *Promoted axonogenesis *Lipid cross-talk
Schafer *et al.* 2023	hIPSC derived EMPs	Brain organoid Analysis: WK15	*Transcriptional profile	**Healthy versus**

			*Response to laser injury, LPS injection	**ASD brain organoid**: iMG acquire disease specific signature
Usui-Ouchi *et al.* 2023	hIPSC derived macrophage progenitors	Retinal organoid Analysis: WK28-31	*Transcriptional profile *Synaptic layer colonization	*Enhanced inflammatory signature
Buonfiglioli *et al.* 2025	hIPSC-derived hematopoietic stem cells	Cerebral organoids Analysis: D32-35	*Transcriptional profile *Immune-sensing properties to LPS, IFNγ, IFNα and IL6	*Decrease in cell density and $OTX2^+$ and $NEUN^+$ cells *Transcriptional profile and structural changes upon **IFNγ-stimulation**
Alternative approach to induce microglia differentiation within organoids				
Cakir *et al* 2022	Forward programming of iMG by PU1 overexpression	Cortical organoid Analysis: D30-75	*Transcriptional profile *Synaptic pruning of postsynaptic material	Alzheimer disease modeling using Aβ42 oligomers
Sun *et al.* 2022	Induced by fusion	Fusion of vessel & brain organoid Analysis: D25-40	*Immune-sensing properties to LPS *Synaptic pruning	Enhanced neuronal maturation

Table continued on next page

Non hIPSC-derived microglia				
Abreu *et al.* 2018	Immortalized microglia (SV40)	Brain spheroids Analysis: WK8	Immune-sensing properties to LPS, Dengue- and Zika virus stimulation	-
Popova *et al.* 2021	Primary prenatal human microglia (from mid gestation cortex)	Cortical organoid Analysis: WK7-10	*Phagocytosis of newborn cells *Elimination of postsynaptic material *Transcriptional profile	*Reduced type I interferon response *Reduced cell stress in radial glia
Ao *et al.* 2021	Immortalized microglia (HMC3)	Tubular forebrain organoids, generated in a hollow mesh (chip)	Immune-sensing properties to LPS and opioids	-

5. Concluding remarks

Beside mimicking important steps of early fetal brain development in a human aspect (Bagley et al. 2017; Camp et al. 2015; Renner et al. 2017; Sloan et al. 2018), brain organoids can be used for disease modelling and drug testing (H. Kim et al. 2019; Lin et al. 2018; Rumsey et al. 2022; Smits et al. 2019). Overall, our results emphasize that it is critical to integrate microglia as they fine-tune neuronal development, and influence both viral- as well as drug-mediated consequences. In their absence, microglia-specific effect will be overlooked and results might be misinterpreted.

6. References

Abreu, Celina Monteiro, Lucio Gama, Susanne Krasemann, Megan Chesnut, Shelly Odwin-Dacosta, Helena T. Hogberg, Thomas Hartung, and David Pamies. 2018. “Microglia Increase Inflammatory Responses in IPSC-Derived Human BrainSpheres.” Frontiers in Microbiology 9:2766. doi: 10.3389/fmicb.2018.02766.

Abud, Edsel M., Ricardo N. Ramirez, Eric S. Martinez, Luke M. Healy, Cecilia H. H. Nguyen, Sean A. Newman, Andriy V. Yeromin, Vanessa M. Scarfone, Samuel E. Marsh, Cristhian Fimbres, Chad A. Caraway, Gianna M. Fote, Abdullah M. Madany, Anshu Agrawal, Rakez Kayed, Karen H. Gylys, Michael D. Cahalan, Brian J. Cummings, Jack P. Antel, Ali Mortazavi, Monica J. Carson, Wayne W. Poon, and Mathew Blurton-Jones. 2017. “IPSC-Derived Human Microglia-like Cells to Study Neurological Diseases.” Neuron 94(2):278-293.e9. doi: 10.1016/j.neuron.2017.03.042.

Adams, S. S., K. F. McCullough, and J. S. Nicholson. 1969. “The Pharmacological Properties of Ibuprofen, an Anti-Inflammatory, Analgesic and Antipyretic Agent.” Archives Internationales de Pharmacodynamie et de Therapie 178(1):115–29.

Adamu, Alhamdu, Shuo Li, Fankai Gao, and Guofang Xue. 2024. “The Role of Neuroinflammation in Neurodegenerative Diseases: Current Understanding and Future Therapeutic Targets.” Frontiers in Aging Neuroscience 16.

Adler, Ruben, and M. Valeria Canto-Soler. 2007. “Molecular Mechanisms of Optic Vesicle Development: Complexities, Ambiguities and Controversies.” Developmental Biology 305(1):1–13.

Ajmone-Cat, Maria Antonietta, Antonietta Bernardo, Anita Greco, and Luisa Minghetti. 2010. “Non-Steroidal Anti-Inflammatory Drugs and Brain Inflammation: Effects on Microglial Functions.” Pharmaceuticals (Basel, Switzerland) 3(6):1949–65. doi: 10.3390/ph3061949.

Alexopoulou, Lena, Agnieszka Czopik Holt, Ruslan Medzhitov, and Richard A. Flavell. 2001. “Recognition of Double-Stranded RNA and Activation of NF-KB by Toll-like Receptor 3.” Nature 2001 413:6857 413(6857):732–38. doi: 10.1038/35099560.

Allen, Nicola J., and Ben A. Barres. 2009. How Do Glia Differ from Neurons?

Alliot, Francoise, Isabelle Godin, and Bernard Pessac. 1999. “Microglia Derive from Progenitors, Originating from the Yolk Sac, and Which Proliferate in the Brain.” Developmental Brain Research 117(2):145–52. doi: 10.1016/S0165-3806(99)00113-3.

Amin, Neal D., Kevin W. Kelley, Konstantin Kaganovsky, Massimo Onesto, Jin Hao, Yuki Miura, James P. McQueen, Noah Reis, Genta Narazaki, Tommy Li, Shravanti Kulkarni, Sergey Pavlov, and Sergiu P. Pașca. 2024. “Generating Human Neural Diversity with a Multiplexed Morphogen Screen in Organoids.” Cell Stem Cell 31(12):1831-1846.e9. doi: 10.1016/j.stem.2024.10.016.

Anderson, Sarah R., Jianmin Zhang, Michael R. Steele, Cesar O. Romero, Amanda G. Kautzman, Dorothy P. Schafer, and Monica L. Vetter. 2019. “Complement Targets Newborn Retinal Ganglion Cells for Phagocytic Elimination by Microglia.” Journal of Neuroscience 39(11):2025–40. doi: 10.1523/JNEUROSCI.1854-18.2018.

Andoh, Megumi, Kazuki Shibata, Kazuki Okamoto, Junya Onodera, Kohei Morishita, Yuki Miura, Yuji Ikegaya, and Ryuta Koyama. 2019. “Exercise Reverses Behavioral and Synaptic Abnormalities after Maternal Inflammation.” Cell Reports 27(10):2817-2825.e5. doi: 10.1016/J.CELREP.2019.05.015.

Andrzejewska, Anna, Barbara Lukomska, and Miroslaw Janowski. 2019. “Concise Review: Mesenchymal Stem Cells: From Roots to Boost.” Stem Cells (Dayton, Ohio) 37(7):855–64. doi: 10.1002/stem.3016.

Angeles-Albores, David, Raymond Y. Raymond, Juancarlos Chan, and Paul W. Sternberg. 2016. “Tissue Enrichment Analysis for C. Elegans Genomics.” BMC Bioinformatics 17(1):366. doi: 10.1186/s12859-016-1229-9.

Ao, Zheng, Hongwei Cai, Zhuhao Wu, Sunghwa Song, Hande Karahan, Byungwook Kim, Hui Chen Lu, Jungsu Kim, Ken Mackie, and Feng Guo. 2021. “Tubular Human Brain Organoids to Model Microglia-Mediated Neuroinflammation.” Lab on a Chip 21(14):2751–62. doi: 10.1039/d1lc00030f.

Arnò, Benedetta, Francesca Grassivaro, Chiara Rossi, Andrea Bergamaschi, Valentina Castiglioni, Roberto Furlan, Melanie Greter, Rebecca Favaro, Giancarlo Comi, Burkhard Becher, Gianvito Martino, and Luca Muzio. 2014. “Neural Progenitor Cells Orchestrate Microglia Migration and Positioning into the Developing Cortex.” Nature Communications 5(1):1–13. doi: 10.1038/ncomms6611.

Artimovich, Elena, Russell K. Jackson, Michaela B. C. Kilander, Yu Chih Lin, and Michael W. Nestor. 2017. “PeakCaller: An Automated Graphical Interface for the Quantification of Intracellular Calcium Obtained by High-Content Screening.” BMC Neuroscience 18(1):72. doi: 10.1186/s12868-017-0391-y.

Ashworth, Kristen E., Jessica Weisbrod, and Brian G. Ballios. 2024. “Inherited Retinal Diseases and Retinal Organoids as Preclinical Cell Models for Inherited Retinal Disease Research.” Genes 15(6).

Auriti, Cinzia, Domenico Umberto De Rose, Alessandra Santisi, Ludovica Martini, Fiammetta Piersigilli, Iliana Bersani, Maria Paola Ronchetti, and Leonardo Caforio. 2021. “Pregnancy and Viral Infections: Mechanisms of Fetal Damage, Diagnosis and Prevention of Neonatal Adverse Outcomes from Cytomegalovirus to SARS-CoV-2 and Zika Virus.” Biochimica et Biophysica Acta. Molecular Basis of Disease 1867(10):166198. doi: 10.1016/J.BBADIS.2021.166198.

Bagley, Joshua A., Daniel Reumann, Shan Bian, Julie Lévi-Strauss, and Juergen A. Knoblich. 2017. “Fused Cerebral Organoids Model Interactions between Brain Regions.” Nature Methods 14(7):743–51. doi: 10.1038/nmeth.4304.

Baines, Kelly J., Dendra M. Hillier, Faraj L. Haddad, Nagalingam Rajakumar, Susanne Schmid, and Stephen J. Renaud. 2020. “Maternal Immune Activation Alters Fetal Brain Development and Enhances Proliferation of Neural Precursor Cells in Rats.” Frontiers in Immunology 11:1145. doi: 10.3389/FIMMU.2020.01145/FULL.

Barresi, Michael J. F. 2020. Developmental Biology. Twelfth ed. New York : Sinauer Associates, [2020].

Bartalska, Katarina, Verena Hübschmann, Medina Korkut-Demirbaş, Ryan John A. Cubero, Alessandro Venturino, Karl Rössler, Thomas Czech, and Sandra Siegert. 2022. “A Systematic Characterization of Microglia-like Cell Occurrence during Retinal Organoid Differentiation.” IScience 25(7):104580. doi: 10.1016/j.isci.2022.104580.

Bates, Douglas, Martin Mächler, Benjamin M. Bolker, and Steven C. Walker. 2015. “Fitting Linear Mixed-Effects Models Using Lme4.” Journal of Statistical Software 67(1). doi: 10.18637/jss.v067.i01.

Bejoy, Julie, Xuegang Yuan, Liqing Song, Thien Hua, Richard Jeske, Sébastien Sart, Qing Xiang Amy Sang, and Yan Li. 2019. “Genomics Analysis of Metabolic Pathways of Human Stem Cell-Derived Microglia-Like Cells and the Integrated Cortical Spheroids.” Stem Cells International 2019. doi: 10.1155/2019/2382534.

Bennett, Mariko L., F. Chris Bennett, Shane A. Liddelow, Bahareh Ajami, Jennifer L. Zamanian, Nathaniel B. Fernhoff, Sara B. Mulinyawe, Christopher J. Bohlen, Aykezar Adil, Andrew Tucker, Irving L. Weissman, Edward F. Chang, Gordon Li, Gerald A. Grant, Melanie G. Hayden Gephart, and Ben A. Barres. 2016. “New Tools for Studying Microglia in the Mouse and Human CNS.” Proceedings of the National Academy of Sciences of the United States of America 113(12):E1738–46. doi: 10.1073/pnas.1525528113.

Ben-Reuven, Lihi, and Orly Reiner. 2019. “Dynamics of Cortical Progenitors and Production of Subcerebral Neurons Are Altered in Embryos of a Maternal Inflammation Model for Autism.” Molecular Psychiatry 2019 26:5 26(5):1535–50. doi: 10.1038/s41380-019-0594-y.

Ben-Yehuda, Hila, Orit Matcovitch-Natan, Alexander Kertser, Amit Spinrad, Marco Prinz, Ido Amit, and Michal Schwartz. 2019. “Maternal Type-I Interferon Signaling Adversely Affects the Microglia and the Behavior of the Offspring Accompanied by Increased Sensitivity to Stress.” Molecular Psychiatry 2019 25:5 25(5):1050–67. doi: 10.1038/s41380-019-0604-0.

Bernardino, Liliana, Fabienne Agasse, Bruno Silva, Raquel Ferreira, Sofia Grade, Jo˜ao Jo˜ao, and O. Malva. 2008. “Tumor Necrosis Factor-α Modulates Survival, Proliferation, and Neuronal Differentiation in Neonatal Subventricular Zone Cell Cultures.” STEM CELLS 26(9):2361–71. doi: 10.1634/STEMCELLS.2007-0914.

Bian, Zhilei, Yandong Gong, Tao Huang, Christopher Z. W. Lee, Lihong Bian, Zhijie Bai, Hui Shi, Yang Zeng, Chen Liu, Jian He, Jie Zhou, Xianlong Li, Zongcheng Li, Yanli Ni, Chunyu Ma, Lei Cui, Rui Zhang, Jerry K. Y. Chan, Lai Guan Ng, Yu Lan, Florent Ginhoux, and Bing Liu. 2020. “Deciphering Human Macrophage Development at Single-Cell Resolution.” Nature 582(7813):571–76. doi: 10.1038/s41586-020-2316-7.

Bloom, William, and G. W. Bartelmez. 1940. “Hematopoiesis in Young Human Embryos.” American Journal of Anatomy 67(1):21–53. doi: 10.1002/aja.1000670103.

Bohlen, Christopher J., F. Chris Bennett, Andrew F. Tucker, Hannah Y. Collins, Sara B. Mulinyawe, and Ben A. Barres. 2017. “Diverse Requirements for Microglial Survival, Specification, and Function Revealed by Defined-Medium Cultures.” Neuron 94(4):759-773.e8. doi: 10.1016/j.neuron.2017.04.043.

Bose, Shambhunath, and Jungsook Cho. 2013. “Role of Chemokine CCL2 and Its Receptor CCR2 in Neurodegenerative Diseases.” Archives of Pharmacal Research 36(9):1039–50. doi: 10.1007/S12272-013-0161-Z/TABLES/3.

Bsibsi, Malika, Carla Persoon-Deen, Ronald W. H. Verwer, Sonja Meeuwsen, Rivka Ravid, and Johannes M. Van Noort. 2006. “Toll-like Receptor 3 on Adult Human Astrocytes Triggers Production of Neuroprotective Mediators.” Glia 53(7):688–95. doi: 10.1002/GLIA.20328.

Bsibsi, Malika, Rivka Ravid, Djordje Gveric, and Johannes M. Van Noort. 2002. “Broad Expression of Toll-Like Receptors in the Human Central Nervous System.” Journal of Neuropathology & Experimental Neurology 61(11):1013–21. doi: 10.1093/JNEN/61.11.1013.

Buchrieser, Julian, William James, and Michael D. Moore. 2017. “Human Induced Pluripotent Stem Cell-Derived Macrophages Share Ontogeny with MYB-Independent Tissue-Resident Macrophages.” Stem Cell Reports 8(2):334–45. doi: 10.1016/j.stemcr.2016.12.020.

Buonfiglioli, Alice, Raphael Kübler, Roy Missall, Renske De Jong, Stephanie Chan, Verena Haage, Stefan Wendt, Ada J. Lin, Daniele Mattei, Mara Graziani, Brooke Latour, Frederieke Gigase, Rebecca Chiu, Ya Zhang, Haakon B. Nygaard, Philip L. De Jager, and Lot D. De Witte. 2025. “A Microglia-Containing Cerebral Organoid Model to Study Early Life Immune Challenges.” Brain, Behavior, and Immunity 123:1127–46. doi: 10.1016/j.bbi.2024.11.008.

Burger, Courtney A., Danye Jiang, Fenge Li, and Melanie A. Samuel. 2020. “C1q Regulates Horizontal Cell Neurite Confinement in the Outer Retina.” Frontiers in Neural Circuits 14. doi: 10.3389/FNCIR.2020.583391/FULL.

Butovsky, Oleg, Mark P. Jedrychowski, Craig S. Moore, Ron Cialic, Amanda J. Lanser, Galina Gabriely, Thomas Koeglsperger, Ben Dake, Pauline M. Wu, Camille E. Doykan, Zain Fanek, Liping Liu, Zhuoxun Chen, Jeffrey D. Rothstein, Richard M. Ransohoff, Steven P. Gygi, Jack P. Antel, and Howard L. Weiner. 2014. “Identification of a Unique TGF-β-Dependent Molecular and Functional Signature in Microglia.” Nature Neuroscience 17(1):131–43. doi: 10.1038/nn.3599.

Cakir, Bilal, Yoshiaki Tanaka, Ferdi Ridvan Kiral, Yangfei Xiang, Onur Dagliyan, Juan Wang, Maria Lee, Allison M. Greaney, Woo Sub Yang, Catherine duBoulay, Mehmet Hamdi Kural, Benjamin Patterson, Mei Zhong, Jonghun Kim, Yalai Bai, Wang Min, Laura E. Niklason, Prabir Patra, and In Hyun Park.

2022. “Expression of the Transcription Factor PU.1 Induces the Generation of Microglia-like Cells in Human Cortical Organoids.” Nature Communications 13(1):1–15. doi: 10.1038/s41467-022-28043-y.

Camp, J. Gray, Farhath Badsha, Marta Florio, Sabina Kanton, Tobias Gerber, Michaela Wilsch-Bräuninger, Eric Lewitus, Alex Sykes, Wulf Hevers, Madeline Lancaster, Juergen A. Knoblich, Robert Lachmann, Svante Pääbo, Wieland B. Huttner, and Barbara Treutlein. 2015. “Human Cerebral Organoids Recapitulate Gene Expression Programs of Fetal Neocortex Development.” Proceedings of the National Academy of Sciences of the United States of America 112(51):15672–77. doi: 10.1073/pnas.1520760112.

Campos, Viviane Souza de, Karin C. Calaza, and Daniel Adesse. 2020. “Implications of TORCH Diseases in Retinal Development—Special Focus on Congenital Toxoplasmosis.” Frontiers in Cellular and Infection Microbiology 10:585727. doi: 10.3389/FCIMB.2020.585727.

Cao, Ou, and Roland W. Herzog. 2008. “TLR3 Signaling Does Not Affect Organ-Specific Immune Responses to Factor IX in AAV Gene Therapy.” Blood 112(3):910. doi: 10.1182/BLOOD-2008-02-137992.

Capowski, Elizabeth E., Kayvan Samimi, Steven J. Mayerl, M. Joseph Phillips, Isabel Pinilla, Sara E. Howden, Jishnu Saha, Alex D. Jansen, Kimberly L. Edwards, Lindsey D. Jager, Katherine Barlow, Rasa Valiauga, Zachary Erlichman, Anna Hagstrom, Divya Sinha, Valentin M. Sluch, Xitiz Chamling, Donald J. Zack, Melissa C. Skala, and David M. Gamm. 2019. “Reproducibility and Staging of 3D Human Retinal Organoids across Multiple Pluripotent Stem Cell Lines.” Development (Cambridge) 146(1). doi: 10.1242/DEV.171686/VIDEO-7.

Catala, Martin. 2019. “Development of the Cerebrospinal Fluid Pathways during Embryonic and Fetal Life in Humans.” Pp. 1–75 in Pediatric Hydrocephalus. Cham: Springer International Publishing.

Chambers, Stuart M., Christopher A. Fasano, Eirini P. Papapetrou, Mark Tomishima, Michel Sadelain, and Lorenz Studer. 2009. “Highly Efficient Neural Conversion of Human ES and IPS Cells by Dual Inhibition of SMAD Signaling.” Nature Biotechnology 27(3):275–80. doi: 10.1038/nbt.1529.

Chen, Guokai. 2014. “Splitting HESC/HiPSC Lines with EDTA in Feeder-Free Conditions.” StemBook. doi: 10.3824/stembook.1.88.1.

Chen, Jiapei, Elizabeth E. Crouch, Miriam E. Zawadzki, Kyle A. Jacobs, Lakyn N. Mayo, Jennifer Ja Yoon Choi, Pin Yeh Lin, Saba Shaikh, Jessica Tsui, Susana Gonzalez-Granero, Shamari Waller, Avani Kelekar, Gugene Kang, Edward J. Valenzuela, Janeth Ochoa Birrueta, Loukas N. Diafos, Kaylee Wedderburn-Pugh, Barbara Di Marco, Wenlong Xia, Claudia Z. Han, Nicole G. Coufal, Christopher K. Glass, Stephen P. J. Fancy, Julieta Alfonso, Arnold R. Kriegstein, Michael C. Oldham, Jose Manuel Garcia-Verdugo, Matthew L. Kutys, Maria K. Lehtinen, Alexis J. Combes, and Eric J. Huang. 2024. “Proinflammatory Immune Cells Disrupt Angiogenesis and Promote Germinal Matrix Hemorrhage in Prenatal Human Brain.” Nature Neuroscience. doi: 10.1038/s41593-024-01769-2.

Chen, Shih Wei, Yu Sheng Hung, Jong Ling Fuh, Nien Jung Chen, Yeh Shiu Chu, Shu Cian Chen, Ming Ji Fann, and Yu Hui Wong. 2021. “Efficient Conversion of Human Induced Pluripotent Stem Cells into Microglia by Defined Transcription Factors.” Stem Cell Reports 16(5):1363–80. doi: 10.1016/j.stemcr.2021.03.010.

Chen, Xianwei, Guoqiang Sun, Lizhao Feng, E. Tian, and Yanhong Shi. 2025. “Human IPSC-Derived Microglial Cells Protect Neurons from Neurodegeneration in Long-Term Cultured Adhesion Brain Organoids.” Communications Biology 8(1):30. doi: 10.1038/s42003-024-07401-0.

Chen, Xiaohong, Yang Yang, Lin Chen, and Kejing Wang. 2024. “Pregnancy Outcomes and Birth Defects in Offspring Following Non-Steroidal Anti-Inflammatory Drugs Exposure during Pregnancy: A Systematic Review and Meta-Analysis.” Reproductive Toxicology 125:108561. doi: 10.1016/J.REPROTOX.2024.108561.

Chen, Yong, John M. Hallenbeck, Christl Ruetzler, David Bol, Karen Thomas, Nancy E. J. Berman, and Stefanie N. Vogel. 2003. “Overexpression of Monocyte Chemoattractant Protein 1 in the Brain Exacerbates Ischemic Brain Injury and Is Associated with Recruitment of Inflammatory Cells.” Journal of Cerebral Blood Flow and Metabolism 23(6):748–55. doi: 10.1097/01.WCB.0000071885.63724.20/ASSET/IMAGES/LARGE/10.1097_01.WCB.0000071885.63724.20-FIG5.JPEG.

Chhor, Vibol, Tifenn Le Charpentier, Sophie Lebon, Marie Virgine Oré, Idoia Lara Celador, Julien Josserand, Vincent Degos, Etienne Jacotot, Henrik Hagberg, Karin Sävman, Carina Mallard, Pierre Gressens, and Bobbi Fleiss. 2013. “Characterization of Phenotype Markers and Neuronotoxic Potential of Polarised Primary Microglia in Vitro.” Brain, Behavior, and Immunity 32:70–85. doi: 10.1016/J.BBI.2013.02.005.

Chichagova, Valeria, Maria Georgiou, Madeleine Carter, Birthe Dorgau, Gerrit Hilgen, Joseph Collin, Rachel Queen, Git Chung, Jila Ajeian, Marina Moya-Molina, Stefan Kustermann, Francois Pognan, Philip Hewitt, Michael Schmitt, Evelyne Sernagor, Lyle Armstrong, and Majlinda Lako. 2023. “Incorporating Microglia-like Cells in Human Induced Pluripotent Stem Cell-Derived Retinal Organoids.” Journal of Cellular and Molecular Medicine 27(3):435–45. doi: 10.1111/JCMM.17670.

Clarkson, Benjamin D. S., Robert J. Kahoud, Christina B. McCarthy, and Charles L. Howe. 2017. “Inflammatory Cytokine-Induced Changes in Neural Network Activity Measured by Waveform Analysis of High-Content Calcium Imaging in Murine Cortical Neurons.” Scientific Reports 2017 7:1 7(1):1–13. doi: 10.1038/s41598-017-09182-5.

Coiro, Pierluca, Ragunathan Padmashri, Anand Suresh, Elizabeth Spartz, Gurudutt Pendyala, Shinnyi Chou, Yoosun Jung, Brittney Meays, Shreya Roy, Nagsen Gautam, Yazen Alnouti, Ming Li, and Anna Dunaevsky. 2015. “Impaired Synaptic Development in a Maternal Immune Activation Mouse Model of Neurodevelopmental Disorders.” Brain, Behavior, and Immunity 50:249–58. doi: 10.1016/J.BBI.2015.07.022.

Collin, Joseph, Rachel Queen, Darin Zerti, Birthe Dorgau, Rafiqul Hussain, Jonathan Coxhead, Simon Cockell, and Majlinda Lako. 2019. “Deconstructing Retinal Organoids: Single Cell RNA-Seq Reveals the Cellular Components of Human Pluripotent Stem Cell-Derived Retina.” STEM CELLS 37(5):593–98. doi: 10.1002/stem.2963.

Colonna, Marco, and Oleg Butovsky. 2017. “Microglia Function in the Central Nervous System During Health and Neurodegeneration.” Annual Review of Immunology 35(1):441–68. doi: 10.1146/annurev-immunol-051116-052358.

Cora, Virginia, Jasmin Haderspeck, Lena Antkowiak, Ulrich Mattheus, Peter H. Neckel, Andreas F. Mack, Sylvia Bolz, Marius Ueffng, Natalia Pashkovskaia, Kevin Achberger, and Stefan Liebau. 2019. “A Cleared View on Retinal Organoids.” Cells 8(5). doi: 10.3390/cells8050391.

Cowan, Cameron S., Magdalena Renner, Martina De Gennaro, Brigitte Gross-Scherf, David Goldblum, Yanyan Hou, Martin Munz, Tiago M. Rodrigues, Jacek Krol, Tamas Szikra, Rachel Cuttat, Annick Waldt, Panagiotis Papasaikas, Roland Diggelmann, Claudia P. Patino-Alvarez, Patricia Galliker, Stefan E. Spirig, Dinko Pavlinic, Nadine Gerber-Hollbach, Sven Schuierer, Aldin Srdanovic, Marton Balogh, Riccardo Panero, Akos Kusnyerik, Arnold Szabo, Michael B. Stadler, Selim Orgül, Simone Picelli, Pascal W. Hasler, Andreas Hierlemann, Hendrik P. N. Scholl, Guglielmo Roma, Florian Nigsch, and Botond Roska. 2020. “Cell Types of the Human Retina and Its Organoids at Single-Cell Resolution.” Cell 182(6):1623-1640.e34. doi: 10.1016/j.cell.2020.08.013.

Cserép, Csaba, Anett D. Schwarcz, Balázs Pósfai, Zsófia I. László, Anna Kellermayer, Zsuzsanna Környei, Máté Kisfali, Miklós Nyerges, Zsolt Lele, István Katona, and Ádám Dénes. 2022. “Microglial Control

of Neuronal Development via Somatic Purinergic Junctions." Cell Reports 40(12):111369. doi: 10.1016/j.celrep.2022.111369.

Cunningham, C. L., V. Martinez-Cerdeno, and S. C. Noctor. 2013. "Microglia Regulate the Number of Neural Precursor Cells in the Developing Cerebral Cortex." Journal of Neuroscience 33(10):4216–33. doi: 10.1523/JNEUROSCI.3441-12.2013.

Daneman, Richard, Lu Zhou, Amanuel A. Kebede, and Ben A. Barres. 2010. "Pericytes Are Required for Blood–Brain Barrier Integrity during Embryogenesis." Nature 468(7323):562–66. doi: 10.1038/nature09513.

Dang, Jason, Shashi Kant Tiwari, Gianluigi Lichinchi, Yue Qin, Veena S. Patil, Alexey M. Eroshkin, and Tariq M. Rana. 2016. "Zika Virus Depletes Neural Progenitors in Human Cerebral Organoids through Activation of the Innate Immune Receptor TLR3." Cell Stem Cell 19(2):258–65. doi: 10.1016/j.stem.2016.04.014.

Davalos, Dimitrios, Jaime Grutzendler, Guang Yang, Jiyun V. Kim, Yi Zuo, Steffen Jung, Dan R. Littman, Michael L. Dustin, and Wen Biao Gan. 2005. "ATP Mediates Rapid Microglial Response to Local Brain Injury in Vivo." Nature Neuroscience 8(6):752–58. doi: 10.1038/nn1472.

Deininger, Martin H., and Hermann J. Schluesener. 1999. "Cyclooxygenases-1 and -2 Are Differentially Localized to Microglia and Endothelium in Rat EAE and Glioma." Journal of Neuroimmunology 95(1–2):202–8. doi: 10.1016/S0165-5728(98)00257-4.

Dermitzakis, Iasonas, Paschalis Theotokis, Paschalis Evangelidis, Efthymia Delilampou, Nikolaos Evangelidis, Anastasia Chatzisavvidou, Eleni Avramidou, and Maria Eleni Manthou. 2023. "CNS Border-Associated Macrophages: Ontogeny and Potential Implication in Disease." Current Issues in Molecular Biology 45(5):4285–4300.

Diaz-Araya, Claudia M., Jan M. Provis, Philip L. Penfold, and Francis A. Billson. 1995. "Development of Microglial Topography in Human Retina." The Journal of Comparative Neurology 363(1):53–68. doi: 10.1002/cne.903630106.

Douvaras, Panagiotis, Bruce Sun, Minghui Wang, Ilya Kruglikov, Gregory Lallos, Matthew Zimmer, Cecile Terrenoire, Bin Zhang, Sam Gandy, Eric Schadt, Donald O. Freytes, Scott Noggle, and Valentina Fossati. 2017. "Directed Differentiation of Human Pluripotent Stem Cells to Microglia." Stem Cell Reports 8(6):1516–24. doi: 10.1016/j.stemcr.2017.04.023.

Dräger, Nina M., Sydney M. Sattler, Cindy Tzu Ling Huang, Olivia M. Teter, Kun Leng, Sayed Hadi Hashemi, Jason Hong, Giovanni Aviles, Claire D. Clelland, Lihong Zhan, Joe C. Udeochu, Lay Kodama, Andrew B. Singleton, Mike A. Nalls, Justin Ichida, Michael E. Ward, Faraz Faghri, Li Gan, and Martin Kampmann. 2022. "A CRISPRi/a Platform in Human IPSC-Derived Microglia Uncovers Regulators of Disease States." Nature Neuroscience 25(9):1149–62. doi: 10.1038/s41593-022-01131-4.

Dragulescu, Adrian A. 2014. Read, Write, Format Excel 2007 (Xlsx) Files.

Dudgeon, J. A. 1967. "Maternal Rubella and Its Effect on the Foetus." Review Article Arch. Dis. Childh 110. doi: 10.1136/adc.42.222.110.

Dunn, Jemma, Sara Ferluga, Vikram Sharma, Matthias Futschik, David A. Hilton, Claire L. Adams, Edwin Lasonder, and C. Oliver Hanemann. 2019. "Proteomic Analysis Discovers the Differential Expression of Novel Proteins and Phosphoproteins in Meningioma Including NEK9, HK2 and SET and Deregulation of RNA Metabolism." EBioMedicine 40:77–91. doi: 10.1016/j.ebiom.2018.12.048.

Easley-Neal, Courtney, Oded Foreman, Neeraj Sharma, Ali A. Zarrin, and Robby M. Weimer. 2019. "CSF1R Ligands IL-34 and CSF1 Are Differentially Required for Microglia Development and Maintenance in White and Gray Matter Brain Regions." Frontiers in Immunology 10:2199. doi: 10.3389/fimmu.2019.02199.

Eiraku, Mototsugu, Nozomu Takata, Hiroki Ishibashi, Masako Kawada, Eriko Sakakura, Satoru Okuda, Kiyotoshi Sekiguchi, Taiji Adachi, and Yoshiki Sasai. 2011. “Self-Organizing Optic-Cup Morphogenesis in Three-Dimensional Culture.” Nature 2011 472:7341 472(7341):51–56. doi: 10.1038/nature09941.

Elkabes, S., E. M. DiCicco-Bloom, and I. B. Black. 1996. “Brain Microglia/Macrophages Express Neurotrophins That Selectively Regulate Microglial Proliferation and Function.” The Journal of Neuroscience : The Official Journal of the Society for Neuroscience 16(8):2508–21. doi: 10.1523/JNEUROSCI.16-08-02508.1996.

Elmore, Monica R. P., Allison R. Najafi, Maya A. Koike, Nabil N. Dagher, Elizabeth E. Spangenberg, Rachel A. Rice, Masashi Kitazawa, Bernice Matusow, Hoa Nguyen, Brian L. West, and Kim N. Green. 2014. “Colony-Stimulating Factor 1 Receptor Signaling Is Necessary for Microglia Viability, Unmasking a Microglia Progenitor Cell in the Adult Brain.” Neuron 82(2):380–97. doi: 10.1016/j.neuron.2014.02.040.

Emdad, Luni, Sunita L. D’Souza, Harini P. Kothari, Zulekha A. Qadeer, and Isabelle M. Germano. 2012. “Efficient Differentiation of Human Embryonic and Induced Pluripotent Stem Cells into Functional Astrocytes.” Stem Cells and Development 21(3):404–10. doi: 10.1089/scd.2010.0560.

Erblich, Bryna, Liyin Zhu, Anne M. Etgen, Kostantin Dobrenis, and Jeffrey W. Pollard. 2011. “Absence of Colony Stimulation Factor-1 Receptor Results in Loss of Microglia, Disrupted Brain Development and Olfactory Deficits.” PLOS ONE 6(10):e26317. doi: 10.1371/JOURNAL.PONE.0026317.

Fabriek, Babs O., Elise S. Van Haastert, Ian Galea, Machteld M. J. Polfliet, Ed D. Döpp, Michel M. Van Den Heuvel, Timo K. Van Den Berg, Corline J. A. De Groot, Paul Van Der Valk, and Christine D. Dijkstra. 2005. “CD163-Positive Perivascular Macrophages in the Human CNS Express Molecules for Antigen Recognition and Presentation.” Glia 51(4):297–305. doi: 10.1002/glia.20208.

Fagerlund, Ilkka, Antonios Dougalis, Anastasia Shakirzyanova, Mireia Gómez-Budia, Anssi Pelkonen, Henna Konttinen, Sohvi Ohtonen, Mohammad Feroze Fazaludeen, Marja Koskuvi, Johanna Kuusisto, Damián Hernández, Alice Pebay, Jari Koistinaho, Tuomas Rauramaa, Šárka Lehtonen, Paula Korhonen, and Tarja Malm. 2021. “Microglia-like Cells Promote Neuronal Functions in Cerebral Organoids.” Cells 11(1):124. doi: 10.3390/cells11010124.

Faial, Tiago, Andreia S. Bernardo, Sasha Mendjan, Evangelia Diamanti, Daniel Ortmann, George E. Gentsch, Victoria L. Mascetti, Matthew W. B. Trotter, James C. Smith, and Roger A. Pedersen. 2015. “Brachyury and SMAD Signalling Collaboratively Orchestrate Distinct Mesoderm and Endoderm Gene Regulatory Networks in Differentiating Human Embryonic Stem Cells.” Development (Cambridge) 142(12):2121–35. doi: 10.1242/dev.117838.

Fan, Yang, Zhilu Chen, Janak L. Pathak, Ana M. D. Carneiro, and Chang Y. Chung. 2018. “Differential Regulation of Adhesion and Phagocytosis of Resting and Activated Microglia by Dopamine.” Frontiers in Cellular Neuroscience 12:389822. doi: 10.3389/FNCEL.2018.00309/BIBTEX.

Feng, Lingling, Brandoch Cook, Su Yi Tsai, Ting Zhou, Brooke LaFlamme, Todd Evans, and Shuibing Chen. 2016. “Discovery of a Small-Molecule BMP Sensitizer for Human Embryonic Stem Cell Differentiation.” Cell Reports 15(9):2063–75. doi: 10.1016/j.celrep.2016.04.066.

Fife, Brian T., Kevin J. Kennedy, Mary C. Paniagua, Nicholas W. Lukacs, Steven L. Kunkel, Andrew D. Luster, and William J. Karpus. 2001. “CXCL10 (IFN-Gamma-Inducible Protein-10) Control of Encephalitogenic CD4+ T Cell Accumulation in the Central Nervous System during Experimental Autoimmune Encephalomyelitis.” Journal of Immunology (Baltimore, Md. : 1950) 166(12):7617–24. doi: 10.4049/JIMMUNOL.166.12.7617.

Fligor, Clarisse M., Sailee S. Lavekar, Jade Harkin, Priya K. Shields, Kirstin B. VanderWall, Kang Chieh Huang, Cátia Gomes, and Jason S. Meyer. 2021. “Extension of Retinofugal Projections in an Assembled

Model of Human Pluripotent Stem Cell-Derived Organoids." Stem Cell Reports 16(9):2228–41. doi: 10.1016/j.stemcr.2021.05.009.

Font-Nieves, Miriam, M. Glòria Sans-Fons, Roser Gorina, Ester Bonfill-Teixidor, Angeĺica Salas-Peŕdomo, Leonardo Maŕquez-Kisinousky, Tomaš Santalucia, and Anna M. Planas. 2012. "Induction of COX-2 Enzyme and Down-Regulation of COX-1 Expression by Lipopolysaccharide (LPS) Control Prostaglandin E2 Production in Astrocytes." The Journal of Biological Chemistry 287(9):6454. doi: 10.1074/JBC.M111.327874.

Forrest, Caroline M., Omari S. Khalil, Mazura Pisar, Robert A. Smith, Lynda Darlington, and Trevor W. Stone. 2012. "Prenatal Activation of Toll-like Receptors-3 by Administration of the Viral Mimetic Poly(I:C) Changes Synaptic Proteins, N-Methyl-D-Aspartate Receptors and Neurogenesis Markers in Offspring." Molecular Brain 5(1):22. doi: 10.1186/1756-6606-5-22.

Forrester, John V, Heping Xu, Lucia Kuffová, Andrew D. Dick, and Paul G. McMenamin. 2010. "Dendritic Cell Physiology and Function in the Eye." Immunological Reviews 234(1):282–304. doi: 10.1111/j.0105-2896.2009.00873.x.

Gabriel, Elke, Walid Albanna, Giovanni Pasquini, Anand Ramani, Natasa Josipovic, Aruljothi Mariappan, Friedrich Schinzel, Celeste M. Karch, Guobin Bao, Marco Gottardo, Ata Alp Suren, Jürgen Hescheler, Kerstin Nagel-Wolfrum, Veronica Persico, Silvio O. Rizzoli, Janine Altmüller, Maria Giovanna Riparbelli, Giuliano Callaini, Olivier Goureau, Argyris Papantonis, Volker Busskamp, Toni Schneider, and Jay Gopalakrishnan. 2021. "Human Brain Organoids Assemble Functionally Integrated Bilateral Optic Vesicles." Cell Stem Cell. doi: 10.1016/j.stem.2021.07.010.

Gao, Mei Ling, Xiao Zhang, Fang Han, Jia Xu, Si Jian Yu, Kangxin Jin, and Zi Bing Jin. 2022. "Functional Microglia Derived from Human Pluripotent Stem Cells Empower Retinal Organ." Science China Life Sciences 65(6):1057–71. doi: 10.1007/S11427-021-2086-0/METRICS.

Garber, Charise, Allison Soung, Lauren L. Vollmer, Marlene Kanmogne, Aisling Last, Jasmine Brown, and Robyn S. Klein. 2019. "T Cells Promote Microglia-Mediated Synaptic Elimination and Cognitive Dysfunction during Recovery from Neuropathogenic Flaviviruses." Nature Neuroscience 22(8):1276–88. doi: 10.1038/s41593-019-0427-y.

Garcez, Patricia P., Erick Correia Loiola, Rodrigo Madeiro Da Costa, Luiza M. Higa, Pablo Trindade, Rodrigo Delvecchio, Juliana Minardi Nascimento, Rodrigo Brindeiro, Amilcar Tanuri, and Stevens K. Rehen. 2016. "Zika Virus: Zika Virus Impairs Growth in Human Neurospheres and Brain Organoids." Science 352(6287):816–18. doi: 10.1126/SCIENCE.AAF6116/SUPPL_FILE/PAPV2.PDF.

Garita-Hernandez, Marcela, Fiona Routet, Laure Guibbal, Hanen Khabou, Lyes Toualbi, Luisa Riancho, Sacha Reichman, Jens Duebel, Jose-Alain Sahel, Olivier Goureau, and Deniz Dalkara. 2020. "AAV-Mediated Gene Delivery to 3D Retinal Organoids Derived from Human Induced Pluripotent Stem Cells." International Journal of Molecular Sciences 21(3):994. doi: 10.3390/ijms21030994.

Geirsdottir, Laufey, Eyal David, Hadas Keren-Shaul, Daniel Erny, Ido Amit, and Marco Prinz. 2019. "Cross-Species Single-Cell Analysis Reveals Divergence of the Primate Microglia Program Identification of Disease-Associated Microglia Gene Expression Modules in Humans." Cell 179:1609–22. doi: 10.1016/j.cell.2019.11.010.

Geissmann, Frederic, Steffen Jung, and Dan R. Littman. 2003. "Blood Monocytes Consist of Two Principal Subsets with Distinct Migratory Properties." Immunity 19(1):71–82. doi: 10.1016/S1074-7613(03)00174-2.

Gerdes, J., H. Lemke, H. Baisch, H. H. Wacker, U. Schwab, and H. Stein. 1984. "Cell Cycle Analysis of a Cell Proliferation-Associated Human Nuclear Antigen Defined by the Monoclonal Antibody Ki-67." The Journal of Immunology 133(4).

Ginhoux, Florent, Melanie Greter, Marylene Leboeuf, Sayan Nandi, Peter See, Mark F. Mehler, Simon J. Conway, Lai Guan Ng, E. Richard Stanley, M. Igor, and Miriam Merad. 2010. “Fate Mapping Analysis Reveals That Adult Microglia Derive from Primitive Macrophages.” Science 330(6005):841–45. doi: 10.1126/science.1194637.Fate.

Ginhoux, Florent, and Marco Prinz. 2015. “Origin of Microglia: Current Concepts and Past Controversies.” Cold Spring Harbor Perspectives in Biology 7(8). doi: 10.1101/cshperspect.a020537.

Giovanoli, Sandra, Ulrike Weber-Stadlbauer, Manfred Schedlowski, Urs Meyer, and Harald Engler. 2016. “Prenatal Immune Activation Causes Hippocampal Synaptic Deficits in the Absence of Overt Microglia Anomalies.” Brain, Behavior, and Immunity 55:25–38. doi: 10.1016/J.BBI.2015.09.015.

Goddery, Emma N., Cori E. Fain, Chloe G. Lipovsky, Katayoun Ayasoufi, Lila T. Yokanovich, Courtney S. Malo, Roman H. Khadka, Zachariah P. Tritz, Fang Jin, Michael J. Hansen, and Aaron J. Johnson. 2021. “Microglia and Perivascular Macrophages Act as Antigen Presenting Cells to Promote CD8 T Cell Infiltration of the Brain.” Frontiers in Immunology 12. doi: 10.3389/fimmu.2021.726421.

Goldmann, Tobias, Peter Wieghofer, Marta Joana Costa Jordão, Fabiola Prutek, Nora Hagemeyer, Kathrin Frenzel, Lukas Amann, Ori Staszewski, Katrin Kierdorf, Martin Krueger, Giuseppe Locatelli, Hannah Hochgerner, Robert Zeiser, Slava Epelman, Frederic Geissmann, Josef Priller, Fabio M. V. Rossi, Ingo Bechmann, Martin Kerschensteiner, Sten Linnarsson, Steffen Jung, and Marco Prinz. 2016. “Origin, Fate and Dynamics of Macrophages at Central Nervous System Interfaces.” Nature Immunology 17(7):797–805. doi: 10.1038/ni.3423.

Gosselin, David, Dylan Skola, Nicole G. Coufal, Inge R. Holtman, Johannes C. M. Schlachetzki, Eniko Sajti, Baptiste N. Jaeger, Carolyn O’Connor, Conor Fitzpatrick, Martina P. Pasillas, Monique Pena, Amy Adair, David D. Gonda, Michael L. Levy, Richard M. Ransohoff, Fred H. Gage, and Christopher K. Glass. 2017. “An Environment-Dependent Transcriptional Network Specifies Human Microglia Identity.” Science 356(6344):eaal3222. doi: 10.1126/science.aal3222.

Greter, Melanie, Iva Lelios, Pawel Pelczar, Guillaume Hoeffel, Jeremy Price, Marylene Leboeuf, Thomas M. Kündig, Karl Frei, Florent Ginhoux, Miriam Merad, and Burkhard Becher. 2012. “Stroma-Derived Interleukin-34 Controls the Development and Maintenance of Langerhans Cells and the Maintenance of Microglia.” Immunity 37(6):1050–60. doi: 10.1016/j.immuni.2012.11.001.

Griswold, Don E., and Jerry L. Adams. 1996. “Constitutive Cyclooxygenase (COX-1) and Inducible Cyclooxygenase (COX-2): Rationale for Selective Inhibition and Progress to Date.” Med Res Rev. 16(2):181–206. doi: 10.1002/(SICI)1098-1128(199603)16:2.

Guizzetti, Marina, Xiaolu Zhang, Calla Goeke, and David P. Gavin. 2014. “Glia and Neurodevelopment: Focus on Fetal Alcohol Spectrum Disorders.” Frontiers in Pediatrics 2(NOV):123.

Guo, Long, Débora Romeo Bertola, Asako Takanohashi, Asuka Saito, Yuko Segawa, Takanori Yokota, Satoru Ishibashi, Yoichiro Nishida, Guilherme Lopes Yamamoto, José Francisco da Silva Franco, Rachel Sayuri Honjo, Chong Ae Kim, Camila Manso Musso, Margaret Timmons, Amy Pizzino, Ryan J. Taft, Bryan Lajoie, Melanie A. Knight, Kenneth H. Fischbeck, Andrew B. Singleton, Carlos R. Ferreira, Zheng Wang, Li Yan, James Y. Garbern, Pelin O. Simsek-Kiper, Hirofumi Ohashi, Pamela G. Robey, Alan Boyde, Naomichi Matsumoto, Noriko Miyake, Jürgen Spranger, Raphael Schiffmann, Adeline Vanderver, Gen Nishimura, Maria Rita dos Santos Passos-Bueno, Cas Simons, Kinya Ishikawa, and Shiro Ikegawa. 2019. “Bi-Allelic CSF1R Mutations Cause Skeletal Dysplasia of Dysosteosclerosis-Pyle Disease Spectrum and Degenerative Encephalopathy with Brain Malformation.” American Journal of Human Genetics 104(5):925–35. doi: 10.1016/J.AJHG.2019.03.004.

Gupta, Tulika, Kanchan Kapoor, Daisy Sahni, and Balbir Singh. 2016. “Mapping the Time Line of Development in Each Layer of Human Foetal Retina.” Journal of Clinical and Diagnostic Research : JCDR 10(3):AC04. doi: 10.7860/JCDR/2016/14936.7372.

Guttikonda, Sudha R., Lisa Sikkema, Jason Tchieu, Nathalie Saurat, Ryan M. Walsh, Oliver Harschnitz, Gabriele Ciceri, Marjolein Sneeboer, Linas Mazutis, Manu Setty, Paul Zumbo, Doron Betel, Lot D. de Witte, Dana Pe'er, and Lorenz Studer. 2021. "Fully Defined Human Pluripotent Stem Cell-Derived Microglia and Tri-Culture System Model C3 Production in Alzheimer's Disease." Nature Neuroscience 24(3):343–54. doi: 10.1038/s41593-020-00796-z.

Haenseler, Walther, Stephen N. Sansom, Julian Buchrieser, Sarah E. Newey, Craig S. Moore, Francesca J. Nicholls, Satyan Chintawar, Christian Schnell, Jack P. Antel, Nicholas D. Allen, M. Zameel Cader, Richard Wade-Martins, William S. James, and Sally A. Cowley. 2017. "A Highly Efficient Human Pluripotent Stem Cell Microglia Model Displays a Neuronal-Co-Culture-Specific Expression Profile and Inflammatory Response." Stem Cell Reports 8(6):1727–42. doi: 10.1016/j.stemcr.2017.05.017.

Hagemeyer, Nora, Katrin Kierdorf, Kathrin Frenzel, Jia Xue, Marc Ringelhan, Zeinab Abdullah, Isabelle Godin, Peter Wieghofer, Marta Joana Costa Jordão, Thomas Ulas, Gülden Yorgancioglu, Frank Rosenbauer, Percy A. Knolle, Mathias Heikenwalder, Joachim L. Schultze, and Marco Prinz. 2016. "Transcriptome-Based Profiling of Yolk Sac-Derived Macrophages Reveals a Role for Irf8 in Macrophage Maturation." The EMBO Journal 35(16):1730–44. doi: 10.15252/embj.201693801.

Hallam, Dean, Gerrit Hilgen, Birthe Dorgau, Lili Zhu, Min Yu, Sanja Bojic, Philip Hewitt, Michael Schmitt, Marianne Uteng, Stefan Kustermann, David Steel, Mike Nicholds, Robert Thomas, Achim Treumann, Andrew Porter, Evelyne Sernagor, Lyle Armstrong, and Majlinda Lako. 2018. "Human-Induced Pluripotent Stem Cells Generate Light Responsive Retinal Organoids with Variable and Nutrient-Dependent Efficiency." STEM CELLS 36(10):1535–51. doi: 10.1002/stem.2883.

Hammond, Timothy R., Connor Dufort, Lasse Dissing-Olesen, Stefanie Giera, Adam Young, Alec Wysoker, Alec J. Walker, Frederick Gergits, Michael Segel, James Nemesh, Samuel E. Marsh, Arpiar Saunders, Evan Macosko, Florent Ginhoux, Jinmiao Chen, Robin J. M. Franklin, Xianhua Piao, Steven A. McCarroll, and Beth Stevens. 2019. "Single-Cell RNA Sequencing of Microglia throughout the Mouse Lifespan and in the Injured Brain Reveals Complex Cell-State Changes." Immunity 50(1):253-271.e6. doi: 10.1016/J.IMMUNI.2018.11.004.

Han, Claudia Z., Rick Z. Li, Emily Hansen, Samantha Trescott, Bethany R. Fixsen, Celina T. Nguyen, Cristina M. Mora, Nathanael J. Spann, Hunter R. Bennett, Olivier Poirion, Justin Buchanan, Anna S. Warden, Bing Xia, Johannes C. M. Schlachetzki, Martina P. Pasillas, Sebastian Preissl, Allen Wang, Carolyn O'Connor, Shreya Shriram, Roy Kim, Danielle Schafer, Gabriela Ramirez, Jean Challacombe, Samuel A. Anavim, Avalon Johnson, Mihir Gupta, Ian A. Glass, Michael L. Levy, Sharona Ben Haim, David D. Gonda, Louise Laurent, Jennifer F. Hughes, David C. Page, Mathew Blurton-Jones, Christopher K. Glass, and Nicole G. Coufal. 2023. "Human Microglia Maturation Is Underpinned by Specific Gene Regulatory Networks." Immunity 56(9):2152-2171.e13. doi: 10.1016/j.immuni.2023.07.016.

Hanisch, Uwe Karsten, and Helmut Kettenmann. 2007. "Microglia: Active Sensor and Versatile Effector Cells in the Normal and Pathologic Brain." Nature Neuroscience 10(11):1387–94. doi: 10.1038/nn1997.

Hattori, Yuki, and Takaki Miyata. 2018. "Microglia Extensively Survey the Developing Cortex via the CXCL12/CXCR4 System to Help Neural Progenitors to Acquire Differentiated Properties." Genes to Cells 23(10):915–22. doi: 10.1111/GTC.12632.

Hattori, Yuki, Yu Naito, Yoji Tsugawa, Shigenori Nonaka, Hiroaki Wake, Takashi Nagasawa, Ayano Kawaguchi, and Takaki Miyata. 2020. "Transient Microglial Absence Assists Postmigratory Cortical Neurons in Proper Differentiation." Nature Communications 11(1). doi: 10.1038/s41467-020-15409-3.

Hay, Elizabeth D. 2005. "The Mesenchymal Cell, Its Role in the Embryo, and the Remarkable Signaling Mechanisms That Create It." Developmental Dynamics 233(3):706–20. doi: 10.1002/dvdy.20345.

Hayashi, Ryuhei, Yuki Ishikawa, Ryousuke Katori, Yuzuru Sasamoto, Yuki Taniwaki, Hiroshi Takayanagi, Motokazu Tsujikawa, Kiyotoshi Sekiguchi, Andrew J. Quantock, and Kohji Nishida. 2017. "Coordinated Generation of Multiple Ocular-like Cell Lineages and Fabrication of Functional Corneal Epithelial Cell Sheets from Human IPS Cells." Nature Protocols 12(4):683–96. doi: 10.1038/nprot.2017.007.

Hayashi, Ryuhei, Yuki Ishikawa, Yuzuru Sasamoto, Ryosuke Katori, Naoki Nomura, Tatsuya Ichikawa, Saori Araki, Takeshi Soma, Satoshi Kawasaki, Kiyotoshi Sekiguchi, Andrew J. Quantock, Motokazu Tsujikawa, and Kohji Nishida. 2016. "Co-Ordinated Ocular Development from Human IPS Cells and Recovery of Corneal Function." Nature 531(7594):376–80. doi: 10.1038/nature17000.

Hayes, Lindsay N., Kyongman An, Elisa Carloni, Fangze Li, Elizabeth Vincent, Chloë Trippaers, Manish Paranjpe, Gül Dölen, Loyal A. Goff, Adriana Ramos, Shin-ichi Kano, and Akira Sawa. 2022. "Prenatal Immune Stress Blunts Microglia Reactivity, Impairing Neurocircuitry." Nature 610(7931):327. doi: 10.1038/s41586-022-05274-z.

He, Yingbo, Natalie Taylor, Xiang Yao, and Anindya Bhattacharya. 2021. "Mouse Primary Microglia Respond Differently to LPS and Poly(I:C) in Vitro." Scientific Reports 2021 11:1 11(1):1–14. doi: 10.1038/s41598-021-89777-1.

Heisenberg, Carl-Philipp, and Lilianna Solnica-Krezel. 2008. "Back and Forth between Cell Fate Specification and Movement during Vertebrate Gastrulation." Current Opinion in Genetics & Development 18(4):311–16. doi: 10.1016/j.gde.2008.07.011.

Hendrickson, Anita. 2016. "Development of Retinal Layers in Prenatal Human Retina." American Journal of Ophthalmology 161:29. doi: 10.1016/J.AJO.2015.09.023.

Hendrickson, Anita, Daniel Possin, Lejla Vajzovic, and Cynthia A. Toth. 2012. "Histologic Development of the Human Fovea From Midgestation to Maturity." American Journal of Ophthalmology 154(5):767-778.e2. doi: 10.1016/j.ajo.2012.05.007.

Hickman, Suzanne E., Nathan D. Kingery, Toshiro K. Ohsumi, Mark L. Borowsky, Li Chong Wang, Terry K. Means, and Joseph El Khoury. 2013. "The Microglial Sensome Revealed by Direct RNA Sequencing." Nature Neuroscience 16(12):1896–1905. doi: 10.1038/nn.3554.

Hirami, Yasuhiko, Michiko Mandai, Sunao Sugita, Akiko Maeda, Tadao Maeda, Midori Yamamoto, Hirofumi Uyama, Satoshi Yokota, Masashi Fujihara, Masataka Igeta, Takashi Daimon, Kanako Fujita, Tomoko Ito, Naoki Shibatani, Chikako Morinaga, Tetsuya Hayama, Aya Nakamura, Kazuki Ueyama, Keiichi Ono, Hidetaka Ohara, Masayo Fujiwara, Suguru Yamasaki, Kenji Watari, Kiyoko Bando, Keigo Kawabe, Atsushi Ikeda, Toru Kimura, Atsushi Kuwahara, Masayo Takahashi, and Yasuo Kurimoto. 2023. "Safety and Stable Survival of Stem-Cell-Derived Retinal Organoid for 2 Years in Patients with Retinitis Pigmentosa." Cell Stem Cell 30(12):1585-1596.e6. doi: 10.1016/j.stem.2023.11.004.

Hirata, Akihiro, Ken Ichi Inada, Tetsuya Tsukamoto, Hiroki Sakai, Tsutomu Mizoshita, Tokuma Yanai, Toshiaki Masegi, Hidemasa Goto, Masaki Inagaki, and Masae Tatematsu. 2004. "Characterization of a Monoclonal Antibody, HTA28, Recognizing a Histone H3 Phosphorylation Site as a Useful Marker of M-Phase Cells." Journal of Histochemistry and Cytochemistry 52(11):1503–9. doi: 10.1369/jhc.4A6285.2004.

Hoeffel, Guillaume, Jinmiao Chen, Yonit Lavin, Donovan Low, Francisca F. Almeida, Peter See, Anna E. Beaudin, Josephine Lum, Ivy Low, E. Camilla Forsberg, Michael Poidinger, Francesca Zolezzi, Anis Larbi, Lai Guan Ng, Jerry K. Y. Chan, Melanie Greter, Burkhard Becher, Igor M. Samokhvalov, Miriam Merad, and Florent Ginhoux. 2015. "C-Myb(+) Erythro-Myeloid Progenitor-Derived Fetal Monocytes Give Rise to Adult Tissue-Resident Macrophages." Immunity 42(4):665–78. doi: 10.1016/j.immuni.2015.03.011.

Hoeffel, Guillaume, and Florent Ginhoux. 2015. “Ontogeny of Tissue-Resident Macrophages.” Frontiers in Immunology 6(SEP). doi: 10.3389/fimmu.2015.00486.

Hoozemans, Jeroen J. M., Robert Veerhuis, Ingrid Janssen, Evert Jan Van Elk, Annemieke J. M. Rozemuller, and Piet Eikelenboom. 2002. “The Role of Cyclo-Oxygenase 1 and 2 Activity in Prostaglandin E2 Secretion by Cultured Human Adult Microglia: Implications for Alzheimer’s Disease.” Brain Research 951(2):218–26. doi: 10.1016/S0006-8993(02)03164-5.

Hoshino, Akina, Rinki Ratnapriya, Matthew J. Brooks, Vijender Chaitankar, Matthew S. Wilken, Chi Zhang, Margaret R. Starostik, Linn Gieser, Anna La Torre, Mario Nishio, Olivia Bates, Ashley Walton, Olivia Bermingham-McDonogh, Ian A. Glass, Rachel O. L. Wong, Anand Swaroop, and Thomas A. Reh. 2017. “Molecular Anatomy of the Developing Human Retina.” Developmental Cell 43(6):763-779.e4. doi: 10.1016/j.devcel.2017.10.029.

Hoshino, Akiyoshi, Satoshi Ueha, Sanshiro Hanada, Toshio Imai, Masako Ito, Kenji Yamamoto, Kouji Matsushima, Akira Yamaguchi, and Tadahiro Iimura. 2013. “Roles of Chemokine Receptor CX3CR1 in Maintaining Murine Bone Homeostasis through the Regulation of Both Osteoblasts and Osteoclasts.” Journal of Cell Science 126(4):1032–45. doi: 10.1242/jcs.113910.

Hothorn, Torsten, Frank Bretz, and Peter Westfall. 2008. “Simultaneous Inference in General Parametric Models.” Biometrical Journal 50(3):346–63. doi: 10.1002/bimj.200810425.

Van Hove, Hannah, Liesbet Martens, Isabelle Scheyltjens, Karen De Vlaminck, Ana Rita Pombo Antunes, Sofie De Prijck, Niels Vandamme, Sebastiaan De Schepper, Gert Van Isterdael, Charlotte L. Scott, Jeroen Aerts, Geert Berx, Guy E. Boeckxstaens, Roosmarijn E. Vandenbroucke, Lars Vereecke, Diederik Moechars, Martin Guilliams, Jo A. Van Ginderachter, Yvan Saeys, and Kiavash Movahedi. 2019. “A Single-Cell Atlas of Mouse Brain Macrophages Reveals Unique Transcriptional Identities Shaped by Ontogeny and Tissue Environment.” Nature Neuroscience 22(6):1021–35. doi: 10.1038/s41593-019-0393-4.

Hu, Yuqiong, Xiaoye Wang, Boqiang Hu, Yunuo Mao, Yidong Chen, Liying Yan, Jun Yong, Ji Dong, Yuan Wei, Wei Wang, Lu Wen, Jie Qiao, and Fuchou Tang. 2019. “Dissecting the Transcriptome Landscape of the Human Fetal Neural Retina and Retinal Pigment Epithelium by Single-Cell RNA-Seq Analysis.” PLOS Biology 17(7):e3000365. doi: 10.1371/JOURNAL.PBIO.3000365.

Huang, Tao, Jianlin Cui, Lei Li, Peter F. Hitchcock, and Yuhao Li. 2012. “The Role of Microglia in the Neurogenesis of Zebrafish Retina.” Biochemical and Biophysical Research Communications 421(2):214. doi: 10.1016/J.BBRC.2012.03.139.

Hübschmann, Verena, Medina Korkut-Demirbaş, and Sandra Siegert. 2022. “Assessing Human IPSC-Derived Microglia Identity and Function by Immunostaining, Phagocytosis, Calcium Activity, and Inflammation Assay.” STAR Protocols 3(4):101866. doi: 10.1016/j.xpro.2022.101866.

Hulshof, Sandra, Elise S. van Haastert, Hedwich F. Kuipers, Peter J. van den Elsen, Corline J. de Groot, Paul van der Valk, Rivka Ravid, and Knut Biber. 2003. “CX 3 CL1 and CX 3 CR1 Expression in Human Brain Tissue: Noninflammatory Control versus Multiple Sclerosis.” Journal of Neuropathology & Experimental Neurology 62(9):899–907. doi: 10.1093/jnen/62.9.899.

Imai, Y., I. Ibata, D. Ito, K. Ohsawa, and S. Kohsaka. 1996. “A Novel Gene Iba1 in the Major Histocompatibility Complex Class III Region Encoding an EF Hand Protein Expressed in a Monocytic Lineage.” Biochemical and Biophysical Research Communications 224(3):855–62. doi: 10.1006/bbrc.1996.1112.

Ito, D., K. Tanaka, S. Suzuki, T. Dembo, and Y. Fukuuchi. 2001. “Enhanced Expression of Iba1, Ionized Calcium-Binding Adapter Molecule 1, after Transient Focal Cerebral Ischemia in Rat Brain.” Stroke 32(5):1208–15. doi: 10.1161/01.str.32.5.1208.

Ito, Daisuke, Yoshinori Imai, Keiko Ohsawa, Kazuyuki Nakajima, Yasuo Fukuuchi, and Shinichi Kohsaka. 1998. “Microglia-Specific Localisation of a Novel Calcium Binding Protein, Iba1.” Molecular Brain Research 57(1):1–9. doi: 10.1016/S0169-328X(98)00040-0.

Jacob, Fadi, Sarshan R. Pather, Wei Kai Huang, Feng Zhang, Samuel Zheng Hao Wong, Haowen Zhou, Beatrice Cubitt, Wenqiang Fan, Catherine Z. Chen, Miao Xu, Manisha Pradhan, Daniel Y. Zhang, Wei Zheng, Anne G. Bang, Hongjun Song, Juan Carlos de la Torre, and Guo li Ming. 2020. “Human Pluripotent Stem Cell-Derived Neural Cells and Brain Organoids Reveal SARS-CoV-2 Neurotropism Predominates in Choroid Plexus Epithelium.” Cell Stem Cell 27(6):937-950.e9. doi: 10.1016/j.stem.2020.09.016.

Jacobson, Marcus, and Giro Hirose. 1978. “Origin of the Retina from Both Sides of the Embryonic Brain: A Contribution to the Problem of Crossing at the Optic Chiasma.” Science 202(4368):637–39.

Jain, Ashish, and Geetu Tuteja. 2019. “TissueEnrich: Tissue-Specific Gene Enrichment Analysis” edited by J. Kelso. Bioinformatics 35(11):1966–67. doi: 10.1093/bioinformatics/bty890.

Janabi, Nazila, Sylviane Peudenier, Bénédicte Héron, Kim Heng Ng, and Marc Tardieu. 1995. “Establishment of Human Microglial Cell Lines after Transfection of Primary Cultures of Embryonic Microglial Cells with the SV40 Large T Antigen.” Neuroscience Letters 195(2):105–8. doi: 10.1016/0304-3940(94)11792-H.

Janetzko, Karin, Gabi Rink, Andrea Hecker, Karen Bieback, Harald Klüter, and Peter Bugert. 2014. “A Single-Tube Real-Time PCR Assay for Mycoplasma Detection as a Routine Quality Control of Cell Therapeutics.” Transfusion Medicine and Hemotherapy : Offizielles Organ Der Deutschen Gesellschaft Fur Transfusionsmedizin Und Immunhamatologie 41(1):83–89. doi: 10.1159/000357096.

Janssen, Astrid, Thorsten J. Maier, Susanne Schiffmann, Ovidiu Coste, Maic Seegel, Gerd Geisslinger, and Sabine Grösch. 2006. “Evidence of COX-2 Independent Induction of Apoptosis and Cell Cycle Block in Human Colon Carcinoma Cells after S- or R-Ibuprofen Treatment.” European Journal of Pharmacology 540(1–3):24–33. doi: 10.1016/J.EJPHAR.2006.04.030.

Jiang, Zhen Huan, Jun Peng, Hui Lin Yang, Xing Li Fu, Jin Zhi Wang, Lei Liu, Jian Nong Jiang, Yong Fei Tan, and Zhi Jun Ge. 2017. “Upregulation and Biological Function of Transmembrane Protein 119 in Osteosarcoma.” Experimental and Molecular Medicine 49(5):329. doi: 10.1038/emm.2017.41.

Johnson, Erik A., Thuy L. Dao, Michelle A. Guignet, Claire E. Geddes, Andrew I. Koemeter-Cox, and Robert K. Kan. 2011. “Increased Expression of the Chemokines CXCL1 and MIP-1α by Resident Brain Cells Precedes Neutrophil Infiltration in the Brain Following Prolonged Soman-Induced Status Epilepticus in Rats.” Journal of Neuroinflammation 8:41. doi: 10.1186/1742-2094-8-41.

Juul, Sandra E., and Robert D. Christensen. 2018. “Developmental Hematology.” Avery’s Diseases of the Newborn: Tenth Edition 5:1113-1120.e3. doi: 10.1016/B978-0-323-40139-5.00078-4.

Kanamoto, Takashi, Koji Mizuhashi, Koji Terada, Takashi Minami, Hideki Yoshikawa, and Takahisa Furukawa. 2009. “Isolation and Characterization of a Novel Plasma Membrane Protein, Osteoblast Induction Factor (Obif), Associated with Osteoblast Differentiation.” BMC Developmental Biology 9(1):70. doi: 10.1186/1471-213X-9-70.

Kassambara, Alboukadel. 2017. Package “ggpubr” Type Package Title “Ggplot2” Based Publication Ready Plots.

Kato, Miyako, Shinichi Nishida, Hidero Kitasato, Natsue Sakata, and Shinichi Kawai. 2010. “Cyclooxygenase-1 and Cyclooxygenase-2 Selectivity of Non-Steroidal Anti-Inflammatory Drugs: Investigation Using Human Peripheral Monocytes.” Journal of Pharmacy and Pharmacology 53(12):1679–85. doi: 10.1211/0022357011778070.

Kawai, Taro, and Shizuo Akira. 2010. “The Role of Pattern-Recognition Receptors in Innate Immunity: Update on Toll-like Receptors.” Nature Immunology 11(5):373–84.

Kelemen, E., and M. Jánossa. 1980. “Macrophages Are the First Differentiated Blood Cells Formed in Human Embryonic Liver.” Experimental Hematology 8(8):996–1000.

Kelley, Kevin W., and Sergiu P. Pașca. 2022. “Human Brain Organogenesis: Toward a Cellular Understanding of Development and Disease.” Cell 185(1):42–61.

Kettenmann, H., A. Faissner, and J. Trotter. 1996. “Neuron-Glia Interactions in Homeostasis and Degeneration.” Pp. 533–43 in Comprehensive Human Physiology. Springer, Berlin, Heidelberg.

Kettenmann, Helmut, Uwe-Karsten Hanisch, Mami Noda, and Alexei Verkhratsky. 2011. “Physiology of Microglia.” Physiological Reviews 91(2):461–553. doi: 10.1152/physrev.00011.2010.

Kierdorf, Katrin, Daniel Erny, Tobias Goldmann, Victor Sander, Christian Schulz, Elisa Gomez Perdiguero, Peter Wieghofer, Annette Heinrich, Pia Riemke, Christoph Hölscher, Dominik N. Müller, Bruno Luckow, Thomas Brocker, Katharina Debowski, Günter Fritz, Ghislain Opdenakker, Andreas Diefenbach, Knut Biber, Mathias Heikenwalder, Frederic Geissmann, Frank Rosenbauer, and Marco Prinz. 2013. “Microglia Emerge from Erythromyeloid Precursors via Pu.1- and Irf8-Dependent Pathways.” Nature Neuroscience 16(3):273–80. doi: 10.1038/nn.3318.

Kierdorf, Katrin, Takahiro Masuda, Marta Joana Costa Jordão, and Marco Prinz. 2019. “Macrophages at CNS Interfaces: Ontogeny and Function in Health and Disease.” Nature Reviews Neuroscience 20(9):547–62.

Kilpinen, Helena, Angela Goncalves, Andreas Leha, Vackar Afzal, Kaur Alasoo, Sofie Ashford, Sendu Bala, Dalila Bensaddek, Francesco Paolo Casale, Oliver J. Culley, Petr Danecek, Adam Faulconbridge, Peter W. Harrison, Annie Kathuria, Davis McCarthy, Shane A. McCarthy, Ruta Meleckyte, Yasin Memari, Nathalie Moens, Filipa Soares, Alice Mann, Ian Streeter, Chukwuma A. Agu, Alex Alderton, Rachel Nelson, Sarah Harper, Minal Patel, Alistair White, Sharad R. Patel, Laura Clarke, Reena Halai, Christopher M. Kirton, Anja Kolb-Kokocinski, Philip Beales, Ewan Birney, Davide Danovi, Angus I. Lamond, Willem H. Ouwehand, Ludovic Vallier, Fiona M. Watt, Richard Durbin, Oliver Stegle, and Daniel J. Gaffney. 2017. “Common Genetic Variation Drives Molecular Heterogeneity in Human IPSCs.” Nature 546(7658):370–75. doi: 10.1038/nature22403.

Kim, Hongwon, Hyeok Ju Park, Hwan Choi, Yujung Chang, Hanseul Park, Jaein Shin, Junyeop Kim, Christopher J. Lengner, Yong Kyu Lee, and Jongpil Kim. 2019. “Modeling G2019S-LRRK2 Sporadic Parkinson’s Disease in 3D Midbrain Organoids.” Stem Cell Reports 12(3):518–31. doi: 10.1016/J.STEMCR.2019.01.020.

Kim, Hyosung, Kun Leng, Jinhee Park, Alexander G. Sorets, Suil Kim, Alena Shostak, Rebecca J. Embalabala, Kate Mlouk, Ketaki A. Katdare, Indigo V. L. Rose, Sarah M. Sturgeon, Emma H. Neal, Yan Ao, Shinong Wang, Michael V. Sofroniew, Jonathan M. Brunger, Douglas G. McMahon, Matthew S. Schrag, Martin Kampmann, and Ethan S. Lippmann. 2022. “Reactive Astrocytes Transduce Inflammation in a Blood-Brain Barrier Model through a TNF-STAT3 Signaling Axis and Secretion of Alpha 1-Antichymotrypsin.” Nature Communications 2022 13:1 13(1):1–18. doi: 10.1038/s41467-022-34412-4.

Kim, Sangbae, Albert Lowe, Rachayata Dharmat, Seunghoon Lee, Leah A. Owen, Jun Wang, Akbar Shakoor, Yumei Li, Denise J. Morgan, Andre A. Hejazi, Ales Cvekl, Margaret M. DeAngelis, Z. Jimmy Zhou, Rui Chen, and Wei Liu. 2019. “Generation, Transcriptome Profiling, and Functional Validation of Cone-Rich Human Retinal Organoids.” Proceedings of the National Academy of Sciences of the United States of America 166(22):10824–33. doi: 10.1073/pnas.1901572116.

Koizumi, Keiichi, Yurika Saitoh, Takayuki Minami, Nobuhiro Takeno, Koichi Tsuneyama, Tatsuro Miyahara, Takashi Nakayama, Hiroaki Sakurai, Yasuo Takano, Miyuki Nishimura, Toshio Imai, Osamu Yoshie,

and Ikuo Saiki. 2009. “Role of CX3CL1/Fractalkine in Osteoclast Differentiation and Bone Resorption.” The Journal of Immunology 183(12):7825–31. doi: 10.4049/jimmunol.0803627.

Kolb, H., E. Fernandez, and B. Jones. 1995. Webvision: The Organization of the Retina and Visual System. Salt Lake City (UT): University of Utah Health Sciences Center.

Konttinen, Henna, Mauricio e. Castro Cabral-da-Silva, Sohvi Ohtonen, Sara Wojciechowski, Anastasia Shakirzyanova, Simone Caligola, Rosalba Giugno, Yevheniia Ishchenko, Damián Hernández, Mohammad Feroze Fazaludeen, Shaila Eamen, Mireia Gómez Budia, Ilkka Fagerlund, Flavia Scoyni, Paula Korhonen, Nadine Huber, Annakaisa Haapasalo, Alex W. Hewitt, James Vickers, Grady C. Smith, Minna Oksanen, Caroline Graff, Katja M. Kanninen, Sarka Lehtonen, Nicholas Propson, Michael P. Schwartz, Alice Pébay, Jari Koistinaho, Lezanne Ooi, and Tarja Malm. 2019. “PSEN1ΔE9, APPswe, and APOE4 Confer Disparate Phenotypes in Human IPSC-Derived Microglia.” Stem Cell Reports 13(4):669–83. doi: 10.1016/j.stemcr.2019.08.004.

Kracht, L., M. Borggrewe, S. Eskandar, N. Brouwer, S. M. Chuva de Sousa Lopes, J. D. Laman, S. A. Scherjon, J. R. Prins, S. M. Kooistra, and B. J. L. Eggen. 2020. “Human Fetal Microglia Acquire Homeostatic Immune-Sensing Properties Early in Development.” Science 369(6503):530–37. doi: 10.1126/SCIENCE.ABA5906/SUPPL_FILE/ABA5906_TABLES_S1_S10.XLSX.

Krenn, Veronica, Camilla Bosone, Thomas R. Burkard, Julia Spanier, Ulrich Kalinke, Arianna Calistri, Cristiano Salata, Raissa Rilo Christoff, Patricia Pestana Garcez, Ali Mirazimi, and Jürgen A. Knoblich. 2021. “Organoid Modeling of Zika and Herpes Simplex Virus 1 Infections Reveals Virus-Specific Responses Leading to Microcephaly.” Cell Stem Cell 28(8):1362-1379.e7. doi: 10.1016/J.STEM.2021.03.004.

Kreutzberg, G. W. 1996. “Microglia: A Sensor for Pathological Events in the CNS.” Trends in Neurosciences 19(8):312–18.

Kuse, Yoshiki, Kazuki Ohuchi, Shinsuke Nakamura, Hideaki Hara, and Masamitsu Shimazawa. 2018. “Microglia Increases the Proliferation of Retinal Precursor Cells during Postnatal Development.” Molecular Vision 24:536.

Lancaster, Madeline A., Magdalena Renner, Carol-Anne Martin, Daniel Wenzel, Louise S. Bicknell, Matthew E. Hurles, Tessa Homfray, Josef M. Penninger, Andrew P. Jackson, and Juergen A. Knoblich. 2013. “Cerebral Organoids Model Human Brain Development and Microcephaly.” Nature 501(7467):373–79. doi: 10.1038/nature12517.

Larsson, Jonas, and Stefan Karlsson. 2005. “The Role of Smad Signaling in Hematopoiesis.” Oncogene 24(37):5676–92. doi: 10.1038/sj.onc.1208920.

Lawson, L. J., V. H. Perry, P. Dri, and S. Gordon. 1990. “Heterogeneity in the Distribution and Morphology of Microglia in the Normal Adult Mouse Brain.” Neuroscience 39(1):151–70.

Leverrier-Penna, S., R. T. Mitchell, E. Becker, L. Lecante, M. Ben Maamar, N. Homer, V. Lavoué, D. M. Kristensen, N. Dejucq-Rainsford, B. Jégou, and S. Mazaud-Guittot. 2018. “Ibuprofen Is Deleterious for the Development of First Trimester Human Fetal Ovary Ex Vivo.” Human Reproduction 33(3):482–93. doi: 10.1093/HUMREP/DEX383.

Li, Fenge, Danye Jiang, and Melanie A. Samuel. 2019. “Microglia in the Developing Retina.” Neural Development 14(1):1–13.

Lima, Isabel Vieira De Assis, Leandro Francisco Silva Bastos, Marcelo Limborço-Filho, Bernd L. Fiebich, and Antonio Carlos Pinheiro De Oliveira. 2012. “Role of Prostaglandins in Neuroinflammatory and Neurodegenerative Diseases.” Mediators of Inflammation 2012:13. doi: 10.1155/2012/946813.

Lin, Yuan-Ta, Jinsoo Seo, Fan Gao, Heather M. Feldman, Hsin-Lan Wen, Jay Penney, Hugh P. Cam, Elizabeta Gjoneska, Waseem K. Raja, Jemmie Cheng, Richard Rueda, Oleg Kritskiy, Fatema Abdurrob, Zhuyu Peng, Blerta Milo, Chung Jong Yu, Sara Elmsaouri, Dilip Dey, Tak Ko, Bruce A. Yankner, and Li-Huei

Tsai. 2018. “APOE4 Causes Widespread Molecular and Cellular Alterations Associated with Alzheimer’s Disease Phenotypes in Human IPSC-Derived Brain Cell Types.” Neuron 98(6):1141-1154.e7. doi: 10.1016/J.NEURON.2018.05.008.

Liu, Aimin, and Lee A. Niswander. 2005. “Bone Morphogenetic Protein Signalling and Vertebrate Nervous System Development.” Nature Reviews Neuroscience 6(12):945–54. doi: 10.1038/nrn1805.

Lively, Starlee, and Lyanne C. Schlichter. 2018. “Microglia Responses to Pro-Inflammatory Stimuli (LPS, IFNγ+TNFα) and Reprogramming by Resolving Cytokines (IL-4, IL-10).” Frontiers in Cellular Neuroscience 12:391869. doi: 10.3389/FNCEL.2018.00215/BIBTEX.

Loayza, Marco, Shuying Lin, Kathleen Carter, Norma Ojeda, Lir Wan Fan, Sumana Ramarao, Abhay Bhatt, and Yi Pang. 2022. “Maternal Immune Activation Alters Fetal and Neonatal Microglia Phenotype and Disrupts Neurogenesis in Mice.” Pediatric Research 2022 93:5 93(5):1216–25. doi: 10.1038/s41390-022-02239-w.

Lopes, M. Beatriz S. 2009. “Meninges: Embryology.” Pp. 25–29 in Meningiomas. London: Springer London.

Ludwig, Allison L., Steven J. Mayerl, Yu Gao, Mark Banghart, Cole Bacig, Maria A. Fernandez Zepeda, Xinyu Zhao, and David M. Gamm. 2023. “Re-Formation of Synaptic Connectivity in Dissociated Human Stem Cell-Derived Retinal Organoid Cultures.” Proceedings of the National Academy of Sciences of the United States of America 120(2):e2213418120. doi: 10.1073/PNAS.2213418120/SUPPL_FILE/PNAS.2213418120.SAPP.PDF.

Lum, Fok Moon, Donovan K. S. Low, Yiping Fan, Jeslin J. L. Tan, Bernett Lee, Jerry K. Y. Chan, Laurent Rénia, Florent Ginhoux, and Lisa F. P. Ng. 2017. “Zika Virus Infects Human Fetal Brain Microglia and Induces Inflammation.” Clinical Infectious Diseases 64(7):914–20. doi: 10.1093/CID/CIW878.

Lun, Melody P., Edwin S. Monuki, and Maria K. Lehtinen. 2015. “Development and Functions of the Choroid Plexus-Cerebrospinal Fluid System.” Nature Reviews Neuroscience 16(8):445–57.

Luo, Ziming, Chaochao Xu, Kaijing Li, Bikun Xian, Yuchun Liu, Kang Li, Ying Liu, Huifeng Rong, Mingjun Tang, Dongpeng Hu, Sijing Yang, Meifang Ye, Xiufeng Zhong, and Jian Ge. 2019. “Islet1 and Brn3 Expression Pattern Study in Human Retina and HiPSC-Derived Retinal Organoid.” doi: 10.1155/2019/8786396.

Lux, Christopher T., Momoko Yoshimoto, Kathleen McGrath, Simon J. Conway, James Palis, and Mervin C. Yoder. 2008. “All Primitive and Definitive Hematopoietic Progenitor Cells Emerging before E10 in the Mouse Embryo Are Products of the Yolk Sac.” Blood 111(7):3435–38. doi: 10.1182/blood-2007-08-107086.

MacCord, Kate. 2012. “Mesenchyme | The Embryo Project Encyclopedia.”

Madry, Christian, Vasiliki Kyrargyri, I. Lorena Arancibia-Cárcamo, Renaud Jolivet, Shinichi Kohsaka, Robert M. Bryan, and David Attwell. 2018. “Microglial Ramification, Surveillance, and Interleukin-1β Release Are Regulated by the Two-Pore Domain K+ Channel THIK-1.” Neuron 97(2):299-312.e6. doi: 10.1016/j.neuron.2017.12.002.

Malik, Nasir, and Mahendra S. Rao. 2013. “A Review of the Methods for Human IPSC Derivation.” Pp. 23–33 in Methods in Molecular Biology. Vol. 997.

Marín-Teva, José Luis, Isabelle Dusart, Catherine Colin, Annie Gervais, Nico Van Rooijen, and Michel Mallat. 2004. “Microglia Promote the Death of Developing Purkinje Cells.” Neuron 41(4):535–47. doi: 10.1016/S0896-6273(04)00069-8.

Marsters, Candace M., Dinushan Nesan, Rena Far, Natalia Klenin, Quentin J. Pittman, and Deborah M. Kurrasch. 2020. “Embryonic Microglia Influence Developing Hypothalamic Glial Populations.” Journal of Neuroinflammation 17(1):1–17. doi: 10.1186/S12974-020-01811-7/FIGURES/9.

Masuda, Takahiro, Roman Sankowski, Ori Staszewski, Chotima Böttcher, Lukas Amann, Sagar, Christian Scheiwe, Stefan Nessler, Patrik Kunz, Geert van Loo, Volker Arnd Coenen, Peter Christoph Reinacher, Anna Michel, Ulrich Sure, Ralf Gold, Dominic Grün, Josef Priller, Christine Stadelmann, and Marco

Prinz. 2019. “Spatial and Temporal Heterogeneity of Mouse and Human Microglia at Single-Cell Resolution.” Nature 566(7744):388–92. doi: 10.1038/s41586-019-0924-x.

Matcovitch-Natan, Orit, Deborah R. Winter, Amir Giladi, Stephanie Vargas Aguilar, Amit Spinrad, Sandrine Sarrazin, Hila Ben-Yehuda, Eyal David, Fabiola Zelada González, Pierre Perrin, Hadas Keren-Shaul, Meital Gury, David Lara-Astaiso, Christoph A. Thaiss, Merav Cohen, Keren Bahar Halpern, Kuti Baruch, Aleksandra Deczkowska, Erika Lorenzo-Vivas, Shalev Itzkovitz, Eran Elinav, Michael H. Sieweke, Michal Schwartz, and Ido Amit. 2016. “Microglia Development Follows a Stepwise Program to Regulate Brain Homeostasis.” Science 353(6301). doi: 10.1126/SCIENCE.AAD8670/SUPPL_FILE/AAD8670-MATCOVITCH-NATAN-SM.TABLES-S1-TO-S10.XLSX.

Matsumoto, Misako, and Tsukasa Seya. 2008. “TLR3: Interferon Induction by Double-Stranded RNA Including Poly(I:C).” Advanced Drug Delivery Reviews 60(7):805–12. doi: 10.1016/J.ADDR.2007.11.005.

Maya-Arteaga, Juan Pablo, Humberto Martínez-Orozco, and Sofía Diaz-Cintra. 2024. “MorphoGlia, an Interactive Method to Identify and Map Microglia Morphologies, Demonstrates Differences in Hippocampal Subregions of an Alzheimer’s Disease Mouse Model.” Frontiers in Cellular Neuroscience 18. doi: 10.3389/fncel.2024.1505048.

McMahon, Courtney L., Hilary Staples, Michal Gazi, Ricardo Carrion, and Jenny Hsieh. 2021. “SARS-CoV-2 Targets Glial Cells in Human Cortical Organoids.” Stem Cell Reports 16(5):1156–64. doi: 10.1016/j.stemcr.2021.01.016.

McQuade, Amanda, Morgan Coburn, Christina H. Tu, Jonathan Hasselmann, Hayk Davtyan, and Mathew Blurton-Jones. 2018. “Development and Validation of a Simplified Method to Generate Human Microglia from Pluripotent Stem Cells.” Molecular Neurodegeneration 13(1):67. doi: 10.1186/s13024-018-0297-x.

Megli, Christina J., and Carolyn B. Coyne. 2021. “Infections at the Maternal–Fetal Interface: An Overview of Pathogenesis and Defence.” Nature Reviews Microbiology 2021 20:2 20(2):67–82. doi: 10.1038/s41579-021-00610-y.

Mellough, Carla B., Roman Bauer, Joseph Collin, Birthe Dorgau, Darin Zerti, David W. P. Dolan, Carl M. Jones, Osagie G. Izuogu, Min Yu, Dean Hallam, Jannetta S. Steyn, Kathryn White, David H. Steel, Mauro Santibanez-Koref, David J. Elliott, Michael S. Jackson, Susan Lindsay, Sushma Grellscheid, and Majlinda Lako. 2019. “An Integrated Transcriptional Analysis of the Developing Human Retina.” Development (Cambridge) 146(2). doi: 10.1242/dev.169474.

Menassa, David A, and Diego Gomez-Nicola. 2018. “Microglial Dynamics During Human Brain Development.” Frontiers in Immunology 9:1014. doi: 10.3389/fimmu.2018.01014.

Meyer, Urs. 2019. “Neurodevelopmental Resilience and Susceptibility to Maternal Immune Activation.” Trends in Neurosciences 42(11):793–806. doi: 10.1016/J.TINS.2019.08.001.

Meyer, Urs, Myriel Nyffeler, Andrea Engler, Adrian Urwyler, Manfred Schedlowski, Irene Knuesel, Benjamin K. Yee, and Joram Feldon. 2006. “The Time of Prenatal Immune Challenge Determines the Specificity of Inflammation-Mediated Brain and Behavioral Pathology.” The Journal of Neuroscience 26(18):4752. doi: 10.1523/JNEUROSCI.0099-06.2006.

Meyer, Urs, Myriel Nyffeler, Benjamin K. Yee, Irene Knuesel, and Joram Feldon. 2008. “Adult Brain and Behavioral Pathological Markers of Prenatal Immune Challenge during Early/Middle and Late Fetal Development in Mice.” Brain, Behavior, and Immunity 22(4):469–86. doi: 10.1016/J.BBI.2007.09.012.

Michael, Benedict D., Laura Bricio-Moreno, Elizabeth W. Sorensen, Tom Solomon, Evelyn A. Kurt-Jones, Andrew D. Luster Correspondence, Yoshishige Miyabe, Jeffrey Lian, and Andrew D. Luster. 2020.

"Astrocyte- and Neuron-Derived CXCL1 Drives Neutrophil Transmigration and Blood-Brain Barrier Permeability in Viral Encephalitis." doi: 10.1016/j.celrep.2020.108150.

Mildner, Alexander, Hao Huang, Josefine Radke, Werner Stenzel, and Josef Priller. 2017. "P2Y12 Receptor Is Expressed on Human Microglia under Physiological Conditions throughout Development and Is Sensitive to Neuroinflammatory Diseases." Glia 65(2):375–87. doi: 10.1002/glia.23097.

Mittelbronn, M., K. Dietz, H. J. Schluesener, and R. Meyermann. 2001. "Local Distribution of Microglia in the Normal Adult Human Central Nervous System Differs by up to One Order of Magnitude." Acta Neuropathologica 101(3):249–55.

Miyamoto, Akiko, Hiroaki Wake, Ayako Wendy Ishikawa, Kei Eto, Keisuke Shibata, Hideji Murakoshi, Schuichi Koizumi, Andrew J. Moorhouse, Yumiko Yoshimura, and Junichi Nabekura. 2016. "Microglia Contact Induces Synapse Formation in Developing Somatosensory Cortex." Nature Communications 7(1):12540. doi: 10.1038/ncomms12540.

Mizee, Mark R., Suzanne S. M. Miedema, Marlijn van der Poel, Adelia, Karianne G. Schuurman, Miriam E. van Strien, Jeroen Melief, Joost Smolders, Debbie A. Hendrickx, Kirstin M. Heutinck, Jörg Hamann, and Inge Huitinga. 2017. "Isolation of Primary Microglia from the Human Post-Mortem Brain: Effects of Ante- and Post-Mortem Variables." Acta Neuropathologica Communications 5(1):16. doi: 10.1186/s40478-017-0418-8.

Mizuhashi, Koji, Takashi Kanamoto, Masako Ito, Takeshi Moriishi, Yuki Muranishi, Yoshihiro Omori, Koji Terada, Toshihisa Komori, and Takahisa Furukawa. 2012. "OBIF, an Osteoblast Induction Factor, Plays an Essential Role in Bone Formation in Association with Osteoblastogenesis." Development, Growth & Differentiation 54(4):474–80. doi: 10.1111/j.1440-169X.2012.01333.x.

Monier, Anne, Homa Adle-Biassette, Anne-Lise Delezoide, Philippe Evrard, Pierre Gressens, and Catherine Verney. 2007. "Entry and Distribution of Microglial Cells in Human Embryonic and Fetal Cerebral Cortex." Journal of Neuropathology and Experimental Neurology 66(5):372–82. doi: 10.1097/nen.0b013e3180517b46.

Monier, Anne, Philippe Evrard, Pierre Gressens, and Catherine Verney. 2006. "Distribution and Differentiation of Microglia in the Human Encephalon during the First Two Trimesters of Gestation." Journal of Comparative Neurology 499(4):565–82. doi: 10.1002/CNE.21123.

Montilla, Alejandro, Alazne Zabala, Carlos Matute, and María Domercq. 2020. "Functional and Metabolic Characterization of Microglia Culture in a Defined Medium." Frontiers in Cellular Neuroscience 14:506355. doi: 10.3389/FNCEL.2020.00022/BIBTEX.

Mor, Gil, and Ingrid Cardenas. 2010. "The Immune System in Pregnancy: A Unique Complexity." American Journal of Reproductive Immunology (New York, N.Y. : 1989) 63(6):425. doi: 10.1111/J.1600-0897.2010.00836.X.

Morgan, Josh, and Rachel Wong. 2007. "Development of Cell Types and Synaptic Connections in the Retina." Webvision: The Organization of the Retina and Visual System.

Mrdjen, Dunja, Anto Pavlovic, Felix J. Hartmann, Bettina Schreiner, Sebastian G. Utz, Brian P. Leung, Iva Lelios, Frank L. Heppner, Jonathan Kipnis, Doron Merkler, Melanie Greter, and Burkhard Becher. 2018. "High-Dimensional Single-Cell Mapping of Central Nervous System Immune Cells Reveals Distinct Myeloid Subsets in Health, Aging, and Disease." Immunity 48(2):380-395.e6. doi: 10.1016/j.immuni.2018.01.011.

Muffat, J., Y. Li, B. Yuan, M. Mitalipova, A. Omer, S. Corcoran, G. Bakiasi, L. H. Tsai, P. Aubourg, R. M. Ransohoff, and R. Jaenisch. 2016. "Efficient Derivation of Microglia-like Cells from Human Pluripotent Stem Cells." Nature Medicine. doi: 10.1038/nm.4189.

Nag, T. C., and S. Wadhwa. 2001. “Differential Expression of Syntaxin-1 and Synaptophysin in the Developing and Adult Human Retina.” Journal of Biosciences 26(2):179–91. doi: 10.1007/BF02703642.

Nakanishi, Masaya, Tetsuhiro Niidome, Satoru Matsuda, Akinori Akaike, Takeshi Kihara, and Hachiro Sugimoto. 2007. “Microglia-Derived Interleukin-6 and Leukaemia Inhibitory Factor Promote Astrocytic Differentiation of Neural Stem/Progenitor Cells.” European Journal of Neuroscience 25(3):649–58. doi: 10.1111/j.1460-9568.2007.05309.x.

Nakano, Tokushige, Satoshi Ando, Nozomu Takata, Masako Kawada, Keiko Muguruma, Kiyotoshi Sekiguchi, Koichi Saito, Shigenobu Yonemura, Mototsugu Eiraku, and Yoshiki Sasai. 2012. “Self-Formation of Optic Cups and Storable Stratified Neural Retina from Human ESCs.” Cell Stem Cell 10(6):771–85. doi: 10.1016/j.stem.2012.05.009.

Nemes-Baran, Ashley D., Donovan R. White, and Tara M. DeSilva. 2020. “Fractalkine-Dependent Microglial Pruning of Viable Oligodendrocyte Progenitor Cells Regulates Myelination.” Cell Reports 32(7). doi: 10.1016/j.celrep.2020.108047.

Nimmerjahn, A., Frank Kirchhoff, and Fritjof Helmchen. 2005. “Resting Microglial Cells Are Highly Dynamic Surveillants of Brain Parenchyma in Vivo.” Science 308(5726):1314–18. doi: 10.1126/science.1110647.

Noctor, Stephen C., Alexander C. Flint, Tamily A. Weissman, Winston S. Wong, Brian K. Clinton, and Arnold R. Kriegstein. 2002. “Dividing Precursor Cells of the Embryonic Cortical Ventricular Zone Have Morphological and Molecular Characteristics of Radial Glia.” The Journal of Neuroscience : The Official Journal of the Society for Neuroscience 22(8):3161–73. doi: 20026299.

Oceguera-Yanez, Fabian, Shin Il Kim, Tomoko Matsumoto, Ghee Wan Tan, Long Xiang, Takeshi Hatani, Takayuki Kondo, Makoto Ikeya, Yoshinori Yoshida, Haruhisa Inoue, and Knut Woltjen. 2016. “Engineering the AAVS1 Locus for Consistent and Scalable Transgene Expression in Human IPSCs and Their Differentiated Derivatives.” Methods 101:43–55. doi: 10.1016/j.ymeth.2015.12.012.

O’Koren, Emily G., Chen Yu, Mikael Klingeborn, Alicia Y. W. Wong, Cameron L. Prigge, Rose Mathew, Joan Kalnitsky, Rasha A. Msallam, Aymeric Silvin, Jeremy N. Kay, Catherine Bowes Rickman, Vadim Y. Arshavsky, Florent Ginhoux, Miriam Merad, and Daniel R. Saban. 2019. “Microglial Function Is Distinct in Different Anatomical Locations during Retinal Homeostasis and Degeneration.” Immunity 50(3):723-737.e7. doi: 10.1016/j.immuni.2019.02.007.

Oosterhof, Nynke, Irene J. Chang, Ehsan Ghayoor Karimiani, Laura E. Kuil, Dana M. Jensen, Ray Daza, Erica Young, Lee Astle, Herma C. van der Linde, Giridhar M. Shivaram, Jeroen Demmers, Caitlin S. Latimer, C. Dirk Keene, Emily Loter, Reza Maroofian, Tjakko J. van Ham, Robert F. Hevner, and James T. Bennett. 2019. “Homozygous Mutations in CSF1R Cause a Pediatric-Onset Leukoencephalopathy and Can Result in Congenital Absence of Microglia.” American Journal of Human Genetics 104(5):936. doi: 10.1016/J.AJHG.2019.03.010.

O’Rahilly, R., and F. Müller. 1986. “The Meninges in Human Development.” Journal of Neuropathology and Experimental Neurology 45(5):588–608.

Ormel, Paul R., Renata Vieira de Sá, Emma J. van Bodegraven, Henk Karst, Oliver Harschnitz, Marjolein A. M. Sneeboer, Lill Eva Johansen, Roland E. van Dijk, Nicky Scheefhals, Amber Berdenis van Berlekom, Eduardo Ribes Martínez, Sandra Kling, Harold D. MacGillavry, Leonard H. van den Berg, René S. Kahn, Elly M. Hol, Lot D. de Witte, and R. Jeroen Pasterkamp. 2018. “Microglia Innately Develop within Cerebral Organoids.” Nature Communications 9(1). doi: 10.1038/s41467-018-06684-2.

Ortmann, Daniel, and Ludovic Vallier. 2017. “Variability of Human Pluripotent Stem Cell Lines.” Current Opinion in Genetics & Development 46:179–85. doi: 10.1016/j.gde.2017.07.004.

Ostrem, Bridget Elaine La Monica, Nuria Domińguez-Iturza, Jeffrey A. Stogsdill, Tyler Faits, Kwanho Kim, Joshua Z. Levin, and Paola Arlotta. 2024. “Fetal Brain Response to Maternal Inflammation Requires Microglia.” Development (Cambridge) 151(10). doi: 10.1242/DEV.202252/347530.

Owusu-Akyaw, Amma, Kavitha Krishnamoorthy, Laura T. Goldsmith, and Sara S. Morelli. 2019. “The Role of Mesenchymal-Epithelial Transition in Endometrial Function.” Human Reproduction Update 25(1):114–33.

Ozaki, Kana, Daisuke Kato, Ako Ikegami, Akari Hashimoto, Shouta Sugio, Zhongtian Guo, Midori Shibushita, Tsuyako Tatematsu, Koichiro Haruwaka, Andrew J. Moorhouse, Hideto Yamada, and Hiroaki Wake. 2020. “Maternal Immune Activation Induces Sustained Changes in Fetal Microglia Motility.” Scientific Reports 10(1). doi: 10.1038/S41598-020-78294-2.

Palomba, Nicole Piera, Katiuscia Martinello, Germana Cocozza, Sara Casciato, Addolorata Mascia, Giancarlo Di Gennaro, Roberta Morace, Vincenzo Esposito, Heike Wulff, Cristina Limatola, and Sergio Fucile. 2021. “ATP-Evoked Intracellular Ca2+ Transients Shape the Ionic Permeability of Human Microglia from Epileptic Temporal Cortex.” Journal of Neuroinflammation 18(1):44. doi: 10.1186/s12974-021-02096-0.

Pandya, Hetal, Michael J. Shen, David M. Ichikawa, Andrea B. Sedlock, Yong Choi, Kory R. Johnson, Gloria Kim, Mason A. Brown, Abdel G. Elkahloun, Dragan Maric, Colin L. Sweeney, Selamawit Gossa, Harry L. Malech, Dorian B. McGavern, and John K. Park. 2017. “Differentiation of Human and Murine Induced Pluripotent Stem Cells to Microglia-like Cells.” Nature Neuroscience. doi: 10.1038/nn.4534.

Paolicelli, Rosa C., Giulia Bolasco, Francesca Pagani, Laura Maggi, Maria Scianni, Patrizia Panzanelli, Maurizio Giustetto, Tiago Alves Ferreira, Eva Guiducci, Laura Dumas, Davide Ragozzino, and Cornelius T. Gross. 2011. “Synaptic Pruning by Microglia Is Necessary for Normal Brain Development.” Science 333(6048):1456–58. doi: 10.1126/SCIENCE.1202529/SUPPL_FILE/PAOLICELLI.SOM.PDF.

Park, Dong Shin, Tatsuya Kozaki, Satish Kumar Tiwari, Marco Moreira, Ahad Khalilnezhad, Federico Torta, Nicolas Olivié, Chung Hwee Thiam, Oniko Liani, Aymeric Silvin, Wint Wint Phoo, Liang Gao, Alexander Triebl, Wai Kin Tham, Leticia Gonçalves, Wan Ting Kong, Sethi Raman, Xiao Meng Zhang, Garett Dunsmore, Charles Antoine Dutertre, Salanne Lee, Jia Min Ong, Akhila Balachander, Shabnam Khalilnezhad, Josephine Lum, Kaibo Duan, Ze Ming Lim, Leonard Tan, Ivy Low, Kagistia Hana Utami, Xin Yi Yeo, Sylvaine Di Tommaso, Jean William Dupuy, Balazs Varga, Ragnhildur Thora Karadottir, Mufeeda Changaramvally Madathummal, Isabelle Bonne, Benoit Malleret, Zainab Yasin Binte, Ngan Wei Da, Yingrou Tan, Wei Jie Wong, Jinqiu Zhang, Jinmiao Chen, Radoslaw M. Sobota, Shanshan W. Howland, Lai Guan Ng, Frédéric Saltel, David Castel, Jacques Grill, Veronique Minard, Salvatore Albani, Jerry K. Y. Chan, Morgane Sonia Thion, Sang Yong Jung, Markus R. Wenk, Mahmoud A. Pouladi, Claudia Pasqualini, Veronique Angeli, Olivier N. F. Cexus, and Florent Ginhoux. 2023. “IPS-Cell-Derived Microglia Promote Brain Organoid Maturation via Cholesterol Transfer.” Nature 623(7986):397–405. doi: 10.1038/S41586-023-06713-1.

Parkhurst, Christopher N., Guang Yang, Ipe Ninan, Jeffrey N. Savas, John R. Yates, Juan J. Lafaille, Barbara L. Hempstead, Dan R. Littman, Wen-Biao Gan, and Wen-Biao Gan. 2013. “Microglia Promote Learning-Dependent Synapse Formation through Brain-Derived Neurotrophic Factor.” Cell 155(7):1596–1609. doi: 10.1016/j.cell.2013.11.030.

Park-Min, Kyung Hyun, Eun Young Lee, Neal K. Moskowitz, Elisha Lim, Sun Kyeong Lee, Joseph A. Lorenzo, Chuanxin Huang, Ari M. Melnick, P. Edward Purdue, Steven R. Goldring, and Lionel B. Ivashkiv. 2013. “Negative Regulation of Osteoclast Precursor Differentiation by CD11b and β 2 Integrin-B-Cell Lymphoma 6 Signaling.” Journal of Bone and Mineral Research 28(1):135–49. doi: 10.1002/jbmr.1739.

Pasca, Anca M., Steven A. Sloan, Laura E. Clarke, Yuan Tian, Christopher D. Makinson, Nina Huber, Chul Hoon Kim, Jin Young Park, Nancy A. O'Rourke, Khoa D. Nguyen, Stephen J. Smith, John R. Huguenard, Daniel H. Geschwind, Ben A. Barres, and Sergiu P. Pasca. 2015. "Functional Cortical Neurons and Astrocytes from Human Pluripotent Stem Cells in 3D Culture." Nature Methods 12(7):671–78. doi: 10.1038/nmeth.3415.

Pecchi, Emilie, Michel Dallaporta, André Jean, Sylvie Thirion, and Jean Denis Troadec. 2009. "Prostaglandins and Sickness Behavior: Old Story, New Insights." Physiology & Behavior 97(3–4):279–92. doi: 10.1016/J.PHYSBEH.2009.02.040.

Pei, Y. F., and J. A. G. Rhodin. 1970. "The Prenatal Development of the Mouse Eye." The Anatomical Record 168(1):105–25.

Pellegrini, Laura, Claudia Bonfio, Jessica Chadwick, Farida Begum, Mark Skehel, and Madeline A. Lancaster. 2020. "Human CNS Barrier-Forming Organoids with Cerebrospinal Fluid Production." Science 369(6500). doi: 10.1126/science.aaz5626.

Perales-Linares, Renzo, and Sonia Navas-Martin. 2013. "Toll-like Receptor 3 in Viral Pathogenesis: Friend or Foe?" Immunology 140(2):153. doi: 10.1111/IMM.12143.

Pesti, István, Ádám Légrádi, and Eszter Farkas. 2024. "Primary Microglia Cell Cultures in Translational Research: Strengths and Limitations." Journal of Biotechnology 386:10–18.

Phares, Timothy W., Stephen A. Stohlman, David R. Hinton, and Cornelia C. Bergmann. 2013. "Astrocyte-Derived CXCL10 Drives Accumulation of Antibody-Secreting Cells in the Central Nervous System during Viral Encephalomyelitis." Journal of Virology 87(6):3382. doi: 10.1128/JVI.03307-12.

Pill, Karoline, Sandra Hofmann, Heinz Redl, and Wolfgang Holnthoner. 2015. "Vascularization Mediated by Mesenchymal Stem Cells from Bone Marrow and Adipose Tissue: A Comparison." Cell Regeneration 4(1):4:8. doi: 10.1186/s13619-015-0025-8.

Plociennikowska, Agnieszka, Jamie Frankish, Thais Moraes, Dolores Del Prete, Franziska Kahnt, Claudio Acuna, Michal Slezak, Marco Binder, and Ralf Bartenschlager. 2021. "TLR3 Activation by Zika Virus Stimulates Inflammatory Cytokine Production Which Dampens the Antiviral Response Induced by RIG-I-Like Receptors." Journal of Virology 95(10). doi: 10.1128/JVI.01050-20/ASSET/05316D5C-7B3F-4F85-BB40-3C9BD27019E2/ASSETS/IMAGES/LARGE/JVI.01050-20-F010.JPG.

Pocock, Jennifer M., and Helmut Kettenmann. 2007. "Neurotransmitter Receptors on Microglia." Trends in Neurosciences 30(10):527–35. doi: 10.1016/j.tins.2007.07.007.

Pont-Lezica, Lorena, Wouter Beumer, Sabrina Colasse, Hemmo Drexhage, Marjan Versnel, and Alain Bessis. 2014. "Microglia Shape Corpus Callosum Axon Tract Fasciculation: Functional Impact of Prenatal Inflammation." European Journal of Neuroscience 39(10):1551–57. doi: 10.1111/ejn.12508.

Popova, Galina, Sarah S. Soliman, Chang N. Kim, Matthew G. Keefe, Kelsey M. Hennick, Samhita Jain, Tao Li, Dario Tejera, David Shin, Bryant B. Chhun, Christopher S. McGinnis, Matthew Speir, Zev J. Gartner, Shalin B. Mehta, Maximilian Haeussler, Keith B. Hengen, Richard R. Ransohoff, Xianhua Piao, and Tomasz J. Nowakowski. 2021. "Human Microglia States Are Conserved across Experimental Models and Regulate Neural Stem Cell Responses in Chimeric Organoids." Cell Stem Cell 28(12):2153-2166.e6. doi: 10.1016/j.stem.2021.08.015.

Pratt, Lorelei, Li Ni, Nicholas M. Ponzio, and G. Miller Jonakait. 2013. "Maternal Inflammation Promotes Fetal Microglial Activation and Increased Cholinergic Expression in the Fetal Basal Forebrain: Role of Interleukin-6." Pediatric Research 74(4):393–401. doi: 10.1038/pr.2013.126.

Prinz, Marco, Daniel Erny, and Nora Hagemeyer. 2017. "Ontogeny and Homeostasis of CNS Myeloid Cells." Nature Immunology 18(4):385–92. doi: 10.1038/ni.3703.

Prinz, Marco, and Josef Priller. 2014. “Microglia and Brain Macrophages in the Molecular Age: From Origin to Neuropsychiatric Disease.” Nature Reviews Neuroscience 15(5):300–312. doi: 10.1038/nrn3722.

Provis, Jan M. 1987. “Patterns of Cell Death in the Ganglion Cell Layer of the Human Fetal Retina.” Journal of Comparative Neurology 259(2):237–46. doi: 10.1002/CNE.902590205.

Provis, Jan M., Philip L. Penfold, Antony J. Edwards, and Diana van Driel. 1995. “Human Retinal Microglia: Expression of Immune Markers and Relationship to the Glia Limitans.” Glia 14(4):243–56. doi: 10.1002/GLIA.440140402.

Qi, Yuchen, Xin Jun Zhang, Nicolas Renier, Zhuhao Wu, Talia Atkin, Ziyi Sun, M. Zeeshan Ozair, Jason Tchieu, Bastian Zimmer, Faranak Fattahi, Yosif Ganat, Ricardo Azevedo, Nadja Zeltner, Ali H. Brivanlou, Maria Karayiorgou, Joseph Gogos, Mark Tomishima, Marc Tessier-Lavigne, Song Hai Shi, and Lorenz Studer. 2017. “Combined Small-Molecule Inhibition Accelerates the Derivation of Functional Cortical Neurons from Human Pluripotent Stem Cells.” Nature Biotechnology 35(2):154–63. doi: 10.1038/nbt.3777.

Qian, Xuyu, Ha Nam Nguyen, Mingxi M. Song, Christopher Hadiono, Sarah C. Ogden, Christy Hammack, Bing Yao, Gregory R. Hamersky, Fadi Jacob, Chun Zhong, Ki-Jun Yoon, William Jeang, Li Lin, Yujing Li, Jai Thakor, Daniel A. Berg, Ce Zhang, Eunchai Kang, Michael Chickering, David Nauen, Cheng-Ying Ho, Zhexing Wen, Kimberly M. Christian, Pei-Yong Shi, Brady J. Maher, Hao Wu, Peng Jin, Hengli Tang, Hongjun Song, and Guo-Li Ming. 2016. “Brain-Region-Specific Organoids Using Mini-Bioreactors for Modeling ZIKV Exposure.” Cell 165(5):1238–54. doi: 10.1016/j.cell.2016.04.032.

Qian, Xuyu, Hongjun Song, and Guo-Li Ming. 2019. “Brain Organoids: Advances, Applications and Challenges.” Development (Cambridge, England) 146(8). doi: 10.1242/dev.166074.

Quick, Eamon D., J. Smith Leser, Penny Clarke, and Kenneth L. Tyler. 2014. “ Activation of Intrinsic Immune Responses and Microglial Phagocytosis in an Ex Vivo Spinal Cord Slice Culture Model of West Nile Virus Infection .” Journal of Virology 88(22):13005–14. doi: 10.1128/jvi.01994-14.

Renner, Magdalena, Madeline A. Lancaster, Shan Bian, Heejin Choi, Taeyun Ku, Angela Peer, Kwanghun Chung, and Juergen A. Knoblich. 2017. “Self-organized Developmental Patterning and Differentiation in Cerebral Organoids.” The EMBO Journal 36(10):1316–29. doi: 10.15252/embj.201694700.

Réu, Pedro, Azadeh Khosravi, Samuel Bernard, Jeff E. Mold, Mehran Salehpour, Kanar Alkass, Shira Perl, John Tisdale, Göran Possnert, Henrik Druid, and Jonas Frisén. 2017. “The Lifespan and Turnover of Microglia in the Human Brain.” Cell Reports 20(4):779–84. doi: 10.1016/j.celrep.2017.07.004.

Rezaie, Payam, Andrew Dean, David Male, and Norbert Ulfig. 2005. “Microglia in the Cerebral Wall of the Human Telencephalon at Second Trimester.” Cerebral Cortex 15(7):938–49. doi: 10.1093/cercor/bhh194.

Rezaie, Payam, and David Male. 2003. “Microglia in Fetal and Adult Human Brain Can Be Distinguished from Other Mononuclear Phagocytes through Their Lack of CD163 Expression.” Neuroembryology 2(3):130–33. doi: 10.1159/000074192.

Romagnani, Paola, and Clara Crescioli. 2012. “CXCL10: A Candidate Biomarker in Transplantation.” Clinica Chimica Acta 413(17–18):1364–73. doi: 10.1016/J.CCA.2012.02.009.

Rosin, Jessica M., Sarthak Sinha, Jeff Biernaskie, and Deborah M. Kurrasch. 2021. “A Subpopulation of Embryonic Microglia Respond to Maternal Stress and Influence Nearby Neural Progenitors.” Developmental Cell 56(9):1326-1345.e6. doi: 10.1016/j.devcel.2021.03.018.

Roy, Kristin. 2012. “Establishment of Microglia Precursors Derived from Human Induced Pluripotent Stem Cells to Model SOD1-Mediated Amyotrophic Lateral Sclerosis.” Thesis.

Rumsey, John W., Case Lorance, Max Jackson, Trevor Sasserath, Christopher W. McAleer, Christopher J. Long, Arindom Goswami, Melissa A. Russo, Shruti M. Raja, Karissa L. Gable, Doug Emmett, Lisa D. Hobson-Webb, Manisha Chopra, James F. Howard, Jeffrey T. Guptill, Michael J. Storek, Miguel

Alonso-Alonso, Nazem Atassi, Sandip Panicker, Graham Parry, Timothy Hammond, and James J. Hickman. 2022. “Classical Complement Pathway Inhibition in a ‘Human-On-A-Chip’ Model of Autoimmune Demyelinating Neuropathies.” Advanced Therapeutics 5(6):2200030. doi: 10.1002/ADTP.202200030.

Dello Russo, Cinzia, Natalia Cappoli, Isabella Coletta, Daniele Mezzogori, Fabiola Paciello, Giacomo Pozzoli, Pierluigi Navarra, and Alessandra Battaglia. 2018. “The Human Microglial HMC3 Cell Line: Where Do We Stand? A Systematic Literature Review.” Journal of Neuroinflammation 15(1).

Rustenhoven, Justin, Antoine Drieu, Tornike Mamuladze, Kalil Alves de Lima, Taitea Dykstra, Morgan Wall, Zachary Papadopoulos, Mitsuhiro Kanamori, Andrea Francesca Salvador, Wendy Baker, Mackenzie Lemieux, Sandro Da Mesquita, Andrea Cugurra, James Fitzpatrick, Sanja Sviben, Ross Kossina, Peter Bayguinov, Reid R. Townsend, Qiang Zhang, Petra Erdmann-Gilmore, Igor Smirnov, Maria Beatriz Lopes, Jasmin Herz, and Jonathan Kipnis. 2021. “Functional Characterization of the Dural Sinuses as a Neuroimmune Interface.” Cell 184(4):1000-1016.e27. doi: 10.1016/j.cell.2020.12.040.

Rustenhoven, Justin, Thomas I. H. Park, Patrick Schweder, John Scotter, Jason Correia, Amy M. Smith, Hannah M. Gibbons, Robyn L. Oldfield, Peter S. Bergin, Edward W. Mee, Richard L. M. Faull, Maurice A. Curtis, E. Scott Graham, and Mike Dragunow. 2016. “Isolation of Highly Enriched Primary Human Microglia for Functional Studies.” Scientific Reports 6(1):1–11. doi: 10.1038/srep19371.

Rymo, Simin F., Holger Gerhardt, Fredrik Wolfhagen Sand, Richard Lang, Anne Uv, and Christer Betsholtz. 2011. “A Two-Way Communication between Microglial Cells and Angiogenic Sprouts Regulates Angiogenesis in Aortic Ring Cultures.” PLoS ONE 6(1). doi: 10.1371/journal.pone.0015846.

Sabate-Soler, Sonia, Sarah Louise Nickels, Cláudia Saraiva, Emanuel Berger, Ugne Dubonyte, Kyriaki Barmpa, Yan Jun Lan, Tsukasa Kouno, Javier Jarazo, Graham Robertson, Jafar Sharif, Haruhiko Koseki, Christian Thome, Jay W. Shin, Sally A. Cowley, and Jens C. Schwamborn. 2022. “Microglia Integration into Human Midbrain Organoids Leads to Increased Neuronal Maturation and Functionality.” Glia 70(7):1267–88. doi: 10.1002/glia.24167.

Sabogal-Guáqueta, Angélica María, Alejandro Marmolejo-Garza, Marina Trombetta-Lima, Asmaa Oun, Jasmijn Hunneman, Tingting Chen, Jari Koistinaho, Sarka Lehtonen, Arjan Kortholt, Justina C. Wolters, Barbara M. Bakker, Bart J. L. Eggen, Erik Boddeke, and Amalia Dolga. 2023. “Species-Specific Metabolic Reprogramming in Human and Mouse Microglia during Inflammatory Pathway Induction.” Nature Communications 2023 14:1 14(1):1–24. doi: 10.1038/s41467-023-42096-7.

Saha, Aindrila, Elizabeth Capowski, Maria A. Fernandez Zepeda, Emma C. Nelson, David M. Gamm, and Raunak Sinha. 2022. “Cone Photoreceptors in Human Stem Cell-Derived Retinal Organoids Demonstrate Intrinsic Light Responses That Mimic Those of Primate Fovea.” Cell Stem Cell 29(3):460-471.e3. doi: 10.1016/J.STEM.2022.01.002.

Sakaguchi, Hideya, Yuki Ozaki, Tomoka Ashida, Takayoshi Matsubara, Naotaka Oishi, Shunsuke Kihara, and Jun Takahashi. 2019. “Self-Organized Synchronous Calcium Transients in a Cultured Human Neural Network Derived from Cerebral Organoids.” Stem Cell Reports 13(3):458. doi: 10.1016/J.STEMCR.2019.05.029.

Samudyata, Ana O. Oliveira, Susmita Malwade, Nuno Rufino de Sousa, Sravan K. Goparaju, Jessica Gracias, Funda Orhan, Laura Steponaviciute, Martin Schalling, Steven D. Sheridan, Roy H. Perlis, Antonio G. Rothfuchs, and Carl M. Sellgren. 2022. “SARS-CoV-2 Promotes Microglial Synapse Elimination in Human Brain Organoids.” Molecular Psychiatry 27(10):3939–50. doi: 10.1038/s41380-022-01786-2.

Santos, Ana M., Ruth Calvente, Mohamed Tassi, Maria-Carmen Carrasco, David Martín-Oliva, José L. Marín-Teva, Julio Navascués, and Miguel A. Cuadros. 2008. “Embryonic and Postnatal Development of Microglial Cells in the Mouse Retina.” The Journal of Comparative Neurology 506(2):224–39. doi: 10.1002/cne.21538.

Sartorius, Rossella, Maria Trovato, Roberta Manco, Luciana D'Apice, and Piergiuseppe De Berardinis. 2021. "Exploiting Viral Sensing Mediated by Toll-like Receptors to Design Innovative Vaccines." Npj Vaccines 2021 6:1 6(1):1–15. doi: 10.1038/s41541-021-00391-8.

Satoh, Jun-ichi, Yoshihiro Kino, Naohiro Asahina, Mika Takitani, Junko Miyoshi, Tsuyoshi Ishida, and Yuko Saito. 2016. "TMEM119 Marks a Subset of Microglia in the Human Brain." Neuropathology 36(1):39–49. doi: 10.1111/neup.12235.

Scanlon, C. S., E. A. Van Tubergen, R. C. Inglehart, and N. J. D'Silva. 2013. "Biomarkers of Epithelial-Mesenchymal Transition in Squamous Cell Carcinoma." Journal of Dental Research 92(2):114–21.

Schaefer, Christof, Marc Oppermann, Evelin Wacker, and Corinna Weber-Schoendorfer. 2012. "Arzneimitteltherapiesicherheit in Der Schwangerschaft - Das Embryotox-Projekt." Zeitschrift Fur Evidenz, Fortbildung Und Qualitat Im Gesundheitswesen 106(10):723–28. doi: 10.1016/j.zefq.2012.11.012.

Schafer, Dorothy P., Emily K. Lehrman, Amanda G. Kautzman, Ryuta Koyama, Alan R. Mardinly, Ryo Yamasaki, Richard M. Ransohoff, Michael E. Greenberg, Ben A. Barres, and Beth Stevens. 2012. "Microglia Sculpt Postnatal Neural Circuits in an Activity and Complement-Dependent Manner." Neuron 74(4):691–705. doi: 10.1016/j.neuron.2012.03.026.

Schafer, Simon T., Abed Al Fatah Mansour, Johannes C. M. Schlachetzki, Monique Pena, Saeed Ghassemzadeh, Lisa Mitchell, Amanda Mar, Daphne Quang, Sarah Stumpf, Irene Santisteban Ortiz, Addison J. Lana, Clara Baek, Raghad Zaghal, Christopher K. Glass, Axel Nimmerjahn, and Fred H. Gage. 2023. "An in Vivo Neuroimmune Organoid Model to Study Human Microglia Phenotypes." Cell 186(10):2111-2126.e20. doi: 10.1016/j.cell.2023.04.022.

Schmid, Christoph, Lauren Sautkulis, Patria Danielson, Judith Cooper, Karl Hasel, Brain Hilbush, J. George Sutcliffe, and Monika J. Carson. 2002. "Heterogeneous Expression of the Triggering Receptor Expressed on Myeloid Cells-2 on Adult Murine Microglia." Journal of Neurochemistry 83(6):1309–20.

Schmied, Verena, Medina Korkut-Demirbaş, Alessandro Venturino, Juan Pablo Maya-Arteaga, and Sandra Siegert. 2025. "Microglia Determine an Immune-Challenged Environment and Facilitate Ibuprofen Action in Human Retinal Organoids." Journal of Neuroinflammation 22(1):98. doi: 10.1186/s12974-025-03366-x.

Schulz, C., E. G. Perdiguero, L. Chorro, H. Szabo-Rogers, N. Cagnard, K. Kierdorf, M. Prinz, B. Wu, S. E. W. Jacobsen, J. W. Pollard, J. Frampton, K. J. Liu, and F. Geissmann. 2012. "A Lineage of Myeloid Cells Independent of Myb and Hematopoietic Stem Cells." Science 336(6077):86–90. doi: 10.1126/science.1219179.

Schulz, Rouven, Medina Korkut-Demirbaş, Gloria Colombo, and Sandra Siegert. 2021. "Chimeric GPCRs Mimic Distinct Signaling Pathways and Modulate Microglia Responses." BioRxiv 2021.06.21.449162. doi: 10.1101/2021.06.21.449162.

Seabold, Skipper, and Josef Perktold. 2010. "Statsmodels: Econometric and Statistical Modeling with Python." Pp. 92–96 in Proceedings of the 9th Python in Science Conference. SciPy.

Seitz, Scott, Penny Clarke, and Kenneth L. Tyler. 2018. "Pharmacologic Depletion of Microglia Increases Viral Load in the Brain and Enhances Mortality in Murine Models of Flavivirus-Induced Encephalitis." Journal of Virology 92(16). doi: 10.1128/jvi.00525-18.

Shang, Yu, Li Tian, Tianjiao Chen, Xiaoying Liu, Jilin Zhang, Dongxin Liu, Jiayi Wei, Wengang Fang, Yuhua Chen, and Deshu Shang. 2019. "CXCL1 Promotes the Proliferation of Neural Stem Cells by Stimulating the Generation of Reactive Oxygen Species in APP/PS1 Mice." Biochemical and Biophysical Research Communications 515(1):201–6. doi: 10.1016/J.BBRC.2019.05.130.

Shiraki, Nobuhiko, Kazuichi Maruyama, Ryuhei Hayashi, Akiko Oguchi, Yasuhiro Murakawa, Tomohiko Katayama, Toru Takigawa, Susumu Sakimoto, Andrew J. Quantock, Motokazu Tsujikawa, and Kohji Nishida. 2022. "PAX6-Positive Microglia Evolve Locally in HiPSC-Derived Ocular Organoids." Stem Cell Reports 17(2):221–30. doi: 10.1016/j.stemcr.2021.12.009.

Sierra, Amanda, Fernando de Castro, Juan del Río-Hortega, José Rafael Iglesias-Rozas, Manuel Garrosa, and Helmut Kettenmann. 2016. "The 'Big-Bang' for Modern Glial Biology: Translation and Comments on Pío Del Río-Hortega 1919 Series of Papers on Microglia." Glia 64(11):1801–40. doi: 10.1002/glia.23046.

Sloan, Steven A., Jimena Andersen, Anca M. Paşca, Fikri Birey, and Sergiu P. Paşca. 2018. "Generation and Assembly of Human Brain Region–Specific Three-Dimensional Cultures." Nature Protocols 13(9):2062–85. doi: 10.1038/s41596-018-0032-7.

Smith, Christopher J., Yan Zhang, Carol M. Koboldt, Jerry Muhammad, Ben S. Zweifel, Alex Shaffer, John J. Talley, Jaime L. Masferrer, Karen Seibert, and Peter C. Isakson. 1998. "Pharmacological Analysis of Cyclooxygenase-1 in Inflammation." Proceedings of the National Academy of Sciences of the United States of America 95(22):13313–18. doi: 10.1073/PNAS.95.22.13313/ASSET/894C7E40-932E-4EF2-B3B1-61718A960DA7/ASSETS/GRAPHIC/PQ2183243007.JPEG.

Smith, Joshua A., Arabinda Das, Swapan K. Ray, and Naren L. Banik. 2012. "Role of Pro-Inflammatory Cytokines Released from Microglia in Neurodegenerative Diseases." Brain Research Bulletin 87(1):10–20.

Smits, Lisa M., Lydia Reinhardt, Peter Reinhardt, Michael Glatza, Anna S. Monzel, Nancy Stanslowsky, Marcelo D. Rosato-Siri, Alessandra Zanon, Paul M. Antony, Jessica Bellmann, Sarah M. Nicklas, Kathrin Hemmer, Xiaobing Qing, Emanuel Berger, Norman Kalmbach, Marc Ehrlich, Silvia Bolognin, Andrew A. Hicks, Florian Wegner, Jared L. Sterneckert, and Jens C. Schwamborn. 2019. "Modeling Parkinson's Disease in Midbrain-like Organoids." NPJ Parkinson's Disease 5(1). doi: 10.1038/S41531-019-0078-4.

Somjen, George G. 1988. "Nervenkitt: Notes on the History of the Concept of Neuroglia." Glia 1(1):2–9.

Song, Eric, Ce Zhang, Benjamin Israelow, Alice Lu-Culligan, Alba Vieites Prado, Sophie Skriabine, Peiwen Lu, Orr El Weizman, Feimei Liu, Yile Dai, Klara Szigeti-Buck, Yuki Yasumoto, Guilin Wang, Christopher Castaldi, Jaime Heltke, Evelyn Ng, John Wheeler, Mia Madel Alfajaro, Etienne Levavasseur, Benjamin Fontes, Neal G. Ravindra, David van Dijk, Shrikant Mane, Murat Gunel, Aaron Ring, Syed A. Jaffar Kazmi, Kai Zhang, Craig B. Wilen, Tamas L. Horvath, Isabelle Plu, Stephane Haik, Jean Leon Thomas, Angeliki Louvi, Shelli F. Farhadian, Anita Huttner, Danielle Seilhean, Nicolas Renier, Kaya Bilguvar, and Akiko Iwasaki. 2021. "Neuroinvasion of SARS-CoV-2 in Human and Mouse Brain." Journal of Experimental Medicine 218(3). doi: 10.1084/JEM.20202135.

Song, Liqing, Xuegang Yuan, Zachary Jones, Cynthia Vied, Yu Miao, Mark Marzano, Thien Hua, Qing Xiang Amy Sang, Jingjiao Guan, Teng Ma, Yi Zhou, and Yan Li. 2019. "Functionalization of Brain Region-Specific Spheroids with Isogenic Microglia-like Cells." Scientific Reports 9(1). doi: 10.1038/s41598-019-47444-6.

Song, Wenzhe, Roberta Mazzieri, Tao Yang, and Glenda C. Gobe. 2017. "Translational Significance for Tumor Metastasis of Tumor-Associated Macrophages and Epithelial-Mesenchymal Transition." Frontiers in Immunology 8(SEP):1106.

Speicher, Anna M., Lisanne Korn, Csat Ari, Laura Gonzalez-Cano, Michael Heming, Christian Thomas, Christina B. Schroeter, David Schafflick, Xiaolin Li, Lukas Gola, Alexander Engler, Thilo Kaehne, Ludovic Vallier, Sven G. Meuth, Gerd Meyer, H€ Orste, Stjepana Kovac, Heinz Wiendl, Hans R. Sch€ Oler, and Matthias Pawlowski. 2022. "Deterministic Programming of Human Pluripotent Stem Cells into Microglia Facilitates Studying Their Role in Health and Disease." doi: 10.1073/pnas.

Spirig, Stefan E., Valeria J. Arteaga-Moreta, Zoltan Raics, Susana Posada-Céspedes, Stephanie Chreng, Olaf Galuba, Inga Galuba, Isabelle Claerr, Steffen Renner, P. Timo Kleindienst, Adrienn Volak, Jannick Imbach, Svitlana Malysheva, Rebecca A. Siwicki, Vincent Hahaut, Yanyan Hou, Simone Picelli, Marco Cattaneo, Josephine Jüttner, Cameron S. Cowan, Myriam Duckely, Daniel K. Baeschlin, Magdalena Renner, Vincent Unterreiner, and Botond Roska. 2023. "Cell Type-Focused Compound Screen in Human Organoids Reveals Molecules and Pathways Controlling Cone Photoreceptor Death." BioRxiv 2023.10.09.561525. doi: 10.1101/2023.10.09.561525.

Squarzoni, Paola, Guillaume Oller, Guillaume Hoeffel, Lorena Pont-Lezica, Philippe Rostaing, Donovan Low, Alain Bessis, Florent Ginhoux, and Sonia Garel. 2014. "Microglia Modulate Wiring of the Embryonic Forebrain." Cell Reports 8(5):1271–79. doi: 10.1016/j.celrep.2014.07.042.

Sridhar, Akshayalakshmi, Akina Hoshino, Connor R. Finkbeiner, Alex Chitsazan, Li Dai, Alexandra K. Haugan, Kayla M. Eschenbacher, Dana L. Jackson, Cole Trapnell, Olivia Bermingham-McDonogh, Ian Glass, and Thomas A. Reh. 2020. "Single-Cell Transcriptomic Comparison of Human Fetal Retina, HPSC-Derived Retinal Organoids, and Long-Term Retinal Cultures." Cell Reports 30(5):1644-1659.e4. doi: 10.1016/J.CELREP.2020.01.007.

Stafford, Jennifer B., and Lawrence J. Marnett. 2008. "Prostaglandin E2 Inhibits Tumor Necrosis Factor-Alpha RNA through PKA Type I." Biochemical and Biophysical Research Communications 366(1):104–9. doi: 10.1016/J.BBRC.2007.11.091.

Stevens, Beth, Nicola J. Allen, Luis E. Vazquez, Gareth R. Howell, Karen S. Christopherson, Navid Nouri, Kristina D. Micheva, Adrienne K. Mehalow, Andrew D. Huberman, Benjamin Stafford, Alexander Sher, Alan M. Litke, John D. Lambris, Stephen J. Smith, Simon W. M. John, and Ben A. Barres. 2007. "The Classical Complement Cascade Mediates CNS Synapse Elimination." Cell 131(6):1164–78. doi: 10.1016/J.CELL.2007.10.036.

Stock, Sarah J. E., and Jane E. Norman. 2019. "Medicines in Pregnancy." F1000Research 8. doi: 10.12688/F1000RESEARCH.17535.1.

Sturrock, R. R. 1987. "A Quantitative Histological Study of Cell Division and Changes in Cell Number in the Meningeal Sheath of the Embryonic Human Optic Nerve." Journal of Anatomy 155:133–40.

Su, Xuan, Peng Yue, Jing Kong, Xin Xu, Yu Zhang, Wenjing Cao, Yuxin Fan, Meixiao Liu, Jingjing Chen, Aihua Liu, and Fukai Bao. 2021. "Human Brain Organoids as an In Vitro Model System of Viral Infectious Diseases." Frontiers in Immunology 12. doi: 10.3389/FIMMU.2021.792316.

Sullivan, Patrick F. 2005. "The Genetics of Schizophrenia." PLoS Medicine 2(7):e212. doi: 10.1371/journal.pmed.0020212.

Sun, Xin Yao, Xiang Chun Ju, Yang Li, Peng Ming Zeng, Jian Wu, Ying Ying Zhou, Li Bing Shen, Jian Dong, Yue Jun Chen, and Zhen Ge Luo. 2022. "Generation of Vascularized Brain Organoids to Study Neurovascular Interactions." ELife 11. doi: 10.7554/eLife.76707.

Takahashi, Kazutoshi, Koji Tanabe, Mari Ohnuki, Megumi Narita, Tomoko Ichisaka, Kiichiro Tomoda, and Shinya Yamanaka. 2007. "Induction of Pluripotent Stem Cells from Adult Human Fibroblasts by Defined Factors." Cell 131(5):861–72. doi: 10.1016/j.cell.2007.11.019.

Takata, Kazuyuki, Tatsuya Kozaki, Christopher Zhe Wei Lee, Morgane Sonia Thion, Masayuki Otsuka, Shawn Lim, Kagistia Hana Utami, Kerem Fidan, Dong Shin Park, Benoit Malleret, Svetoslav Chakarov, Peter See, Donovan Low, Gillian Low, Marta Garcia-Miralles, Ruizhu Zeng, Jinqiu Zhang, Chi Ching Goh, Ahmet Gul, Sandra Hubert, Bernett Lee, Jinmiao Chen, Ivy Low, Nurhidaya Binte Shadan, Josephine Lum, Tay Seok Wei, Esther Mok, Shohei Kawanishi, Yoshihisa Kitamura, Anis Larbi, Michael Poidinger, Laurent Renia, Lai Guan Ng, Yochai Wolf, Steffen Jung, Tamer Önder, Evan Newell, Tara Huber, Eishi Ashihara, Sonia Garel, Mahmoud A. Pouladi, and Florent Ginhoux. 2017. "Induced-Pluripotent-Stem-Cell-Derived Primitive Macrophages Provide a Platform for Modeling Tissue-

Resident Macrophage Differentiation and Function." Immunity 47(1):183-198.e6. doi: 10.1016/j.immuni.2017.06.017.

Tanaka, Ken Ichiro, Hiroshi Kaji, Toru Yamaguchi, Ippei Kanazawa, Lucie Canaff, Geoffrey N. Hendy, and Toshitsugu Sugimoto. 2014. "Involvement of the Osteoinductive Factors, Tmem119 and BMP-2, and the ER Stress Response PERK-EIF2α-ATF4 Pathway in the Commitment of Myoblastic into Osteoblastic Cells." Calcified Tissue International 94(4):454–64. doi: 10.1007/s00223-013-9828-1.

TCW, Julia, Minghui Wang, Anna A. Pimenova, Kathryn R. Bowles, Brigham J. Hartley, Emre Lacin, Saima I. Machlovi, Rawan Abdelaal, Celeste M. Karch, Hemali Phatnani, Paul A. Slesinger, Bin Zhang, Alison M. Goate, and Kristen J. Brennand. 2017. "An Efficient Platform for Astrocyte Differentiation from Human Induced Pluripotent Stem Cells." Stem Cell Reports 9(2):600–614. doi: 10.1016/J.STEMCR.2017.06.018.

Thau, Lauren, Vamsi Reddy, and Paramvir Singh. 2022. Anatomy, Central Nervous System. Treasure Island (FL): StatPearls Publishing.

Thiery, Jean Paul, Hervé Acloque, Ruby Y. J. Huang, and M. Angela Nieto. 2009. "Epithelial-Mesenchymal Transitions in Development and Disease." Cell 139(5):871–90. doi: 10.1016/j.cell.2009.11.007.

Thompson, Kimberly M., Emily A. Simons, Kamran Badizadegan, Susan E. Reef, and Louis Z. Cooper. 2016. "Characterization of the Risks of Adverse Outcomes Following Rubella Infection in Pregnancy." Risk Analysis 36(7):1315–31. doi: 10.1111/RISA.12264.

Thomson, J. A., J. Itskovitz-Eldor, S. S. Shapiro, M. A. Waknitz, J. J. Swiergiel, V. S. Marshall, and J. M. Jones. 1998. "Embryonic Stem Cell Lines Derived from Human Blastocysts." Science (New York, N.Y.) 282(5391):1145–47. doi: 10.1126/SCIENCE.282.5391.1145.

Timmerman, Raissa, Saskia M. Burm, and Jeffrey J. Bajramovic. 2018. "An Overview of in Vitro Methods to Study Microglia." Frontiers in Cellular Neuroscience 12:242. doi: 10.3389/fncel.2018.00242.

Töndury, Gian, and David W. Smith. 1966. "Fetal Rubella Pathology." The Journal of Pediatrics 68(6):867–79. doi: 10.1016/S0022-3476(66)80204-4.

Town, Terrence, David Jeng, Lena Alexopoulou, Jun Tan, and Richard A. Flavell. 2006. "Microglia Recognize Double-Stranded RNA via TLR3." The Journal of Immunology 176(6):3804–12. doi: 10.4049/jimmunol.176.6.3804.

Ubogu, Eroboghene E., Melissa K. Callahan, Barbara H. Tucky, and Richard M. Ransohoff. 2006. "Determinants of CCL5-Driven Mononuclear Cell Migration across the Blood-Brain Barrier. Implications for Therapeutically Modulating Neuroinflammation." Journal of Neuroimmunology 179(1–2):132–44. doi: 10.1016/J.JNEUROIM.2006.06.004.

Ueno, Masaki, Yuki Fujita, Tatsuhide Tanaka, Yuka Nakamura, Junichi Kikuta, Masaru Ishii, and Toshihide Yamashita. 2013. "Layer v Cortical Neurons Require Microglial Support for Survival during Postnatal Development." Nature Neuroscience 16(5):543–51. doi: 10.1038/nn.3358.

Uhlén, Mathias, Linn Fagerberg, Bjö M. Hallström, Cecilia Lindskog, Per Oksvold, Adil Mardinoglu, Åsa Sivertsson, Caroline Kampf, Evelina Sjöstedt, Anna Asplund, Ing Marie Olsson, Karolina Edlund, Emma Lundberg, Sanjay Navani, Cristina Al Khalili Szigyarto, Jacob Odeberg, Dijana Djureinovic, Jenny Ottosson Takanen, Sophia Hober, Tove Alm, Per Henrik Edqvist, Holger Berling, Hanna Tegel, Jan Mulder, Johan Rockberg, Peter Nilsson, Jochen M. Schwenk, Marica Hamsten, Kalle Von Feilitzen, Mattias Forsberg, Lukas Persson, Fredric Johansson, Martin Zwahlen, Gunnar Von Heijne, Jens Nielsen, and Fredrik Pontén. 2015. "Tissue-Based Map of the Human Proteome." Science 347(6220). doi: 10.1126/science.1260419.

Usui-Ouchi, Ayumi, Sarah Giles, Sarah Harkins-Perry, Elizabeth A. Mills, Roberto Bonelli, Guoqin Wei, Yasuo Ouchi, Nobuyuki Ebihara, Shintaro Nakao, Martin Friedlander, and Kevin T. Eade. 2023.

"Integrating Human IPSC-Derived Macrophage Progenitors into Retinal Organoids to Generate a Mature Retinal Microglial Niche." Glia. doi: 10.1002/GLIA.24428.

Utz, Sebastian G., Peter See, Wiebke Mildenberger, Morgane Sonia Thion, Aymeric Silvin, Mirjam Lutz, Florian Ingelfinger, Nirmala Arul Rayan, Iva Lelios, Anne Buttgereit, Kenichi Asano, Shyam Prabhakar, Sonia Garel, Burkhard Becher, Florent Ginhoux, and Melanie Greter. 2020. "Early Fate Defines Microglia and Non-Parenchymal Brain Macrophage Development." Cell 181(3):557-573.e18. doi: 10.1016/j.cell.2020.03.021.

Vankriekelsvenne, Elise, Uta Chrzanowski, Katerina Manzhula, Theresa Greiner, Andreas Wree, Alexander Hawlitschka, Gemma Llovera, Jiangshan Zhan, Sarah Joost, Christoph Schmitz, Peter Ponsaerts, Sandra Amor, Erik Nutma, Markus Kipp, and Hannes Kaddatz. 2022. "Transmembrane Protein 119 Is Neither a Specific nor a Reliable Marker for Microglia." Glia 70(6):1170–90. doi: 10.1002/glia.24164.

Vaughan-Jackson, Alun, Szymon Stodolak, Kourosh H. Ebrahimi, Cathy Browne, Paul K. Reardon, Elisabete Pires, Javier Gilbert-Jaramillo, Sally A. Cowley, and William S. James. 2021. "Differentiation of Human Induced Pluripotent Stem Cells to Authentic Macrophages Using a Defined, Serum-Free, Open-Source Medium." Stem Cell Reports 16:1735–48. doi: 10.1016/j.stemcr.2021.05.018.

Venegas, Carmen, and Michael T. Heneka. 2017. "Danger-Associated Molecular Patterns in Alzheimer's Disease." Journal of Leukocyte Biology 101(1):87–98. doi: 10.1189/jlb.3mr0416-204r.

Vezzani, Annamaria, and Barbara Viviani. 2015. "Neuromodulatory Properties of Inflammatory Cytokines and Their Impact on Neuronal Excitability." Neuropharmacology 96:70–82. doi: 10.1016/J.NEUROPHARM.2014.10.027.

Victor, Matheus B., Noelle Leary, Xochitl Luna, Hiruy S. Meharena, Aine Ni Scannail, P. Lorenzo Bozzelli, George Samaan, Mitchell H. Murdock, Djuna von Maydell, Audrey H. Effenberger, Oyku Cerit, Hsin Lan Wen, Liwang Liu, Gwyneth Welch, Maeve Bonner, and Li Huei Tsai. 2022. "Lipid Accumulation Induced by APOE4 Impairs Microglial Surveillance of Neuronal-Network Activity." Cell Stem Cell 29(8):1197-1212.e8. doi: 10.1016/J.STEM.2022.07.005.

Wagstaff, Ellie L., Anneloor L. M. A. ten Asbroek, Jacoline B. ten Brink, Nomdo M. Jansonius, and Arthur A. B. Bergen. 2021. "An Alternative Approach to Produce Versatile Retinal Organoids with Accelerated Ganglion Cell Development." Scientific Reports 2021 11:1 11(1):1–17. doi: 10.1038/s41598-020-79651-x.

Wahlin, Karl J., Julien A. Maruotti, Srinivasa R. Sripathi, John Ball, Juan M. Angueyra, Catherine Kim, Rhonda Grebe, Wei Li, Bryan W. Jones, and Donald J. Zack. 2017. "Photoreceptor Outer Segment-like Structures in Long-Term 3D Retinas from Human Pluripotent Stem Cells." Scientific Reports 2017 7:1 7(1):1–15. doi: 10.1038/s41598-017-00774-9.

Wang, Yaming, Kristy J. Szretter, William Vermi, Susan Gilfillan, Cristina Rossini, Marina Cella, Alexander D. Barrow, Michael S. Diamond, and Marco Colonna. 2012. "IL-34 Is a Tissue-Restricted Ligand of CSF1R Required for the Development of Langerhans Cells and Microglia." Nature Immunology 13(8):753–60. doi: 10.1038/NI.2360.

Wenzel, Tyler J., Joseph D. Desjarlais, and Darrell D. Mousseau. 2024. "Human Brain Organoids Containing Microglia That Have Arisen Innately Adapt to a β-Amyloid Challenge Better than Those in Which Microglia Are Integrated by Co-Culture." Stem Cell Research and Therapy 15(1). doi: 10.1186/s13287-024-03876-0.

Wheeler, D. Lori, Alan Sariol, David K. Meyerholz, and Stanley Perlman. 2018. "Microglia Are Required for Protection against Lethal Coronavirus Encephalitis in Mice." Journal of Clinical Investigation 128(3):931–43. doi: 10.1172/JCI97229.

Wickham, Hadley. 2016. "Ggplot2: Elegant Graphics for Data Analysis." Pp. 3–10 in Springer.

Wickham, Hadley, Romain Francois, Lionel Henry, and Kirill Mueller. 2021. “A Grammar of Data Manipulation [R Package Dplyr Version 1.0.7].”

Wu, Yumei, Hui Peng, Min Cui, Nicholas P. Whitney, Yunlong Huang, and Jialin C. Zheng. 2009. “CXCL12 Increases Human Neural Progenitor Cell Proliferation through Akt-1/FOXO3a Signaling Pathway.” Journal of Neurochemistry 109(4):1157–67. doi: 10.1111/J.1471-4159.2009.06043.X.

Xiang, Yangfei, Yoshiaki Tanaka, Bilal Cakir, Benjamin Patterson, Kun Yong Kim, Pingnan Sun, Young Jin Kang, Mei Zhong, Xinran Liu, Prabir Patra, Sang Hun Lee, Sherman M. Weissman, and In Hyun Park. 2019. “HESC-Derived Thalamic Organoids Form Reciprocal Projections When Fused with Cortical Organoids.” Cell Stem Cell 24(3):487-497.e7. doi: 10.1016/J.STEM.2018.12.015.

Xu, Ranjie, Andrew J. Boreland, Xiaoxi Li, Caroline Erickson, Mengmeng Jin, Colm Atkins, Zhiping P. Pang, Brian P. Daniels, and Peng Jiang. 2021. “Developing Human Pluripotent Stem Cell-Based Cerebral Organoids with a Controllable Microglia Ratio for Modeling Brain Development and Pathology.” Stem Cell Reports 16(8):1923–37. doi: 10.1016/j.stemcr.2021.06.011.

Xu, Yan Peng, Yang Qiu, Boya Zhang, Guilai Chen, Qi Chen, Miao Wang, Fan Mo, Jiuyue Xu, Jin Wu, Rong Rong Zhang, Meng Li Cheng, Na Na Zhang, Bao Lyu, Wen Liang Zhu, Meng Hua Wu, Qing Ye, Da Zhang, Jiang Hong Man, Xiao Feng Li, Jie Cui, Zhiheng Xu, Baoyang Hu, Xi Zhou, and Cheng Feng Qin. 2019. “Zika Virus Infection Induces RNAi-Mediated Antiviral Immunity in Human Neural Progenitors and Brain Organoids.” Cell Research 2019 29:4 29(4):265–73. doi: 10.1038/s41422-019-0152-9.

Yamashita, Nami, Eriko Tokunaga, Makoto Iimori, Yuka Inoue, Kimihiro Tanaka, Hiroyuki Kitao, Hiroshi Saeki, Eiji Oki, and Yoshihiko Maehara. 2018. “Epithelial Paradox: Clinical Significance of Coexpression of E-Cadherin and Vimentin With Regard to Invasion and Metastasis of Breast Cancer.” Clinical Breast Cancer 18(5):e1003–9. doi: 10.1016/j.clbc.2018.02.002.

Yao, Min, Wei Zhou, Simren Sangha, Andrew Albert, Albert J. Chang, Thomas C. Liu, and M. Michael Wolfe. 2005. “Effects of Nonselective Cyclooxygenase Inhibition with Low-Dose Ibuprofen on Tumor Growth, Angiogenesis, Metastasis, and Survival in a Mouse Model of Colorectal Cancer.” Clinical Cancer Research 11(4):1618–28. doi: 10.1158/1078-0432.CCR-04-1696.

Yaqubi, Moein, Adam M. R. Groh, Marie France Dorion, Elia Afanasiev, Julia Xiao Xuan Luo, Hadi Hashemi, Sarthak Sinha, Nicholas W. Kieran, Manon Blain, Qiao Ling Cui, Jeff Biernaskie, Myriam Srour, Roy Dudley, Jeffery A. Hall, Joshua A. Sonnen, Nathalie Arbour, Alexandre Prat, Jo Anne Stratton, Jack Antel, and Luke M. Healy. 2023. “Analysis of the Microglia Transcriptome across the Human Lifespan Using Single Cell RNA Sequencing.” Journal of Neuroinflammation 20(1). doi: 10.1186/s12974-023-02809-7.

Yu, J. Y., Maxim A. Vodyanik, Kim Smuga-Otto, Jessica Antosiewicz-Bourget, Jennifer L. Frane, Shulan Tian, Jeff Nie, Gudrun A. Jonsdottir, Victor Ruotti, Ron Stewart, Igor I. Slukvin, and James A. Thomson. 2007. “Induced Pluripotent Stem Cell Lines Derived from Human Somatic Cells.” Science 318(5858):1917–20. doi: 10.1126/science.1151526.

Zhang, Chi, Wan-Qing Yu, Akina Hoshino, Jing Huang, Fred Rieke, Thomas A. Reh, and Rachel O. L. Wong. 2019. “Development of ON and OFF Cholinergic Amacrine Cells in the Human Fetal Retina.” Journal of Comparative Neurology 527(1):174–86. doi: 10.1002/cne.24405.

Zhang, P., J. Li, Z. Tan, C. Wang, T. Liu, L. Chen, J. Yong, W. Jiang, X. Sun, L. Du, M. Ding, and H. Deng. 2008. “Short-Term BMP-4 Treatment Initiates Mesoderm Induction in Human Embryonic Stem Cells.” Blood 111(4):1933–41. doi: 10.1182/blood-2007-02-074120.

Zhang, Pengbo, Jian Li, Zhijia Tan, Chengyan Wang, Ting Liu, Lin Chen, Jun Yong, Wei Jiang, Xiaomeng Sun, Liying Du, Mingxiao Ding, and Hongkui Deng. 2008. “Short-Term BMP-4 Treatment Initiates Mesoderm Induction in Human Embryonic Stem Cells.” Blood 111(4):1933–41. doi: 10.1182/blood-2007-02-074120.

Zhang, Pingbo, Craig Dufresne, Randi Turner, Sara Ferri, Vidya Venkatraman, Rabia Karani, Gerard A. Lutty, Jennifer E. Van Eyk, and Richard D. Semba. 2015. “The Proteome of Human Retina.” PROTEOMICS 15(4):836–40. doi: 10.1002/pmic.201400397.

Zhang, Pingbo, Rabia Karani, Randi L. Turner, Craig Dufresne, Sara Ferri, Jennifer E. Van Eyk, and Richard D. Semba. 2016. “The Proteome of Normal Human Retrobulbar Optic Nerve and Sclera.” PROTEOMICS 16(19):2592–96. doi: 10.1002/pmic.201600229.

Zhang, Pingbo, David Kirby, Craig Dufresne, Yan Chen, Randi Turner, Sara Ferri, Deepak P. Edward, Jennifer E. Van Eyk, and Richard D. Semba. 2016. “Defining the Proteome of Human Iris, Ciliary Body, Retinal Pigment Epithelium, and Choroid.” PROTEOMICS 16(7):1146–53. doi: 10.1002/pmic.201500188.

Zhang, Weifeng, Dan Xiao, Qinwen Mao, and Haibin Xia. 2023. “Role of Neuroinflammation in Neurodegeneration Development.” Signal Transduction and Targeted Therapy 2023 8:1 8(1):1–32. doi: 10.1038/s41392-023-01486-5.

Zhang, Xijing, Liangwei Chen, Yazhou Wang, Yinxiu Ding, Zhengwu Peng, Li Duan, Gong Ju, Yi Ren, and Xi Wang. 2013. “Macrophage Migration Inhibitory Factor Promotes Proliferation and Neuronal Differentiation of Neural Stem/Precursor Cells through Wnt/β-Catenin Signal Pathway.” International Journal of Biological Sciences 9(10):1108–20. doi: 10.7150/IJBS.7232.

Zhong, Xiufeng, Christian Gutierrez, Tian Xue, Christopher Hampton, M. Natalia Vergara, Li Hui Cao, Ann Peters, Tea Soon Park, Elias T. Zambidis, Jason S. Meyer, David M. Gamm, King Wai Yau, and M. Valeria Canto-Soler. 2014. “Generation of Three-Dimensional Retinal Tissue with Functional Photoreceptors from Human IPSCs.” Nature Communications 5(1):1–14. doi: 10.1038/ncomms5047.

Zhou, Ting, Lei Tan, Gustav Y. Cederquist, Yujie Fan, Brigham J. Hartley, Suranjit Mukherjee, Mark Tomishima, Kristen J. Brennand, Qisheng Zhang, Robert E. Schwartz, Todd Evans, Lorenz Studer, and Shuibing Chen. 2017. “High-Content Screening in HPSC-Neural Progenitors Identifies Drug Candidates That Inhibit Zika Virus Infection in Fetal-like Organoids and Adult Brain.” Cell Stem Cell 21(2):274-283.e5. doi: 10.1016/j.stem.2017.06.017.

Zhu, Gang, Motohiro Okada, Shukuko Yoshida, Fumiaki Mori, Shinya Ueno, Koichi Wakabayashi, and Sunao Kaneko. 2006. “Effects of Interleukin-1β on Hippocampal Glutamate and GABA Releases Associated with Ca2+-Induced Ca2+ Releasing Systems.” Epilepsy Research 71(2–3):107–16. doi: 10.1016/j.eplepsyres.2006.05.017.